



The
University
Of
Sheffield.

The Medical School
Department of Oncology and Human Metabolism

The use of a novel TIMP3 peptide to specifically target therapeutic drugs to tumours

Mohammed Saeed K Aldughaim

Supervised by:

Dr. Mike Barker

& Dr Munitta Muthana

**A project dissertation in partial fulfilment of the requirements for the
Doctor of Philosophy degree in Cellular and Molecular Medicine of the
University of Sheffield**

November 2017

Dedication

I dedicate this work to my parents, my wife, Ghadah and my son, Saeed.

Acknowledgement

My overwhelming gratitude goes to the Almighty Allah (SWT), the most Gracious and the most Merciful for HIS mercy on me and my family; and for seeing me through, right from the beginning of my creation, through to this moment of my life. He is the pillar upon which I stand and the reason for the success of this PhD thesis. Next are my lovely parents; I sincerely appreciate them for their show of unique love and words of wisdom to me. And to my dear wife and son, I say thank you to them for their love, patience and support, which made my PhD life less stressful and incredibly wonderful.

This acknowledgement remains incomplete without appreciating unrelenting and unwavering support extended to me by my supervisor, Dr Mike Barker. I am indeed grateful to him for his massive contributions and painstaking efforts; right from the beginning to the end of my studies and towards ensuring this thesis comes out in its very best. I strongly believe, posterity would never forget his efforts at ensuring my PhD life went smoothly. I also wish to acknowledge the contributions of my second supervisor, Dr Munitta Muthana; I am indeed grateful for her support by complementing efforts of my first supervisor towards ensuring overall success of my research.

I cannot lose sight of the immense contributions and care extended to me by Dr Simon Tazzyman, who was always there to help anytime I turned to him. I am also extremely grateful to Dr Russel Hughes, all my colleagues, my siblings and friends, who were instrumental to the successful completion of my PhD studies, I acknowledge and appreciate you all.

Finally, the sponsorship of my PhD research by Prince Mohammed Medical City (PMMC), Saudi Arabia is also acknowledged.

Abstract

Background

Tissue inhibitor of metalloproteinases-3 (TIMP3) is an extracellular matrix protein with a number of novel properties such as inhibition of matrix metalloproteinases. Another of its ability is to inhibit vascular endothelial growth factor receptor 2 (VEGFR2), a key mediator of angiogenesis. Our laboratory has begun to investigate the interaction sites between TIMP3 and VEGFR2 and have identified several regions within the C-terminal domain of TIMP3 that play a role in this interaction including a short sixteen amino-acid peptide (p700) inhibits VEGFR2 and other receptors which are upregulated in either tumour vasculature or tumour cells in several cancers.

The aims of this study were to utilize p700 as a novel delivery vehicle for cytotoxic drugs to treat cancer and to engineer identified residues from the TIMP3 C-terminal into a chimeric protein of TIMP3 and TIMP4 for VEGFR2 inhibition.

Results

P700 retained its receptor binding after successful coupling to Doxil®. In contrast to Doxil alone, P700-Doxil was rapidly internalized by H5V cells, mouse (4T1) and human (MCF7) breast cancer cells but not HUVEC cells, showing approximately 100-fold increase in uptake relative to Doxil alone. Furthermore, this enhanced uptake significantly increased the sensitivity of breast cancer cells to Doxil in vitro but not in vivo.

Recombinant CPG2 was highly expressed in *E. coli* and successfully purified by nickel affinity chromatography. Biolayer interferometry showed that CPG2-p700 had a 100-fold increase in binding affinity for VEGFR2 compared with CPG2 alone. Recombinant CGP2-p700 retained its catalytic activity for MTX. In the presence of CPG2-p700, the ZD2676P pro-drug showed significant cytotoxicity for 4T1 cells compared with prodrug alone or CPG2 alone.

Finally, we successfully transfected H5V endothelial cell line with TIMP3-TIMP4 chimeras for stable expression. Initial phosphorylation assays showed T3T4V inhibited VEGFR2 phosphorylation in H5V cells transfected while T3T4 that lacks these residues did not.

List of content

| | |
|--|-------------|
| Dedication | ii |
| Acknowledgement | iii |
| Abstract | iv |
| List of content | v |
| List of Figures | xi |
| List of Tables | xiii |
| List of Abbreviations | xiv |
| CHAPTER 1 | 1 |
| General Introduction | 1 |
| 1 Introduction | 2 |
| 1.1 Hallmarks of cancer | 2 |
| 1.1.1 The cancer hallmark and cancer cell survival | 3 |
| 1.1.2 Induction of angiogenesis and lymphangiogenesis as a cancer hallmark | 10 |
| 1.2 The tumour microenvironment contributes to the hallmarks of cancer | 11 |
| 1.3 Tumour angiogenesis | 14 |
| 1.3.1 VEGF is the major angiogenic growth factor | 14 |
| 1.3.1.1 VEGF: The canonical angiogenic factor exists in soluble and matrix bound forms | 17 |
| 1.3.1.2 VEGF signalling with neuropilin is crucial to endothelial cell migration and angiogenesis..... | 21 |
| 1.3.2 Other proangiogenic factors highly expressed in cancer | 21 |
| 1.3.3 The PDGF/PDGFR system | 22 |
| 1.3.4 FGF and FGFR | 23 |
| 1.3.5 Targeting angiogenesis in cancer | 24 |
| 1.4 The Metzincins | 25 |
| 1.4.1 A disintegrin and metalloproteinases (ADAMs)..... | 25 |
| 1.4.2 A disintegrin and metalloproteinase protease with thrombospondin motif (ADAMTS)..... | 26 |
| 1.4.3 Matrix metalloproteinases (MMPs) | 27 |
| 1.4.3.1 Structure of MMP | 28 |
| 1.4.3.2 Proteolytic activation of MMPs | 28 |
| 1.5 Metalloproteinases in tumour growth and invasion | 31 |
| 1.6 MMPs as therapeutic target in clinical trials | 32 |
| 1.7 Regulation of metzincins | 33 |
| 1.7.1 Transcriptional expression | 33 |
| 1.7.2 Post translational regulation of metzincins | 33 |

| | | |
|------------------------------|--|-----------|
| 1.8 | Regulation of metzinc proteins by TIMPS | 34 |
| 1.9 | TIMPs | 36 |
| 1.9.1 | Structure-function properties of TIMPs..... | 36 |
| 1.9.2 | Regulation of TIMP proteins..... | 40 |
| 1.9.3 | TIMPs in cancer..... | 41 |
| 1.9.3.1 | TIMP1..... | 41 |
| 1.9.3.2 | TIMP2..... | 42 |
| 1.9.3.3 | TIMP3..... | 42 |
| 1.9.3.4 | TIMP4..... | 43 |
| 1.9.4 | TIMP3: Structural and functional features..... | 46 |
| 1.9.4.1 | TIMP3 association with the ECM..... | 48 |
| 1.9.4.2 | TIMP3 Inhibition of adamalysin metalloproteinases..... | 48 |
| 1.9.4.3 | TIMP3 and apoptosis..... | 49 |
| 1.9.4.4 | TIMP3 and EFEMP1..... | 50 |
| 1.9.4.5 | TIMP3 in the retina..... | 51 |
| 1.9.4.5.1 | TIMP3 in the pathogenesis of Sorsby’s fundus dystrophy..... | 51 |
| 1.9.4.5.2 | TIMP3 and age-related macular degeneration (AMD)..... | 51 |
| 1.9.4.6 | TIMP3 and angiogenesis..... | 53 |
| 1.9.4.6.1 | TIMP3 inhibition of VEGFR2..... | 53 |
| 1.10 | Targeted drug delivery systems in cancer therapy | 53 |
| 1.10.1 | Lipid based DDS..... | 56 |
| 1.10.2 | Polymeric nanoparticle..... | 58 |
| 1.10.3 | Peptide DDS..... | 58 |
| 1.10.4 | Prodrug approach..... | 58 |
| 1.11 | Work that has led to this project | 59 |
| 1.12 | Hypotheses and aims | 60 |
| CHAPTER 2 | | 62 |
| General Methods | | 62 |
| 2.1. | Methods | 63 |
| 2.1.1. | Transformation <i>E. coli</i> :..... | 63 |
| 2.1.2. | Bacterial suspension culture:..... | 63 |
| 2.1.3. | Small scale (Miniprep) and Large scale (Maxiprep) plasmid DNA purification:..... | 63 |
| 2.1.4. | Restriction enzyme digestion of plasmid DNA:..... | 64 |
| 2.1.5. | Agarose gel electrophoresis for DNA analysis or purification:..... | 65 |
| 2.1.6. | Ligation of DNA..... | 65 |
| 2.1.7. | Verification of ligated constructs:..... | 66 |
| 2.1.8. | Methods for mammalian cell culture..... | 66 |

| | | |
|---|---|------------|
| 2.1.8.1. | H5V 4T1 and MCF-7 cell culture:..... | 66 |
| 2.1.8.2. | Passaging of mammalian cell lines:..... | 67 |
| 2.1.9. | Cryopreservation of cells | 67 |
| 2.1.10. | Determining protein concentration: | 68 |
| 2.1.11. | SDS-PAGE | 68 |
| 2.1.11.1. | Gel preparation:..... | 68 |
| 2.1.11.2. | Electrophoresis: | 69 |
| 2.1.12. | Western blotting..... | 69 |
| 2.1.12.1. | Semi-dry Protein transfer onto nitrocellulose membrane: | 69 |
| 2.1.12.2. | Blocking of Nitrocellulose membrane:..... | 70 |
| 2.1.12.3. | Antibody probing for protein identification: | 70 |
| 2.1.12.4. | Protein band detection and blot development: | 70 |
| 2.1.12.5. | Stripping of blots for reprobing: | 71 |
| 2.1.13. | MTS Cell Proliferation Assay..... | 71 |
| CHAPTER 3 | | 72 |
| Coupling of p700 peptide to PEGylated liposomal doxorubicin (Doxil®)..... | | 72 |
| 3.1. | Introduction..... | 73 |
| 3.1.1. | Aims and objectives of the study | 75 |
| 3.2.1. | Conjugation of p700 peptide to PEGylated liposomal doxorubicin | 76 |
| 3.2.2. | Coupling reaction..... | 78 |
| 3.2.2.1. | Purification of coupled products..... | 80 |
| 3.2.3. | Confirmation of coupling by flow cytometry | 80 |
| 3.2.4. | Confirmation of cellular binding of p700-conjugated liposomal doxorubicin.... | 81 |
| 3.2.5. | Confirmation to cellular uptake of p700-conjugated liposomal doxorubicin | 82 |
| 3.2.6. | Cell viability assays | 83 |
| 3.2.7. | Cytotoxicity assay..... | 83 |
| 3.3. | Results | 85 |
| 3.3.1. | Coupling assessment..... | 85 |
| 3.3.2. | Binding evaluation | 87 |
| 3.3.3. | Cellular uptake and internalisation..... | 93 |
| 3.3.4. | Growth assessment..... | 100 |
| 3.3.5. | Cytotoxic effect of conjugates | 102 |
| 3.4. | Discussion..... | 104 |
| 3.5. | Conclusion | 107 |
| CHAPTER 4 | | 108 |
| Coupling of p700 peptide to carboxypeptidase G2 for pro-drug activation..... | | 108 |
| 4.1. | Introduction: | 109 |

| | | |
|-------------|--|-----|
| 4.1.1. | Aim | 110 |
| 4.2. | Methods | 113 |
| 4.2.1. | Synthesis of CPG2 codon-optimized synthetic gene | 113 |
| 4.2.2. | Sub-cloning of the codon optimised CPG2-His gene into pET28a and insertion of the p700 and T3C peptide sequences)..... | 113 |
| 4.2.3. | Transformation of CPG2 constructs into competent <i>E. coli</i> | 114 |
| 4.2.4. | Small scale induction of CPG2-only and CPG2 fusion protein expression | 114 |
| 4.2.5. | Protein detection by SDS-PAGE and Coomassie Brilliant Blue staining..... | 115 |
| 4.2.6. | Solubility test of recombinant proteins | 115 |
| 4.2.7. | Large scale induction of recombinant CPG2 expression | 116 |
| 4.2.8. | Whole bacterial cell lysis and separation into soluble and insoluble fractions . | 116 |
| 4.2.9. | Inclusion body Preparation | 117 |
| 4.2.9.1. | Insoluble fraction | 117 |
| 4.2.9.2. | Washes..... | 117 |
| 4.2.9.3. | Inclusion Body | 117 |
| 4.2.9.4. | Screening..... | 118 |
| 4.2.10. | CPG2 purification from the insoluble fraction by Ni ²⁺ -NTA chromatography | 118 |
| 4.2.10.1. | Preparation of Ni ²⁺ column: | 118 |
| 4.2.10.2. | Protein purification | 118 |
| 4.2.10.3. | Elution | 118 |
| 4.2.11. | Protein quantification of eluent fractions..... | 119 |
| 4.2.12. | Enzyme activity assay | 119 |
| 4.2.13. | Assessment of zinc-dependence of recombinant CPG2-fusion protein enzyme activity | 120 |
| 4.2.14. | Kinetic analysis of CPG2-p700 binding to VEGFR2 by Bio-Layer Interferometry (BLITZ) | 120 |
| 4.2.15. | Cytotoxicity assay..... | 123 |
| 4.3. | Results | 125 |
| 4.3.1. | Construction of CPG2, CPG2-p700 and CPG2-T3C cDNA clones | 125 |
| 4.3.2. | Small scale induction of CPG2 expression | 127 |
| 4.3.3. | Solubility Test..... | 129 |
| 4.3.4. | Large scale expression of CPG2 and CPG2 fusion proteins..... | 131 |
| 4.3.5. | Inclusion body preparation for CPG2 | 133 |
| 4.3.6. | Purified CPG2 recombinants proteins:..... | 135 |
| 4.3.7. | Assessment of the enzymatic activity of the purified recombinant CPG2 proteins | 137 |
| 4.3.8. | Determination of the ability of CPG2-p700 recombinant protein to bind to VEGFR2 by bio-layer interferometry..... | 139 |

| | |
|---|------------|
| 4.3.9. Cytotoxicity assays to determine the ability of recombinant CPG2 proteins to activate the ZD2676P prodrug: | 141 |
| 4.4. Discussion | 143 |
| 4.5. Conclusion | 145 |
| CHAPTER 5 | 146 |
| Assessment of the efficacy of Doxil-p700 in an <i>in vivo</i> model of breast cancer | 146 |
| 5.1 Introduction | 147 |
| 5.1.1 Aim of this chapter..... | 148 |
| 5.2 Transplant of cancer cells into BALB/c mice | 150 |
| 5.2.1 Treatment | 152 |
| 5.2.2 Fixed Tissue Preparation..... | 153 |
| 5.2.3 Haematoxylin and eosin staining | 153 |
| 5.2.4 Immunohistochemistry staining for caspase-3 | 154 |
| 5.2.5 Immunofluorescence staining for CD31 | 156 |
| 5.2.6 Analysis for stained tumour or lung sections:..... | 157 |
| 5.3 Results | 158 |
| 5.3.1 Health assessment of mice | 158 |
| 5.3.2 Effect of Doxil and Doxil-p700 treatment on tumour growth | 160 |
| 5.3.3 Induction of necrosis by Doxil and Doxil-p700..... | 162 |
| 5.3.4 Caspase activation by Doxil and Doxil-p700..... | 164 |
| 5.3.5 Effect of Doxil and Doxil-p700 treatment on tumour vascularisation..... | 166 |
| 5.3.6 Effect of Doxil and Doxil-p700 treatment on lung metastasis of 4T1 cells..... | 171 |
| 5.4 Discussion | 174 |
| 5.5 Conclusion | 176 |
| CHAPTER 6 | 177 |
| Identifying TIMP3 residues responsible for inhibition of VEGFR2 to facilitate rational drug design | 177 |
| 6.1 Introduction | 178 |
| 6.1.1 Aim of this chapter..... | 179 |
| 6.2 Methods | 180 |
| 6.2.1 Polymerase chain reaction (PCR) for adding the V5-[His] ₆ tag to TIMP chimeras | 180 |
| 6.2.2 Digestion and ligation of PCR products and pcDNA6 vector | 182 |
| 6.2.3 Transformation of T3T4 constructs into competent E-coli..... | 182 |
| 6.2.4 Diagnostic restriction digest..... | 182 |
| 6.2.5 Transfection of cell lines..... | 182 |
| 6.2.6 Phosphorylation assay..... | 183 |
| 6.3 Results | 185 |

| | | |
|---------------------------|---|------------|
| 6.3.1 | Creation of V5-His-tagged chimeras | 185 |
| 6.3.2 | Optimisation of H5V cell transfection | 188 |
| 6.3.3 | Stable transfection of H5V cells with the TIMP constructs..... | 188 |
| 6.3.4 | Confirmation of VEGFR2 autophosphorylation in untransfected H5V cells ... | 192 |
| 6.3.5 | VEGFR2 autophosphorylation assay in H5V cells transfected with the TIMP chimeras | 194 |
| 6.4 | Discussion | 196 |
| 6.5 | Conclusion | 197 |
| CHAPTER 7 | | 198 |
| General Discussion | | 198 |
| 7.1. | Novelty of the p700 peptide | 199 |
| 7.2. | Coupling of CPG2 to p700 | 201 |
| 7.3 | Coupling of p700 to liposomal doxorubicin (Doxil®) | 202 |
| 7.4 | Assessment of p700-Doxil® <i>in vivo</i> | 203 |
| 7.5 | Identification of VEGFR2 binding residues on TIMP3 | 203 |
| 7.6 | Conclusion | 204 |
| 7.7 | Future work | 205 |
| 8 | Bibliography | 208 |
| 9 | Appendix | 227 |

List of Figures

| | |
|--|-----|
| Figure 1.1. Extrinsic and intrinsic apoptotic pathways | 5 |
| Figure 1.2. Mechanism of apoptosis evasion by cancer cells | 6 |
| Figure 1.3. Enabling and emerging hallmarks of cancer cells | 9 |
| Figure 1.4. VEGF isoforms and their receptors that mediate angiogenesis | 16 |
| Figure 1.5. Hypoxia activation of NOTCH and VEGFR-2 signalling during vascularisation ... | 19 |
| Figure 1.6. Protein isoforms of VEGF-A..... | 20 |
| Figure 1.7. MMP classification based on shared structural domains and substrates | 30 |
| Figure 1.8. The primary structure of TIMPs | 38 |
| Figure 1.9. Box shade alignment of the TIMP protein family showing sequence similarities and conserved domains..... | 39 |
| Figure 1.10. TIMPs regulate key aspects of the tumour microenvironment..... | 45 |
| Figure 1.11. Overview of TIMP3 regulatory properties | 47 |
| Figure 1.12. Schematic diagram of various Targeted Drug Delivery Systems (TDDS)..... | 55 |
| Figure 1.13. Delivery of liposomal drug to peripheral tissues and tumours | 57 |
| Figure 3.1 The SPAAC reaction for conjugating p700 to Doxil..... | 79 |
| Figure 3.2. Assessment of p700 coupling to PEGylated liposome | 86 |
| Figure 3.3 The effect of coupling p700 peptide on the binding of Doxil to the H5V..... | 88 |
| Figure 3.4. The effect of coupling p700 on the binding of Doxil® to the 4T1 | 89 |
| Figure 3.5 The effect of coupling p700 on the binding of Doxil to the MCF-7 | 90 |
| Figure 3.6 Effect of coupling p700 on binding of Doxil® to primary human dermal microvascular endothelial cells..... | 91 |
| Figure 3.7 Comparison of the binding of Doxil-p700 between primary HuDMEC and the three cell lines | 92 |
| Figure 3.8 Uptake of Doxil and Doxil-p700 by the 4T1 cell line | 95 |
| Figure 3.9 Uptake of empty liposome-p700 by the 4T1 cell line | 96 |
| Figure 3.10 Uptake of empty p700 conjugated liposomes by the H5V cell line | 97 |
| Figure 3.11 Uptake of Doxil® and Doxil-p700 by the MCF-7 cell line..... | 98 |
| Figure 3.12 Uptake of Doxil and Doxil-p700 by HuDMEC..... | 99 |
| Figure 3.13 Growth rate of 4T1, H5V and HuDMEC cells over 72 h..... | 101 |
| Figure 3.14 Effect of increasing concentrations of empty liposome-p700-FITC, Doxil-FITC and Doxil-p700-FITC on the viability of 4T1, H5V, MCF-7 and HuDMEC..... | 103 |
| Figure 4.1 Strategy for prodrug activation by CPG2-p700..... | 112 |
| Figure 4.2 Conversion of methotrexate to 2,4-diamino methylpteroic acid by CPG2 can be determined by measuring the decrease in methotrexate absorbance at 320 nm..... | 119 |
| Figure 4.3 BLI technology enables label-free, real-time kinetic analysis of protein/protein interactions..... | 122 |
| Figure 4.4 Subcloning of CPG2, p700 and T3C into the pET28a vector | 126 |
| Figure 4.5 SDS-PAGE analysis of recombinant CPG-2 protein expression in BL21 <i>E. coli</i> ... | 128 |
| Figure 4.6 Solubility test to determine localisation of recombinant CPG2 protein expression in BL21 <i>E. coli</i> | 130 |
| Figure 4.7 Large-scale expression of CPG2 recombinant proteins in BL21 <i>E. coli</i> | 132 |
| Figure 4.8 CPG2 proteins present in different fractions of BL21 <i>E. coli</i> cell lysate | 134 |
| Figure 4.9 Purification of recombinant CPG2 proteins on nickel-chelate resin from urea washes derived from the insoluble fraction of BL21 <i>E. coli</i> cell lysates..... | 136 |

| | |
|---|-----|
| Figure 4.10 Confirmation of the zinc-dependent enzymatic activity of purified recombinant CPG2 proteins..... | 138 |
| Figure 4.11 A representative bio-layer interferometry experiment comparing the interaction between recombinant CPG2 or CPG2-p700 and VEGFR2 | 140 |
| Figure 4.12 The effect of increasing concentrations of prodrug ZD2676P on the viability of the mouse breast cancer cell line 4T1 in the presence or absence of CPG2 or CPG2-p700..... | 142 |
| Figure 5.1 Abdominal cavity of BALB/c mice showing location of mammary fat pad (white) and 4T1 cell injection site (indicated by black arrow)..... | 151 |
| Figure 5.2 Doxil and Doxil-p700 do not significantly affect the weight of tumour bearing mice | 159 |
| Figure 5.3 Doxil and Doxil-p700 significantly reduce tumour growth of orthotopically implanted 4T1 mammary tumours..... | 161 |
| Figure 5.4 Identification and scoring of necrotic areas post-treatment with Doxil and Doxil-p700 | 163 |
| Figure 5.5 Caspase 3 activation after Doxil and Doxil-p700 treatment..... | 165 |
| Figure 5.6A Effect of Doxil and Doxil-p700 on CD31 expression as a measure of vascularisation..... | 167 |
| Figure 5.6B Effect of Doxil and Doxil-p700 on CD31 expression as a measure of vascularisation..... | 168 |
| Figure 5.6C Effect of Doxil and Doxil-p700 on CD31 expression as a measure of vascularisation..... | 169 |
| Figure 5.6D Effect of Doxil and Doxil-p700 on CD31 expression as a measure of vascularisation..... | 170 |
| Figure 5.7 Effect of Doxil and Doxil-p700 on lung metastasis of 4T1 cancer cells..... | 172 |
| Figure 6.1 Preparation of T3T4 chimeras for insertion into the pcDNA6 vector | 186 |
| Figure 6.2 Diagnostic restriction digest of final TIMP constructs..... | 187 |
| Figure 6.3 Transfection of H5V cells with pmaxGFP using Lipofectamine 2000 | 189 |
| Figure 6.4 Transfection of H5V cells with pmaxGFP plasmid using TransIT-LT1 | 190 |
| Figure 6.5 Expression of TIMP proteins by stably transfected H5V cells..... | 191 |
| Figure 6.6 VEGFR2 phosphorylation in the H5V cell line..... | 193 |
| Figure 6.7 VEGFR2 phosphorylation in transfected H5V cell lines..... | 195 |

List of Tables

| | |
|--|-----|
| Table 1.1 Human TIMPs and their general properties..... | 37 |
| Table 2.1 Preparation of SDS-PAGE gels for western blot..... | 69 |
| Table 3.1 Lipid concentration of liposomes..... | 77 |
| Table 3.2 Structure of p700-FITC and control FITC..... | 77 |
| Table 5.1 Treatment group and dosage of Doxil or Doxil-p700 per body weight of mice..... | 152 |
| Table 6.1 PCR mastermix preparation used to add the V5-[His] ₆ tag | 182 |

List of Abbreviations

| | |
|-------------------|--|
| μM | Micromolar |
| 4T1 | Mouse breast cancer cell line |
| ADAM | a disintegrin and metalloproteinase |
| ADAMTS | ADAM proteases with thrombospondin motifs |
| ADEPT | Antibody directed enzyme pro-drug therapy |
| AMD | Age-related macular degeneration |
| ARPE19 | A human retinal pigment epithelial cell line |
| BLI | Bio-Layer Interferometry |
| Ca^{2+} | Calcium ion |
| CNV | Choroidal neovascularisation |
| COS-7 | Fibroblast-like cell lines from immortalised CV-1 cells |
| CPG2 | Carboxypeptidases G2 |
| DBCO | Dibenzocyclooctyl |
| TDDS | Targeted Drug delivery system |
| dH ₂ O | Deionised water |
| Dox | Doxorubicin |
| Doxil | Liposomal doxorubicin |
| ECM | Extracellular matrix |
| EDTA | Ethylene diamine tetra acetate |
| EFEMP1 | Epidermal growth factor–containing fibulin-like extracellular matrix protein 1 |
| EGF/R | Epidermal growth factor/receptor |
| EMT | Epithelial-mesenchymal transition |
| EPR | Enhanced permeability and retention effect |
| FBS | Foetal bovine serum |
| FGF/R | Fibroblast growth factor/receptor |
| H5V | Murine cardiac endothelial cells |
| HEK-293 | Human embryonic kidney cell line |
| HuDMEC | Primary human dermal microvascular endothelial cells |
| IGF | Insulin growth factor |
| IPTG | isopropyl thiogalactopyranoside |
| kDa | Kilo Dalton |
| MCF-7 | Human breast adenocarcinoma cell line |
| mM | Millimolar |

| | |
|-------------------|--|
| MMP | Matrix metalloproteinase |
| mRNA | Messenger RNA |
| MSC | Mesenchymal stem cells |
| MTX | Methotrexate |
| NiCl ₂ | Nickel chloride |
| NRP | Neuropillin |
| P700 | short peptide derived from TIMP3 carboxyl domain |
| PBS | Phosphate buffered saline |
| PDGF/R | Platelet derived growth factor/receptor |
| PEG | Polyethylene glycol |
| PFA | Paraformaldehyde |
| ROS | Reactive oxygen species |
| RT | Room temperature |
| SDS-PAGE | Sodium dodecyl sulphate polyacrylamide electrophoresis |
| SEM | Standard error of mean |
| SFD | Sorsby's fundus dystrophy |
| T3C | TIMP3 C terminus |
| TACE | TNF- α converting enzyme |
| TAM | Tumour associated macrophages |
| TDDS | Targeted drug delivery system |
| TGF | Transforming growth factor |
| TIMP | Tissue inhibitor of MMP |
| TNF | Tumour necrosis factor |
| TNFR1 | TNF α receptor 1 |
| V | Voltage |
| VEGF | Vascular endothelial growth factor |
| VEGFR | VEGF receptor |
| vWF | Von Willebrand factor |
| ZnSO ₄ | Zinc sulphate |

CHAPTER 1

General Introduction

1 Introduction

Our understanding of the complex mechanisms of cancer development has progressed greatly in recent years and can be summarised in what are described as “the hallmarks of cancer” (see section 1.1 below). This rapid progression in our understanding has led to the development of many highly specific drugs that seek to more effectively target the disease, whilst reducing the, often very severe, side-effects of conventional chemotherapy. Many of these drugs target aberrant receptor signalling by the tumour cells themselves, such as that mediated by the epidermal growth factor receptor (EGFR) or the human epidermal growth factor receptor 2 (HER2). Other, more recent, approaches have included targeting the tumour microenvironment, such as drugs that target tumour vasculature, cutting off the blood supply that is essential for tumour growth and metastasis. However, a disadvantage of these highly specific drugs is that cells in the tumour microenvironment can rapidly acquire resistance, and they are almost always used in combination with established, broad spectrum, chemotherapeutics with their inherent toxicity.

One approach that aims to circumvent the disadvantages of both highly specific tumour targeting and broad-spectrum chemotherapeutics, is to combine them in tumour-specific delivery of broad-spectrum cytotoxic drugs and this is the main subject of this thesis.

1.1. Hallmarks of cancer

Cancer develops through the accumulation of genetic changes that eventually result in the conversion of normal cells into hyperplastic ones. Several such changes are necessary to overcome host defence mechanisms that would normally result in apoptosis and clearance of aberrant cells. These changes impart specific characteristics on the cells that enable growth and spread (metastasis) of the tumour and were first referred to as the “hallmarks

of cancer by Hanahan and Weinberg in 2000 (Hanahan and Weinberg, 2000) and re-addressed in 2011 (Hanahan and Weinberg, 2011). A fundamental understanding of these pathways and processes has thus provided a way of deciphering how cancer cells are able to survive death during their transition into the malignant state and these will be discussed in the following sections.

1.1.1 The cancer hallmark and cancer cell survival

One major hallmark of cancer cells is their resistance to apoptosis. Apoptosis, or programmed cell death, is a major pathway employed to eliminate damaged or diseased cells from the body in a controlled manner. The apoptosis occurs via the intrinsic pathway that senses changes within the cell, most notably outer mitochondrial membrane permeabilization, and the extrinsic pathway that senses external signals that activate cell surface death receptors which are members of the tumour necrosis alpha receptor superfamily both eventually activating caspase dependent cell death (Figure 1.1) (Fernald and Kurokawa, 2013).

Cancer cells constantly encounter genotoxic or cytotoxic stress due to chemotherapy or during cancer development, which would normally activate death pathways. However, these cells modulate apoptotic pathways by regulation of key factors through upregulation or downregulation of their genes or keeping the protein in constantly activated or deactivated states (Figure 1.2). These events are not mutually exclusive and tumour cells often employ several of these mechanisms to ensure their continued proliferation.

Although all possible cellular stressors that could activate apoptosis are yet to be determined, many of the factors that sense abnormalities have been identified. Most important of these sensing factors is that of p53 protein, a transcriptional factor that is found mutated in most human cancers (Muller and Vousden, 2013). When there is substantial DNA damage, such as DNA strand breaks or chromosomal aberrance, p53 is

activated and it in turn activates transcription of PUMA and Noxa BH3-only proteins. Deficiency in this pathway in tumour cells usually involves loss of function of p53 protein resulting in suppression or total loss in PUMA and Noxa expression. The subsequent inability to activate apoptosis thus fuels cancer cell survival and proliferation.

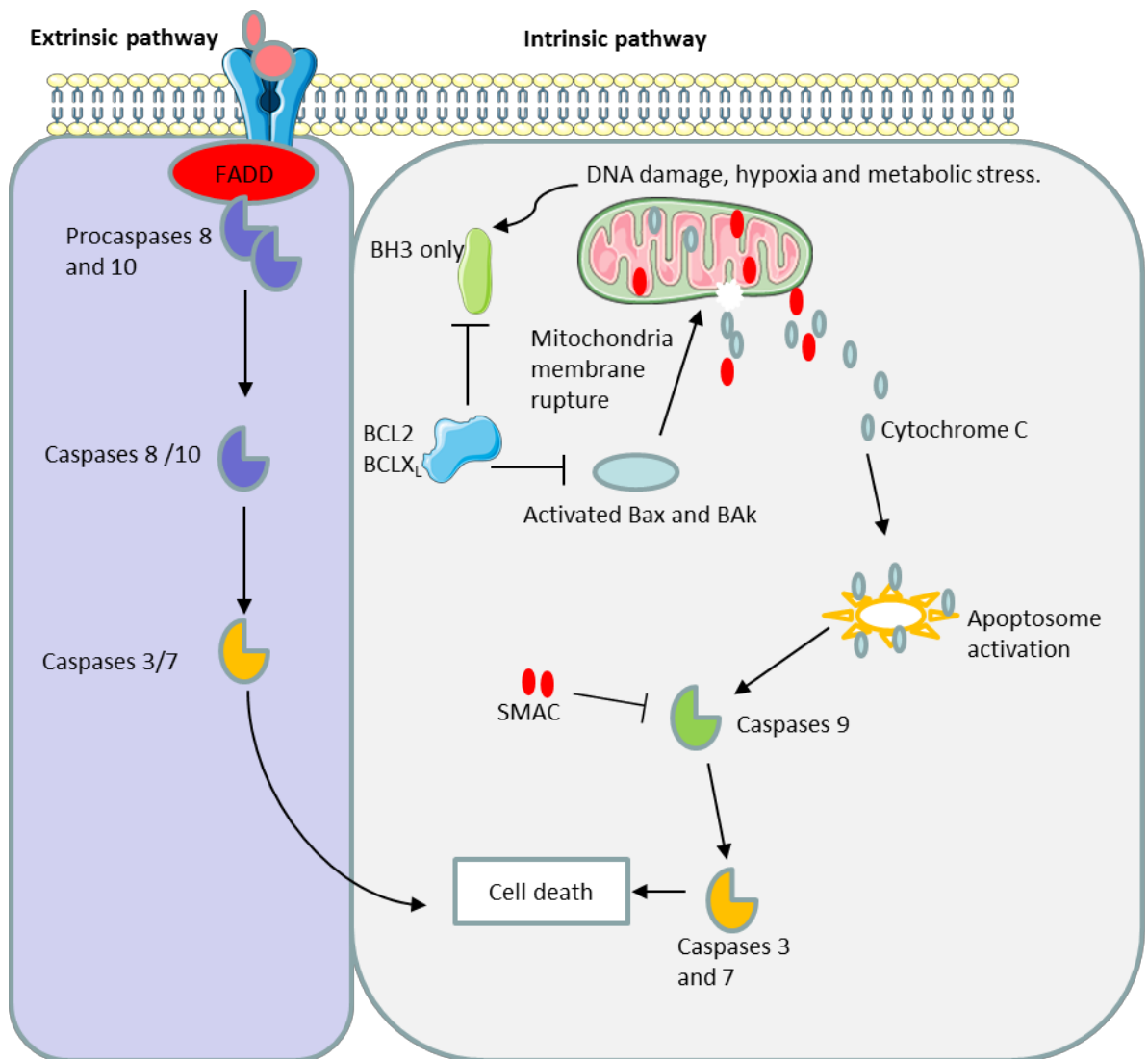


Figure 1.1. Extrinsic and intrinsic apoptotic pathways

The extrinsic pathway involves binding of extracellular ligands to death receptors which then activated initiator caspases 8 and 10 through FAS-associated death domain protein (FADD). The activated caspase 8 and 10 can proteolytically activate the executioner caspases 3 and 7 or the BCL2 protein Bid to truncated Bid (tBID) which cause apoptosis or mitochondrial membrane permeabilisation respectively. The intrinsic pathway starts with an internal stimulus which activates pro-apoptotic BCL2 family proteins, such as Bax and Bak, which cause the permeabilisation of the mitochondrial outer membrane. This causes the release of cytochrome C which interacts with Apaf1 to form the apoptosome which in turn activates caspase 9. Caspase-9 then activates the executioner caspases 3 and 7. Based on Ichim and Tait (2016), with permission.

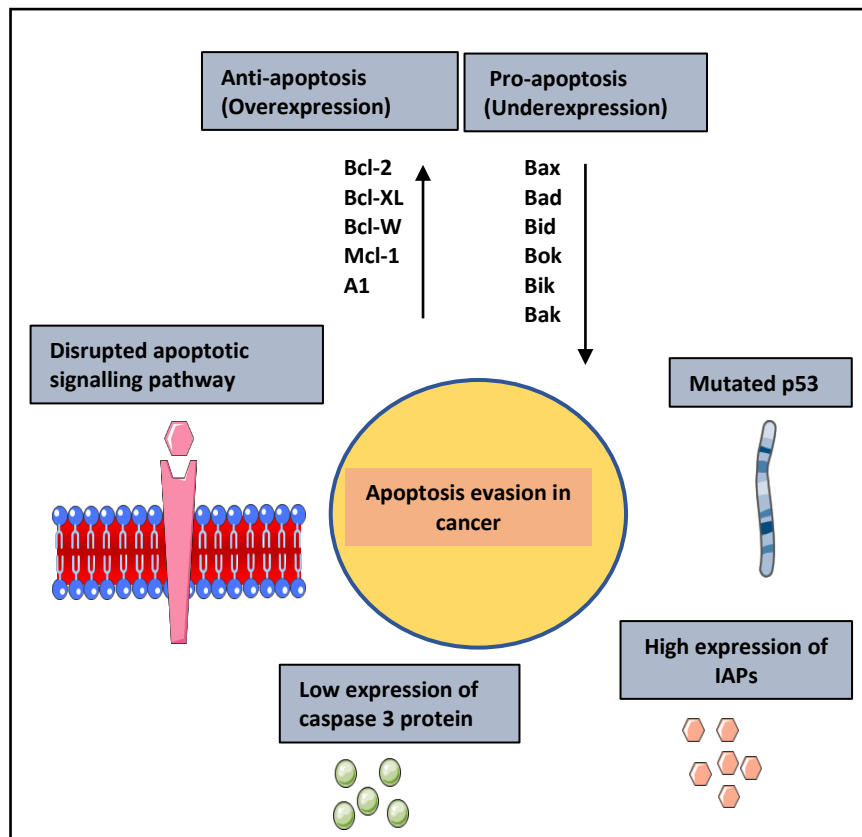


Figure 1.2. Mechanism of apoptosis evasion by cancer cells

Death receptors that signal apoptosis may become downregulated, p53 which is known as the guardian of the genome may become defective, caspases and IAP are usually downregulated while anti-apoptotic proteins such as BCL-2 are upregulated resulting in increased survival and resistance to cell death. Based on (Wong, 2011).

Uncontrolled proliferation of cancer cells is also fuelled by their ability to evade growth suppressing signals that play roles in, for example, induction of senescence, apoptosis or cell cycle arrest. Mutations in genes encoding tumour suppressors such as *TP53* (the gene that encodes p53), *RB* and *PTEN* have been identified in different studies investigating genetic alterations in animal or human cancers. In fact, about 50% of human cancers are known to contain mutations or deletions in *TP53* and individuals with just one allelic loss in *TP53*, causing haplo-insufficiency, are prone to development of Li-Fraumeni syndrome, resulting in increased susceptibility to certain cancers (Gutschner and Diederichs, 2012). In addition to this, loss of p53 function results in annulment of p53 dependent growth suppression including defective cell cycle arrest and activation of growth factor expressions (Yang et al., 2017), leading to yet another hallmark, which is uncontrolled proliferation. This usually involves constitutive activation of cell surface receptor tyrosine kinases by the growth factors, or through mutation that activates pathways allowing unregulated progression of cells through the cell cycle (Lemmon and Schlessinger, 2010, Witsch *et al.*, 2010).

To support the uncontrolled proliferation, cancer cells need to find a way of indefinitely replicating their DNA while progressing through the cell cycle irrespective of genomic errors or mutations they have accumulated. Normal cells control ageing through shortening of the telomere that eventually results in loss of DNA content and subsequent cell death. Like stem cells during embryogenesis, cancer cells upregulate telomerases that repairs the chromosome ends to allow for continued replication (Bernadotte et al., 2016, Stewart et al., 2012, Cairney and Keith, 2008). Due to the high expression and subsequent high activity of telomerase, cancer cells are able to resist senescence and apoptosis while initiating replicative immortality (Figure 1.3).

The uncontrolled growth of cancer cells results in aggressive phenotype which gives birth to another key cancer hallmark, the invasive and metastatic ability of tumour cells to secondary sites another key hallmark of progressive cancer (Hanahan and Weinberg, 2011). This is dependent on epigenetic and genetic heterogeneity within the tumour, coupled with external signals within the tumour microenvironment. In cancers arising from epithelial tissues, progression to higher grade malignancy is characterised by epithelial to mesenchymal transition (EMT) (Cavallaro and Christofori, 2004), where the immotile epithelial cells transform into motile mesenchymal stem cells. Tumour tissue as opposed to normal tissues are characterised with loose cell junctions causing weak cell to cell interaction causing them to easily migrate out of the tumour microenvironment to secondary site. E-cadherin is an important factor that maintains tight junctions gap and cell interactions but its inhibition by cancer cells prevents its interaction with other proteins needed to maintain the integrity of the cell junctions (Onder *et al.*, 2008, Sawada *et al.*, 2008, Zschiesche *et al.*, 1997).

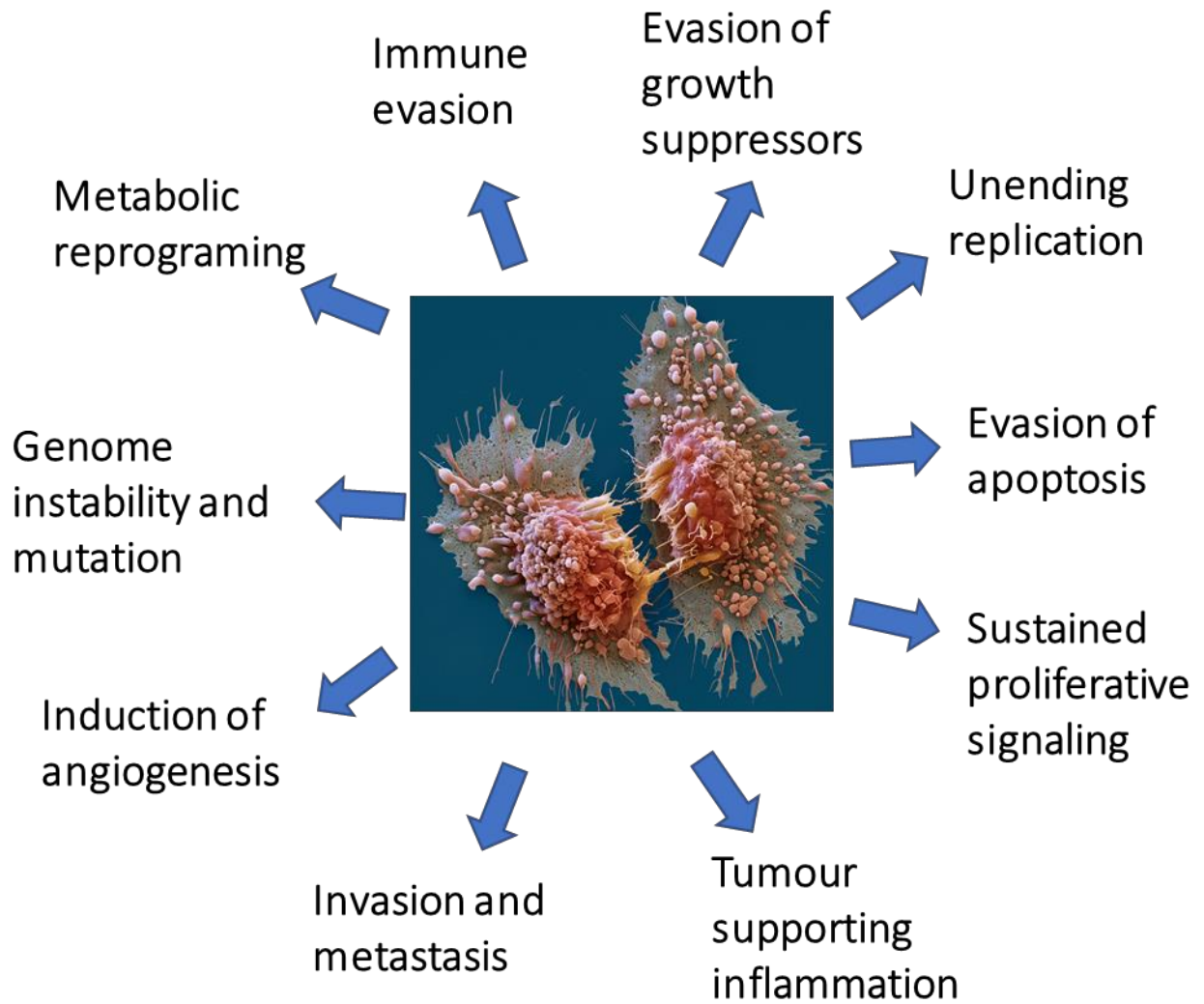


Figure 1.3. Enabling and emerging hallmarks of cancer cells

Aside their ability to discussed hallmarks, cancer cells have emerging hallmarks that enable their survival such as their ability to evade immune response or reprogram their metabolism during unfavourable conditions in the tumour microenvironment that attracts immune cells exhibit high pH and reduced nutrient/oxygen. In addition, tumour cells constantly accumulate somatic mutation to activate pathways that are otherwise dormant in tumour cells (Hanahan and Weinberg, 2011).

1.1.2 Induction of angiogenesis and lymphangiogenesis as a cancer hallmark

Oxygen and nutrients are essential for cell growth and survival, and these are supplied through the vasculature. As cells grow and multiply into tissues and organs, as found in multicellular organisms during embryogenesis, there is a need for increased growth of blood vessels to keep up with the demand through assembly of newly birthed endothelial cells (vasculogenesis) and sprouting/branching of existing vessels (angiogenesis). These processes are regulated by pro- and anti-angiogenic factors in a tightly control manner. The tipping of these factors in favour of angiogenesis is termed the “angiogenic switch”. The vasculature is generally quiescent after morphogenesis but the angiogenic switch becomes temporarily activated in adulthood during the female reproductive cycle or in wound healing. Dysregulation in this processes is often encountered in different diseases, especially in cancer (Carmeliet, 2003).

Like normal cells, tumour cells require nutrients and oxygen and thus require vascularisation. However, cancer cells permanently turn the angiogenic switch on for continuous growth of the vasculature to supply nutrients to newly formed cancer cells (Hanahan and Weinberg, 2011). This switch is triggered by various factors, including metabolic stress due to nutrient and oxygen deprivation, immune responses affecting production of inflammatory molecules, mechanical stress and mutations in key genes such as those inactivating tumour suppressors or activating oncogenes (Liao and Johnson, 2007). However, the manner in which genetic and environmental factors interact in influencing angiogenesis is not completely understood. Notwithstanding, research has shown that both pro- and anti-angiogenic factors are largely produced by blood cells, cancer cells, endothelial cells and the extracellular matrix (ECM) dependent on the requirement in the tumour microenvironment during cancer progression (Carmeliet and Jain, 2000). Most of these molecules are proteins that bind cell surface receptors on

vascular endothelial cells such as thrombospondin (TSP) and vascular endothelial growth factors (VEGF) which act as inhibitor and inducer of angiogenesis respectively. The role of VEGFs are known to be by stimulating and maintaining the growth of blood vessels, however, this growth is kept in check by TSP known to maintain vascular quiescence through prevention of endothelial cell migration and survival (Olfert, 2016). In the tumour tissue however, cancer cells are known to overexpress VEGFs while the TSPs expressions are inhibited resulting in unregulated growth of blood vessels supplying the tumour tissue with nutrients and oxygen and even channel for cancer cells to metastasise to secondary site (Kazerounian et al., 2008).

Aside contributing to the metabolic activities of cells within the tumour microenvironment, angiogenesis is a key factor determining the aggressiveness and metastatic potential of the tumour cells and lymphangiogenesis plays a crucial role in this aspect. Like angiogenesis, lymphangiogenesis does not occur in normal cells except during embryogenesis or inflammation when blood supply is needed, and it involves sprouting of blood vessels from existing lymphatic vessels. Tumour cells induce lymphangiogenesis by overexpressing lymphangiogenic growth factors such as VEGF-C, VEGF-D and VEGFR3, and the expression of these factors is known to correlate with lymph node metastasis and lymphatic vessel density (Maekawa et al., 2007, Thiele and Sleeman, 2006). As a result, both angiogenesis and lymphangiogenesis contribute immensely to the aggressiveness of a particular tumour and for this reason, angiogenic and lymphangiogenic factors have been targeted as therapeutic targets in different cancers.

1.2 The tumour microenvironment contributes to the hallmarks of cancer

The tumour microenvironment is made up of many different components in addition to the tumour cells themselves and these all contribute to malignant transformation.

Although different tumour types at different stages of malignancy will contain several cell types, the components of the tumour microenvironment are broadly categorised into cells with haematopoietic and mesenchymal origin, and non-cellular components (Pattabiraman and Weinberg, 2014).

Cells of haematopoietic origin develop from the bone marrow and these comprise the immune cells which are also classified into the lymphoid and myeloid cells. Lymphoid cells consist of T cells, B cells and natural killer cells while the myeloid cells include tumour-associated macrophages (TAMs). Although these immune cells have the potential to destroy tumours, the tumour microenvironment can bring about phenotypic changes that result in a pro-tumourigenic phenotype, such that targeting the immune system is now a major focus in the development of novel therapeutics (de Visser *et al.*, 2006, Restifo *et al.*, 2012, Pollard, 2004).

Cells of mesenchymal origin comprise of mesenchymal stem cells (MSC), myofibroblasts, fibroblasts and endothelial cells, which play a key role in vasculogenesis. The role of MSCs in promoting tumour growth is still controversial but it has been demonstrated that MSC and myofibroblasts both promote tumour progression by creating a supportive microenvironment that meets the need of neoplastic cells to become malignant (Quante *et al.*, 2011). Endothelial cells are abundantly present in the tumour microenvironment and within the solid tumour. This is because of the major role they play in formation of blood vessels to supply the nutrients and oxygen required by the growing tumour. Neovascularisation of the tumour is driven by a host of factors, such as VEGF-A, produced by both the tumour cells themselves and other cells, such as TAMs, within the tumour, driven primarily by the hypoxic microenvironment. However the blood vessels that form within the tumour are abnormal, being irregular and leaky and

there is evidence that these abnormalities actually contribute to tumour growth (Dudley, 2012).

The ECM is the major non-cellular component of the tumour microenvironment, as it is within normal tissues and organs, and is comprised of many structural biomolecules that include fibrous proteins, such as collagens and elastin, proteoglycans, such as syndecans and aggrecan, and it is also a reservoir for a host of bioactive molecules that include various growth factors. The ECM provides the main structural scaffolding for cells in addition to initiating the mechanical and biochemical cues required for the maintenance of cellular morphogenesis, differentiation and tissue homeostasis (Frantz *et al.*, 2010). The ECM is subdivided into the basement membrane, which is made up of type IV collagen, fibronectin and laminin and the interstitial stroma, which is made up of fibrillar collagens, glycoproteins and proteoglycans. All of these molecules provide the support that gives the tissue its tensile strength (Lu *et al.*, 2012). The ECM contributes to tumour growth in several ways. Alterations in ECM composition and hypoxia trigger signalling cascades that increase the expression of soluble and cell surface proteinases, such as matrix metalloproteinases (MMPs), that not only create space for tumours to expand, become vascularised and metastasise, but also result in the activation or release of several growth factors and pro-angiogenic molecules. For example, the pro-angiogenic growth factors, basic fibroblast growth factor (bFGF) and VEGF are sequestered in the ECM by binding to glycosaminoglycans and released upon proteolytic cleavage of these molecules. Moreover, MMPs play a role in the cleavage and activation of E-cadherin and the release of transforming growth factor β (TGF- β) from its inactivating protein, both of which play critical roles in EMT (Kessenbrock *et al.*, 2010).

1.3 Tumour angiogenesis

The transformation of cells into a neoplastic state is a gradual process that requires sustenance of proliferative signalling and resistance to apoptosis using all manner of processes. As discussed in 1.1.6 above, angiogenesis is a key hallmark of cancer that enables growth and metastasis of the tumour mass

1.3.1 VEGF is the major angiogenic growth factor

As tumours grow, tumour cells respond to the needs of new neoplastic cells by secreting and releasing growth factors that mediate angiogenesis and regulate infiltration of inflammatory molecules into the tumour microenvironment. These growth factors engage in multiple ligand-receptor signalling cascades in a similar manner to that found during foetal development and wound healing. These ligand-receptor mediated signalling pathways mainly involve VEGF and its receptors, reviewed in Otrrock *et al.* (2007). In mammals the VEGF family comprise five members, VEGF-A, -B, -C, -D and placental growth factor (PlGF), although VEGF-A is primarily referred to simply as VEGF. The interaction between these family members and their cognate tyrosine kinase receptors, VEGFR-1, -2 and -3 and co-receptors, the neuropilins (NP-1 and NP-2) is essential for the development and/or maintenance of the vasculature (reviewed in Simons *et al.* (2016)). The binding specificity of these ligands/receptors is illustrated in Figure 1.4, although this is probably a simplification as all three VEGF receptors are able to form heterodimers (Huang *et al.*, 2001, Nilsson *et al.*, 2010).

The interaction between VEGF-A and VEGFR-2 is the main driver of angiogenesis in both development and adulthood. In contrast, VEGFR-1 is a negative regulator of angiogenesis on endothelial cells, acting as a decoy receptor for VEGFR-2, but also appears to play a role in monocyte recruitment, acting as a chemoattractant receptor on these cells (Barleon *et al.*, 1996, Tchaikovski *et al.*, 2008) and as such may play a role in

tumour angiogenesis by recruiting TAMs. VEGFR-3 is expressed by blood and lymphatic endothelial cells during development but expression is largely restricted to lymphatic cells in adulthood. However, expression of VEGFR-3 is highly upregulated in angiogenic sprouts (Tammela *et al.*, 2008) and may play a role in angiogenesis in cancer (Valtola *et al.*, 1999).

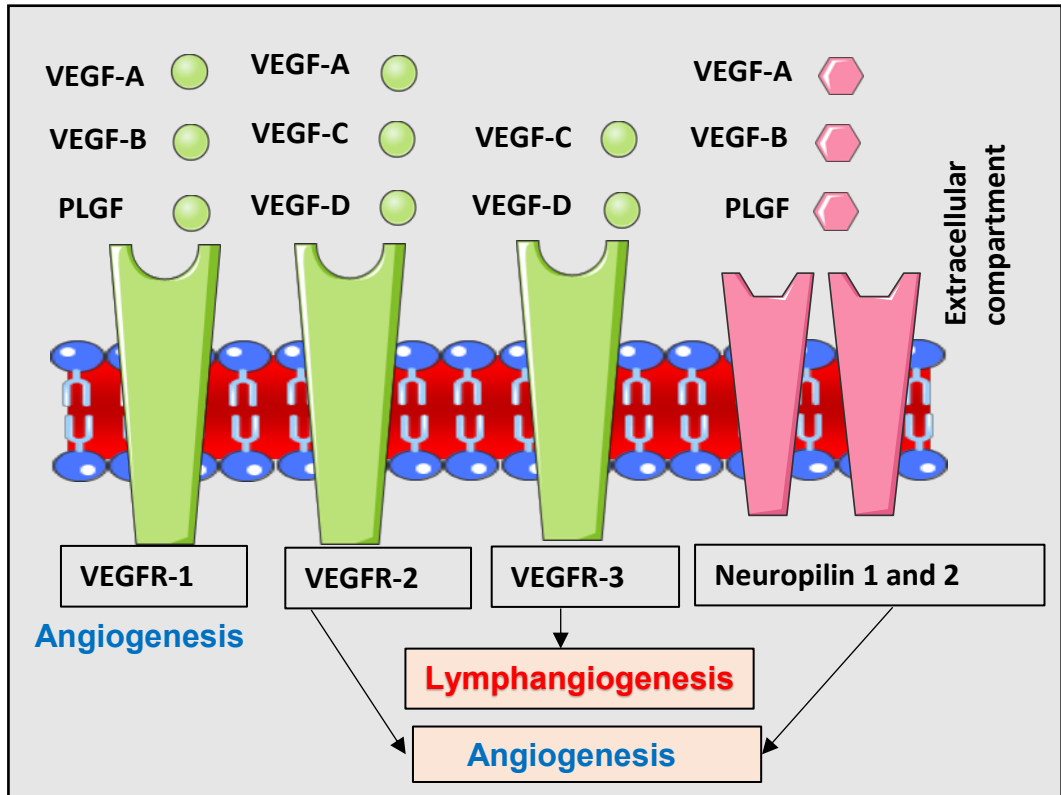


Figure 1.4. VEGF isoforms and their receptors that mediate angiogenesis

Different VEGF family members bind different receptors. VEGFA and VEGFB can bind VEGFR-1 and Neuropilin 1 and 2 to activate angiogenesis in a similar way to VEGFA, VEGFC and VEGFD binding to VEGFR-2. However, VEGFC and VEGFD can bind VEGFR-3 to activate Lymphangiogenesis.

1.3.1.1 VEGF: The canonical angiogenic factor exists in soluble and matrix bound forms

Like all family members, VEGF (VEGF-A) is a homodimer and receptor binding brings about dimerisation of VEGFR2, resulting in phosphorylation of the receptor and activation of downstream signalling cascades that mediate cell survival, proliferation, migration, vessel formation and increased vascular permeability (Figure 1.5). VEGF is expressed and secreted in different isoforms due to alternative splicing during transcription of its gene. All VEGF isoforms can interact with VEGF receptors -1 and -2 using the receptor binding domain encoded by VEGF exons 2 to 5 (Ferrara, 2010), however interaction with heparan sulphate proteoglycans (HSPG) in the ECM is determined by exons 6-8, such that the shortest isoform, VEGF121 in humans, is completely soluble and VEGF206 entirely localised to the ECM with those in between showing varying degrees of affinity for the ECM. Additionally, these latter domains determine interaction with co-receptors, such as neuropilins, which may in turn explain differences in downstream signalling initiated by the different isoforms (Whitaker *et al.*, 2001).

Mice expressing only soluble VEGF isoform 120 (VEGF120) have been shown to exhibit less sprouting during embryogenesis with a high mortality rate during the early stage of life (Ruhrberg *et al.*, 2002). In another study, MMP-cleaved soluble VEGF113-induced blood vessels showed less sprouting but larger vessel formation in a tumour xenograft compared to the matrix bound VEGF164 and VEGF108-118 induced vessels which were thinner and had more branches (Lee *et al.*, 2005b). These data suggest the soluble form of VEGF is responsible for expansion of blood vessels within the tumour while the matrix bound forms help in sprouting to access inner tumour cells, making both forms possible therapeutic targets.

As mentioned, interaction of VEGFR2 with either the soluble or matrix bound VEGF forms produces different outcomes due to the differing downstream signalling cascades activated. VEGFR2 binding with matrix bound VEGF causes phosphorylation of tyrosine 1214 which is a residue that has been shown to activate stress-activated protein kinase (SAPK)2/p38 to induce endothelial cell migration (Lamallice *et al.*, 2004). This may explain why sprouting is induced by this form of VEGF. Although both soluble and matrix bound VEGFs can activate p38MAPK and Akt, only matrix bound VEGF can maintain prolonged activation of p38MAPK while soluble VEGF causes prolonged activation of Akt. Interestingly, collagen matrix-bound VEGF clusters VEGFR2 and maintains prolonged phosphorylation at specific tyrosine residues, allowing VEGFR2 to interact with β 1-integrins to mediate activation of divergent downstream signalling cascades (Chen *et al.*, 2010). This interaction, however, disfavours interaction of VEGFR2 with NRP1, another important binding partner for VEGFR2.

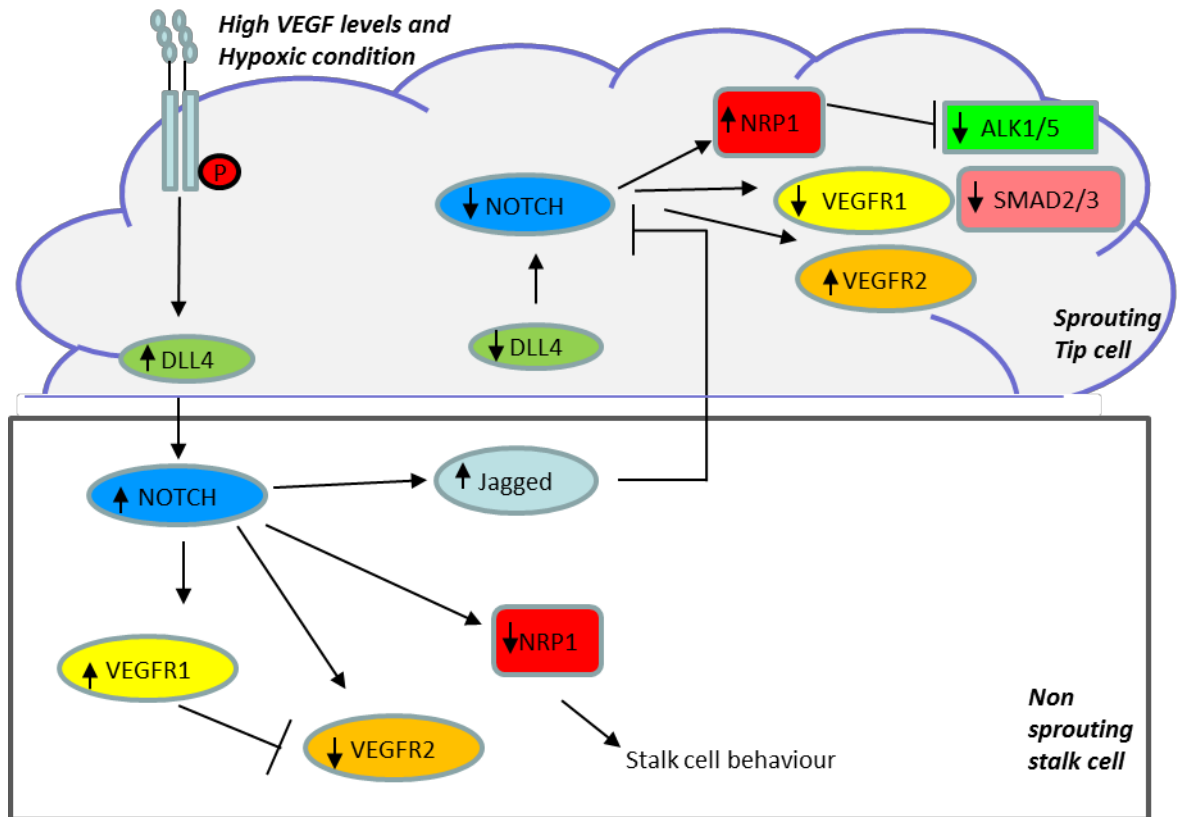


Figure 1.5. Hypoxia activation of NOTCH and VEGFR-2 signalling during vascularisation

Hypoxia induces VEGF binding to VEGFR-2 to trigger blood vessel formation through NOTCH signalling pathway which involves DLL-4, NOTCH, and JAGGED. Based on Simons *et al.* (2016), with permission.

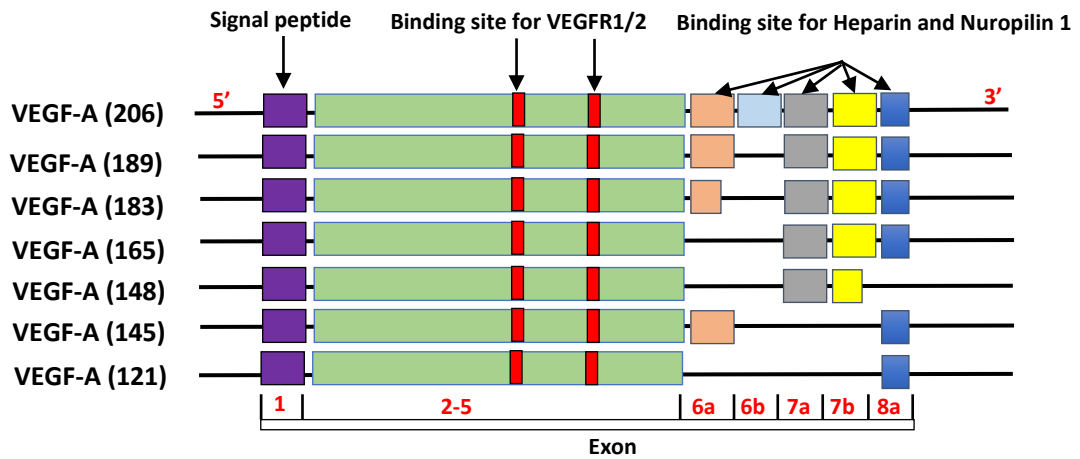


Figure 1.6. Protein isoforms of VEGF-A

Schematic representation of seven VEGF-A family members, with the important domains- signal peptide, binding sites for VEGFR1/2 and binding site for Heparin and Neuropilin-1. Based on (Grunewald *et al.*, 2010, Penn *et al.*, 2008).

1.3.1.2 VEGF signalling with neuropilin is crucial to endothelial cell migration and angiogenesis

Neuropilin has two major forms NRP1 and NRP2 both of which are transmembrane glycoproteins expressed in variety of cell types including cancer and endothelial cells (Jubb *et al.*, 2012). NRP-1 interacts with VEGF through the VEGF C-terminal domain and its involvement in vascular development is exemplified by the fact that NRP1 null mice exhibit neuronal and cardiovascular defects that eventually lead to death (Kitsukawa *et al.*, 1997). NRP1 interacts with VEGF through its b1b2 extracellular domain, serving as a secondary receptor. Binding of NRP1 with VEGF enhances the interaction between VEGF and VEGFR2 and two major amino acid residues, Y297 and D320 of human NRP1 have been demonstrated to be responsible for this interaction (Herzog *et al.*, 2011). Inhibition of NRP1 activities through point mutation in these residues resulted in reduced NRP1 binding with VEGF and anti-VEGF effects such as reduced VEGF-induced angiogenesis and endothelial cell migration. These data show the importance of NRP1 to VEGF signalling via VEGFR2. However, inhibition of NRP1 interaction with VEGF does not influence VEGFR2 downstream signalling. NRP2 is primarily expressed on lymphatic endothelial cells and is thought to play a similar role in VEGF-C and -D mediated activation of VEGFR3 in lymphangiogenesis (Wang *et al.*, 2016).

1.3.2 Other proangiogenic factors highly expressed in cancer

Aside from VEGF, several other growth factors and their receptors are known to play a role in the angiogenic process. Some of these proangiogenic factors, such as platelet-derived growth factor (PDGF) and fibroblast growth factor (FGF) are often highly expressed in cancer to support proliferation, survival and metastasis and often indicate reduced patient survival.

1.3.3 The PDGF/PDGFR system

PDGF is a dimeric growth factor that is comprised of two subunits which can be made up of two A, two B or both A and B subunits. PDGF binds PDGF receptors (PDGFR) which comprise two closely related proteins, PDGFR α and PDGFR β , coded by the PDGFRA and PDGFRB genes, respectively. Both are tyrosine kinases that binds PDGF dimers to initiate signalling resulting in cell growth, survival and migration (Heldin, 2013). Both PDGFR α and PDGFR β are structurally similar with both having five immunoglobulin-like extracellular domains and intracellular kinase domains. However, both receptors bind to PDGF ligands with different affinities, resulting in different signalling and cellular functions such that different PDGF polypeptide combinations determine what receptor dimers they bind. For instance, PDGF-AA will bind PDGFR α receptor dimer while PDGF-AB will bind dimerised PDGFR α and PDGFR- β (Andrae *et al.*, 2008).

To drive tumourigenesis, PDGF or its receptors are often mutated or highly expressed both resulting in hyperactivity of the receptors. Point mutations, resulting in kinase hyperactivity, are found in critical residues of PDGFR α and this is known to occur in 5% of gastrointestinal stromal tumours (GIST) and in about 5 to 10% of glioblastoma multiforme, the gene is overexpressed (Puputti *et al.*, 2006, Heinrich *et al.*, 2003). PDGFR in epithelial tumours plays a crucial role in tumourigenesis by facilitating EMT and thus, their invasiveness and metastasis. Overexpression of PDGFR occurs in these cells such that tumour cells that were not responsive to PDGF initially becomes responsive. In EMT, PDGF often has an autocrine effect on the tumour cells to stimulate PDGFR expression in cells not expressing the receptor initially (Jechlinger *et al.*, 2006). PDGFR has been implicated in several other cancers and has been explored as a therapeutic target. A preclinical model of prostate cancer showed that anti-PDGFR antibody treatment of mice inoculated with prostate cancer cells resulted in inhibition of

skeletal metastasis and knockdown of PDGFR α and PDGFR β in prostate cancer cells inoculated into another mouse model resulted in suppression of angiogenesis (Russell *et al.*, 2009, Park *et al.*, 2011). PDGF-A and PDGFR α mRNA levels are often found to be very high in patients with cholangiocarcinoma and treatment of cholangiocarcinoma cell lines with PDGFR kinase inhibitors, sunitinib or imatinib, reduces cell migration and cancer cell viability (Boonjaraspinyo *et al.*, 2012).

1.3.4 FGF and FGFR

Fibroblast growth factors comprise a large family of glycoproteins, of which FGF1-10 signal through cell surface tyrosine kinase receptors (FGFR1-4). FGF 1 and 2 are also known as acidic and basic FGF, respectively. FGFs bind to heparan sulphate proteoglycans (HPSG) in the ECM. The release of FGF from the ECM is mediated by heparinases or proteases and the released FGF binds to cell surface heparan sulphate proteoglycans (HPSG), which stabilises the interaction between FGF and FGFR (Turner and Grose, 2010). FGFR signalling is crucial to many cellular and developmental processes such as embryonic patterning of the mesoderm and development of different organ systems (De Moerlooze *et al.*, 2000). FGFR signalling is also known to be involved in disease pathogenesis, most importantly in cancer. Mutations in *FGFR1* and *FGFR2* has been found in breast and lung cancers (Matsuda *et al.*, 2011) *FGFR2* is known to be highly expressed in colorectal cancer, contributing to tumour growth angiogenesis and tissue invasion (Antoniou *et al.*, 2008, Davies *et al.*, 2005, Matsuda *et al.*, 2011). In rectal cancer, high *FGFR2* expression has been shown to also correlate with advanced tumour stage, poor response to chemotherapy and poor survival (Li *et al.*, 2014).

A role for the FGF/FGFR signalling pathway in tumour angiogenesis has been demonstrated in many different studies. Investigation of the FGF1 expression profile in ovarian tumour samples showed that FGF1 level correlates with microvessel density

(Birrer *et al.*, 2007). This suggests that FGF1 expression is linked to vessel formation and that FGF1 may have some form of paracrine effect in stimulating angiogenesis. FGF2 is known to support angiogenesis in different cancers including prostate cancer, astrocytoma and hepatocellular carcinoma. (Giri *et al.*, 1999). Increased FGF2, FGFR2, FGFR3 and FGFR4 expression has been found in oral squamous cell carcinoma and colon cancer and their expression is likely involved in dysplastic transition of normal cells to carcinoma (Nayak *et al.*, 2015, Turkington *et al.*, 2014). As a result of the aberrations in the FGF/FGFR signalling pathways in different malignancies, this ligand-receptor signalling pathway is being investigated for its therapeutic potential (Babina and Turner, 2017).

1.3.5 Targeting angiogenesis in cancer

As discussed above, numerous proangiogenic factors amongst other cellular and non-cellular components are responsible for regulating tumour angiogenesis. However, evidence that VEGF and its cognate receptor, VEGFR2 are the major factors stimulating angiogenesis in the tumour microenvironment led to the conclusion that targeting these two proteins would prove to be an important therapeutic strategy for many cancers in sustaining prolonged antiangiogenic and subsequently antitumour response (Carmeliet and Jain, 2011). This led to the development of several anti-VEGF or anti-VEGFR2 drugs and these proved to be highly effective in animal models. While some of these drugs, such as the anti-VEGF antibody, bevacizumab, have been approved after improving patient survival and prognosis compared to radiotherapy and chemotherapeutic agents alone across several indications (Iacovelli *et al.*, 2015, Tewari *et al.*, 2014, Poulsen *et al.*, 2014), they have not proved to be as effective as had been hoped. This may, at least in part, be due to development of resistance in the form of activation of other signalling

pathways involving FGFR and PDGFR and their ligands in stimulating angiogenesis and tumour growth.

1.4 The Metzincins

Extracellular proteinases are essential for the turnover of the ECM, dissolution of cell-cell interactions and the release or activation of a multitude of growth factors and pro-angiogenic molecules and as such play a central role in tumour growth, angiogenesis and metastasis. Of these the metzincin family are undoubtedly the most important class. Their name is derived from the presence of a conserved methionine residue at their active site and utilisation of a zinc ion for catalysis (Rivera *et al.*, 2010b). The metzincin family comprises of a disintegrin and metalloproteinase (ADAM), ADAM proteases with thrombospondin motifs (ADAMTS), matrix metalloproteinases (MMP), pappalysin and astacin sub-families, although the first three are by far the most abundant of these in the ECM.

1.4.1 A disintegrin and metalloproteinases (ADAMs)

ADAM proteins were first discovered for their role in sperm egg fusion (Blobel *et al.*, 1992). ADAMs are zinc bearing membrane anchored proteins containing a disintegrin and a metalloproteinase domain. Some ADAMs are responsible for “juxtamembrane cleavage” i.e. shedding of other membrane associated-proteins including cytokines, cell adhesion molecules, growth factors and growth factor receptors and are thus referred to as sheddases (Gough *et al.*, 2004, Hurskainen *et al.*, 1999). This shedding activity is required for the activation of the pro-forms of several cytokines and growth factors. This is exemplified by ADAM17 in the shedding of tumour necrosis factor α (TNF α).

Twenty-seven human and thirty-seven mouse ADAM genes have been identified. However, only 13 human ADAM proteins are currently known to possess proteolytic activity while the others have been suggested to be involved in other biological functions,

largely cell adhesion (Rivera et al., 2010a, Bahudhanapati et al., 2015). ADAM proteins are similar to MMPs (see later) except the haemopexin domain of MMPs is replaced by a disintegrin domain which is responsible for their interactions with integrins (Bridges and Bowditch, 2005). Besides ADAM15, all ADAM proteins lack the RGD integrin binding motif but rather possess the (D/E)ECD motif, which exhibits a dual function of integrin binding specificity and cell adhesion augmentation (Gupta *et al.*, 2000). ADAM protein members play important roles in ECM metabolism and turnover, and these activities have significant biological impacts such as in wound healing, tissue development and development of diseases such as asthma, Alzheimer disease, and cancer (Tanaka *et al.*, 2005, Lee *et al.*, 2006a, Postina *et al.*, 2004).

1.4.2 A disintegrin and metalloproteinase protease with thrombospondin motif (ADAMTS)

ADAMTS proteins are structurally similar to ADAM proteins with the only difference being that ADAMTS are secreted (in active form) proteinases and the transmembrane domain of ADAM proteins is replaced by thrombospondin-like repeats (Porter *et al.*, 2005). Nineteen ADAMTS proteins have been identified in man (Wagstaff *et al.*, 2011) with ADAMTS1, ADAMTS4, ADAMTS5, ADAMTS9 and ADAMTS13 currently known to have important biological functions that have already been reported in the literature. ADAMTS13 for instance mediates the cleavage of von Willebrand factor (vWF). Impairment of this process results in thrombotic thrombocytopenia purpura (Zhou *et al.*, 2010b). Some ADAMTS proteins, such as ADAMTS4 and ADAMTS5, are known as aggrecanases or more generally termed as hyalactanases because of their activities in cleaving hyaluronan-lectican proteoglycan components of the ECM and have been associated with arthritis (Gao *et al.*, 2002, Sandy *et al.*, 2001, Jones and Riley, 2005). Some ADAMTS also have important function in the nervous system, such as the involvement of ADAMTS4 and ADAMTS5 in synaptic plasticity and glioma invasion

through the cleavage of brevican (Matthews *et al.*, 2000, Yuan *et al.*, 2002). There is also evidence of ADAMTS proteins in the development of neurodegenerative disorders such as increased expression of ADAMTS1 in Alzheimer's disease and Down syndrome, and ADAMTS1, ADAMTS4 and ADAMTS9 in cerebral ischemia (Miguel *et al.*, 2005, Tian *et al.*, 2007, Reid *et al.*, 2009).

In addition to the above, ADAMTS functions affect cell adhesion, proliferation, migration and even angiogenesis, thus their activities were proposed to influence cancer development (Cal and Lopez-Otin, 2015). Indeed, expression of some ADAMTS proteins have been found altered in different cancers resulting in either a protective effect against tumour development or tumour promoting effects. For instance, ADAMTS1 is believed to have a tumour inhibitory role due to its restriction of endothelial cell proliferation. This is brought about by the ADAMTS1 proteolysis of TSP-1 and -2 into fragments that can inhibit vascularisation of liver metastasis (Lee *et al.*, 2010). On the contrary, ADAMTS1 has also been found to be overexpressed in pancreatic cancer and its overexpression is also associated with high risk of breast cancer metastasis to the bone (Minn *et al.*, 2005, Masui *et al.*, 2001).

1.4.3 Matrix metalloproteinases (MMPs)

MMPs consist of a large family of secreted or membrane associated zinc-dependent enzymes that function in an array of physiological processes such as catalysing the turnover of ECM, cell migration, and wound healing/tissue repair (Garcia-Irigoyen *et al.*, 2013). Twenty-four human and twenty-three murine MMP genes have been identified and include secreted and membrane associated members. MMPs were initially categorised according to the substrates they were found to cleave or by cellular localisation, leading to five main types: collagenases (MMP1, MMP8 and MMP13); gelatinases (MMP2 and MMP9); stromelysins (MMP3, MMP10 and MMP11),

matrilysins (MMP7 and MMP26), and the membrane type MMPs (MT-MMPs e.g. MMPs 14-17). As these proteins were sequenced, the enzymes have been further categorised according to key structural motifs (see Figure 1.7).

1.4.3.1 Structure of MMP

With the exception of MMP7, MMP23, and MMP26 that lacks the linker and hemopexin domain, MMPs are structurally made up of four parts. These are the 170-amino acid catalytic metalloproteinase domain, a variable length peptide linker, a 200-amino acid hemopexin domain and an 80-amino acid pro-peptide region. The common structural signature of MMPs are the zinc binding motif characterised by the HEXXHXXGXXH amino acids present in the catalytic domain as well as the hepta-peptide cysteine switch motif-PRCGXPD, present in the propeptide region. Both the cysteine switch and the zinc motifs are important for MMP catalysis as the 3 His amino acids in the zinc binding motif and the Cys in the cysteine coordinate with the catalytic Zn^{2+} . The formation of a Cys- Zn^{2+} prevents water molecule that is necessary for catalysis from entering into the catalytic cleft to bind the Zn^{2+} thus keeping the MMP in an inactive state (Nagase et al., 2006).

1.4.3.2 Proteolytic activation of MMPs

MMPs are initially synthesised as pre-proenzymes that contains a signal peptide upstream of the propeptide region in addition to the above mentioned domains. This peptide is removed during translation of the mRNA into a zymogen, pro-MMP. The pro-MMPs are secreted by the cells and are then proteolytically converted to the matured MMP in an important regulatory step preceding MMP activity. Usually, the pro-MMP is present as a protein complex in the inactive form. For example, pro-MMP2 in its inactive form is tightly bound to TIMP-2 via the C-terminal of the endogenous inhibitor, using its hemopexin domain (Ellerbroek et al., 2001). This complex is essential for the activation

of pro-MMP2 by MT1-MMP because MT1-MMP is able to bind the complex via the N terminal of TIMP2 for access to pro-MMP2. Pro-MMP9 on the other hand is activated in a different fashion as it has been described that downregulation of TIMP-1 is required for activation of pro-MMP9 by TNF- α (Han et al., 2002). This is because TIMP-1 association with pro-MMP9 prevents access of TNF- α to pro-MMP9. This variation is likely due to difference in the requirements for the different MMPs in maintenance of cellular homeostasis. For instance, while MMP2 is a collagenase that is required for the degradation of the ECM with role in cancer cell migration, MMP9 plays crucial role in ECM degradation, neovascularisation, wound healing and immune response (Yabluchanskiy et al., 2013, Koo et al., 2012).

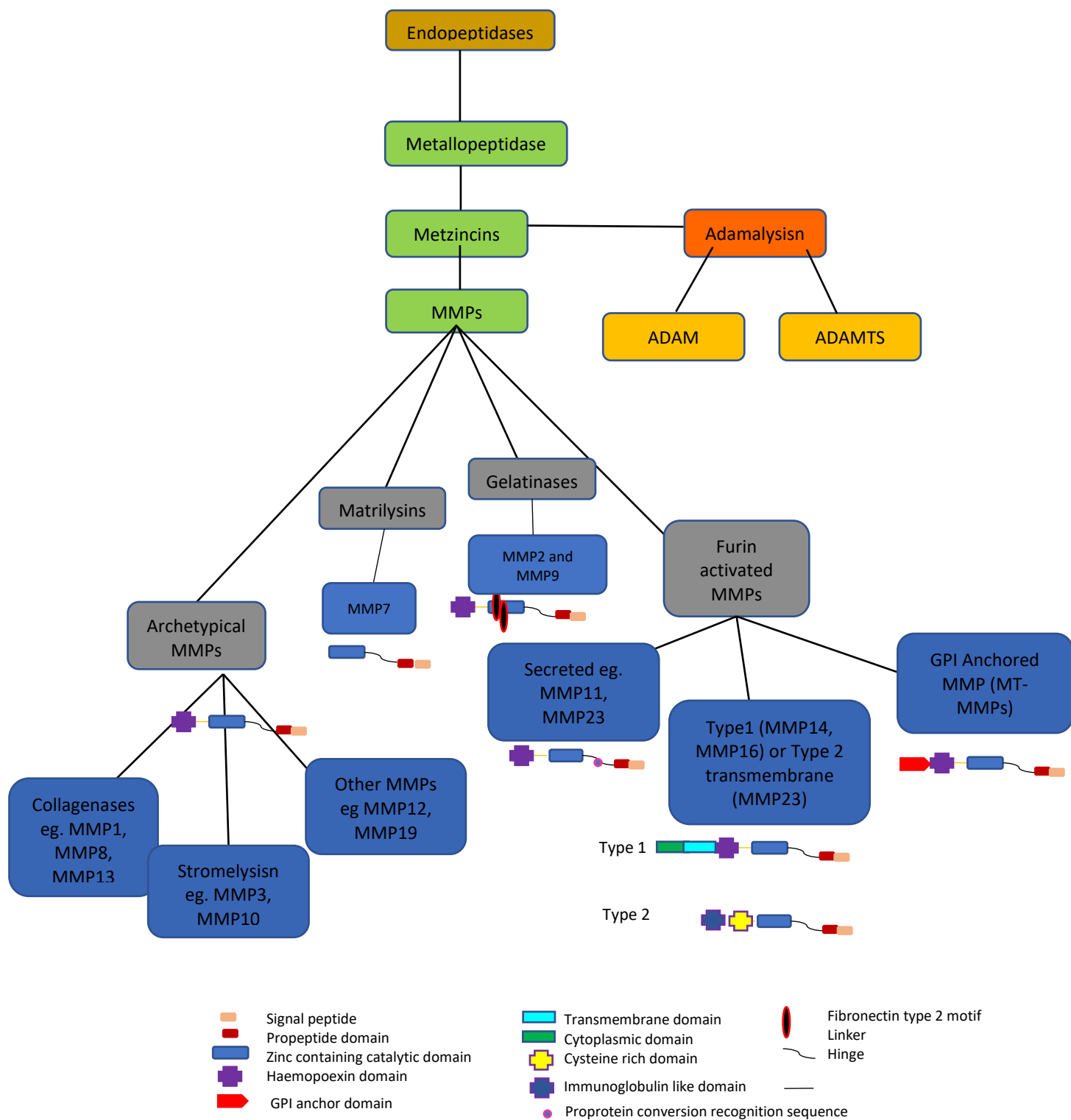


Figure 1.7. MMP classification based on shared structural domains and substrates

Collagenases (MMPs 1, 8, and 13) and stromelysins (MMPs 3 and 10) contain the basic domains: hemopexin-like carboxyl-terminal domain, zinc containing catalytic domain, linker sequence, signal peptide and propeptide domains which other classes build on. Matrilysins (MMPs 7 and 29) are void of the hinge region and hemopexin domain, gelatinases (MMPs 2 and 9) have fibronectin motif within the zinc containing catalytic domain. Membrane-type MMPs are anchored to the membrane by either a transmembrane domain (MMPs 14, 15, 16 and 24) or GPI (MMPs 17 and 25). Based on (Vandenbroucke and Libert, 2014), with permission.

1.5 Metalloproteinases in tumour growth and invasion

Tumour growth, angiogenesis and metastasis are dependent on degradation of the ECM. However, the role of metalloproteinases in these processes is not limited to ECM catabolism and these molecules play often complex roles in most, if not all aspects of the cancer hallmarks.

Metalloproteinases, for example, play a central role in epithelial to mesenchymal transition (EMT) by both cleaving E-cadherin (Noe *et al.*, 2001, Maretzky *et al.*, 2005) and liberating transforming growth factor- β (Illman *et al.*, 2006). Liberation and/or activation of many other growth factors and chemotactic molecules by metalloproteinases is a common theme in cancer progression and the ADAM sheddases are major players in this area. For example, ADAM10 is involved in ectodomain shedding of EGF resulting in EGFR activation and tumour promotion (Sahin *et al.*, 2004). Moreover, ADAMs can also shed pro-apoptotic receptors, inhibiting apoptosis (Ahonen *et al.*, 2003). Death receptor cleavage is not limited to the ADAMS as MMP7 has also been shown to cleave Fas ligand from the cell surface of lung cancer cells treated with doxorubicin (Liu *et al.*, 2008). MMP3 and MMP7 are known to also cleave E cadherin to release bioactive fragments of the E cadherin that promote cancer cell invasion and EMT in breast cancer cells. Furthermore, MMP2 and MMP9 activate latent TGF β to promote tumour angiogenesis and cancer cell invasion (Radisky and Radisky, 2010). In addition to this, MMP9 can induce the release of VEGF from existing cancer cells creating a feedback loop that further induces VEGF dependent expression of MMP9 expression in non-metastatic tissue such that tumour cells in the tissue acquire metastatic potential (Belotti *et al.*, 2003, Hiratsuka *et al.*, 2002).

In addition, MMPs release ECM bound pro-angiogenic factors such as FGF and VEGF (Neve *et al.*, 2014) which in turn stimulate further release of collagenases and gelatinases enhancing tumour angiogenesis and metastasis (Unemori *et al.*, 1992, Lamoreaux *et al.*, 1998). VEGF also induces expression of integrins which can then be further acted upon by several MMPs. For instance, MMP2 binds directly to $\alpha\beta$ 3 integrin to initiate

endothelial cell proliferation and survival and disruption of this interaction between MMP2 and the integrin results in antiangiogenic effects (Siletta *et al.*, 2001).

This central role played by metalloproteinases in cancer progression led to the development of several metalloproteinase inhibitors for cancer treatment. However, these failed in the clinic due to severe side-effects and lack of clinical efficacy. The reasons for this mostly relate to the fact that these drugs were broad spectrum and targeted most metalloproteinases, severely limiting the maximum tolerated dose and, therefore, potential efficacy. This was largely due to the limited understanding of the many complex roles played by these enzymes in the body at the time and, in fact, there is also evidence that some metalloproteinases can limit tumourigenesis by, for example, liberating or activating anti-tumourigenic molecules (Acuff *et al.*, 2006, Balbin *et al.*, 2003, Houghton *et al.*, 2006, McCawley *et al.*, 2004). While more specific metalloproteinase inhibitors are still being explored in cancer treatment (reviewed in (Cathcart *et al.*, 2015)), the functional redundancy of many of these enzymes could still compromise their clinical potential.

1.6 MMPs as therapeutic target in clinical trials

Conventional anticancer agents have largely focused on mutational effect of genes in cancer treatment. However, the importance of ECM remodelling and the role of MMPs in this process have made them crucial targets for cancer therapy. Several investigation and research have developed inhibitors against different MMPs targeting specific domains that are required for MMP catalysis. For instance, early inhibitors including some peptidomimetics were specifically developed to target the catalytic domain in an irreversible manner preventing catalysis. The first set of peptidomimetics developed used hydroxamic acid to chelate the Zn^{2+} at the catalytic domain but the problem with this drugs was the lack of specificity of hydroxamic acid for the Zn^{2+} as it binds to other

divalent metal ions (Overall and Kleifeld, 2006). Batismat was another peptidomimetic that went to into clinical trial based on its inhibitory effects on MMPs like MMP1, MMP2, MMP3 and MMP9. However, poor oral bioavailability resulted in development in more soluble analogue, marismat which also failed in clinical trials due to toxicity at low dose (Gialeli et al., 2011). Prinomastat is a small molecule inhibitor used as antiangiogenic with significant effects in both stages I and II clinical trials but failure to produce significant efficacy in patients with late disease at phase III clinical trial resulted in its termination. Several other small molecule inhibitors were also developed but all failed due to lack of efficacy at some point in clinical trials (Cathcart et al., 2015). This failure is likely stem from poor design of the clinical trials since the drugs have significant efficacy at the initial stage of the trials. It is likely that patients used in the later stage are diverse from those used initially. As such better design of the trial could have resulted in better performance of the drugs.

1.7 Regulation of metzincins

1.7.1 Transcriptional expression

Most metalloproteinases are highly regulated at the transcriptional level. Findings over the last decade have implicated microRNAs (miRNA) in the post-transcriptional regulation of MMP expression (Reviewed in (Li and Li, 2013), giving a broader mode of regulation. For example, ectopic expression of miRNA-224 has been shown to promote breast cancer metastasis to the lungs by repressing MMP1 through inhibition of *RKIP* gene targeting its 3' untranslated region (Huang *et al.*, 2012).

1.7.2 Post translational regulation of metzincins

MMPs and metzincin proteins in general are synthesised as zymogens and activated by proteases. For the secreted MMPs activation takes place in the ECM by various proteases including plasmin and other MMPs. MT-MMPs, ADAMS and ADAMTS are activated in the Golgi network by furin, which is a proprotein convertase, so that the zymogen form

of the protein can be activated before shuttling to the outside of the cell (Loffek *et al.*, 2011, Wang *et al.*, 1996). The inactive forms of metzincins are maintained in that state due to a cysteine residue in the prodomain bound to the zinc at the active site. As such the MMPs that are expressed constitutively are maintained in an inactive state until the prodomain is cleaved, a process known as the “cysteine switch”. Once activated, their proteolytic activities are regulated by different inhibitors, α 2-macroglobulin, reversion-inducing cysteine-rich protein with Kazal motifs (RECK), and their endogenous inhibitors, known as the tissue inhibitors of metalloproteinases (TIMPs) (section 1.9). Cleavage of α 2-macroglobulins by MMPs and ADAMs causes a conformational change in the inhibitor, blocking the enzymes’ catalytic site (reviewed in (Baker *et al.*, 2002)). RECK, a membrane bound inhibitor, has been shown to inhibit ADAMs, MT-MMPs and some MMPs in the context of cancer development. However, there is also evidence RECK is acting by transcriptionally controlling the gene expression of the metzincins as RECK expression has been shown to negatively control promoter activities of MMP9 (Takagi *et al.*, 2009).

1.8 Regulation of metzinc proteins by TIMPS

TIMPs inhibit many metalloproteinases in the ECM, modulating various tumour processes. TIMPs can block proteolytic activation of TGF β . TIMP1 and TIMP3 modulate signalling from the plasma membrane by controlling ADAM-mediated cleavage of NOTCH and TGF β receptor-1 (TGF β R1) inhibiting transcriptional activation of these proteins by the fragments that would be generated. This blockage can also inhibit proteoglycan cleavage preventing ligand interaction with their receptors. Shedding of membrane bound proteins like EGF, amphiregulin and betacellulin for EGFR activation can be inhibited by TIMP inhibition of receptor tyrosine kinases (RTK). TIMPs can alternatively prevent receptor loss via ectodomain shedding by inhibiting proteases

regulating the signalling such as TIMP3 protection of TNF receptor from ADAM17 or TIMP1 protection of MET receptor from ADAM10 sheddases (Jackson et al. 2017).

1.9 TIMPs

TIMPs non-covalently inhibit all MMPs in a 1:1 stoichiometry, although the strength of inhibition of these TIMPs towards specific MMPs varies. TIMPs and MMPs exist in balance regulating physiological processes such as development, tissue repair and angiogenesis; however, dysregulation of the balance between TIMPs and MMPs has been associated with several disease processes including tumour growth and metastasis, (Castagna *et al.*, 2013, Lukaszewicz-Zajac *et al.*, 2013).

1.9.1 Structure-function properties of TIMPs

Mammalian TIMPs comprise two distinct domains; an N-terminal domain which spans about 125 amino acid residues and a C-terminal domain containing about 65 amino acid residues with three disulphide bonds stabilising each domain (Wisniewska *et al.*, 2008). These disulphide bonds create 6 different loops in the protein with 3 in each domain (Figure 1.8). The TIMP protein family comprises of four different homologous proteins, TIMP1-4 (Table 1.1), all with known physiological roles including cell proliferation, differentiation, invasion, migration and apoptosis (Das *et al.*, 2013). TIMP proteins are relatively small proteins of between 21 and 28 kDa in molecular weight, depending on the level of glycosylation, and are structurally similar with an average 40% sequence identity amongst them (Lambert *et al.*, 2004). TIMP2 and TIMP4 have about 50% identity while TIMP1 and TIMP3 have approximately 37% sequence identity (Figure 1.9). The N- and C-terminal domains of TIMPs can fold independently to form stable structures and this reveals that the N-domain is responsible for MMP inhibition whereas the C-domain is responsible for some family member specific functions such as pro-MMP binding and VEGFR2 inhibition (Chen *et al.*, 2014, Kashiwagi *et al.*, 2001, Wu *et al.*, 2011, Nagase and Murphy, 2008).

Table 1.1 Human TIMPs and their general properties (Adapted with permission from Jackson *et al.* (2017))

| Feature | TIMP1 | TIMP2 | TIMP3 | TIMP4 |
|--------------------------------------|--|--|--|---------------------------|
| Human chromosome | X11p11.23–11.4 | 17q23–25 | 22q12.1–q13.2 | 3p25 |
| Mouse chromosome | X A1.3 | 11 E2 | 10C1–D1 | 6 E3 |
| Molecular weight (kDa) | 21 | 22 | 22 | 22 |
| Amino acid residues | 184 | 194 | 188 | 194 |
| Localization | Soluble and cell surface | Soluble and cell surface | Extracellular matrix and cell surface | Soluble and cell surface |
| N-glycosylation sites | 2 | 0 | 1 | 0 |
| MMP inhibition | Weak for MT-MMPs (MMP14, MMP16, MMP19 and MMP24) | All | All | MMP2 and MMP4 |
| ADAM inhibition | ADAM10 | ADAM12 | ADAM10, ADAM12, ADAM17, ADAM28 and ADAM33; ADAMTS1, ADAMTS2, ADAMTS4 and ADAMTS5 | ADAM17, ADAM28 and ADAM33 |
| ProMMP binding | proMMP9 | proMMP2 | proMMP2 and proMMP9 | proMMP2 |
| Non-protease binding partners | CD63 and LRP1 | α 3 β 1 integrin and LRP1 | EFEMP1, VEGFR2 and AGTR1 | |

AGTR1, type-1 angiotensin II receptor; EFEMP1, epidermal growth factor-containing fibulin-like extracellular matrix protein 1; LRP1, lipoprotein receptor-related protein 1; VEGFR2, vascular endothelial growth factor receptor 2.

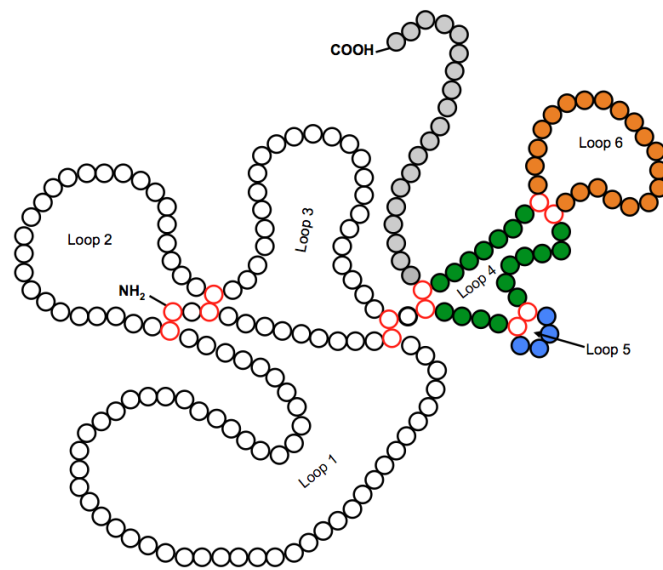


Figure 1.8. The primary structure of TIMPs

The amino and carboxyl domains each comprise 3 different loops constrained by 3 disulfide bonds formed by twelve cysteine residues (red).

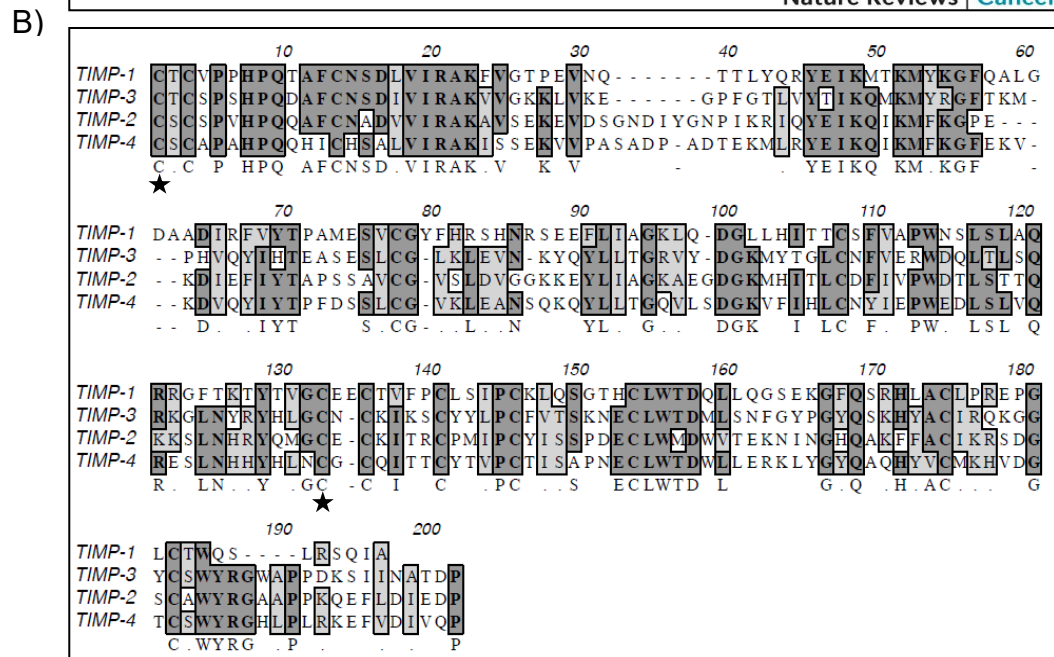
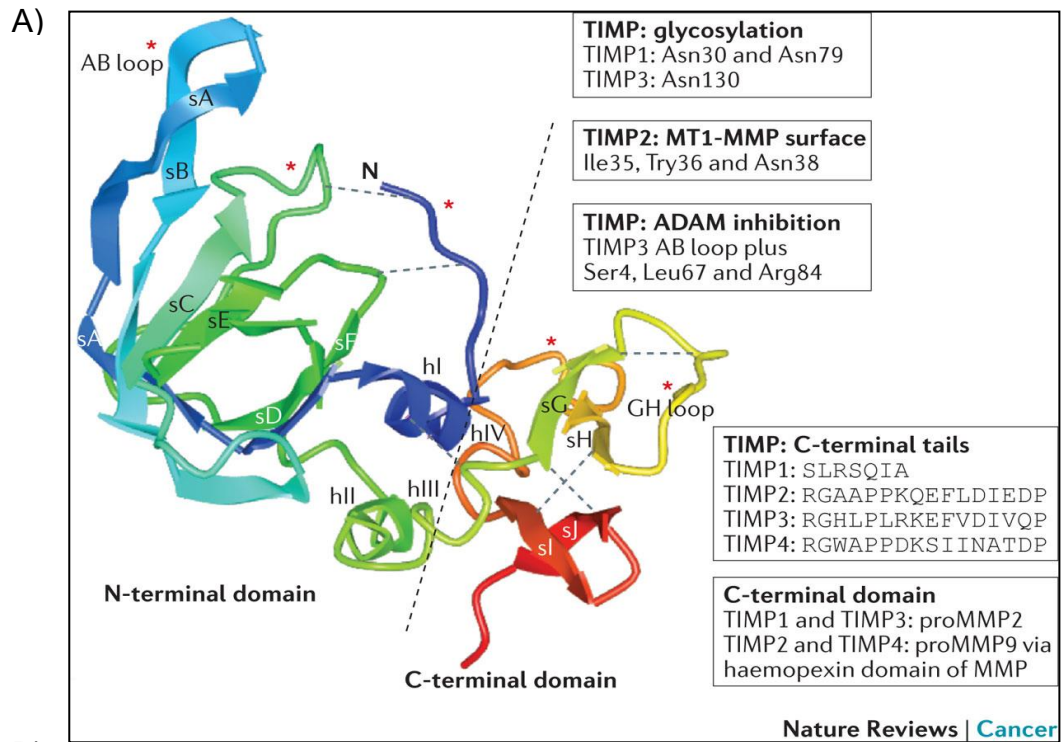


Figure 1.9. Box shade alignment of the TIMP protein family showing sequence similarities and conserved domains

(A) 3D structure highlights the common domain structure of all TIMPs. The N- and C-terminal domains as well as the disulfide bridges (broken lines) are shown, the four α -helices denoted hI to hIV and the ten β strands are also denoted as sA to sJ (Jackson et. al, 2017). (B) Identical residues have dark shading and similar residues lighter shading. Black star indicates conserved residue for the NTR domain of all TIMPs used for regulation of metalloproteinase activities.

1.9.2 Regulation of TIMP proteins

Like MMPs, the regulation of TIMPs is mainly at the transcriptional level and this is facilitated by a variety of cytokines, chemokines and growth factors. Recent advancement in TIMP research has also uncovered some epigenetic modifications. TIMP expression shows a characteristic tissue and developmental stage-dependent pattern (Nuttall et al., 2004, Li et al., 2016). In addition to this, specific cell types activate or repress the expression of *TIMP* genes using signalling from mitogen activated protein kinase (MAPK), Smad and nuclear factor- κ B (NF κ B) pathways (Sampieri *et al.*, 2008, Akool el *et al.*, 2005, Baker *et al.*, 2002).

Analysis of *TIMP1-4* genes, with the exception of *TIMP2*, shows that they contain a canonical retinoid X receptor response element (RXRR) about 1 kb upstream sequence (Clark *et al.*, 2008). The nuclear receptor related-1 (NURR1) is one transcriptional factor that binds the retinoid X receptor, and the control of TIMP expression via the RXRR was shown to mediate upregulation of TIMP1 by NURR1 (Mix *et al.*, 2007). Like most MMPs, *TIMP1*, *TIMP2* and *TIMP3* have GC boxes which allows the binding of GC proteins like Sp1 and Sp3 to such sites. Binding of these proteins to the GC boxes either activate or repress the transcription of the *TIMP* genes depending on the context and the distribution of the GC boxes to which they bind (Dean *et al.*, 2000, Clark *et al.*, 2008). In addition to the RXRR and the GC boxes, *TIMP1*, *TIMP2* and *TIMP4* also have NF- κ B sites upstream of their transcription sites. Binding of p50 and p65 subunits of NF- κ B to the regulatory sequence upstream of *TIMP1* is required for IL-1-dependent transcriptional activation of the gene during inflammation (Wilczynska *et al.*, 2006). NF- κ B is often highly expressed and it is implicated in tumourigenesis of different cancers and the interplay between NF- κ B activation and TIMP1 upregulation for instance, plays an

important role in development of specific cancers such as thyroid cancer (Bommarito *et al.*, 2011).

1.9.3 TIMPs in cancer

In recent years, altered expression of TIMPs has been found to be one of the recurrent molecular signatures of tumour progression, suggesting an important role for these molecules in tumourigenesis (Figure 1.10).

1.9.3.1 TIMP1

Correlation between upregulated expression of TIMP1 and poor prognosis in breast and pancreatic cancers has been shown in many different studies and clinical trials. For instance, there is an increased level of TIMP1 in patients with breast, endometrial and brain cancer as well as in advanced tumour stages in patients having shorter time to relapse (Dechaphunkul *et al.*, 2012, Aaberg-Jessen *et al.*, 2009, Honkavuori *et al.*, 2008). Lack of TIMP1 in immunostained tissue sample of patients with high grade breast carcinoma was associated with positive prognosis (Kuvaja *et al.*, 2005). In addition, increased cytosolic TIMP1 in breast tumour tissue of patients receiving adjuvant chemotherapy correlated significantly with shorter overall patient survival (Dechaphunkul *et al.*, 2012). In pancreatic cancer, increased urine and serum levels of TIMP1 have been observed and are also considered to function as a diagnostic indicator in patients with pancreatic ductal carcinoma containing desmoplastic reaction (Jenkinson *et al.*, 2015, Grünwald *et al.*, 2016). TIMP1's mechanism of action has been recently shown to be through its inhibition BCL2 apoptotic protein, thus inhibiting apoptosis in cancer cells (Nalluri *et al.*, 2015). Overexpression of TIMP1 was shown to suppress BCL2 expression and the inhibition of apoptosis was shown to occur through p90RSk phosphorylation of BAD proapoptotic protein which results in reduction in BAX protein level.

1.9.3.2 TIMP2

TIMP2 plays an essential role in the regulation of cell growth, remodelling of the ECM, angiogenesis and apoptosis all of which are important for cancer development and tumour progression. Both increased and decreased expression of TIMP2 has been reported in different clinical trials investigating its expression in lung, breast and colorectal cancers (Jackson *et al.*, 2017). Expression of TIMP2 is also found to be epigenetically silenced via hypermethylation of its promoter in different cancer cell lines (Pulukuri *et al.*, 2007). Increased levels of TIMP2 are associated with poor prognosis in bladder cancer patients (Grignon *et al.*, 1996). In addition, increased expression of TIMP2 together with MMP2 is also correlated with poor prognosis in patients with thymic epithelial cancer (Sogawa *et al.*, 2003). However, *in vitro* studies have shown that TIMP2 overexpression inhibited tumour growth, angiogenesis and stimulate cancer cell apoptosis (Bourboulia *et al.*, 2011). Difference in experimental design could be the reason for the differences in the above observation. *In vitro* experiments do not totally reflect what occurs in the biological system and it is possible there are several other factors contribute to TIMP2 promotion of cancer progression.

1.9.3.3 TIMP3

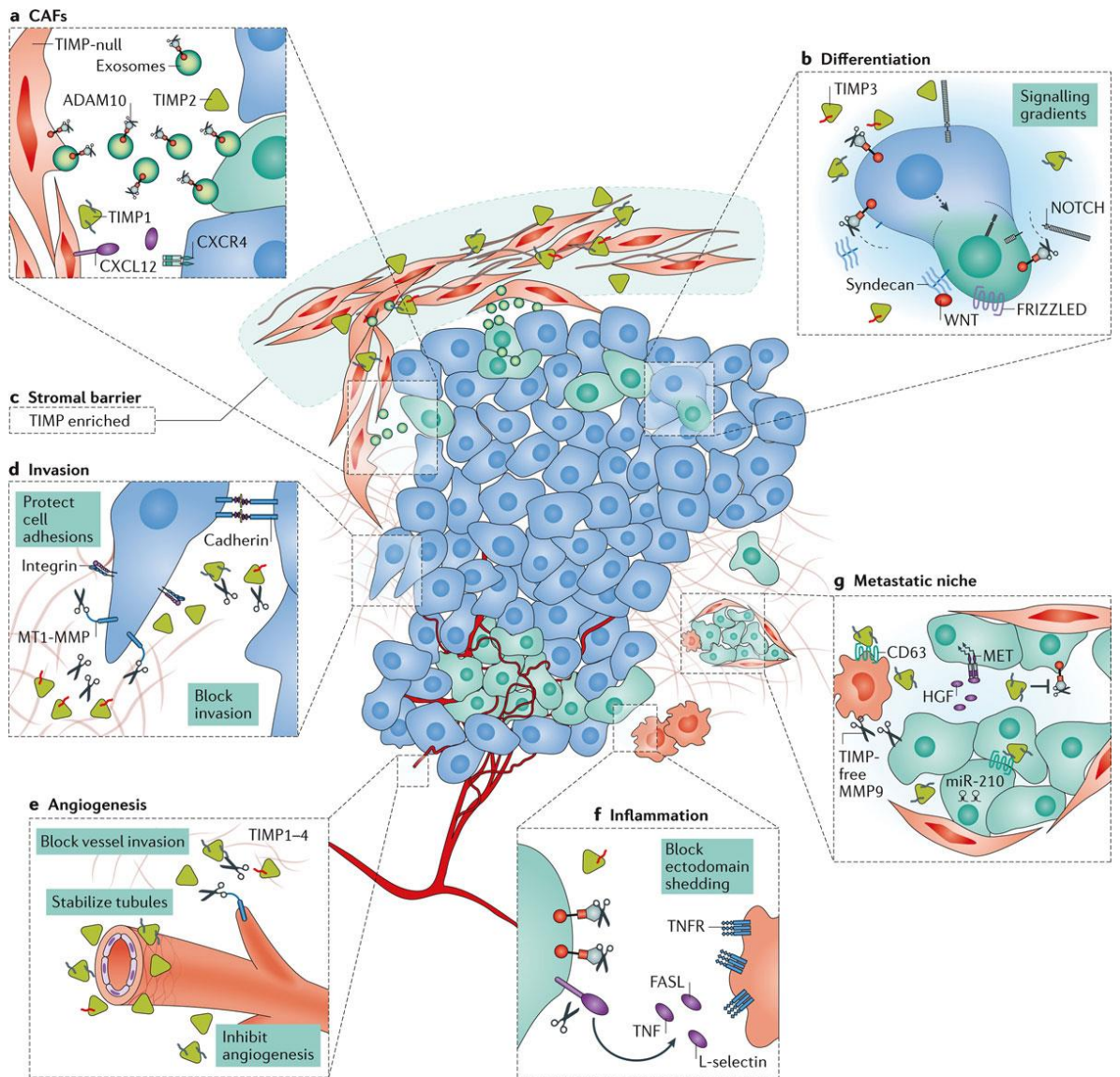
Changes in TIMP3 expression in cancer are the most widely reported in the family and this loss of TIMP3 expression in cancer is usually associated with hypermethylation of the TIMP3 promoter region (Barski *et al.*, 2010, Catusus *et al.*, 2013). Multiple studies have described the downregulation of TIMP3 in different cancers. Loss of *TIMP3* is associated with poor prognosis and advanced disease in colorectal, brain, breast, glioblastoma and kidney cancer (Gu *et al.*, 2008, Bachman *et al.*, 1999, Shinojima *et al.*, 2012). Interestingly, breast cancer with high levels of TIMP3 show a better response to endocrine treatment (Helleman *et al.*, 2008). Gene expression analysis of the four TIMP proteins in breast cancer showed TIMP3 served as a prognostic factor for determining

progression free survival in patients treated with tamoxifen (Span *et al.*, 2004). Gene mapping study by Nakamura *et al.* (2005) on several glioblastoma tissue samples showed a loss of heterozygosity of one of the *TIMP3* alleles while the other allele is hypermethylated. In contrast to all previous studies, where loss of *TIMP3* expression is associated with cancer, two relatively recent reports have linked expression of *TIMP3* to tumourigenesis. One used two independent mouse breast cancer models to show that *TIMP3* knockout increased resistance to tumour development and disease progression indicating a tumour promoting role for *TIMP3* (Jackson *et al.*, 2015). This effect appeared to be dependent on TNF receptor 1 expression. TNFR-1 on mammary tumour cells can increase their proliferation, and the authors suggest that the consequent decrease in shedding of this receptor is one possible cause. Additionally, a second report demonstrated *TIMP3* knockout increased resistance to carcinogen-induced hepatocellular carcinoma (Defamie *et al.*, 2015). In this case this appeared to be independent of TNF signalling, but associated with upregulation of p53, p38 and Notch pathways. However, these variation of *TIMP3* expression in the different cancers mentioned here may be due to heterogeneity of the cell lines because different cells type have variations in gene expression to perform their unique biological functions.

1.9.3.4 TIMP4

Like *TIMP2*, both upregulation and downregulation of *TIMP4* has been reported in different cancers (Melendez-Zajgla *et al.*, 2008). For example, increased *TIMP4* expression has been reported in the early stages of prostate and breast cancer, which was later suppressed at more advanced and invasive stages (Lee *et al.*, 2006b, Liss *et al.*, 2009). Interestingly, analysis of all *TIMP* expression in malignant renal cell carcinoma cell lines showed *TIMP4* expression is suppressed due to chromosomal loss (Hagemann *et al.*, 2001). Overexpression of *TIMP4* in a mouse breast cancer model showed recession

of tumour growth and inhibition of metastasis (Wang *et al.*, 1997). Like TIMP3, these variations in TIMP4 expression is likely dependent on difference in the cancer cell lines used in these studies.



Nature Reviews | Cancer

Figure 1.10. TIMPs regulate key aspects of the tumour microenvironment

ECM remodelling plays key role in the survival of cancer cells within the tumour microenvironment and TIMPs are key player in ECM metabolism. a) TIMPs absence allows for tumour promoting processes in stromal fibroblast with null TIMP expression making them act like cancer associated fibroblasts b) cellular differentiation is regulated by TIMPs by controlling NOTCH and WNT signalling c) many tumour stroma associated TIMPs promote tumour formation and invasion d) TIMPs inhibit uncontrolled migration and invasion through their protective roles on adhesion molecules like E cadherin from proteolytic degradation by inhibiting MMPs e) TIMPs also block angiogenesis and invasion of endothelial cells but they also stabilised already formed vessels f) TIMPs regulate shedding of chemokines that recruits inflammatory cells thus inhibiting tumour dependent environmental changes g) TIMP1 can inhibit ADAM10 shedding of MET receptor, creating a metastatic niche or by acting as a ligand for CD63 receptor. Based on Jackson *et al.* (2017), with permission.

1.9.4 TIMP3: Structural and functional features

Of all the TIMPs, TIMP3 is probably the most interesting as it has several unique properties that will be discussed in later sections. This is illustrated by the fact that TIMP3 knockout animal models have been demonstrated to develop several different disease conditions such as interstitial nephritis and fibrosis (Kassiri *et al.*, 2009). Many of these relate to an increased pro-inflammatory environment due to increases in TNF α shedding by ADAM17 (see section 1.7) and increased MMP activation. In one *Timp3* knockout mouse study, antigen induced arthritis led to an aggravated inflammatory response with increased TNF α production compared to wild type mice (Mahmoodi *et al.*, 2005). In another study, *Timp3* knockout mice injected with angiotensin II developed abdominal aortic aneurysms, which were not observed in mice expressing wild type *Timp3* (Basu *et al.*, 2012). *Timp3* knockout mice have also been shown to exhibit impaired cognitive functions compared to mice expressing the wild type protein (Baba *et al.*, 2009), reflecting the complex role of MMPs and TIMPs in neurological function (Yong, 2005). The multiple targets of TIMP3 and its role in disease are summarised in Figure 1.11 and these will be discussed in more detail below.

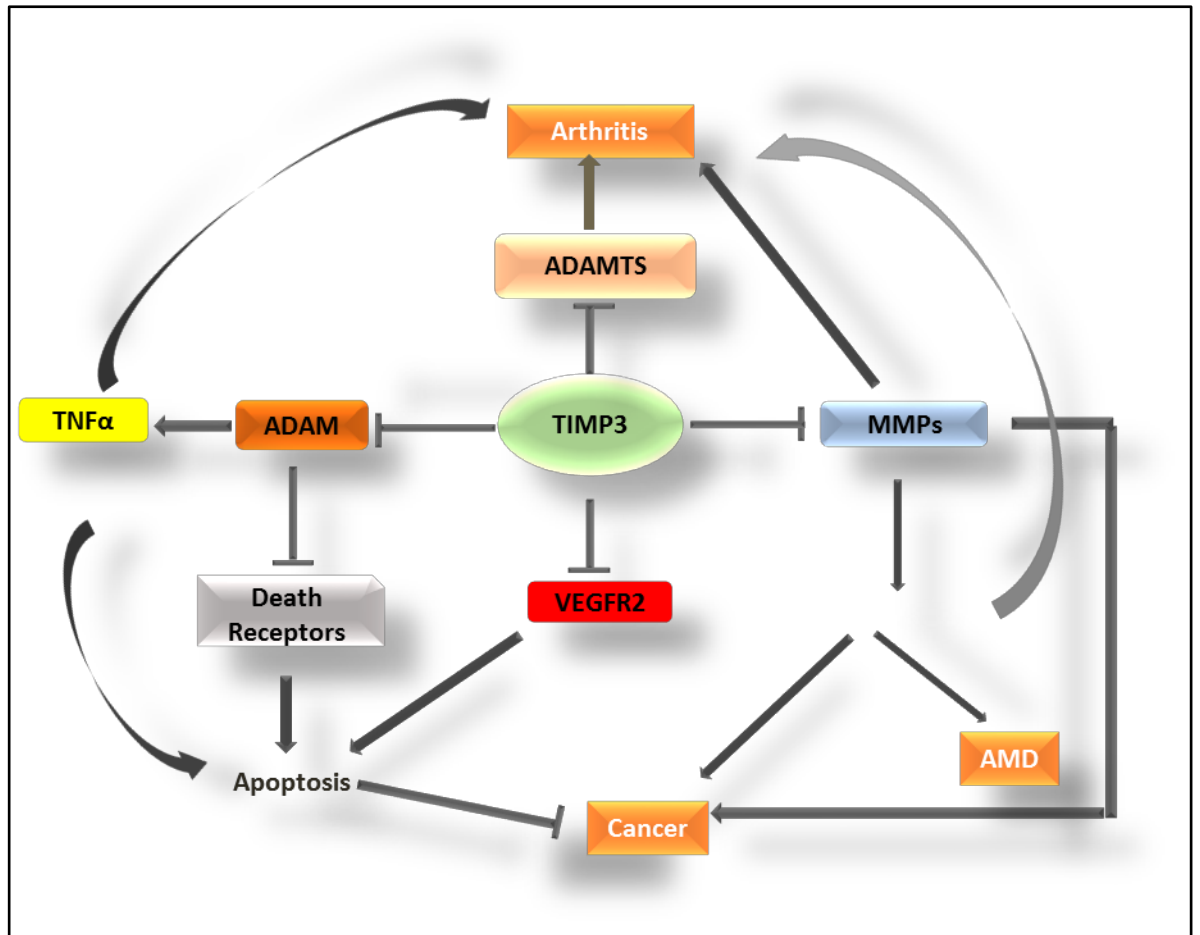


Figure 1.11. Overview of TIMP3 regulatory properties

TIMP3 promotes apoptosis through inhibition of ADAMs, which shed death receptors, and by inhibiting the anti-apoptotic VEGFR2 on some cells. VEGFR2 inhibition, together with inhibition of MMPs also inhibits angiogenesis, which plays a key role in cancer progression and age-related macular degeneration (AMD). TIMP3 can also inhibit arthritis by inhibiting MMPs (e.g. collagenases), ADAMTSs (i.e. aggrecanases) and ADAMs (preventing the shedding of pro-inflammatory cytokines such as $\text{TNF}\alpha$).

1.9.4.1 TIMP3 association with the ECM

Like the other TIMP family members, TIMP3 is a secreted protein but differs from them in its high binding affinity for the ECM, associating its functionality to the cell surface (Lee et al., 2007, Basu et al., 2013). It is sequestered to the ECM in both glycosylated and unglycosylated forms (Langton *et al.*, 1998), unlike TIMP1, TIMP2 and TIMP4, which are soluble proteins. It has been shown in post-partum rat liver that TIMP3 associates with glycosaminoglycans such as chondroitin sulphate, heparin, heparin sulphate and other sulphated compounds like pentosan and suramin (Yu et al., 2000, Troeberg et al., 2014). Lee *et al.* (2007), using N- and C-domain chimeras of TIMPs 1-4, as well as site-directed mutagenesis of TIMP3, identified residues that contributed to ECM binding. Specifically, they showed that Lys26, Lys27, Lys30, Lys76 at the N-terminal domain and Arg163, Lys165 at the C-terminal domain are responsible for the binding of TIMP3 to the ECM. Lysine to glutamate and arginine to glutamine substitution of these residues, resulted in a soluble TIMP3 molecule. More interestingly, these residues were also introduced into TIMP1, which ordinarily does not bind to ECM, producing an ECM binding protein.

1.9.4.2 TIMP3 Inhibition of adamalysin metalloproteinases

One of the unique properties of TIMP3 is its function as the only inhibitor of several ADAM and ADAMTS protein members. One of these is ADAM17, also known as TNF- α converting enzyme (TACE), which processes the shedding of the membrane anchored immunomodulatory and proinflammatory cytokine, tumour necrosis factor- α (TNF- α) by proteolytic cleavage of its ectodomain (Hiraoka *et al.*, 2008). TACE is also involved in the shedding of other membrane bound proteins such as amyloid precursor protein (De Francesco *et al.*, 2013) and transforming growth factor α (TGF- α) (Hiraoka *et al.*, 2008). Analysis of the binding profile of truncated catalytic domain form and full-length recombinant TACE with the N-terminal domain of TIMP3 (N-TIMP3) and the wild type

protein showed the N-TIMP3 binds to TACE with as great an affinity as the full length TIMP3. At basal conditions, the affinity of interaction of TIMP3 with TACE is highest when TACE forms a dimer, although this interaction is relieved through TACE activation by the Erk and p38, a mitogen activated protein kinase (Xu *et al.*, 2012). Mutagenesis studies showed that the N-TIMP3, N-TIMP4 or full length TIMP3 and not TIMP1, 2 or full length TIMP4 inhibits TACE (Lee *et al.*, 2001, Lee *et al.*, 2005a). Loss of TIMP3 expression in bone marrow derived macrophages from TIMP3 deficient mice causes increased TNF shedding as seen during inflammation. In TIMP3 knockout mice, there was also increased serum TNF concentration as compared with mice expressing TIMP3 (Lee *et al.*, 2005a). This suggests TIMP3 may regulate inflammation through TACE.

TIMP3 is unique among the TIMP family in also inhibiting certain members of the ADAMTS family. Notably, TIMP3 is able to inhibit the aggrecanases, ADAMTS-4 and ADAMTS-5, whose activities are associated with the development of osteoarthritis through the degradation of this proteoglycan component of cartilage (Kashiwagi *et al.*, 2001). Understanding this interaction may assist in the development of novel therapeutics for the treatment of osteoarthritis.

1.9.4.3 TIMP3 and apoptosis

TIMP3 over-expression in different cancer cells and human vascular smooth muscle cells has been shown to reduce migration and promote cell death (Baker *et al.*, 1999, Ahonen *et al.*, 1998). This activity lies in the N-terminal domain of TIMP3, is metalloproteinase dependent and is, at least in part, due to stabilisation of three different death receptors, TNF α receptor 1 (TNFR1), FAS, and TNF-related apoptosis inducing ligand receptor 1 (TRAIL-R1) (Ahonen *et al.*, 2003), probably due to inhibition of sheddases such as TACE.

Conversely, TIMP3 knock-out mice indicate an anti-apoptotic role for TIMP3. Fata *et al.*, 2001 showed *Timp3*^{-/-} mice demonstrated alveolar epithelial loss, increased collapse of the lumen, adipose reconstitution and increased apoptosis of mammary gland epithelial cells during mammary gland involution. TIMP3 deficient mice were also found to have increased fibrosis and renal damage which resembles nephritis seen in the ageing kidney (Kassiri *et al.*, 2009). The authors proposed that this may in part be due to increased activity of MMP2 resulting in increased ECM breakdown and loss of ECM-mediated cell survival signals. It is possible that these anti-apoptotic effects of TIMP3 are also mediated via inhibition of TACE. TACE activates TNF- α through cleavage to mediate apoptosis. Interestingly, Kassiri *et al.* (2009) found increased apoptosis in renal cells of TIMP3 deficient mice that was alleviated in *Tnf- α* ^{-/-} double mutant mice.

1.9.4.4 TIMP3 and EFEMP1

Epidermal growth factor–containing fibulin-like extracellular matrix protein 1 (EFEMP1) is an extracellular glycoprotein containing tandem EGF-like repeats and a fibulin type C terminal module. EFEMP1 is a fibulin (also known as fibulin 3), proteins that are widely expressed in elastic tissues and the vasculature with almost exclusive association to these tissues (Kobayashi *et al.*, 2007). A specific mutation in EFEMP1 (Arg345Trp) has been implicated in the pathogenesis of a type of macular degeneration, Malattia Leventinese (ML), a disease affecting the retina leading to blindness, often in middle age (Marmorstein *et al.*, 2002). EFEMP1 and TIMP3 have been shown to bind one another and there is high accumulation and significant expression overlap between TIMP3 and EFEMP1 in the retinal pigment epithelia as well as Bruch’s membrane in patients suffering from ML and age related macular degeneration (AMD) (Klenotic *et al.* (2004).

1.9.4.5 TIMP3 in the retina

1.9.4.5.1 TIMP3 in the pathogenesis of Sorsby's fundus dystrophy

Sorsby's fundus dystrophy (SFD) is a rare disease inherited in an autosomal dominant mode and is characterised by early onset maculopathy associated with neovascularisation of the choroid resulting in the rapid loss of central and subsequently the peripheral vision (Lin *et al.*, 2006). SFD is caused by mutations in *TIMP3* and, to date, 15 different mutations in the gene have been discovered in patients with SFD. Most these are missense mutations in exon 5 which change a residue to a cysteine, although there are some exceptions such as Glu139Lys and His158Arg. There is also one reported nonsense mutation, Glu139X, and a mutation at the intron 4/exon 5 splice junction (Lin *et al.*, 2006). To date, the mechanism of these mutations in the pathogenesis of the disease is not fully understood. It was initially proposed that haploinsufficiency, due to loss of function of one allele is the cause of the disease, however this is not supported by *Timp3*^{-/-} mice and in fact eyes from SFD patients show increased deposition of TIMP3 in the retina (Fariss *et al.*, 1998).

It has subsequently been shown that the unpaired Cys residues in the mutant TIMP3 molecule lead to TIMP3 dimerisation and/or multimerisation and this decreases TIMP3 turnover (Langton *et al.*, 2005, Langton *et al.*, 2000). It was postulated that this leads to the observed deposition of the mutant protein in Bruch's membrane of the retina causing impaired turnover of the ECM and subsequent thickening of the membrane, which could in turn trigger neovascularisation due to hypoxia. In fact all mutations, including those that do not result in a change to a cysteine residue, have now been shown to form disulfide bonded dimers (Alsaffar, 2017).

1.9.4.5.2 TIMP3 and age-related macular degeneration (AMD)

Neovascularisation in the eye is linked to many diseases, most importantly AMD, and it is a major cause of blindness in elderly people with recent treatments aimed at blocking

new blood vessels formation (Ristic *et al.*, 2013). AMD is a complex multifactorial disease with both genetic and environmental risk factors (Abecasis *et al.*, 2004). There are two forms of AMD which are dry AMD, in which there is no neovascularisation and the wet, exudative, AMD where patients present with choroidal neovascularisation (CNV). Although TIMP3 is mutated in SFD, *TIMP3* mutations have not been detected in AMD (Kamei and Hollyfield, 1999). However, as mentioned above, TIMP3 is highly expressed in Bruch's membrane of AMD patients and this has been suggested to likely prevent ECM turnover. The genetic risk factor that has been most strongly associated with the development of AMD is variation in the gene encoding complement factor H (*CFH*); however a recent association study has revealed certain variations in non-coding regions of *TIMP3* may also be associated with the disease (Kaur *et al.*, 2010). Interestingly, it has been shown that EFEMP1 binds to CFH in a yeast-2-hybrid screen, suggesting a possible common mechanism for TIMP3 and EFEMP1 in the pathogenesis of SFD, ML and AMD (Wyatt *et al.*, 2013).

CNV membranes have been shown to be highly reactive towards VEGFA antibody suggesting it is highly expressed in this tissue (Lopez *et al.*, 1996). Clearly, VEGF-A is an important factor in the pathogenesis of AMD and drugs targeting this molecule, such as ranibizumab, have proven to be highly effective at limiting CNV in AMD. It is now known that the regulation of VEGFA and other proangiogenic factors in CNV is modulated by interaction between the cell and ECM. During this process, MMPs are highly expressed in CNV membranes altering cell matrix interactions to promote the growth of new blood vessels (Das *et al.*, 2003).

1.9.4.6 TIMP3 and angiogenesis

1.9.4.6.1 TIMP3 inhibition of VEGFR2

CNV results from angiogenesis, the formation of new blood vessels from pre-existing ones. This process is essential in organ and tissue development, reproduction and in wound healing or tissue repair (Bourlev *et al.*, 2006, Zhou *et al.*, 2013, Kaygusuz *et al.*, 2014). Migration of vascular cells in angiogenesis is dependent on MMPs to degrade the ECM and therefore TIMPs inhibit this process. However, TIMP3 has also been shown to have MMP independent anti-angiogenic properties. Specifically, TIMP3 inhibits VEGF mediated neovascularisation and angiogenesis by serving as a competitive binding partner of VEGF for VEGFR2 (Qi *et al.*, 2013, Qi *et al.*, 2003). Using structure function relationship analyses and recombinant peptides of TIMP3, Qi *et al.* (2013) showed that the C-terminus of TIMP3 is responsible for binding to VEGFR2 and this binding leads to marked inhibition of VEGF mediated signalling events such as epithelial cell migration, VEGF-mediated actin development and reorganisation and epithelial cell proliferation. TIMP3 derived C-terminal peptides were shown in the same study to inhibit CNV in mouse models. Interestingly, mice lacking *TIMP3* have been shown to have increased VEGF mediated angiogenesis and aggravation of CNV induced by laser (Ebrahim *et al.*, 2011).

1.10 Targeted drug delivery systems in cancer therapy

A major issue in the development of any new drug is poor delivery and sustained availability and in fact, more than 70% of drugs produced have poor pharmacokinetics (Khadka *et al.*, 2014). This is no different for cancer treatments. In addition to this, most conventional anticancer drugs target any dividing cells making them toxic to normal cells. This results in the severe side effects that are commonly associated with conventional anticancer drugs such as alopecia, anaemia and loss of appetite. For this reason, much research has focussed on improving the bioavailability and specificity of cancer

treatments by developing drug delivery systems (DDS) that can target the tumour microenvironment (Figure 1.12).

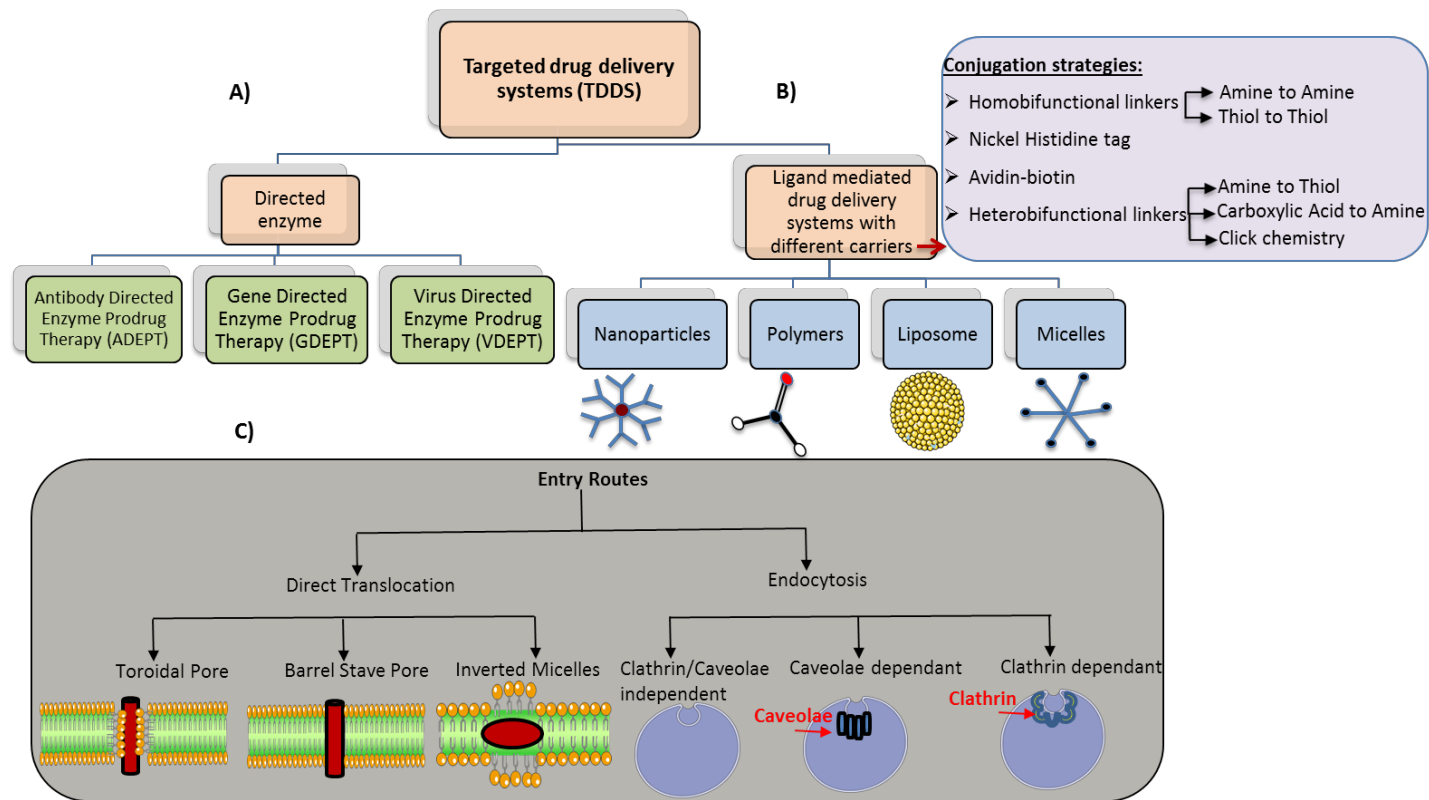


Figure 1.12. Schematic diagram of various Targeted Drug Delivery Systems (TDDS)

Targeting of drugs to specific region can be done by either (A) directed enzyme to tumour target using either antibody, gene, or virus respectively abbreviated as ADEPT, GDEPT, or VDEPT. (B) By encapsulating the active drug in a protected carrier (DDS) which are then conjugated to ligands for targeted delivery to the tumour site. The conjugation of the ligands to carriers can be done using different strategies, including Histidine tag, avidin-biotin, homobifunctional linkers and heterobifunctional linkers which utilise click chemistry, being of great advantage. (C) Internalisation mechanisms of DDS can be divided into two main routes; Endocytosis (clathrin/caveolae dependent or nondependent) and direct translocation (barrel stave pore, toroidal pore and inverted micelles).

1.10.1 Lipid based DDS

Liposomes are a very common DDS that have been used to help improve delivery of many conventional anticancer drugs to tumour sites. This improved delivery is attributable to the enhanced permeability and retention effect (EPR) of liposomes, allowing them to traverse the leaky vessels and localise at the tumour microenvironment (Bolkestein *et al.*, 2016) as shown in Figure 1.13. Liposomes are made up of lipid bilayers with an inner solvated core, that can mimic the cell membrane of living cells. Because initial findings showed liposomes to be unstable at physiological pH resulting in low bioavailability, liposomes have been conjugated to different chemical moieties to increase their circulation time. This includes conjugation of polyethyleneglycol (PEG) to the liposome surface. In addition, liposomes have also been conjugated to monoclonal antibodies or peptide fragments to increase their specificity for the target cells. For example, a study conjugated an anti-SLC22A1 monoclonal antibody to liposomes carrying an MMP2 substrate. The anti-SLC22A1 recognises nucleosomes that are expressed on cancer cells, thus having dual specificity of localising to the tumour microenvironment by means of the antibody and being effective only in cells overexpressing MMP2 which will cleave the peptide to allow internalisation of the liposome for the delivery of encapsulated drug (Zhu *et al.*, 2012).

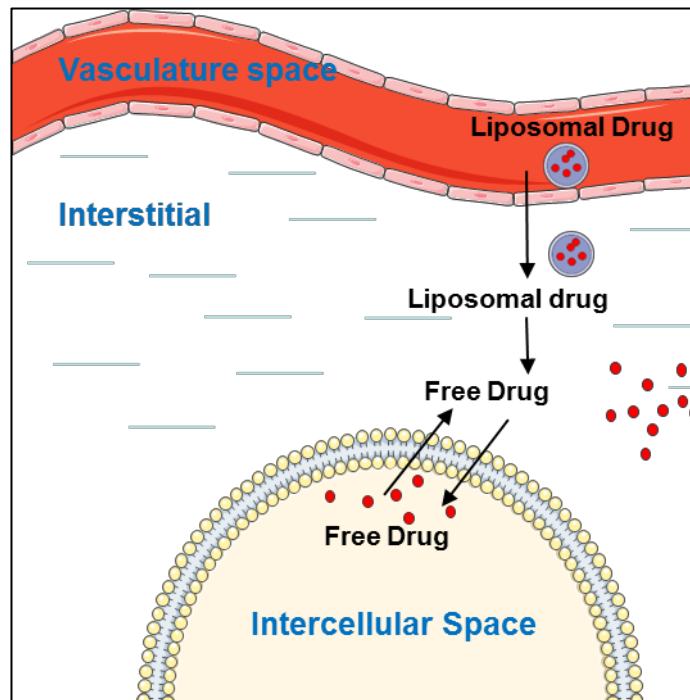


Figure 1.13. Delivery of liposomal drug to peripheral tissues and tumours

Liposomal drugs are released into the interstitial space in tissues with increased vascular permeability such as tumours and once there, liposomes release free drug into the interstitial fluid compartment. The free drug is then able to move by diffusion into the intercellular space and once taken up by the cell, can then carry out the intended pharmacological processes.

1.10.2 Polymeric nanoparticle

Synthetic and natural polymeric nanoparticles can also enhance drug delivery and are being investigated in the treatment of different diseases, including cancer. Chitosan is a natural polymeric nanoparticle with cationic amino groups which enable mucoadhesion, controlled substance release and enhanced uptake into cells (Bernkop-Schnurch and Dunnhaupt, 2012). N-trimethyl chitosan was used to encapsulate camptothecin, a DNA topoisomerase I inhibitor that has shown great promise in the treatment of cancer but which has very poor solubility and gives rise to severe side effects. However, chitosan encapsulated camptothecin successfully inhibited tumour growth and lymphatic metastasis in a mouse model of ovarian cancer with minimal toxicity (Zhou *et al.*, 2010a).

1.10.3 Peptide DDS

Peptide fragments of known proteins in both linear and cyclic forms have been investigated for drug targeting, based on their ease of synthesis and potentially low immunogenicity. The rationale is that cells that express receptors that bind specific proteins will also recognise the peptide fragments, even when conjugated to drugs (Majumdar and Siahaan, 2012), facilitating targeted delivery and entry of the conjugate into the cells. For example, somatostatins are a family of peptide hormones whose receptors are highly upregulated in many cancer cells and these receptors are often targeted for drug delivery in cancer treatment (Barbieri *et al.*, 2013). An Fab fragment of anti-c-Met antibody has been previously conjugated to doxorubicin for targeted delivery in hepatocellular carcinoma chemotherapy (Chen *et al.*, 2013a). It was found that the protein-drug conjugate possessed less cytotoxic effect, enhanced antitumour effects and reduced side effects compared with free doxorubicin.

1.10.4 Prodrug approach

This approach involves the use of a non-toxic compound that can be administered *in vivo* and is then enzymatically metabolised into a toxic drug to exert its effect at a specific site.

The main problem addressed by the prodrug approach is to minimise toxicity of drugs on normal cells and tissues (Rautio *et al.*, 2008, Hu, 2004). One such approach has been antibody-directed enzyme pro-drug therapy (ADEPT). The ADEPT strategy developed by (Andrady *et al.*, 2011), involved coupling a tumour specific antibody to an enzyme that converts the prodrug into a toxic drug for local administration into solid tumours. The limitations of this approach include being able to effectively target the enzyme to the desired site and ensuring unbound enzyme is cleared from the circulation before administration of the prodrug. An alternative approach that circumvents some of these issues is to exploit the tumour microenvironment itself. Reactive oxygen species (ROS) are often generated in the tumour microenvironment (Mates and Sanchez-Jimenez, 2000). As a result, prodrugs that are activated by ROS have been designed and developed over the years and many have been tried in different clinical studies. A hydrogen peroxide-activated boron based MMP inhibitor was recently developed by creating a prodrug with protected boronic ester hydroxyl group on the zinc binding moiety of the drug (Major Jourden and Cohen, 2010). Another good example is the drug ICT2588, a vascular disrupting agent specifically converted into the active form by MT1-MMP that is highly expressed on the surface of many tumour cells (Gill *et al.*, 2014).

1.11 Work that has led to this project

In our laboratory, we have identified a short 16 amino acid fragment of the C-terminus of TIMP3 (KIKSCYYLPCFVTSKN), designated as p700 (present in loop 4 and 5 of full length TIMP3), that potently inhibits VEGFR2 (Chen *et al.*, 2014). However, unlike the peptides described by Qi *et al.* (2013), which apparently retain TIMP3's specificity for VEGFR2, p700 shows a broader binding specificity as it not only inhibits VEGFR2 but also VEGFR1, VEGFR3, PDGFR α , FGFR1, FGFR2, FGFR3 and FGFR4. This broad specificity may account for its demonstrated potency in inhibiting tumour growth in a

syngeneic mouse breast cancer model. Moreover, p700 also significantly inhibited inflammation in a mouse model of rheumatoid arthritis (Chen *et al.*, 2014). The latter ability probably results from p700's wider inhibitory profile as it was demonstrated that the peptide strongly inhibited PDGF-mediated invasion of synovial cells from rheumatoid arthritis patients. While the peptide prevented tumour growth it did not actually kill the tumours, thus leading to tumour regrowth after prolonged treatment or treatment withdrawal (unpublished observation). As such, using it as a sole therapeutic agent may not be successful.

However, utilising p700 in combination with other drug delivery strategies could potentially improve its therapeutic efficacy. For instance, VEGFR2 and VEGFR3 are highly upregulated in the tumour vasculature of several solid tumours such as in malignant colorectal, lung and breast tumours (Smith *et al.*, 2010). In colorectal cancer, VEGFR1 is upregulated and activated in conjunction with epithelial-mesenchymal transformation (EMT) both of which are essential for development of an invasive phenotype (Bates *et al.*, 2003). Additionally, PDGF receptor has been shown to be highly expressed on myofibroblasts and fibroblasts of the stroma of solid tumours and/or tumour vasculature (Heldin, 2013) while FGF receptor is often overexpressed in cancers such as oestrogen receptor (ER)-positive breast cancer and lung (Kato and Nakagama, 2014).

1.12 Hypotheses and aims

We hypothesise that, while in itself p700 peptide may not actually kill tumours, it could be used to target cytotoxic drugs that do. This will be tested by;

- Coupling of p700 to Doxil, liposome encapsulated doxorubicin, a chemotherapeutic agent able to kill tumour cells (but also any other dividing cells to enable specific targeting of the p700-Doxil conjugate to tumour cells expressing high levels of p700's receptors.

- Coupling p700 peptide to carboxypeptidases G2 (CPG2), an enzyme previously used in ADEPT (see section 1.10.4 above) that can convert a prodrug of nitrogen mustard containing an L-glutamate into a cytotoxic drug. This conjugate will be tested for its ability to retain receptor binding and enzyme activity.
- Lastly by introducing six residues from TIMP3 C terminus previous shown in our lab to show binding activity with VEGFR2 into the C-domain of TIMP4 of a recombinant protein with TIMP3 N terminus. The recombinant protein will be expressed in mammalian cells for inhibition of VEGFR2. If this confirms the importance of these residues, it may aid the rational design of new small molecule drugs to target this family of receptors.

CHAPTER 2

General Methods

2.1. Methods

2.1.1. Transformation *E. coli*:

50 µl of aliquots of chemically competent *E. coli cells* retrieved from -80°C were thawed on ice, after which 150 ng of DNA was added to the cells and mixed gently. The mixture was then heat shocked at 42°C for 45sec and then reincubated on ice for 2 mins. The cell mixture was transferred into a microfuge tube containing 500 µl LB broth preheated to 42°C. The mixture was incubated at 37°C with agitation for 1 h. Afterwards, the bacteria mixtures were spread on LB agar containing 100 µg/ml of carbenicillin or 50 µg/ml kanamycin, as required, and incubated overnight at 37°C.

2.1.2. Bacterial suspension culture:

After transformation, single colonies from the agar plate were picked and added to 4 ml of sterile LB broth containing 100 µg/ml of carbenicillin or 50 µg/ml kanamycin and incubated at 37°C overnight with agitation. These were used directly for small scale (miniprep) plasmid preps (in 5 ml LB) or used to inoculate a pre-culture (10ml LB) for maxi- plasmid preparations (200 ml cultures).

2.1.3. Small scale (Miniprep) and Large scale (Maxiprep) plasmid DNA purification:

Using GenElute™ Plasmid Miniprep kit, plasmid DNA was extracted from 1.5 ml of each miniprep culture following the manufacturer's instruction. Briefly, the steps include the following; bacterial cells from the cultured broth were centrifuged at 13000 rpm for 10 mins and the LB broth was aspirated leaving the bacterial pellet. The pellets were each resuspended in 200 µl of solution containing RNase. This was followed by lysis of the cells and denaturation of bacterial proteins and DNA using 200 µl of SDS/NaOH solution, followed by addition of 350 µl of acetate buffer for rapid neutralisation. The proteins and chromosomal DNA that precipitated were then removed by centrifugation at 12000 rpm for 20 mins and the supernatant were gently poured into a spin column and centrifuged at

12000 rpm for 1 min to bind the plasmid to the silica gel in the column followed by elution with dH₂O.

The GenElute™ Maxiprep kit works in the same way as the GenElute Miniprep kit but using larger volumes of reagents, according to the manufacturer's protocol. However, the Qiagen Endofree plasmid kits, which were used for mammalian cell transfections, use a slightly different principle in that the precipitated material is removed using a filter and plasmids are bound to an ion-exchange resin, rather than silica, and then eluted in high salt buffer. Briefly, the bacteria pellet was re-suspended in 10 ml of buffer P1 and gently vortexed before adding 10 ml of buffer P2 to lyse the cells. The tubes were inverted for 4-6 times and incubated at room temperature for 5 mins. 10 ml of buffer P3 was added to the lysate and mixed thoroughly by inversion after which the solution was poured into the Qiagen filter cartridge and incubated at room temperature for 10 mins. The plunger was inserted gently to filter out the lysate into a 50-ml tube. 2.5 ml buffer ER was added and incubated for 30 min on ice. Buffer QBT (10 ml) was added afterwards to equilibrate the tip and was emptied by gravity. Filtered lysate was then applied and allowed to enter the resin by gravity. Qiagen tip was then washed twice (30 ml each) using Buffer QC. The DNA was then eluted with 15 ml QN elution buffer and precipitated with 10.5 ml isopropanol. The solution was mixed and centrifuged at 15,000 rpm for 30 min at 4°C and the isopropanol was decanted. The pellet was washed with 5 ml 70% ethanol and centrifuged as above for 15 min. The DNA was finally reconstituted in endotoxin free water at room temperature.

2.1.4. Restriction enzyme digestion of plasmid DNA:

Insertion of the cDNA sequences of choice into vectors was done by using compatible restriction enzymes to digest both plasmid and cDNA according to the manufacturer's instruction. One step digestion was used since all restriction enzymes used had

compatible reaction buffers. The concentration of enzyme used was never greater than 10% of the final digest volume to avoid star activity which can be caused by high concentrations of glycerol.

2.1.5. Agarose gel electrophoresis for DNA analysis or purification:

As required, a specific amount of DNA (usually 1 µg) was mixed with 6X DNA loading buffer (Promega) to make 1X concentration of loading buffer each time. The samples were then loaded into the wells of the agarose gel (0.8-1% as required). A predefined molecular weight marker (Hyperladder I™, Bionline) was included in the first lane of the gel. The gel was run at a constant voltage of 80 V until the Orange G dye was approximately two-thirds of the way down the gel and then the bands were visualised and recorded using a Bio-Rad Gel Doc EZ. A UV transilluminator (Spectroline, TX-312A) was used to visualise bands for excision, minimising ultraviolet exposure time to limit damage to the DNA. The visibility was achievable due to the presence of EtBr in the gel which binds to DNA and fluoresces under ultraviolet light

DNA was purified from excised bands using the GenElute™ Gel Extraction kit, following the manufacturer's instructions. Briefly, the desired bands were excised and weighed. The excised slices were then dissolved in 3X v/w of solubilisation solution followed by heating for 10 min at 50°C and gently vortexing every 3 mins until the gel dissolved. A volume (equivalent to one slice of the gel) of isopropanol was added to the dissolved mixture which was then loaded onto a silica spin column and then centrifuged to bind the DNA. DNA on the spin column was then washed in the supplied wash buffer to remove contaminants and the DNA eluted using the Tris elution buffer.

2.1.6. Ligation of DNA

Forty nanograms of digested vector was used for the ligation of inserts at a molar ratio of 3:1 of insert to vector. This was calculated using the formula;

$$\text{Insert (ng)} = \frac{\text{vector (ng)} \times \text{insert size (Kb)}}{\text{vector size (Kb)}} \times \frac{\text{insert}}{\text{vector}} \text{ ratio}$$

The reaction was prepared using the calculated amount of the vector and insert, T4 DNA ligase and T4 DNA ligase buffer, and water used to make up the solution to 20 μ l. The mixtures were incubated for 2 hs at 4°C followed by incubation for 18 hs at 16°C. 10 μ l of ligation mix was then used to transform 50 μ l of competent cells (section 2.1.1).

2.1.7. Verification of ligated constructs:

Plasmid DNA was digested with appropriate restriction enzymes to confirm the insertion of cDNA sequences into the vectors and the digested DNA run on 1% agarose gels and compared to the Hyperladder I reference. The sequence of successfully ligated inserts was then determined by automated DNA sequencing using an Applied Biosystems 3730 DNA sequencer and specific primer that anneals at the desired region. Maxipreps (section 2.1.3) were prepared from verified plasmids and used to transfect the mammalian cells (section 6.2.5).

2.1.8. Methods for mammalian cell culture

2.1.8.1. H5V 4T1 and MCF-7 cell culture:

H5V cells are derived from mouse cardiac endothelial cells and express both VEGFR1 and VEGFR2. In particular, the phosphorylation of VEGFR2 in response to VEGF can readily be detected (Kanthou *et al.*, 2014). 4T1 cells are derived from a mouse mammary gland tumour and when grafted into BALB/c mice, represent a well-established animal model of metastatic human breast cancer (Tao *et al.*, 2008, Fantozzi and Christofori, 2006). MCF-7 cells are derived from human oestrogen and progesterone receptor positive invasive ductal carcinoma cells and have low metastatic potential.

H5V and 4T1 cell lines were grown in DMEM high glucose (4.5g/L) media (for H5V) containing 1:1 potassium penicillin/streptomycin sulphate solution (stock 10000U/ml) at 10 μ L/ml, 10% FBS, 2 mM L-glutamine and 56 mM of sodium bicarbonate (NaHCO₃)

at 37°C and 5% CO₂. MCF-7 cells on the other hand were cultured in Dulbecco's Modified Eagle Medium (DMEM-F12) that was supplemented with 10% FBS, 1% penicillin/streptomycin, non-essential amino acids (0.1 mM), Insulin (10 ug/mL) and Sodium pyruvate (1 mM).

Primary human dermal microvascular endothelial cells (HuDMECs) used in this study were obtained from PromoCell, Heidelberg, Germany. HuDMEC cells were grown in endothelial cell growth medium, supplemented with 5% FCS, 1 µg/ml hydrocortisone, 10 ng/ml EGF and 0.4% Endothelial Cell Growth Supplement/Heparin (ECGS/H) at 37°C and 5% CO₂.

2.1.8.2. Passaging of mammalian cell lines:

All cells were grown in T75 flasks and maintained until they were between 80-90% confluent after which they were passaged. Briefly, the cells were initially washed using DPBS followed by detachment from the flask using 3 ml of prewarmed sterile trypsin and incubating at 37°C for 5-8 mins. The action of trypsin was stopped by adding 3 ml of complete medium. The cells were harvested and centrifuged at 500 g, and then the cell pellets resuspended in 3 ml of growth medium. Part of the cell suspension was seeded into T75 flasks containing 10 ml of fresh medium or, when required, frozen (see below).

2.1.9. Cryopreservation of cells

Cells were cryopreserved by resuspending at $1 \times 10^6 \text{ ml}^{-1}$ in FBS containing 10% DMSO in a 1 ml cryovial. Cells were then slowly frozen to -80°C by placing the vials in an insulated box (MR freeze) in a -80°C freezer for at least 24 hrs before transfer to liquid nitrogen. To thaw frozen cells, cryovials from the freezer or liquid nitrogen were retrieved and defrosted at 37°C before resuspending in complete growth medium and culturing as described above

2.1.10. Determining protein concentration:

Protein concentration was determined using the bicinchoninic (BCA) method prior to western blotting to ascertain that equal amounts of protein was loaded into each well of the sodium dodecyl sulphate polyacrylamide electrophoresis (SDS-PAGE) gels. A standard curve was plotted from six different concentrations of bovine serum albumin (BSA) ranging from 0 - 1 mg/ml. For test protein samples, each sample to be tested contained 10% protein and 90% 1X sample buffer (not containing bromophenol blue). 25 μ L of each standard or sample was pipetted into wells of 96-well plates in triplicate and to each well, 200 μ l of a solution containing BCA and 4% copper II sulphate (50:1) present was added. The standard curve plotted was used to estimate the protein concentration.

2.1.11. SDS-PAGE

2.1.11.1. Gel preparation:

Gels containing 7.5% or 10% acrylamide and 1.5 mm thick were prepared using the reagents in Table 2 below. After preparation of the resolving gel, the mixture was poured immediately into the assembled plates. Water saturated butanol was gently pipetted onto the top of the gel to remove bubbles and level the gel. Once the resolving gel was set, the butanol was carefully decanted and the top of the cast was rinsed with water about 3 times. Excess water was carefully removed with filter paper. The stacking gel was prepared as below and a 1.5 mm comb inserted until the gel set. The comb was then removed prior to loading the gel.

Table 2.1 Preparation of SDS-PAGE gels for western blot

| Component | 7.5% | 10% | (Stacking) 4% |
|--|-------------|------------|----------------------|
| Resolving Gel Buffer (1.5 M Tris-HCl, pH 8.8) (ml) | 2.5 | 2.5 | - |
| 40% Acrylamide-Bis Solution 37.5:1 (ml) | 1.88 | 2.5 | 1 |
| dH ₂ O (ml) | 5.45 | 4.85 | 6.36 |
| Stacking Gel Buffer (0.5 M Tris-HCl, pH 6.8) (ml) | - | - | 2.5 |
| 10% SDS (μl) | 100 | 100 | 100 |
| 10% Ammonium Persulphate APS (μl) | 50 | 50 | 50 |
| TEMED (μl) | 25 | 25 | 25 |

2.1.11.2. Electrophoresis:

For the gel electrophoresis, equal amounts of the quantified proteins (20-50μg) were pipetted into microfuge tubes and 2X sample buffer added to give a 1X final concentration and the samples loaded into the SDS-PAGE gels prepared as above. Novex Sharp Pre-stained standard protein ladder was loaded into the first lane in order to allow estimation of the molecular weight of bands. The samples were run in a tank containing 1X running buffer at 80 V for 20 mins followed by 120 V for 1 h, until the tracking dye was about 1 cm from the base of the gel.

2.1.12. Western blotting

2.1.12.1. Semi-dry Protein transfer onto nitrocellulose membrane:

Protein transfer was carried out after electrophoresis using the Trans-Blot® Turbo™ Blotting System and Nitrocellulose Transfer Packs, following the manufacturer's instructions. Briefly, each gel was placed on a nitrocellulose membrane that was pre-soaked with CAPS transfer buffer and the membrane was sandwiched in a cassette

containing two buffer-saturated ion reservoir stacks. The assembled apparatus was then run at 1.3 A and 25 V for one mini gel or 2.5 A and 25 V for two mini gels for 7 min.

2.1.12.2. Blocking of Nitrocellulose membrane:

After successful transfer of the proteins, the membrane was blocked with 20 ml of blocking buffer (5% skimmed milk solution in TBST) on a shaker at RT for at least 6 hours. This was done to prevent non-specific binding of the antibodies to be used in subsequent steps.

2.1.12.3. Antibody probing for protein identification:

The Nitrocellulose membrane was incubated at 4°C overnight on a shaker with the stated primary antibody in blocking buffer. Afterwards it was rinsed in TBST 5 times for 5 mins each wash to remove unbound antibody. The membrane was incubated in a secondary antibody conjugated to horseradish peroxidase (HRP), prepared in blocking buffer, at RT for 1 h on a shaker. The membrane was washed 5 times in TBST as above.

2.1.12.4. Protein band detection and blot development:

The secondary antibody was detected using the LumiGLO Reserve Chemiluminescent Substrate Kit according to the manufacturer's instruction. The reagent was added directly to the membrane, after removing excess TBST, and left to react for about a min. The excess reagent was gently drained and the blot placed in cling film then in a light-proof cassette. Film (Amersham Hyperfilm ECL 5x7inches) was placed on the blot and exposed in the film cassette for 30 secs to 15 mins depending on the intensity of the bands. Following exposure, the film was placed in developing solution until the bands appeared (usually about 1-3 mins) then washed under running water. The developing solution was prepared by adding 100 ml of developer (Carestream® Kodak®-Sigma-Aldrich) to 900ml of water (1:9) and stored at RT in the dark. The film was transferred into fixing solution for 30 secs then washed under running water.

2.1.12.5. Stripping of blots for reprobing:

To avoid repeating electrophoresis and protein transfer steps with the same samples, some blots were stripped with stripping buffer and then reprobed with a different antibody (although sensitivity is reduced). This was done by incubating the previously processed blot in stripping buffer at 50°C for 30 mins. The membrane was then rinsed 5 times in TBST for 10 mins each wash and then blocked probed as described above (sections 2.1.12.2).

2.1.13. MTS Cell Proliferation Assay

The CellTiter 96® AQueous One Solution Cell Proliferation Assay is a colorimetric method for determining the metabolic activity of cells based on the ability of NAD(P)H-dependent cellular oxidoreductase enzymes in the cell to reduce a tetrazolium dye; 3-(4,5-dimethylthiazol-2-yl)-5-(3-carboxymethoxyphenyl)-2-(4-sulphophenyl)-2H-tetrazolium (MTS) in the presence of an electron coupling reagent, phenazine ethosulphate (PES) to a soluble coloured product. The method can be used to determine relative numbers of viable cells in, for example, cell proliferation or cytotoxicity assays.

The viability assays were performed by addition of a small amount of CellTiter 96® AQueous One Solution Reagent (20µl) into culture wells, followed by incubation for 3 h. The absorbance of the wells was recorded at 490nm with a 96-well plate reader. For each cell line, all experiments were repeated three times in six wells of each 96 well plates. Wells containing media-only were used to establish background absorbance. All data were analysed by Microsoft Excel and the background absorbance was subtracted from each value obtained in test wells before the results were graphically presented using GraphPad Prism software (v7.0).

CHAPTER 3

Coupling of p700 peptide to PEGylated liposomal doxorubicin (Doxil[®])

3.1. Introduction

Doxorubicin (Dox) is an anthracycline derivative that has been used as an anticancer chemotherapeutic in many different forms of human cancer, including breast cancer, soft tissue sarcomas, multiple myeloma and some leukaemias. Dox's mechanism of action primarily involves intercalation of both chromosomal and mitochondrial DNA and inhibition of topoisomerase II, an enzyme that relaxes the DNA making it accessible to DNA polymerase, thus inhibiting DNA replication. However, Dox binds to many cellular proteins in addition to topoisomerase, and also results in free radical production, increasing DNA damage and activation of apoptosis (reviewed in Westman *et al.* (2012)).

Dox has been used successfully for cancer treatment over many years; however, the application of the drug is limited due to a wide range of serious side-effects, such as liver and kidney damage and cardiotoxicity (Tacar *et al.*, 2013), and these restrict dosing regimens and, therefore, potential efficacy.

Novel drug delivery systems have since been employed in an attempt to limit such toxicity and improve targeting of these drugs. For instance, there is numerous evidence in the literature that encapsulation of cytotoxic drugs in liposomes helps alleviate the side effects and at the same time improves delivery (Brown and Khan, 2012, Meng *et al.*, 2016, Leriche *et al.*, 2017). In fact, encapsulation of Dox in PEGylated (polyethylene glycol-coated) liposomes (e.g. Doxil®/Caelyx®) has been demonstrated to improve its delivery and minimise side effects (Green and Rose, 2006, Shoji *et al.*, 2014) by decreasing uptake by the mononuclear phagocyte system in the liver and spleen, greatly increasing circulation time and decreasing cardiotoxicity. Localisation is dependent on micelle size, preventing penetration of normal tissue, but allowing accumulation in cancer tissue with its abnormal, leaky vasculature. This is known as the enhanced permeability and retention (EPR) effect of tumours (Maeda, 2012). However, one of the side-effects

of Doxil® is palmar planter erythrodysesthesia (PPE or hand-foot syndrome, a skin condition that particularly affects these limbs), probably due to increased circulation times resulting in accumulation of liposomes in capillaries below the skin (Patil *et al.*, 2008). For this reason, Doxil is licenced for the treatment of the AIDS-related skin cancer, Kaposi's sarcoma.

PEGylation of liposomes, however, confers the nanocarrier with poor intracellular permeabilization and slower drug release which have been previously shown to affect the efficacy of such drugs (Judson *et al.*, 2001). For this reason, modified liposomal formulations have been investigated that might enable more specific targeting of the drug to the tumour microenvironment and enhance uptake. These include the addition of peptides and antibodies that can serve as ligands to specific receptors or antigens that are uniquely expressed by tumour cells (Lukyanov *et al.*, 2004, Pan *et al.*, 2007, Wu *et al.*, 2006), as well as cytosolic/nuclear membrane penetrating peptides, such as those derived the human immunodeficiency virus type-1 (HIV-1) transactivating transcriptional factor (TAT) protein, which contains an oligoarginine sequence that facilitates cellular entry (Futaki *et al.*, 2001).

As previously alluded to, p700 alone inhibits tumour growth but fails to kill the tumour cells, which eventually regrow. In the following chapter, we showed that it is possible to couple p700 to CPG2, an enzyme that can activate cytotoxic pro-drugs, whilst still retaining its ability to bind to its target receptors. We hypothesised, therefore, that it might also be possible to couple p700 directly to a cytotoxic drug, thus localising the cytotoxic drug to the tumour tissue. This could potentially circumvent some of the disadvantages of the ADEPT type approach of immunogenicity and the need for enzyme clearance prior to administration of the prodrug.

In fact, it has been shown that it is possible to directly couple doxorubicin to cancer targeting peptides via a hydrolysable cross-linker, increasing specificity for cancer cells (Soudy *et al.*, 2013). However, there are several disadvantages of this approach. Firstly, modification in this way requires quite complex chemistry; secondly, modification of the drug may impair efficacy and, finally, the number of molecules of Dox delivered will be equal to the number of target receptors, potentially reducing dosage to below a therapeutic concentration. This approach also assumes that the targeting peptide is internalised by the cells, and this was not known for p700.

An alternative strategy would be to couple p700 to the surface of a liposomal encapsulated doxorubicin, such as Doxil®. This has several potential advantages over direct coupling. Firstly, the chemistry is potentially more straight-forward and does not modify the doxorubicin itself. Secondly, one receptor can potentially enable delivery of many molecules of doxorubicin. Thirdly, each liposome can be coated in many copies of the peptide, potentially greatly enhancing avidity to the cell. Lastly, even if the p700 peptide is not internalised by the cell, localisation of the liposomes to the cell surface may still enable delivery of a therapeutic dose of Dox.

3.1.1. Aims and objectives of the study

The aim of this chapter was to couple p700 to the surface of Doxil® and determine the effect of coupling on binding, internalisation and cytotoxicity of the Doxil-p700 complex, relative to Doxil alone, by both human and mouse breast cancer cell lines and by primary human dermal microvascular endothelial cells and a mouse endothelial cell line.

3.2. Methods

3.2.1. Conjugation of p700 peptide to PEGylated liposomal doxorubicin

Dibenzocyclooctyl (DBCO)-functionalised, PEGylated-liposomal doxorubicin (Doxil®) was commercially available from Encapsula® Nanomedicines (Brentwood TN, USA). The DBCO group covalently cross-links with azido groups at neutral pH and temperature in a highly efficient, copper-free “click chemistry” reaction, permitting efficient coupling of peptides containing azide groups to the surface of the liposome under physiological conditions (Figure 3.1).

Empty DBCO-functionalised liposomes (without doxorubicin) were also purchased for use as a negative control. Liposomes were stored at 4°C and schematic representations are shown in Figure 3.1A and B, respectively.

The lipid composition of the liposomes (with or without doxorubicin) is summarised in Table 3.1 below. Only the total lipid concentration was supplied by the manufacturer (15.96 mg/ml) and this was converted into an approximate total lipid molarity of 0.022M. As the DSPE-PEG-DBCO component comprises 1% of this, the molarity of DBCO groups was estimated to be 220µM. In the liposomes containing the active drug, (Doxil®), the doxorubicin concentration was 2 mg/ml.

Table 3.1 Lipid concentration of liposomes (with or without doxorubicin)

| | *HSPC | Cholesterol | **DSPE-PEG | DSPE-PEG-DBCO |
|---|--------------|--------------------|-------------------|----------------------|
| Molecular weight (MW) | 783.8 | 386.5 | 2790.5 | 3077.8 |
| Ratio in liposome (%) | 55 | 40 | 4 | 1 |
| Proportionally-corrected MW | 431.1 | 154.6 | 111.6 | 30.8 |
| Total lipid MW (corrected average MW of lipid) | 728.1 | | | |
| Molarity of 15.96mg/ml lipid solution | 0.022M | | | |

*HSPC = Hydrogenated soybean phosphatidylcholine

**DSPE = 1,2-Distearoyl-sn-glycero-3-phosphoethanolamine

Custom synthesis of an azide-functionalised, FITC-labelled p700 peptide, with a twelve carbon polyethylene glycol spacer (p700-FITC), and an identical control but lacking the p700 peptide sequence (control-FITC), was carried out by Cambridge Research Biochemicals (Cambridge, UK) (see Table 3.2).

Both p700-FITC and control-FITC were supplied in 1 mg freeze dried aliquots and dissolved in water to make 3.3 mM stock solutions. Stocks were then stored at -20°C.

Table 3.2 Structure of p700-FITC and control FITC

| Abbreviation | Molecular weight | Structure |
|---------------------|-------------------------|--|
| Control-FITC | 1159.5 | Azido-PEG12-Lys(5-FITC)-amide |
| P700-FITC | 3032.4 | Azido-PEG12-KIKSCYYLPCFVTSKN-Lys(5-FITC)-amide |

3.2.2. Coupling reaction

A click chemistry reaction was used to couple the p700-FITC (or control-FITC) to DBCO-Doxil® (or empty liposome). Each click reaction contained 250µl (55×10^{-9} moles) DBCO stock and 50µl (165×10^{-9} moles) of the azido-peptide stock in a 0.5 ml microfuge reaction tube. The reaction tube was then wrapped in foil and placed on a blood mixer at room temperature for at least 4 hours and then overnight at 4°C. Reaction products were stored at 4°C in the dark until dialysis.

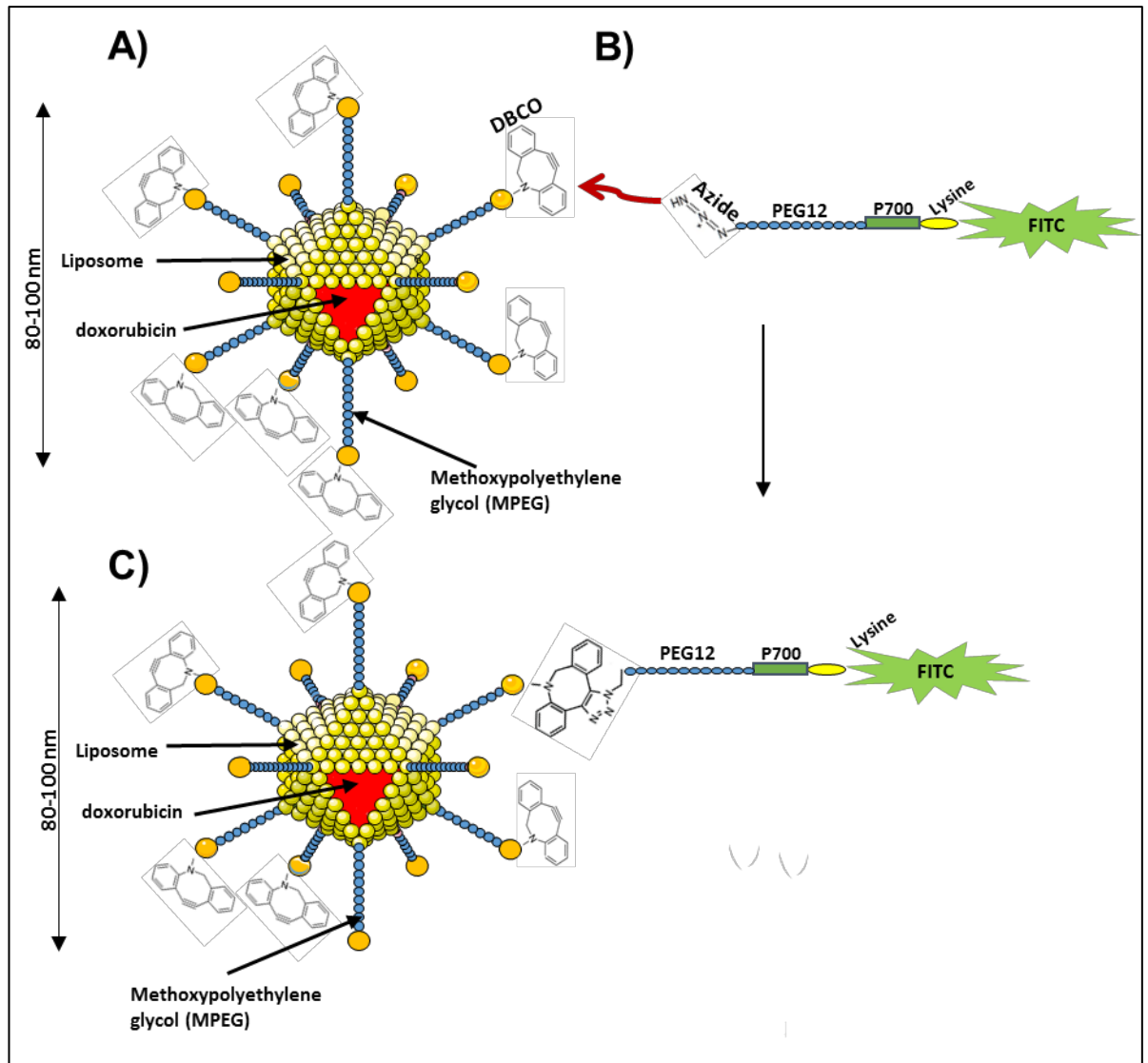


Figure 3.1 The SPAAC reaction for conjugating p700 to Doxil

PEGylated Doxil®, conjugated with DBCO (A) is linked with FITC-labelled p700 containing an azide group (B) in what is known as a strain-promoted alkyne azide cycloaddition (SPAAC) reaction, resulting in a stable triazole group linking the two components (C). Unlike conventional click chemistry the reaction does not require a copper catalyst that would be potentially toxic in biological systems.

3.2.2.1. Purification of coupled products

Separation of the coupled and uncoupled peptide and purification of the coupled products was carried out by cellulose ester membrane dialysis using the Float-a-Lyzer G2 (Spectrum® Labs USA) with a 100 KDa molecular weight cut off, according to the manufacturer's instructions. Based on their size, this process removes any uncoupled peptides from the reaction, leaving only liposomes and any coupled peptide.

Briefly, the Float-A-Lyzer G2 device was first soaked in 10% ethanol and then thoroughly flushed and soaked in H₂O before dialysis to remove the glycerine present on the membrane. The reaction sample (300 µl) was then carefully loaded into the bottom of the dialysis chamber and the device re-capped to create a closed seal. A floatation ring was then attached to the device and it was placed in a beaker containing 1 litre of PBS, which was gently mixed on a magnetic stirrer. Dialysis was performed at 4°C against three changes of 1 L PBS after 4, 6 and 12 hs.

After dialysis, the cap was removed and the total sample in the inner chamber retrieved using a pipette. Final volumes following dialysis were variable and made up to 500 µl with PBS. Based on a starting volume of Doxil of 250µl, and assuming all of the DBCO groups reacted with the azido-peptide, the final concentration of p700 in the final coupled stock was estimated to be 110µM, with a final doxorubicin concentration of 1mg/ml (1.7mM).

Purified stock conjugate solutions were stored at 4°C in the dark and used within 2 weeks.

3.2.3. Confirmation of coupling by flow cytometry

Flow cytometry was used to confirm coupling of FITC-labelled peptide to liposomal doxorubicin. Briefly, 30 µl of the post-dialysis sample was diluted in a 1:10 ratio with PBS and assayed using a BD LSR II flow cytometer.

Samples were excited using the blue laser at an excitation wavelength of 488nm and emissions of 530 nm and 575 nm were used to detect green fluorescence (FITC) and red auto-fluorescence (doxorubicin), respectively. Uncoupled, empty liposomes were used to set the negative values for both channels, and uncoupled Doxil® was used as a positive control for the red channel and p700-FITC as a positive control for the green channel. Data was analysed using FlowJo software.

3.2.4. Confirmation of cellular binding of p700-conjugated liposomal doxorubicin

Cellular binding of the p700-conjugated liposomal doxorubicin to the human and mouse breast cancer cell lines MCF-7 and 4T1, respectively, was evaluated by flow cytometry. The mouse cardiac endothelial cell line, H5V, which expresses high levels of VEGFR2 (Kanthou *et al.*, 2014) was used as a positive control, and primary human dermal microvascular endothelial cells (HuDMEC), were used to determine uptake by normal endothelial cells.

Cells were cultured overnight in a 6-well plate at a density of 5×10^4 per well for H5V, MCF-7 and 4T1, and 1×10^5 per well, for HuDMECs (due to their longer doubling time). To each well containing 2ml culture media, 5ul of either Doxil®-p700-FITC or Doxil-FITC stock solution (i.e. 275 nM peptide) was added and incubated at 37°C for 4 hs in the dark. The media was then removed and the cells washed once with PBS.

To detach cells, 800 µl of Accutase (SIGMA) was then added to each well and incubated for 2-3min at 37°C. Culture media (800 µl) was added to stop the Accutase action and the cell suspension transferred to a polystyrene falcon tube and spun for 5 min at 1000 rpm. The supernatant was removed and cell pellet resuspended in 300 µl FACS buffer (see appendix).

The samples were then examined on an LSR II flow cytometer using compensated-blue laser at the same excitation and mission described in Section 3.2.3 and 10,000 events

collected. Using FlowJo software, data from treated and untreated cells were plotted as side incidental light scatter (SSC) against green fluorescence. For each sample, the percentage of cells with green fluorescence intensity above that of untreated cells was then determined.

3.2.5. Confirmation to cellular uptake of p700-conjugated liposomal doxorubicin

Cellular uptake and localisation of the p700-conjugated liposomal doxorubicin (Doxil[®]-p700-FITC) by MCF-7, 4T1, H5V and HuDMEC cells was evaluated by confocal microscopy. Cells were cultured overnight in a glass 4-well chamber slide (Lab-Tek[®]II) at a density of 3×10^4 per well (for H5V, MCF-7 and 4T1) and 5×10^4 per well (for HuDMECs). To each well containing 700 μ l media, 1.75 μ l of Doxil[®]-p700-FITC; Doxil-FITC or empty liposome-p700-FITC (ie lacking doxorubicin) stock solution was added (equivalent to 275 nM peptide in each case). The cells were then incubated at 37°C in the dark for 4, 9 or 24 hours. The media was then removed and the cells washed once with HBSS to remove any phenol-red containing media, which can autofluoresce. Cells were subsequently fixed by incubating for 20 mins at room temperature with 500 μ l per well of 4% paraformaldehyde (diluted in HBSS).

Fixed cells were then washed twice in PBS followed by a 5-min incubation in 0.1M glycine (pH 7.4) at room temperature. They were then washed thrice in PBS and their nuclei stained with DAPI (diluted 1:100 in PBS) by incubation for 1-2 min at room temperature. Another wash with PBS was then performed and the plastic chamber then detached from the glass slide. Any excess PBS was removed, but the slide not allowed to dry before mounting with Prolong Gold Antifade (Life Technologies) and covering with a glass coverslip. The slides were then allowed to set overnight (in the dark) before being examined on a laser scanning (Nikon A1) confocal microscope equipped with FITC

(EX/EM 488/530 nM), Red (EX/EM 562/570 nM) and UV-Blue (EX/EM 405/480 nM).

Pictures were then further analysed using Image J software.

3.2.6. Cell viability assays

Cell viability assays using MTS were performed on the 4T1, H5V and HuDMEC cell lines. Initial experiments were performed using untreated cells seeded at different densities in order to determine their baseline proliferation rate.

Cultured 4T1, H5V and HuDMEC cells at around 80% confluence were trypsinised and then seeded at densities of 2×10^3 , 3×10^3 and 4×10^3 per well, containing 100 μ l of cultures media, in 96-well plates and incubated at 37°C as normal. MTS assays were carried out after 24, 48 and 72 hours of culture (section 2.1.13). Each seeding density and time point was set up in triplicate and three independent repeats were performed. The absorbance data was analysed and growth curves were drawn using GraphPad Prism v7.0.

3.2.7. Cytotoxicity assay

The cytotoxic effect of increasing concentrations of Doxil®-p700-FITC compared with Doxil-FITC and empty liposome-p700-FITC was evaluated using the MTS assay. Cultured 4T1, H5V and HuDMEC cells at around 80% confluence were trypsinised and then seeded at densities of 2×10^3 per well containing 100 μ l culture media in a 96-well plate and incubated at 37°C overnight as before. Based on the growth curves in Section 3.2.6 this seeding density was chosen as most appropriate for cytotoxicity assays for the 4T1, H5V and HuDMEC cell because it showed the largest magnitude of change in viable cell number with time. For MCF7 cells, however a seeding density of 4×10^3 per well was chosen based on previously published studies (Guan *et al.*, 2015).

Cells were treated with Doxil®-p700-FITC; Doxil-FITC and empty liposome-p700-FITC at 0, 2.5, 5, 10, 25, 50 and 100 μ M doxorubicin concentration (or equivalent liposome concentration for the empty liposomes) for 4 hours at 37°C, before being washed twice

with fresh media to remove any unbound drug. They were subsequently incubated for a further 24 hours in fresh media at 37°C before an MTS assay was performed as described in (section 2.1.13). Each dose level was performed in triplicate and three independent repeat experiments were completed. Statistical analysis was performed using two-way ANOVA-multiple comparison test and percentage cell viability curves were drawn using GraphPad Prism software v7.0.

3.3.Results

3.3.1. Coupling assessment

Following the coupling reaction and dialysis, flow cytometry was used to confirm coupling of the azido-FITC peptides to either empty DBCO-liposomes or DBCO-Doxil (Figure 3.2). The empty liposomes were primarily used as a control to enable confirmation of cross-linking in case the doxorubicin fluorescence of the Doxil interfered with the FITC fluorescence.

As can be seen in panel (A) for azido-p700-FITC and panel (B) for azido-FITC only, there was a pronounced shift in the green fluorescence associated with the liposomes before (blue peak) and after (green peak) coupling, indicating efficient cross-linking of both azido-molecules to the liposomes. This result was mirrored for coupling of azido-p700-FITC and azido-FITC only (panels (C) and (D) respectively) to DBCO-Doxil. Although the background green fluorescence was slightly higher for the Doxil than the empty liposomes prior to coupling (red peak), the shift following coupling (green peak) was also more pronounced, again confirming efficient coupling of both azido-FITC molecules to DBCO-Doxil.

Panels (E) and (F) compare the red fluorescence (associated with doxorubicin) of the final cross-linked products (blue peak, empty liposomes and red peak, Doxil), which confirmed doxorubicin was still present in the Doxil following coupling.

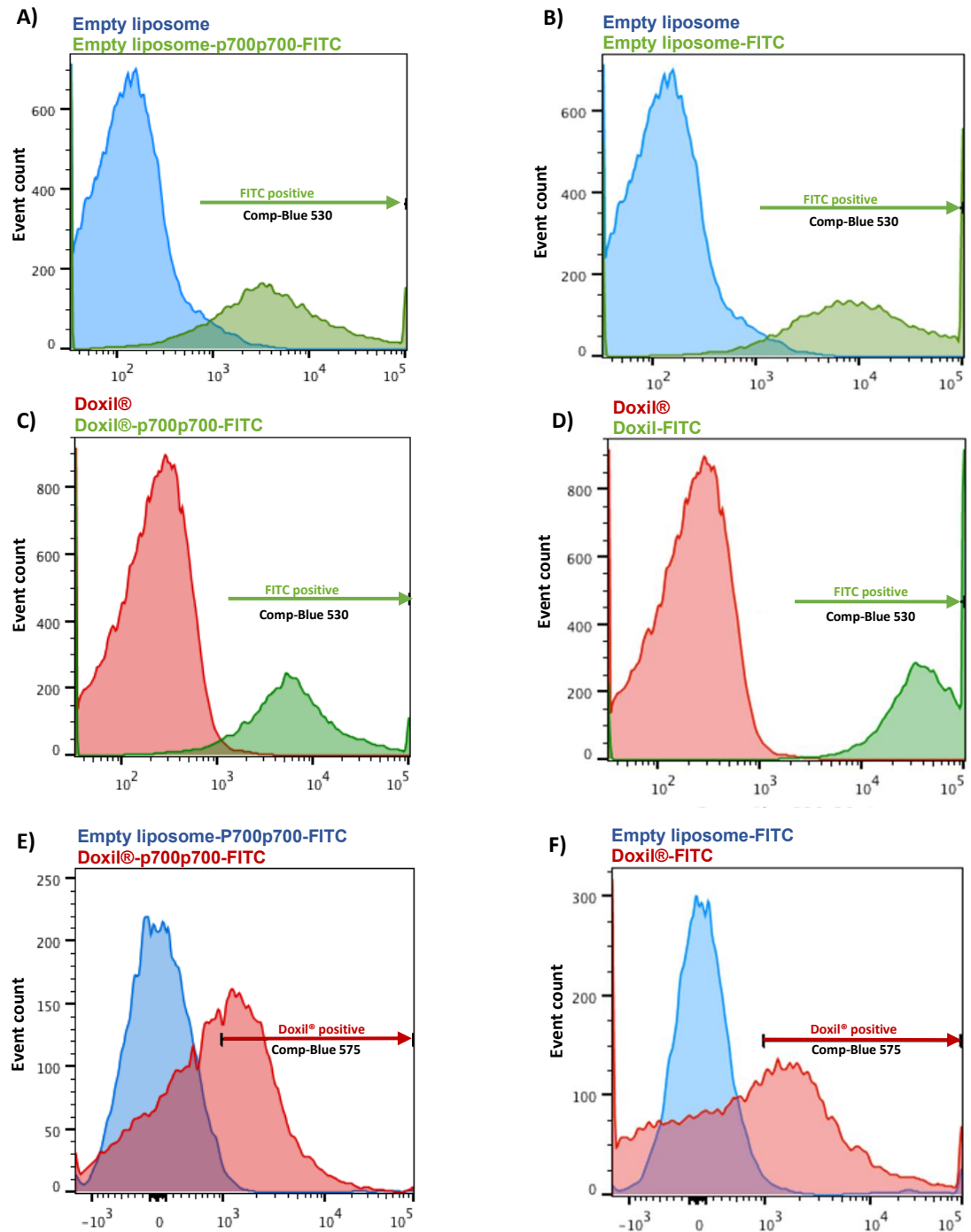


Figure 3.2. Assessment of p700 coupling to PEGylated liposome

Flow cytometric analysis of coupling of: (A) empty DBCO-liposome to azido-p700-FITC; (B) empty DBCO-liposome to azido-FITC only; (C) DBCO-Doxil to azido-p700-FITC; (D) DBCO-Doxil to azido-FITC only. Panels A-D show the shift in green (FITC) fluorescence before (blue or red peaks) and after (green peaks) coupling. Panels (E), for p700-FITC and (F), for FITC-only, compare the red (doxorubicin) fluorescence of the empty liposomes (blue peaks) versus Doxil (red peaks) following coupling, confirming the presence of doxorubicin in the coupled Doxil.

3.3.2. Binding evaluation

The next step of this study was to evaluate binding of Doxil-p700 to a panel of cell lines to determine whether p700 enhances binding of Doxil to mouse and human breast tumour cell lines (4T1 and MCF-7, respectively) or a mouse endothelial cell line (H5V) known to highly express VEGFR2, relative to normal primary microvascular endothelial cells (HuDMEC). Doxil-FITC only was used as a negative control.

As shown in Figure 3.3., Figure 3.4. and Figure 3.5., 96-99% of the MCF-7, 4T1 and H5V cells treated with Doxil-p700-FITC showed positive FITC staining, compared to 3% or less of those cells treated with Doxil-FITC only. In contrast, only about 15% of HuDMEC showed positive FITC staining with Doxil-p700-FITC (Figure 3.6), with those treated with the Doxil-FITC alone showing less than 2% positive FITC staining. This difference in staining between the cell lines and the primary microvascular endothelial cells was highly significant, as illustrated in Figure 3.7.

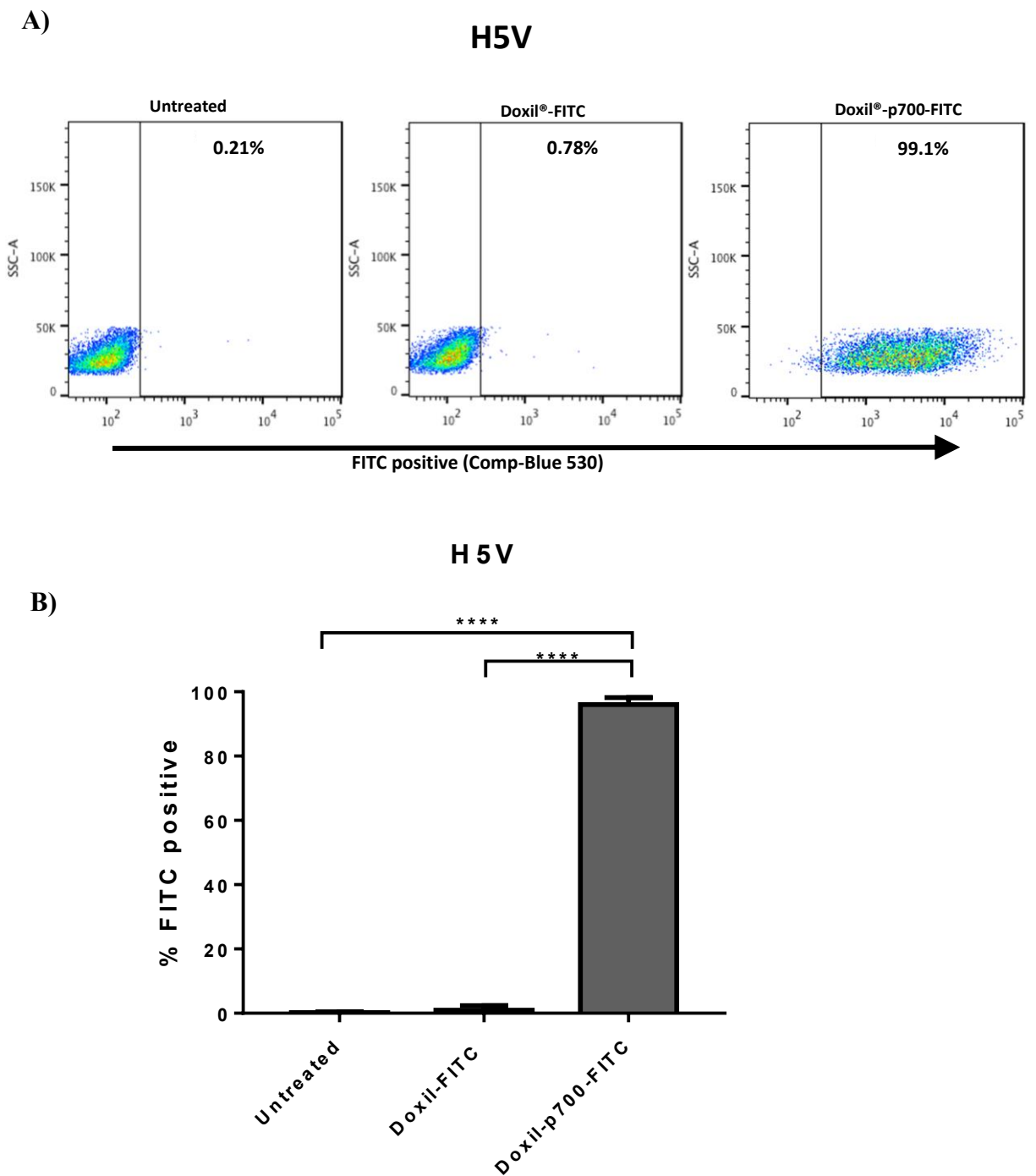


Figure 3.3 The effect of coupling p700 peptide on the binding of Doxil to the H5V mouse endothelial cell line

A) Flow cytometry of cells untreated (left panels) and treated with 275 nM Doxil-FITC (middle panels) or Doxil-p700-FITC (right panels) for 4hrs at 37°C. Percentages relate to numbers of cells with a fluorescence intensity above that of untreated cells. B) Data presented are means \pm SEM three independent repeat experiments (**** $p < 0.0001$ indicates significance, one-way ANOVA, multiple comparison test).

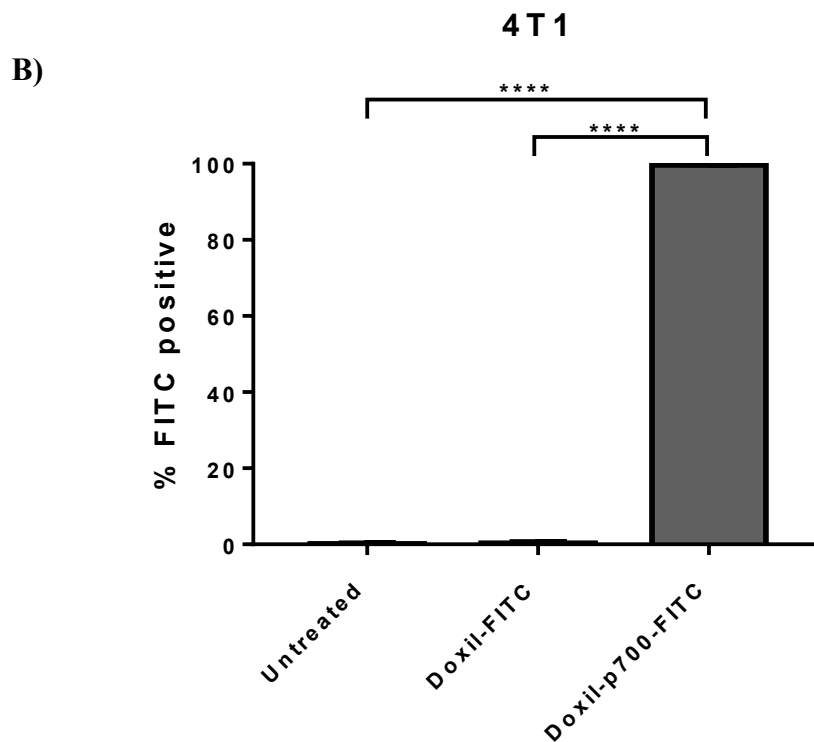
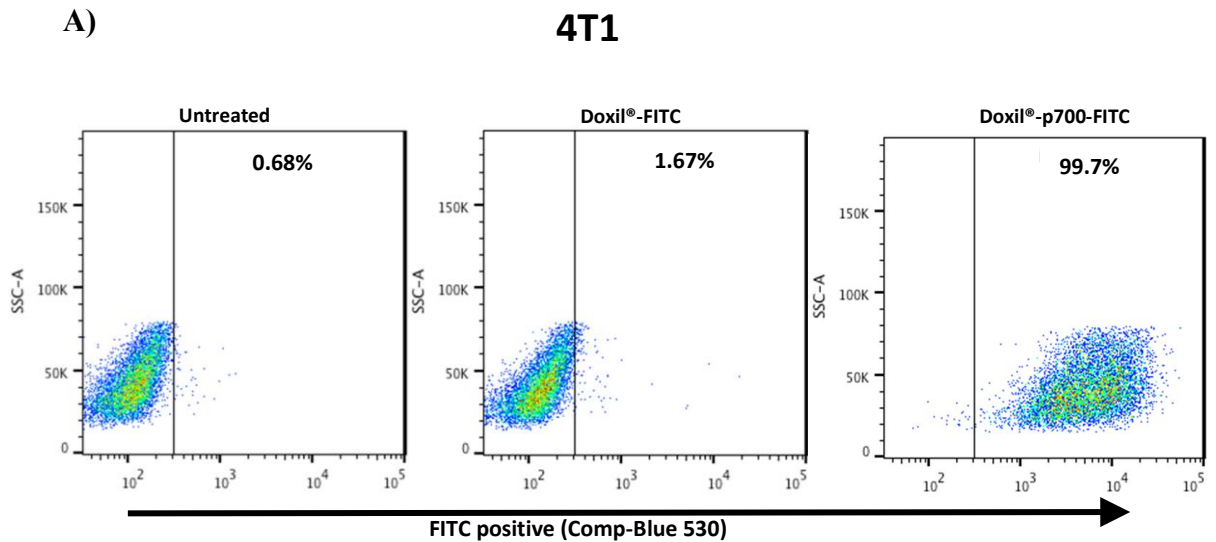


Figure 3.4. The effect of coupling p700 on the binding of Doxil® to the 4T1 mouse breast cancer cell line

A) Flow cytometry of cells untreated (left panels) and treated with 275 nM Doxil-FITC (middle panels) or Doxil-p700-FITC (right panels) for 4hrs at 37°C. Percentages relate to numbers of cells with a fluorescence intensity above that of untreated cells. B) Data presented are means \pm SEM three independent repeat experiments (**** $p < 0.0001$ indicates significance, one-way ANOVA, multiple comparison test).

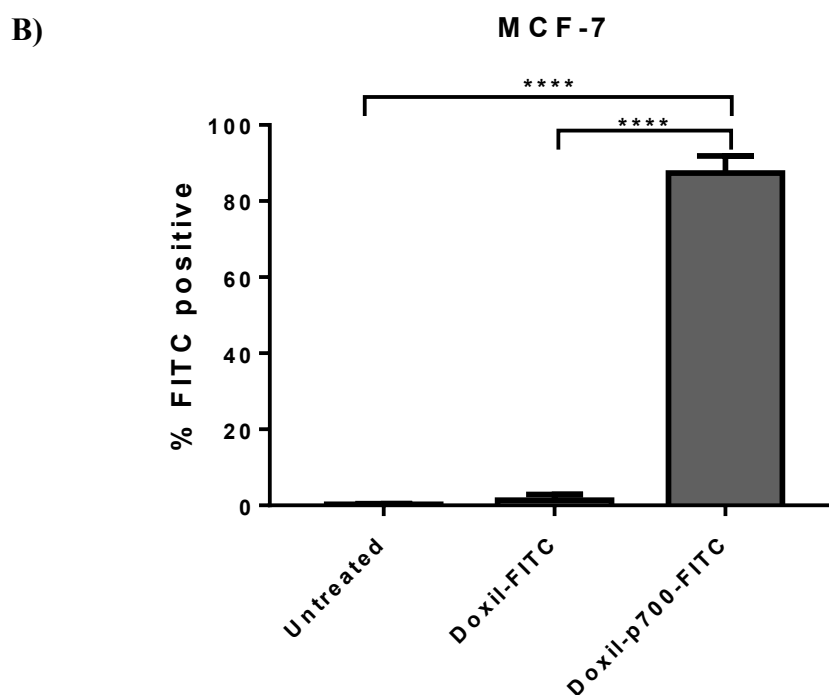
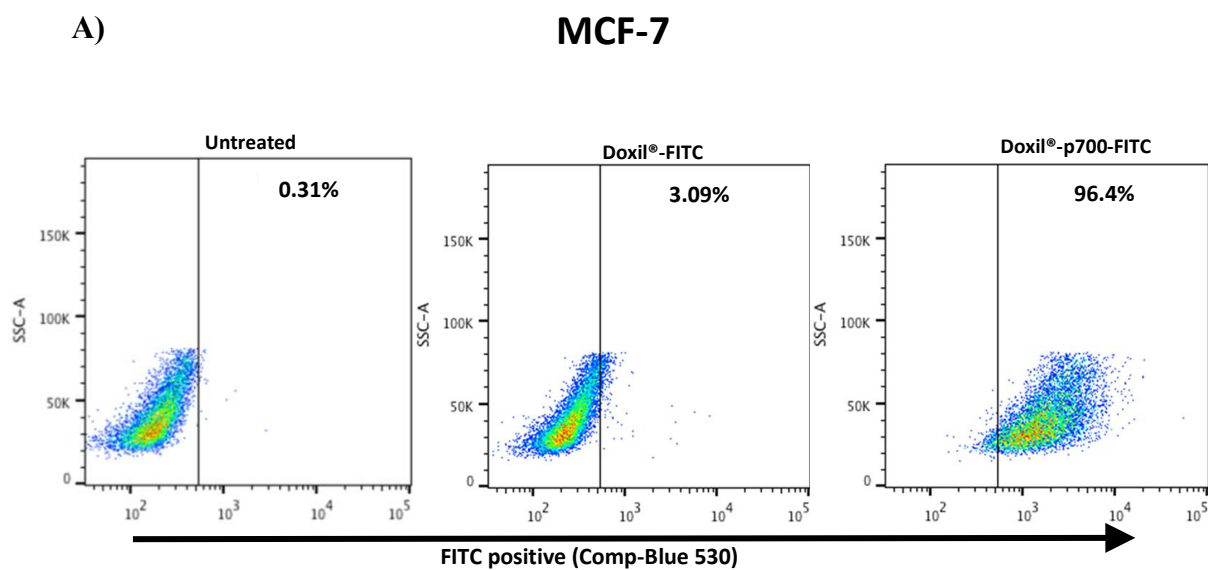


Figure 3.5 The effect of coupling p700 on the binding of Doxil to the MCF-7 breast tumour cell line

A) Flow cytometry of cells untreated (left panels) and treated with 275 nM Doxil-FITC (middle panels) or Doxil-p700-FITC (right panels) for 4hrs at 37°C. Percentages relate to numbers of cells with a fluorescence intensity above that of untreated cells. B) Data presented are means \pm SEM three independent repeat experiments (**** $p < 0.0001$ indicates significance, one-way ANOVA, multiple comparison test).

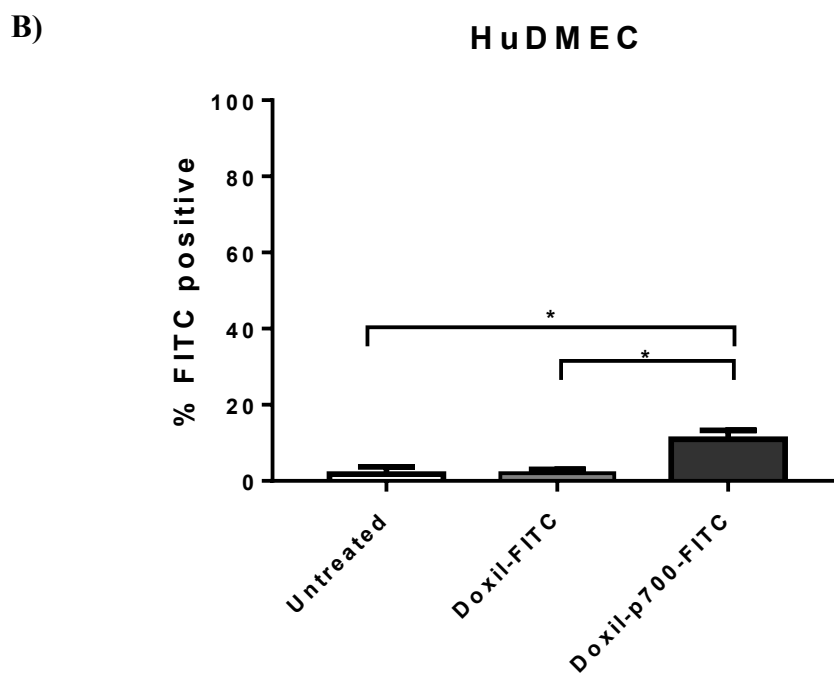
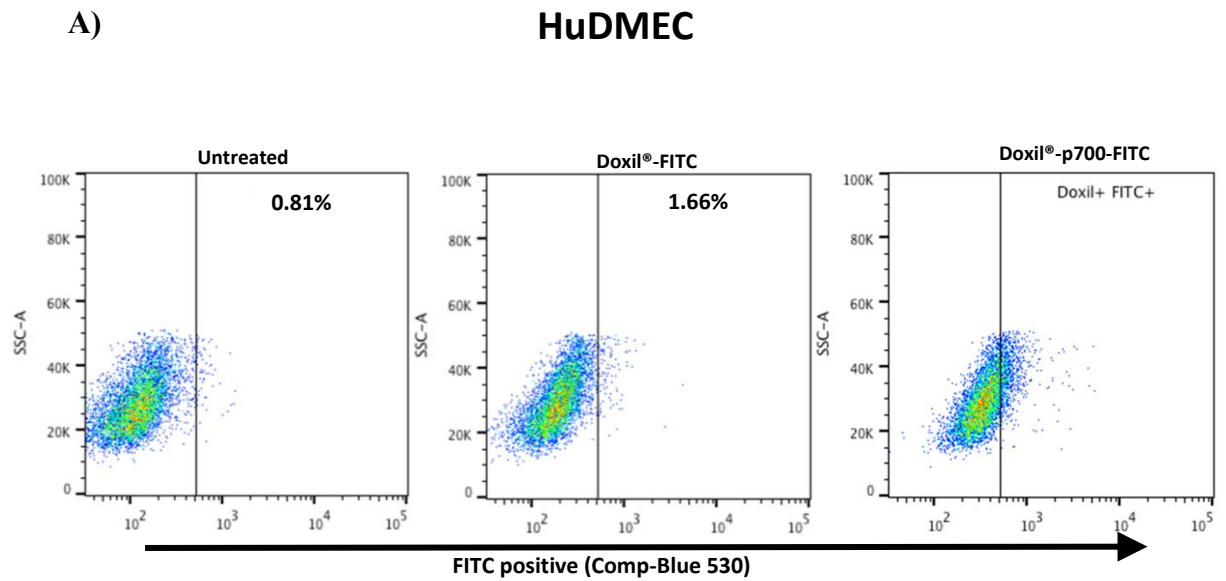


Figure 3.6 Effect of coupling p700 on binding of Doxil® to primary human dermal microvascular endothelial cells

A) Flow cytometry of cells untreated (left panels) and treated with 275 nM Doxil-FITC (middle panels) or Doxil-p700-FITC (right panels) for 4hrs at 37°C. Percentages relate to numbers of cells with a fluorescence intensity above that of untreated cells. B) Data presented are means \pm SEM three independent repeat experiments (** $p < 0.012$ indicates significance, one-way ANOVA, multiple comparison test).

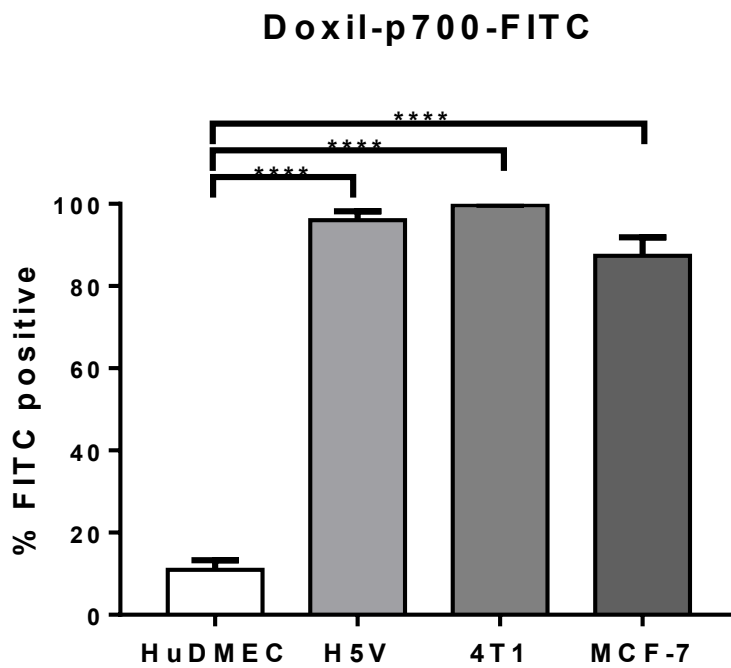


Figure 3.7 Comparison of the binding of Doxil-p700 between primary HuDMEC and the three cell lines

Data presented are means \pm SEM of three independent repeat experiments (**** $p < 0.0001$ indicates significance, one-way ANOVA, multiple comparison test).

3.3.3. Cellular uptake and internalisation

The purpose of coupling p700 to Doxil was to specifically target the cytotoxic drug doxorubicin to tumour tissue. While flow cytometry confirmed that p700 greatly enhances binding of Doxil to tumour cells and also endothelial cells that show up-regulation of target receptors, it is vital that the doxorubicin is then taken up by the cells in order to be effective. Localisation of Doxil to the cell surface may be sufficient to enhance doxorubicin uptake by the cells, however whether p700 would be internalised following binding and thus potentially facilitate cellular entry of the doxorubicin, was unknown.

To examine cellular internalisation after binding, we incubated 4T1 cells with Doxil-FITC only or Doxil-p700-FITC for 4, 9 and 24 hrs, after which cellular internalisation of both peptide (as determined by the FITC label) and doxorubicin (as determined by doxorubicin fluorescence) were evaluated using confocal microscopy (Figure 3.8).

In the absence of the p700 sequence, no FITC fluorescence was seen to be associated with the cells (Figure 3.8A) although there was some red fluorescence, presumably due to passive uptake of doxorubicin. In contrast, in cells treated with Doxil-p700 (Figure 3.8B), there was very strong FITC fluorescence, largely associated with what are presumably endosomal granules in the cytoplasm, and this co-localised with strong red fluorescence, presumed to be from the doxorubicin (observed as a yellow colour in the merged images). Fluorescence was maximal at the 9 hour time point, becoming somewhat diminished at 24 hours. The fact that the red fluorescence was indeed due to doxorubicin was confirmed by repeating the experiment with the empty liposomes coupled to p700 (Figure 3.9), where only green fluorescence was observed.

The experiment was then repeated for H5V and MCF-7 cells, but omitting the 24 h time point as the 4T1 cell line had established sufficient internalisation is achieved at 9 hs

(Figure 3.10 and Figure 3.11). Again, the p700 sequence clearly greatly enhanced uptake of FITC and doxorubicin, with no green and little red fluorescence observed in the cells treated with Doxil-FITC only, although for MCF-7 this was not quite as pronounced as for the mouse cell lines.

The experiment was then repeated using HuDMECs at all three-time points, however in this case no detectable green or red fluorescence was observed, suggesting little internalisation of the drug (Figure 3.12).

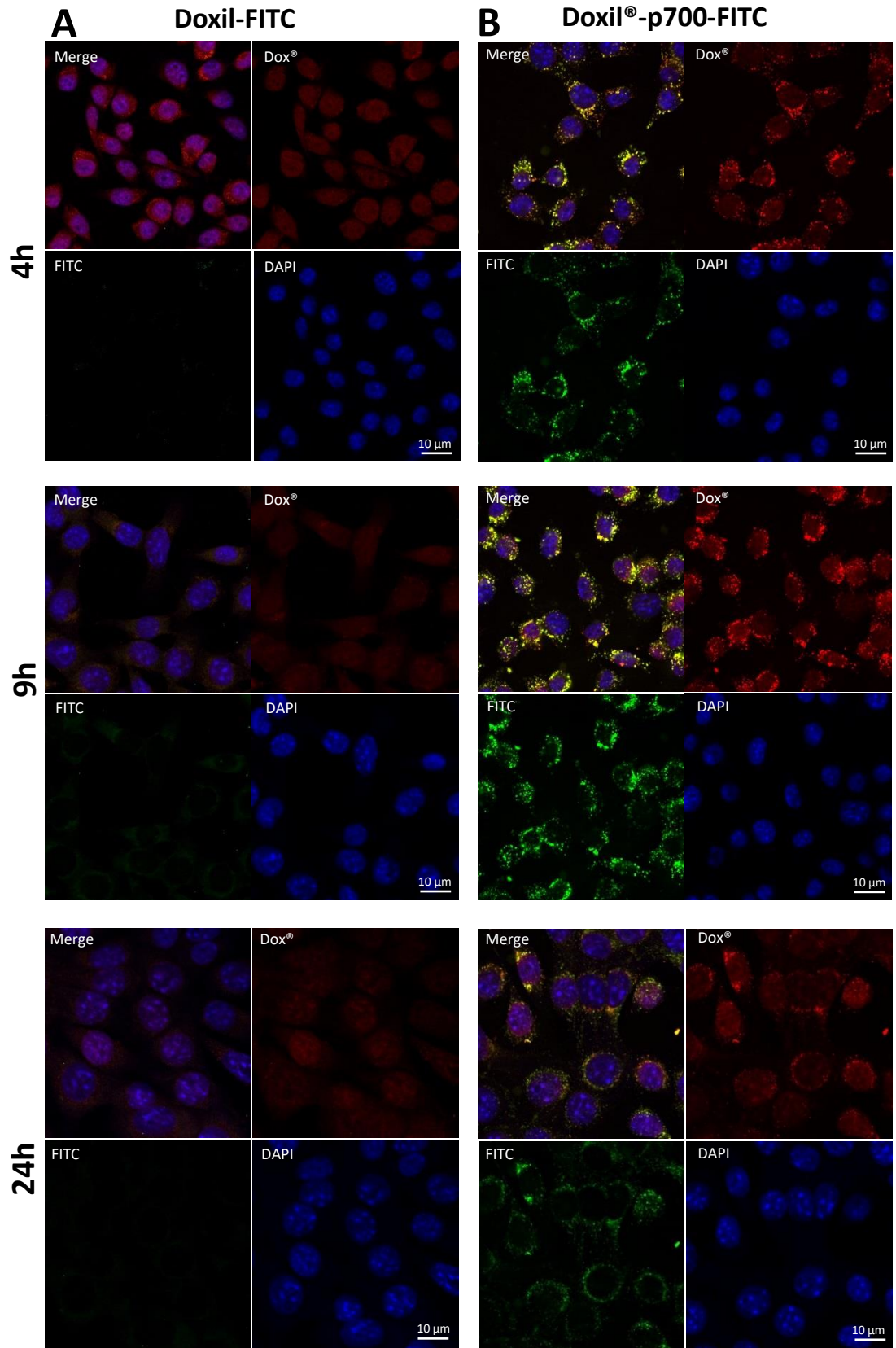


Figure 3.8 Uptake of Doxil and Doxil-p700 by the 4T1 cell line

4T1 mouse breast cancer cells were treated with (A) Doxil-FITC or (B) Doxil-p700-FITC at 275 nM for 4, 9 and 24 hs at 37°C and then imaged by confocal microscopy. Red staining is doxorubicin, green staining is FITC on the peptide conjugate and blue DAPI nuclear stain. (h) indicates hours of treatment.

Empty liposome-p700-FITC

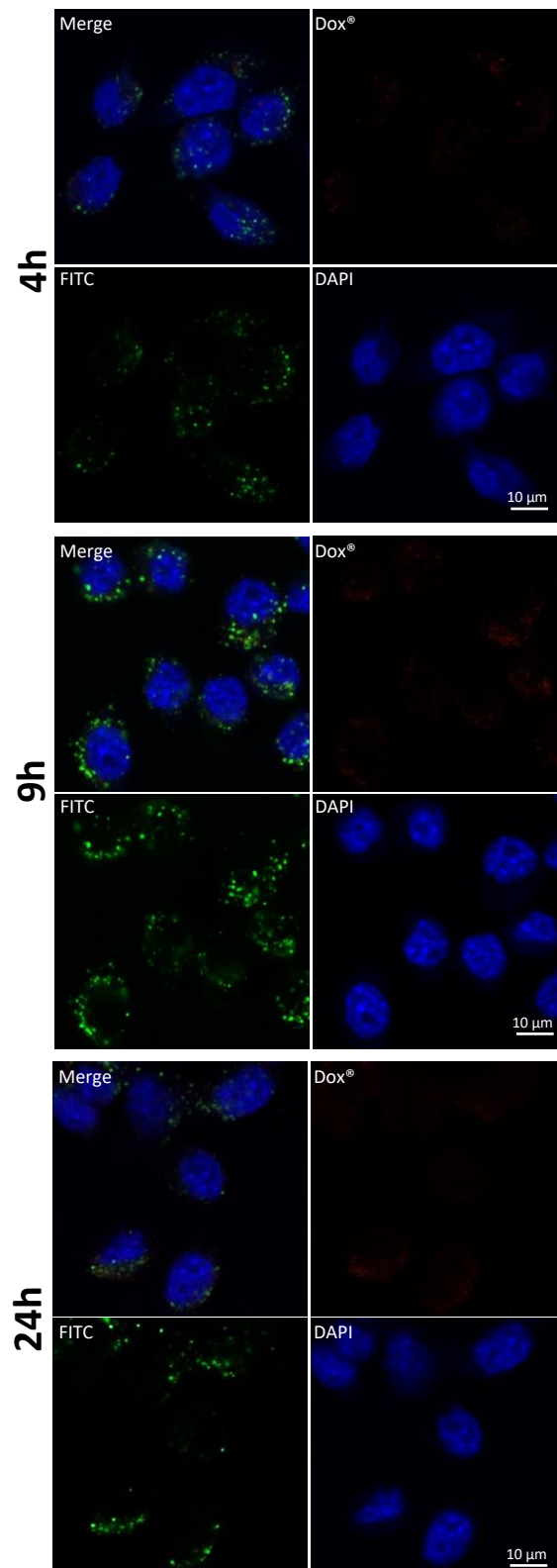


Figure 3.9 Uptake of empty liposome-p700 by the 4T1 cell line

4T1 mouse breast cancer cells were treated with empty liposome-p700-FITC at 275 nM for 4, 9 and 24 hs at 37°C and then imaged by confocal microscopy. Red staining is doxorubicin, green staining is FITC on the peptide conjugate and blue DAPI nuclear stain. (h) indicates hs of treatment.

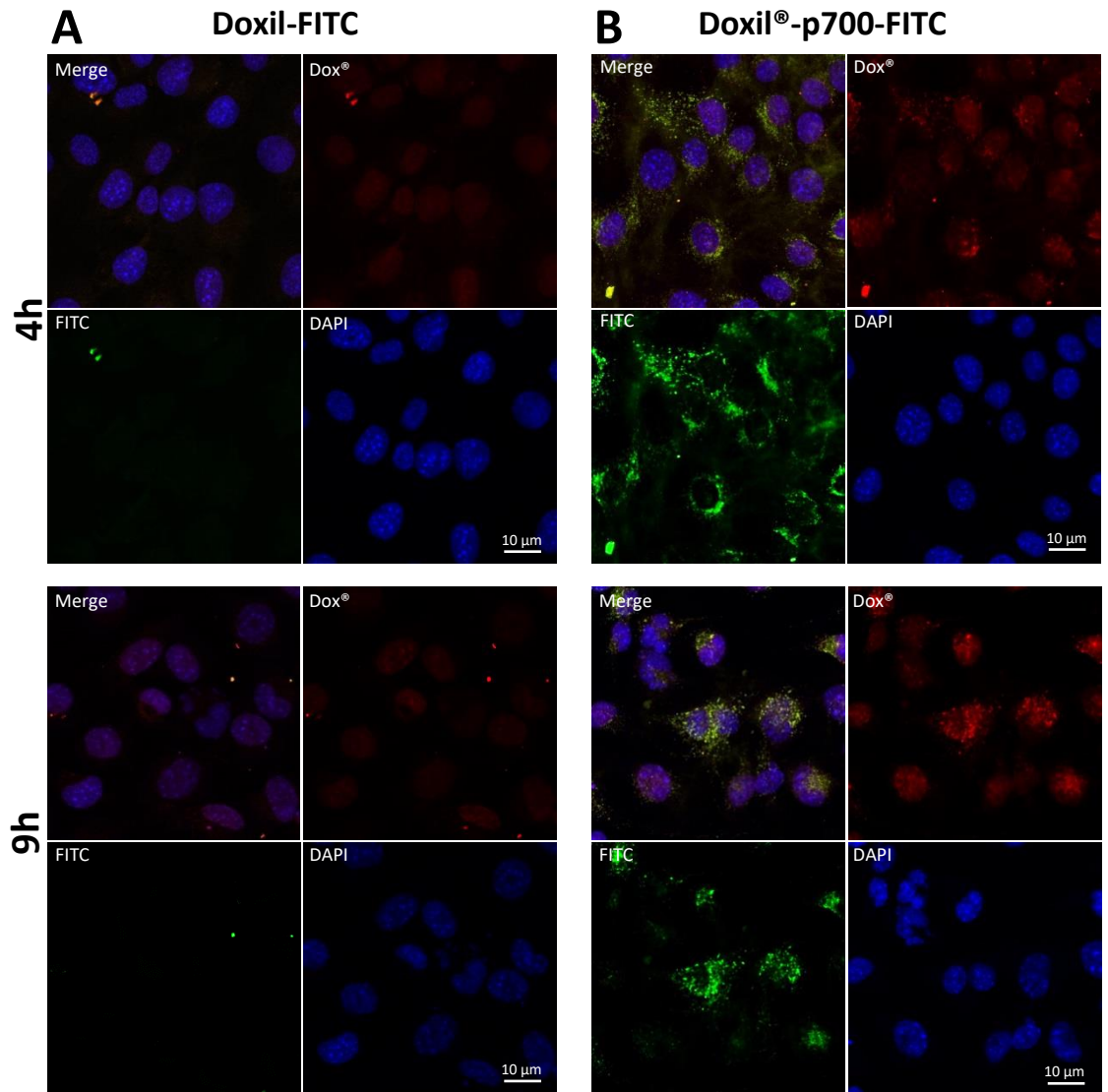


Figure 3.10 Uptake of empty p700 conjugated liposomes by the H5V cell line

Mouse cardiac endothelial cells, H5V, were treated with (A) Doxil-FITC or (B) Doxil-p700-FITC at 275 nM for 4 and 9 hs at 37°C and then imaged by confocal microscopy. Red staining is doxorubicin, green staining is FITC on the peptide conjugate and blue DAPI nuclear stain. (h) indicates hs of treatment.

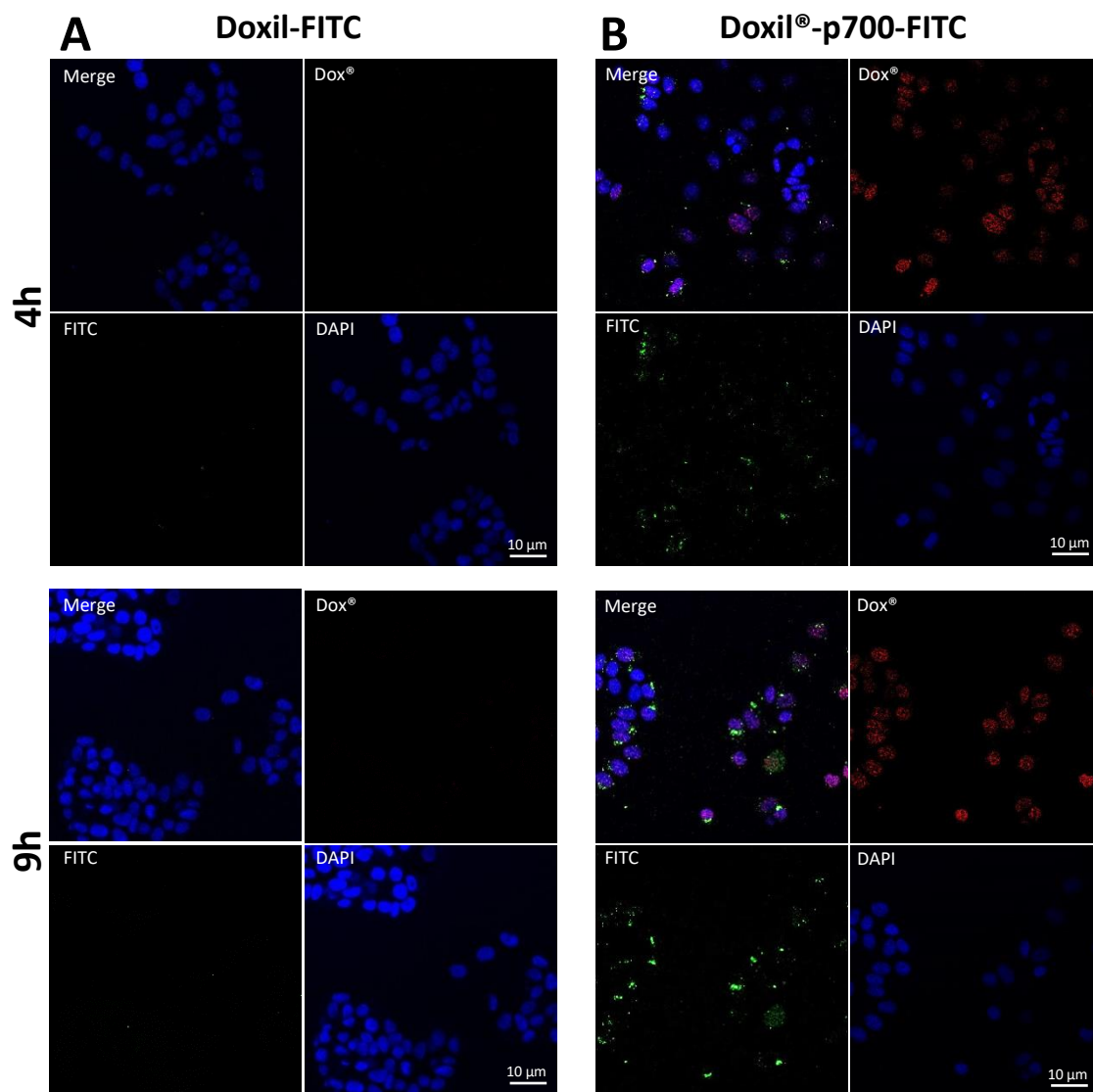


Figure 3.11 Uptake of Doxil[®] and Doxil-p700 by the MCF-7 cell line

MCF-7 breast cancer cells were treated with (A) Doxil-FITC or (B) Doxil-p700-FITC at 275 nM for 4 and 9 hs at 37°C and then imaged by confocal microscopy. Red staining is doxorubicin, green staining is FITC on the peptide conjugate and blue DAPI nuclear stain. (h) indicates hs of treatment.

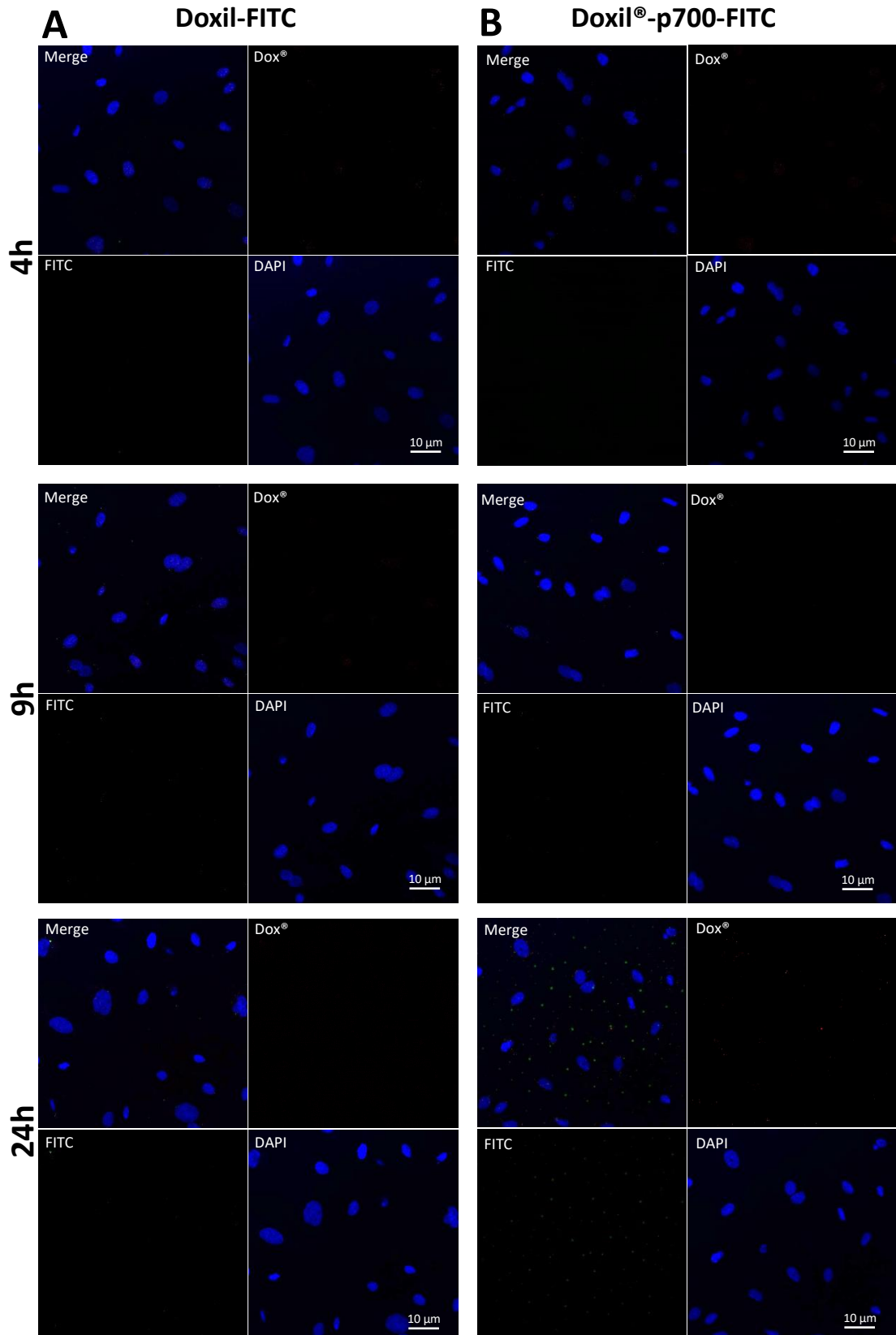


Figure 3.12 Uptake of Doxil and Doxil-p700 by HuDMEC

Primary human dermal microvascular endothelial cells (HuDMEC) were treated with (A) Doxil-FITC or (B) Doxil-p700-FITC at 275 nM for 4, 9 and 24 hs at 37°C and then imaged by confocal microscopy. Red staining is doxorubicin, green staining is FITC on the peptide conjugate and blue DAPI nuclear stain. (h) indicates hs of treatment.

3.3.4. Growth assessment

In order to establish any cytotoxic effect of Doxil®-p700 on the cell lines, it was initially important to determine an optimal seeding density in order to observe this. As such we evaluated the growth rate of H5V, 4T1 and HuDMEC cells from 0 to 72 hs at 2×10^3 , 3×10^3 and 4×10^3 cells per well of a 96-well plate. We did not carry out growth assessment for MCF-7 since its growth rate is well established in the literature (Guan *et al.*, 2015, McGowan *et al.*, 2011, Prados *et al.*, 2010). The result showed that the cell density of all cell lines at least doubled between 24 and 48 hs with 4T1 increasing three-fold (Figure 3.13). This high growth rate for the 4T1 cells resulted in some reduction in growth rate over the subsequent 24 h time period, presumably due to the cells reaching confluence and/or nutrient depletion and so for this reason the lowest seeding density (2×10^3 cell/well) was used in the subsequent cytotoxicity assays. However, we used 4×10^3 cells/ml for MCF-7 as documented in the literature (Guan *et al.*, 2015).

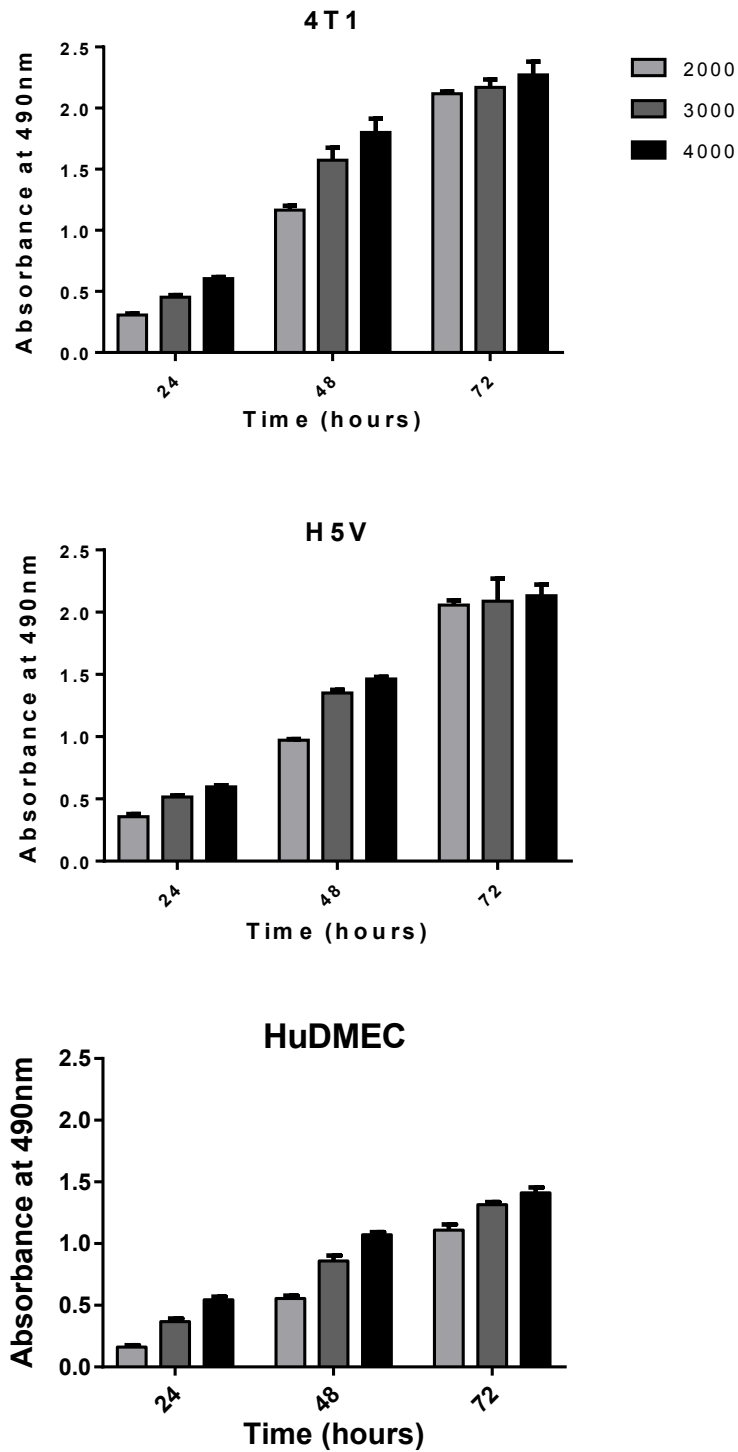


Figure 3.13 Growth rate of 4T1, H5V and HuDMEC cells over 72 h

All cell lines were seeded at 2×10^3 , 3×10^3 and 4×10^3 and incubated for up to 72 h before assessing the cell viability. Experiments were performed in triplicate and data is presented as mean \pm SEM of three independent repeats.

3.3.5. Cytotoxic effect of conjugates

The next step in the study was to evaluate the cell viability of the H5V, 4T1, MCF-7 and HuDMEC cell lines 24 hrs after a 4 hrs exposure to varying concentrations of Doxil-p700-FITC or Doxil-FITC. Empty liposome-p700-FITC was use as a control to confirm any cytotoxicity seen was due to the doxorubicin content of the Doxil and not the liposome or p700 peptide.

As shown in Figure 3.14, 4T1, MCF-7 and H5V cells treated with the highest dose of Doxil-p700-FITC all showed a significant increase in cell death, relative to both empty p700-liposomes and Doxil-FITC only. While the HuDMECs also showed a significant increase in cell death with Doxil-p700, relative to the empty p700-liposomes, this was not significantly greater than that seen with Doxil-FITC only.

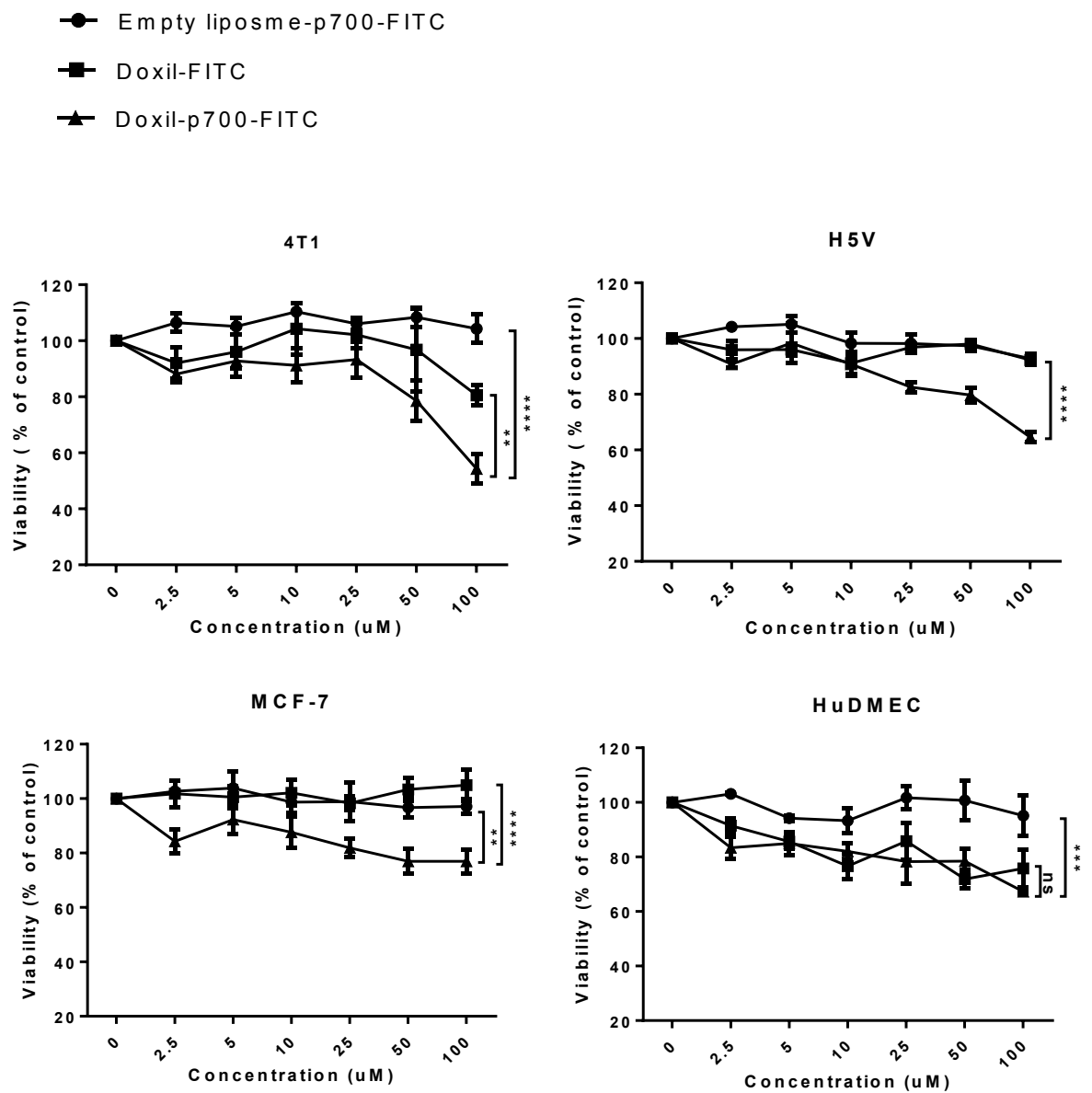


Figure 3.14 Effect of increasing concentrations of empty liposome-p700-FITC, Doxil-FITC and Doxil-p700-FITC on the viability of 4T1 (top left), H5V (top right), MCF-7 (bottom left) and HuDMEC (bottom right)

Cells were treated for 4 hrs with the stated dose of each agent, washed and then incubated for a further 24hrs in complete growth medium before performing an MTS cell viability assay. Experiments were performed in triplicate and data is presented as mean \pm SEM of three independent repeats (**= $p < 0.01$, ***= $p < 0.001$, ****= $p < 0.0001$ indicates significance, two-way ANOVA, multiple comparison test).

3.4. Discussion

Targeted delivery of liposomal encapsulated drugs, such as doxorubicin, exploits the enhanced permeability and retention (EPR) effect of solid tumours (Maeda, 2012). Usually, these liposomal drugs are found around the tumour cells and are not totally internalised into the cells (Mastrobattista *et al.*, 1999). So while liposomal encapsulation enhances tumour specificity, the stability of PEGylated liposomes can result in slow release of the liposomal content around the tumour, reducing cytotoxicity to the extent that there may be no net benefit over non-encapsulated drugs (Tseng *et al.*, 2002). In addition, drugs released extracellularly into the tumour microenvironment may not be able to overwhelm the pumping action of multidrug resistant transporters. This could possibly explain why liposomal doxorubicin only has a marginal effect on tumours that are refractory to most conventional chemotherapeutics, a notable exception being Kaposi's sarcoma, for reasons outlined earlier. As such, active transportation of the liposome into the cells is likely to greatly improve the efficacy of the stable liposomal drug.

In this chapter we sought to exploit the multi-receptor binding profile of p700 (Chen *et al.*, 2014) to target PEGylated doxorubicin (Doxil) to tumour cells. Although this is not a novel concept, p700 may offer several advantages over monoclonal antibodies in this respect due to its reduced size, ease of synthesis, low immunogenicity and ability to target multiple receptors, potentially reducing resistance. As mentioned in the introduction to this chapter, an alternative approach has been to exploit cell-penetrating peptides such as those derived from TAT (Futaki *et al.*, 2001), although such peptides are not tumour specific and so risk increased off-target effects.

For Doxil-p700 to have therapeutic potential it was important to answer a number of questions:

- Does p700 retain its ability to bind receptors after coupling?
- Does p700 enhance uptake of doxorubicin into tumour cells?
- Is any increased uptake associated with increased cytotoxicity?
- Does p700 confer specificity for tumour cells over normal cells?

The data reported in this chapter appear to affirm all of these questions. Although we had shown that linking p700 to CPG2 (Chapter 4) did not appear to affect its ability to bind target receptors, this was not assured in this case as, synthetically, it was much more practical to add the azido group to the N-terminal end of the peptide and thus couple via the N-terminus as opposed to the C-terminus used for CPG2 coupling. While we were unable to perform successful kinetic analysis of the binding of Doxil-p700 to VEGFR2 by BLItz, as we did for CPG2 (data not shown), possibly due to the fact that the liposomes are not of identical size, p700 greatly enhanced binding of Doxil to cells known to express the target receptors.

Moreover, p700 and its payload, doxorubicin, were clearly internalised into the target cells. Again, this was not at all assured prior to this work as, although there was evidence that FGFR and VEGFR2, for example, are internalised into the cell upon ligand binding, in a process facilitated by E-cadherin (Santos *et al.*, 2007, Bryant *et al.*, 2005), we had no evidence that this was also the case for the peptide. However enhanced internalisation does not necessarily equate to enhanced cytotoxicity if the doxorubicin is retained in endosomes and cannot reach the nucleus. After internalisation of liposomal drugs, the liposome is usually metabolised in the endolysosomal pathway where the liposome is degraded by the acidic medium of the lysosome (Burks *et al.*, 2015). The reduction in Doxil-p700-FITC concentration in the cytoplasm after 9 hs could be as a result of degradation of the peptide and the liposome. The fact that there was a clear enhancement

of cytotoxicity of Doxil-p700 over Doxil only, for the cell lines, indicates that at least some of the doxorubicin is then released to the nucleus.

Binding and uptake of Doxil-p700 by the human MCF-7 breast tumour cells was somewhat less than for the mouse 4T1 breast tumour cells and this may explain the reduced killing of MCF-7 relative to 4T1 tumours. However MCF-7 is also known to be resistant to doxorubicin with specific point mutations shown to confer this cell line with resistance to anthracyclines (Coley, 2008). Indeed, this is probably reflected in Figure 3.14, in which MCF-7 is the only cell line where Doxil alone is not cytotoxic, relative to the empty liposomes. The fact that Doxil-p700 does still show some killing of this cell line demonstrates the benefit of targeted delivery.

Lastly, and perhaps surprisingly, uptake of Doxil-p700 by tumour cells was much greater than for primary human microvascular endothelial cells (HuDMEC), despite the fact that these cells do bear VEGFR2. In contrast uptake by the H5V mouse endothelial cell line was much higher. This may, in part, be due to the differential expression of VEGFR2 by these cells and could be said to mimic the fact that VEGFR2 is upregulated in tumour microvasculature compared to normal tissue. It is also possible that, as a retrovirally transformed cell line (Garlanda *et al.*, 1994), H5V also bears FGF and/or PDGF receptors, which are not expressed significantly by HuDMEC. Despite this, Doxil-p700 did show significant killing of HuDMECs, relative to the empty liposomes. However, this probably reflects the fact that primary cells lack some of the drug resistance mechanisms of tumour cells and in fact the level of killing seen with Doxil-p700 was no greater than for Doxil alone, suggesting that the doxorubicin was largely internalised passively into these cells. Moreover, normal vasculature is unlikely to be exposed to such high concentrations of Doxil-p700 as the tumour tissue where it should be concentrated.

3.5.Conclusion

The data presented here demonstrate that Doxil-p700 has significant potential as a cancer therapeutic with the ability to actively target doxorubicin to tumour tissue. Enhanced localisation to the tumour may decrease circulation time throughout the body, relative to unmodified Doxil, potentially reducing off target effects such as palmar planter erythrodysesthesia. Additionally, p700 enabled active internalisation of the conjugate, potentially enhancing drug delivery into the tumour cells. While some cells, such as MCF-7, show resistance to doxorubicin, the other advantage of this technique is that it can be used to target any drug that can be encapsulated in this way.

Clearly, as with CPG2-p700, the next step in validating the Doxil-p700 would be to undertake an *in vivo* study to confirm efficacy in an animal model of cancer. However, the Doxil-p700 conjugate may be a much more promising therapeutic candidate than CPG2-p700. CPG2-p700 still retains one of the main disadvantages of ADEPT in that the enzyme is immunogenic and unproven in a clinical setting. In contrast Doxil is an established therapeutic drug. As p700 is derived from an extracellular human protein it is unlikely to be significantly immunogenic or toxic and so the conjugate is unlikely to be any more harmful than Doxil alone and, due to increased specificity, possibly less so. This greatly enhances its chances of successful progression through clinical trials, should it prove advantageous in animal models.

For this reason, and due to budget constraints, it was decided to only test Doxil-p700 *in vivo* and this is the topic of the next chapter.

CHAPTER 4

Coupling of p700 peptide to carboxypeptidase G2 for pro-drug activation

4.1. Introduction:

Broad-spectrum cytotoxic drugs, such as nitrogen mustards, have been the mainstay of cancer therapy for decades. However, such drugs target all proliferating cells, not just cancer cells and the resulting severe side-effects limits dosage and potential efficacy in the long-term. Many mechanisms have been used to target chemotherapies specifically to the cancer sites, including antibody directed enzyme prodrug therapy (ADEPT), as described in section 1.10.4. As mentioned, in ADEPT, enzymes that convert prodrugs to active drugs are first targeted to the cancer site. After clearance of the enzyme from normal tissue, the prodrug is administered to be activated at the cancer site (Goda *et al.*, 2009).

A *Pseudomonas aeruginosa* strain RS-16-derived enzyme, carboxypeptidase G2 (CPG2 or glucarpidase), has been used in this staged therapy. This is partly because its activity is not found in humans, reducing the chance of toxicity to healthy tissue as the prodrug will be activated only by the localized exogenous enzyme. This zinc-dependent enzyme naturally catalyzes the hydrolysis of the C-terminal glutamic acid residue of folic acid and synthetic folate analogues such as the cancer chemotherapy agent, methotrexate (MTX). For this reason, CPG2 is sometimes used clinically for clearing excess MTX in patient blood after high dose therapy to control its side effects. In ADEPT system, the CPG2 can be used to activate prodrugs such as nitrogen mustard L-glutamate prodrugs into nitrogen mustards, which cross-link DNA leading to apoptosis (Dowell *et al.*, 1996).

The enzyme is normally directed to the cancer tissue by a tumour-specific antibody. However, there are several drawbacks to the use of antibodies in this procedure. Non-humanised antibodies are likely to be immunogenic, potentially preventing repeat dosage and leading to neutralisation of the antibody (Sharma *et al.*, 1992). The size of the antibody also greatly increases circulation time of the enzyme which needs to be cleared

from the circulation prior to pro-drug administration to avoid off target activation of the pro-drug. Longer circulation times also increase the risk of an immune response. While antibodies can be humanised, this is an expensive and time-consuming process. Additionally, antibodies are mono-specific and tumours often rapidly evolve to lose expression of the target molecule. While several different antibodies could be used, this increases the complexity and cost, particularly if humanisation is required.

4.1.1. Aim

The aim of this chapter was to use p700 to target CPG2 to tumour cells. Using our peptide instead of a monoclonal antibody has several potential advantages:

- The peptide is derived from a human extracellular protein and should not be immunogenic.
- The small size of the peptide should enable much more rapid clearance of the complex, further reducing any potential immunogenicity and non-targeted prodrug activation.
- The peptide targets multiple receptors on both tumours and tumour vasculature, greatly decreasing the likely development of drug resistance.

The CPG2 enzyme, being of bacterial origin, is still potentially immunogenic. While alternative humanised enzymes have now been reported (Afshar *et al.*, 2009), this chapter is primarily concerned with proof of principle and CPG2 is well studied and can be readily over-expressed in *E. coli* (Goda *et al.*, 2009).

Two approaches to coupling the peptide were considered. One possibility would have been to chemically cross-link the p700 to CPG2. This has the potential advantage that multiple copies could be linked to a single enzyme molecule, potentially increasing affinity to the target cells. However, this approach is more likely to result in inactivation of the enzyme or peptide as the location of coupling, and number of peptides coupled, are

difficult to control. Instead the approach selected was to fuse the p700 sequence onto the amino-terminus of CPG2 by constructing a novel cDNA clone. As an alternative to the p700 sequence it was also decided to utilise the C-terminal TIMP3 sequence (T3C), SWYRGWAPPDKSIINATDP, shown previously to bind to VEGFR2 (Qi *et al.*, 2013). While this sequence was shown to be specific for VEGFR2 only, unlike p700, it does not contain a disulfide bond which could be problematic in a bacterial expression system. The sequences would also incorporate a flexible [Gly₄Ser]₄ linker (Chen *et al.*, 2013b) to decrease the likelihood that proximity of the peptide sequences to CPG2 would sterically inhibit their ability to bind receptors.

The final construct utilised a C-terminal [His]₆ tagged CPG2 sequence, codon-optimised for expression in *E. coli* (Goda *et al.*, 2009). The *AgeI* restriction site, present towards the amino-terminus of CPG2 was used to allow insertion of either p700 or T3C peptide sequences, both with the [Gly₄Ser]₄ linker. Recombinant proteins could then be then purified using Ni²⁺ chelate column chromatography and affinity for VEGFR2 tested using Bio-Layer Interferometry (BLI). The enzymatic activity of the CPG2 fusion proteins would be determined by methotrexate (MTX) cleavage. The cytotoxic effects of the non-toxic pro-drug, ZD2676P, in the presence of CPG2 or CPG2 fused to the TIMP3 peptides would then be assessed in 4T1 mouse breast cancer cells (Figure 4.1).

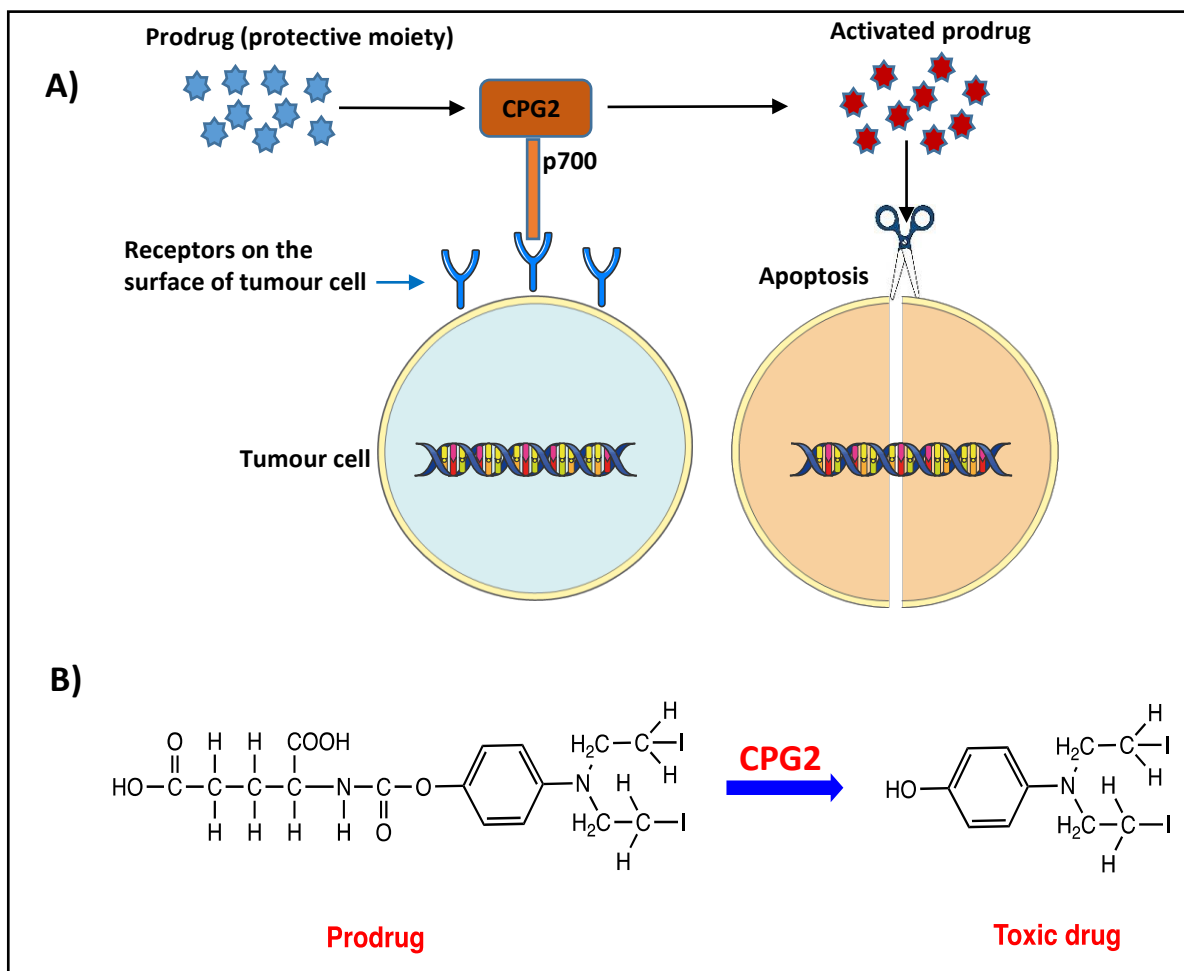


Figure 4.1 Strategy for prodrug activation by CPG2-p700

A) CPG2 is targeted to the cell surface by means of fused p700 which binds growth factor receptors on the cell surface. This allows for localised conversion of prodrug, ZD2767P into an active cytotoxic drug at the cell surface. B) shows the chemical structure of ZD2767P prodrug and its hydrolytic conversion to active drug, ZD2767D, by CPG2 enzyme.

4.2. Methods

4.2.1. Synthesis of CPG2 codon-optimized synthetic gene

The codon-optimized CPG2 gene was synthesised by Eurofins Genomics (see Appendix Figure A1 for the full sequence). The sequence was identical to that described by Goda *et al* 2009, except the second *AgeI* site at base 1050 was silently engineered out to leave a single *AgeI* site at position 106 and 5' *NdeI* and 3' *HindIII* and *NotI* restriction sites were added to facilitate cloning into pET28a bacterial expression vector. It was supplied in a kanamycin resistant cloning vector; pEX-K4. p700 and T3C peptide sequences with 5' *NdeI* sites were also synthesised by Eurofins, including the [Gly₄Ser]₄ linker and the CPG2 sequence up to the *AgeI* site (Appendix Figure A1). These were supplied in an ampicillin-resistant cloning vector, pEX-A2 and could then be cut and ligated onto the 5' end of the codon-optimised CPG2 using the *NdeI* and *AgeI* sites.

Unmodified CPG2, supplied in pET28a at the *NdeI* and *NotI* restriction sites, was a kind gift from Sandra Hemmington, Mologic (UK).

For all the plasmids, transformation into α -Select chemically-competent *E. coli*, followed by mini-prep purification, as described in Section 2.1.3 was used to provide sufficient stocks for subsequent experiments.

4.2.2. Sub-cloning of the codon optimised CPG2-His gene into pET28a and insertion of the p700 and T3C peptide sequences)

Codon-optimised CPG2-His (approximately 1200bp in length) was excised from pEX-K4 by digestion with *NdeI* and *NotI* and ligated into the bacterial expression vector, pET28a, after cutting out the unmodified CPG2 with the same enzymes, as described in sections 2.1.4 and 2.1.6. Agarose gel electrophoresis was used to confirm successful restriction and ligation (section 2.1.5).

Once the codon-optimised CPG2 was cloned into the pET28a vector, either the p700 or the T3C sequences were cloned into the *NdeI* and *AgeI* restriction sites (see Figure A1 in Appendix). Three vector constructs were therefore generated for synthesis of CPG2 only and CPG2 with either p700 or T3C peptide at the N-terminus.

4.2.3. Transformation of CPG2 constructs into competent *E. coli*

All three constructs were transformed into α -Select chemically-competent *E. coli* (Bioline) following the manufacturer's instructions (section 2.1.1). Miniprep and maxiprep plasmid purifications were then performed (section 2.1.3). Automated DNA sequencing was carried out to confirm cloned plasmid sequences.

4.2.4. Small scale induction of CPG2-only and CPG2 fusion protein expression

Following confirmation of DNA sequences for all three CPG2 constructs, plasmid DNA was transformed into host *E. coli* BL21 (DE3) for protein expression. Transformed bacteria were selected by growing on LB agar plates containing 50 μ g/ml kanamycin and 0.2% glucose (to suppress the lac promoter). A single colony was then transferred to a tube containing 10ml LB broth and 50 μ g/ml kanamycin and incubated overnight at 37°C on a rotating shaker. Two 500 μ l aliquots of the bacterial culture were added to an equal volume of 100% glycerol in sterile microfuge tubes (glycerol stocks) and stored at -80°C. For induction, the remaining 9ml bacterial culture was then inoculated into 100ml of LB broth (plus antibiotic) and further incubated until the optical density (OD) reached 0.5 – 0.6. A 1ml pre-induction sample was removed prior to addition of the synthetic lac promoter, isopropyl- β -D-thiogalactopyranoside (IPTG) at a final concentration of 1 mM. This was followed by further incubation and samples were then removed at 1, 2, 3 and 4-h time points post-induction. All pre- and post-induction samples were centrifuged at 14 x 10³ g for 2 min, the supernatant was discarded and the pellets stored at -20°C until protein analysis could be carried out.

4.2.5. Protein detection by SDS-PAGE and Coomassie Brilliant Blue staining

The pellets were re-suspended in 50µl dH₂O and 40µl of the suspension returned to the freezer at -20°C. The remaining 10µl suspension was diluted with an equivalent volume of 2X Laemmli sample buffer (Bio-Rad®) and 1µl of 1M dithiothreitol (DTT) was added. Sample tubes were then placed on a heating block at 95°C for 5 min after which the samples were transferred to QIAshredder tubes and centrifuged at 14×10^3 g for 2 min to remove debris and shear the genomic DNA.

From each sample, 15µl was then loaded onto a 10% gel for SDS-PAGE as described in Section 2.1.11. The gel was then washed twice with dH₂O and stained by incubating in a 1:9 mixture of ethanol and colloidal Coomassie G250 stain (National Diagnostics). After ensuring that there were visible bands, the gel was then washed twice with dH₂O and imaged using a Bio-Rad® Gel DOC™ EZ imager.

4.2.6. Solubility test of recombinant proteins

A solubility test was carried out to determine whether the expressed proteins were in the soluble fraction (supernatant) or the insoluble fraction (pellet) of bacterial cell lysates. Briefly, IPTG induced *E. coli* expressing CPG2 and CPG2-fusion proteins were grown in LB broth supplemented with 50µg/ml kanamycin for 4 h after which a 1ml sample was taken and centrifuged at 14×10^3 g for 2 min. The supernatant was discarded and the pellet was resuspended in 2ml of dH₂O containing Roche Protease Inhibitor Cocktail (1 tablet in 50 ml) followed by mixing. Then 40 µl of lysosome (10mg/ml) was added followed by incubation on ice for 20 min with flicking every 2 min. Next, 80µl of sodium deoxycholate (25mg/ml) was added followed by 20 min incubation on ice with mixing at 2 min intervals. Thereafter, the cells were lysed by sonication (4 cycles at 10 seconds/cycle) on ice. The lysate was centrifuged at 14×10^3 g for 25 min (at 4°C) and the supernatant collected in a fresh tube while the pellet was resuspended in 2ml dH₂O.

10µl aliquots of the whole cells lysate, supernatant and resuspended pellet were analysed on a Coomassie Blue stained SDS-PAGE gel along with 10µl protein ladder (Bio-Rad®) as previously described in section 4.2.5.

4.2.7. Large scale induction of recombinant CPG2 expression

Following the confirmation of expression of CPG2 and CPG2-fusion proteins the expression was induced on a large scale. A glycerol stock of each expression construct was streaked on an agar plate containing (50µg/ml kanamycin) and 2% glucose and grown overnight at 37°C. A starter culture was generated by inoculating 3ml LB broth with a colony from each agar plate and grown for 6-8 h. Thereafter, each starter culture was diluted in 1 L of LB broth containing (50µg/ml kanamycin) and grown at 37°C with shaking. At an OD of 0.5-0.6 the cells were induced with IPTG to a 1 mM final concentration with a 1ml sample taken before induction. Cells were incubated for a further 3-4 h at 37°C with shaking. At the end of the incubation period a 1ml aliquot was taken to confirm induction and the remaining cells were harvested using polycarbonate centrifuge pots (250 ml) at 5500 g for 15 min at 4°C. The supernatant was discarded and the pellet was either processed immediately or stored at -80°C. After confirming induction, pellets were processed as described below.

4.2.8. Whole bacterial cell lysis and separation into soluble and insoluble fractions

Pellets from the large-scale expression (1L culture) were resuspended in 20ml Tris buffer (20mM Tris, 137mM NaCl, 1 mM EDTA pH 7.6) supplemented with protease inhibitor cocktail (Roche) followed by mixing. Cells were then lysed by adding 400µl of 10mg/ml lysozyme (final concentration of 200 µg/ml) followed by incubation on ice for 30 min with gentle mixing every 2 min. Subsequently, 800µl of 25mg/ml sodium deoxycholate detergent was added to the lysate (final concentration of 25µg/ml) followed by 20 min incubation on ice with regular mixing every 2 min. Four one-min sonication cycles, were

then carried out with 60 seconds rest intervals on ice between successive cycles to prevent overheating. Cell lysate was then centrifuged at 15,000g for 25 min at 4°C. The supernatant was transferred into a sterile tube and kept for analysis as a soluble fraction. The pellet was further processed for the insoluble fraction as explained below.

4.2.9. Inclusion body Preparation

4.2.9.1. Insoluble fraction

The pellet from the whole cell lysate centrifugation step was resuspended in 20ml of Tris buffer with urea (20mM Tris, 137mM NaCl, 2M urea, 1 mM EDTA pH 8) and mixed thoroughly until all clumps disappeared. A 50µl aliquot of the suspension was then transferred to a microfuge tube and labelled insoluble fraction for subsequent analysis.

4.2.9.2. Washes

The remaining cell suspension was then centrifuged at 15000 x g for 30 min. The supernatant (Wash 1) was transferred into a fresh sterile tube and stored at 4°C until subsequent analysis (within 24 h to avoid protein degradation). The pellet was again re-suspended in Tris buffer with urea, centrifuged at 15000 x g for 30 min and supernatant (Wash 2) transferred to a fresh sterile tube and stored at 4°C. The pellet re-suspension and centrifugation steps were then repeated two more times and the resulting supernatant collected and labelled as Washes 3 and Wash 4, respectively.

4.2.9.3. Inclusion Body

A sterile pipette tip was used to take a small sample of the final pellet (inclusion body), which was transferred to a microfuge tube and re-suspended in 50µl of dH₂O for SDS-PAGE analysis. The rest of the inclusion body was immediately transferred to a freezer at -80°C for storage.

4.2.9.4. Screening

Coomassie Blue staining and SDS-PAGE analysis was then used for screening detection of protein in the soluble fraction, insoluble fraction, all four washes and the inclusion body as previously described (Sections 2.1.11 and 4.2.5)

4.2.10. CPG2 purification from the insoluble fraction by Ni²⁺-NTA chromatography

4.2.10.1. Preparation of Ni²⁺ column:

The Ni²⁺ column (SIGMA-ALDRICH) was initially equilibrated by adding 20ml dH₂O which was allowed to run through by gravity. The column was then charged by allowing 10ml of 10mM NiCl₂ to run through, again by gravity, followed by a further 20ml of water. Without allowing the column to dry and avoiding bubble formation, 10 ml of wash buffer 1, (20mM Tris, 137mM NaCl, 2M urea; pH 8) was then run through the column.

4.2.10.2. Protein purification

Washes 1 – 4 (section 4.2.9.2) were pooled together (making a total of approximately 60ml) and 300µl of 4M imidazole was added to make a final imidazole concentration of 20mM. This was then loaded onto the column and allowed to run thorough by gravity and the flow through collected for SDS-PAGE analysis to ensure that the protein had bound to the column. The column was then washed with 10ml of filtered wash buffer 2 (20mM Tris, 137mM NaCl, 1M urea; pH 8). Again, the flow through was collected for SDS-PAGE analysis.

4.2.10.3. Elution

Buffer solutions with differing imidazole concentrations (Elution buffers 1 and 2) were used to identify the optimal elution buffer composition. His tagged protein bound to the column was eluted by adding 10ml Elution buffer 1 (20mM tris, 137mM NaCl, 500mM urea, 200mM imidazole; pH 8) to the column. The eluent was collected in 1ml fractions in Eppendorf tubes for SDS-PAGE analysis. Without allowing the column to dry, 10ml Elution buffer 2 (20mM Tris, 137mM NaCl, 500mM urea, 500mM imidazole; pH 8) was

added to the column and again, 1ml fractions of the eluent were collected for SDS-PAGE analysis.

4.2.11. Protein quantification of eluent fractions

The eluent fractions in which recombinant CPG2 protein was detectable by SDS PAGE were then analysed using a BSA concentration standard curve to quantify the protein content as described in Section (2.1.10)

4.2.12. Enzyme activity assay

Recombinant CPG2 fusion protein activity was assessed using methotrexate (MTX) as substrate (Figure 4.2) with a modified protocol of Goda *et al.* (2009). Briefly, 1ml of 100mM TrisHCl pH 7.3 containing 0.2 mM ZnSO₄ and 60μM of MTX was added to a cuvette and incubated at 37°C for 5-10 min. Purified recombinant CPG2 fusion protein was then added (final concentration of 16μg/ml) to the cuvettes which were placed directly into a spectrophotometer, maintained at 37°C. Tris buffer without MTX was used as background control and decrease in absorbance at 320 nm was measured at 5-min intervals.

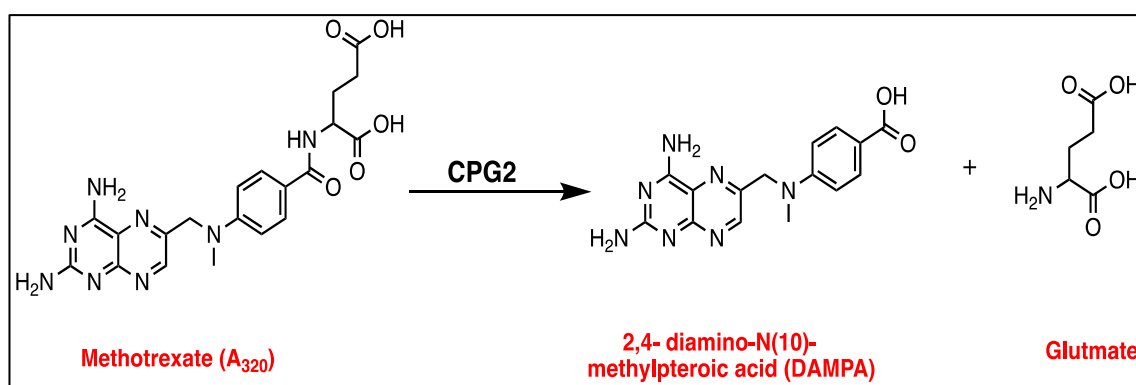


Figure 4.2 Conversion of methotrexate to 2,4-diamino methylpteroic acid by CPG2 can be determined by measuring the decrease in methotrexate absorbance at 320 nm.

4.2.13. Assessment of zinc-dependence of recombinant CPG2-fusion protein enzyme activity:

Zinc-dependence of the purified recombinant CPG2 fusion proteins was evaluated in two ways. In one experiment, the enzyme activity assay was performed as described in Section 4.2.12 in the absence of ZnSO₄. In the second, the enzyme activity assay was performed in the presence of ZnSO₄ with the addition of 10mM EDTA as a zinc chelating agent. Absorbance readings were plotted against time and data was analysed using GraphPad Prism software (v7.0).

4.2.14. Kinetic analysis of CPG2-p700 binding to VEGFR2 by Bio-Layer Interferometry (BLITZ)

Bio-Layer Interferometry (BLI) was used to perform real-time kinetic analysis of the interaction between recombinant CPG-p700 and its ligand, VEGFR2. BLI was performed using the BLItz® system which emits white light down a biosensor coated with a ligand and collects any light reflected (Figure 4.3.). The wavelength of the reflected light is affected by the thickness of coating on the biosensor. When the protein being analysed is added, any protein-ligand interaction results in a change in the number of molecules bound to the biosensor and causes a shift in the interference pattern, which is then recorded by a spectrometer. This wavelength shift is a direct measure of the change in optical thickness (nm) of the biological layer.

Briefly, probes (biosensors), pre-coated in protein A, were hydrated by soaking in PBS for at least 10 min and then loaded on to the biosensor mount. An initial baseline was established by lowering the probe into 250µl of PBS in the tube holder for 60 seconds. VEGFR2 ligand solution, 5µl at a concentration of 250 µg/ml, was then loaded into the drop holder and the biosensor inserted for 300 seconds. A further baseline step was then established before the CPG2 recombinant proteins (CPG2 or CPG2-p700) were introduced into the drop holder for the association and dissociation steps. Control runs

were performed with only PBS and only VEGFR2 (no recombinant proteins added) for comparison.

The experiment was then repeated five times with subsequent sample (CPG2 or CPG2-p700) concentrations ranging from 600nM-10 μ M. The binding affinity (K_d), was then calculated by the BLItz® software based on the binding signal (nm), sample concentration and molecular weight.

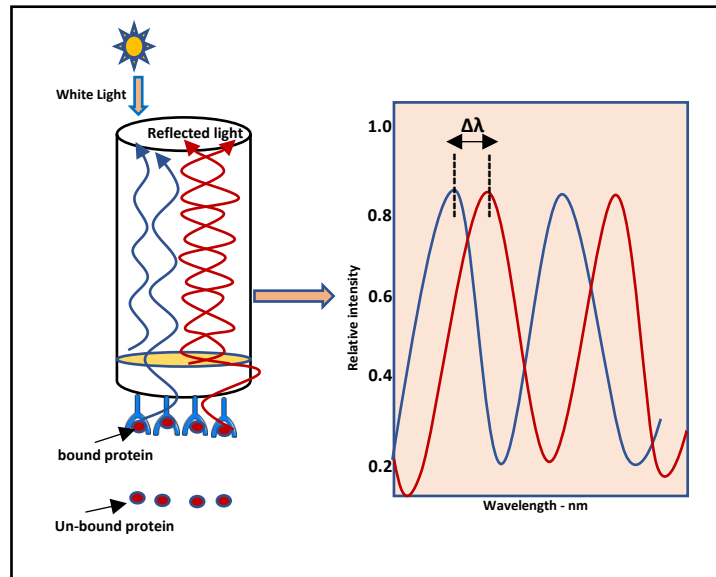


Figure 4.3 BLI technology enables label-free, real-time kinetic analysis of protein/protein interactions

White light is sent down the biosensor to two regions (interface between the glass fiber and the proprietary bio-compatible layer, and the interface between the surface chemistry and solution) and reflected light collected. Different wavelengths in the reflected light from the two regions are affected by the difference in thickness of the regions, resulting in constructive and destructive interference of the constituent wavelengths of the light resulting in an interferometric profile peculiar to the system. When molecules bind to the protein at the biosensor tip, the interferometric profile shifts, resulting in a wavelength shift $\Delta\lambda$ measured in nanometer (nm) which is proportional to the thickness of the protein bio-layer or the amount of bound protein.

4.2.15. Cytotoxicity assay

The ability of the purified CPG2 recombinant proteins to activate the nitrogen mustard pro-drug ZD2676P ((2*S*)-2-[(4-[bis(2-iodoethyl)amino]phenoxy-carbonyl)amino]pentanedioic acid hydroiodide - High Force Research, Durham) was evaluated using a cytotoxicity assay with the mouse breast cancer cell line 4T1.

Viable 4T1 cells were seeded into three 96-well plates at a density of 2×10^3 cells per well and then cultured overnight at 37°C. This cell density was based on previous optimization experiments (section 3.2.6). In one of the 96-well plates, the medium in all wells was replaced with 100µl medium containing recombinant codon-optimised CPG2-only protein at a concentration of 16µg/ml, the same concentration at which maximal enzyme activity was demonstrated in previous experiments (Section 4.2.12). In a second 96-well plate, the medium in all wells were replaced with medium containing recombinant CPG2-p700 at the same concentration (16µg/ml), while the medium in the third plate was replaced with 100µl fresh medium only.

The plates were then incubated for 4 h at 37°C to allow binding of the CPG2-p700. The media in all wells were then aspirated completely and the cells washed twice with PBS to remove any unbound CPG2 residues.

The 10mM stock of ZD2676P prodrug (dissolved in DMSO) was serially diluted in culture media to make 2, 4, 6, 8, 10, 12 and 14 µM concentrations. Media containing each prodrug concentration were then added (in triplicate) to labelled wells in all three plates and further incubated at 37°C for one hour (as recommended by the pro-drug supplier). The media in all wells were then completely aspirated, replaced with fresh growth medium and the plates incubated for 3 - 4 days before 20µl of MTS solution was added into each well to determine the proportion of viable cells as described in Section 2.1.13. Three independent repeat experiments were performed and statistical analysis was

performed using two-way ANOVA and Bonferroni multi-comparison. Percentage cell viability curves were drawn using GraphPad prism software (v7.0).

4.3. Results

4.3.1. Construction of CPG2, CPG2-p700 and CPG2-T3C cDNA clones

Figure 4.4A shows the successful digestion of pET28a (which contained an unmodified form of CPG2) and codon-optimised CPG2 in pEX-K4 with *NdeI* and *NotI* prior to purification and ligation of the codon-optimised CPG2 into the pET28a vector. Following successful ligation, the purified pET28a-CPG2 was then digested with *NdeI* and *AgeI* to allow for insertion of the similarly digested p700 or T3C sequences from the pEX-A2 vector (Figure 4.4B). The inserts were then gel purified and ligated into the 5' end of the codon optimised CPG2.

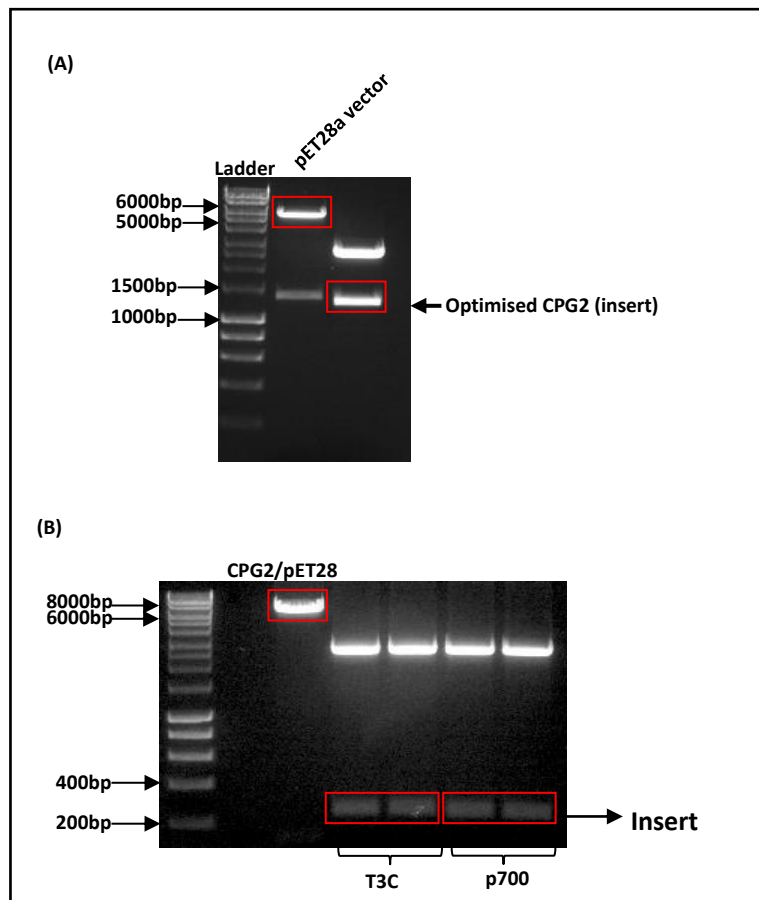


Figure 4.4 Subcloning of CPG2, p700 and T3C into the pET28a vector

A) pET28a vector containing unmodified CPG2 (left) and pEX-K4 vector containing the codon-optimised CPG2 (right) were digested with *NdeI* and *NotI* and separated on an agarose gel. The highlighted bands were then gel purified and ligated.

B) pET28a vector containing codon-optimised CPG2-His (left) was digested with *NdeI* and *AgeI*; pEX-A2 vector containing T3C and p700 (paired lanes to the right, respectively) digested with *NdeI* and *AgeI* and run on an agarose gel. The highlighted bands were then gel purified and ligated.

4.3.2. Small scale induction of CPG2 expression

Following successful ligation and sequence verification of the CPG2 fusion clones, they were transformed into BL21 cells and small scale induction of protein expression carried out. The expressed recombinant proteins were analysed by SDS-PAGE after 1, 2, 3 and 4 h of induction and the results are shown in Figure 4.5. These show a clear induction of expression of proteins at the expected sizes (approximately 43kDa for CPG2 alone and approximately 47kDa for the CPG2 fusion proteins) with time, relative to the uninduced cells.

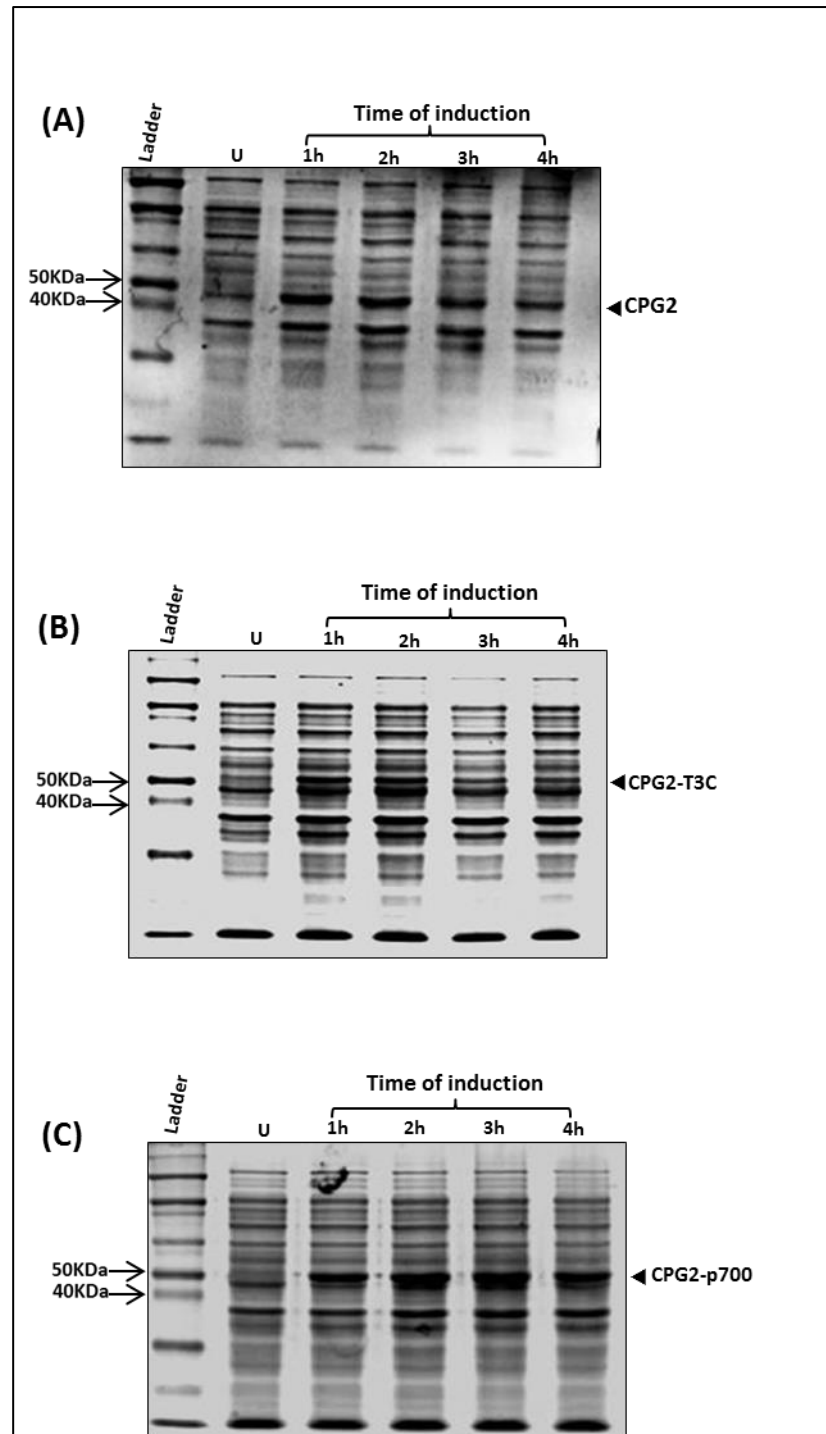


Figure 4.5 SDS-PAGE analysis of recombinant CPG-2 protein expression in BL21 *E. coli*
 CPG2 (A), CPG2-T3-C-terminal (B) and CPG2-p700 (C) fusion expression constructs transformed into BL21 *E. coli* were induced with 1 mM IPTG for 4 h. Protein expression was analysed by Coomassie blue staining of a 10% SDS-PAGE gel for uninduced (u, lane 2) and 1-h intervals post-induction. The predicted MW for CPG2 is 43kDa while both CPG2-T3C and CPG2-p700 have predicted molecular weights of 47kDa.

4.3.3. Solubility Test

Solubility testing was carried out to determine whether the CPG2 was expressed predominantly in the cytosol (soluble fraction) or in subcellular organelles (insoluble fraction). After 3 hrs of IPTG induction, expression of the CPG2, CPG2-T3C and CPG2-p700 was found to be minimal in both initial whole cell lysate and in the soluble fraction of the cells which was derived from supernatants of centrifuged whole cell lysate (Figure 4.6). However, the insoluble fraction derived from pellets of centrifuged whole cell lysate showed high expression of the CPG2 and CPG2-p700 proteins. There was also a clear increase in expression of CPG2-T3C; however, in this case there were two apparent bands, possibly indicating some cleavage of this fusion protein.

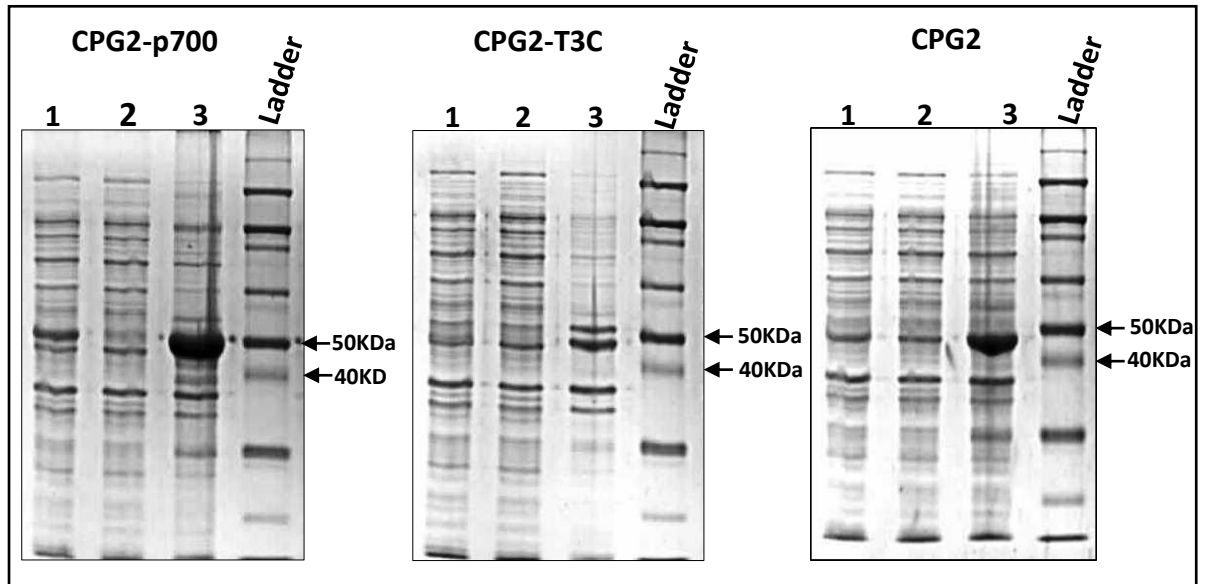


Figure 4.6 Solubility test to determine localisation of recombinant CPG2 protein expression in BL21 *E. coli*

Coomassie Blue staining following SDS-PAGE of samples of whole cell lysate (lane 1), supernatant (lane 2) and re-suspended pellet (lane 3) of IPTG induced BL21 *E. coli* expressing CPG2-p700, CPG2-T3C or CPG2 proteins respectively from left to right, along with protein standards (ladder). The arrow-heads indicate over-expressed protein bands at the expected sizes (43-47kDa) in the re-suspended pellets for all three proteins.

4.3.4. Large scale expression of CPG2 and CPG2 fusion proteins

After determining that the recombinant proteins were maximally expressed after 3 hrs, a large-scale IPTG-induced expression of the recombinant proteins was carried out to determine if the expression could be replicated in bulk. As shown in Figure 4.7, by both Coomassie blue staining and western blotting, there is clear, high-level expression of CPG2 and CPG2-p700 after 3 hrs, confirming the result from the small-scale induction. However, once again CPG2-T3C ran as two distinct bands, indicating degradation of this recombinant protein.

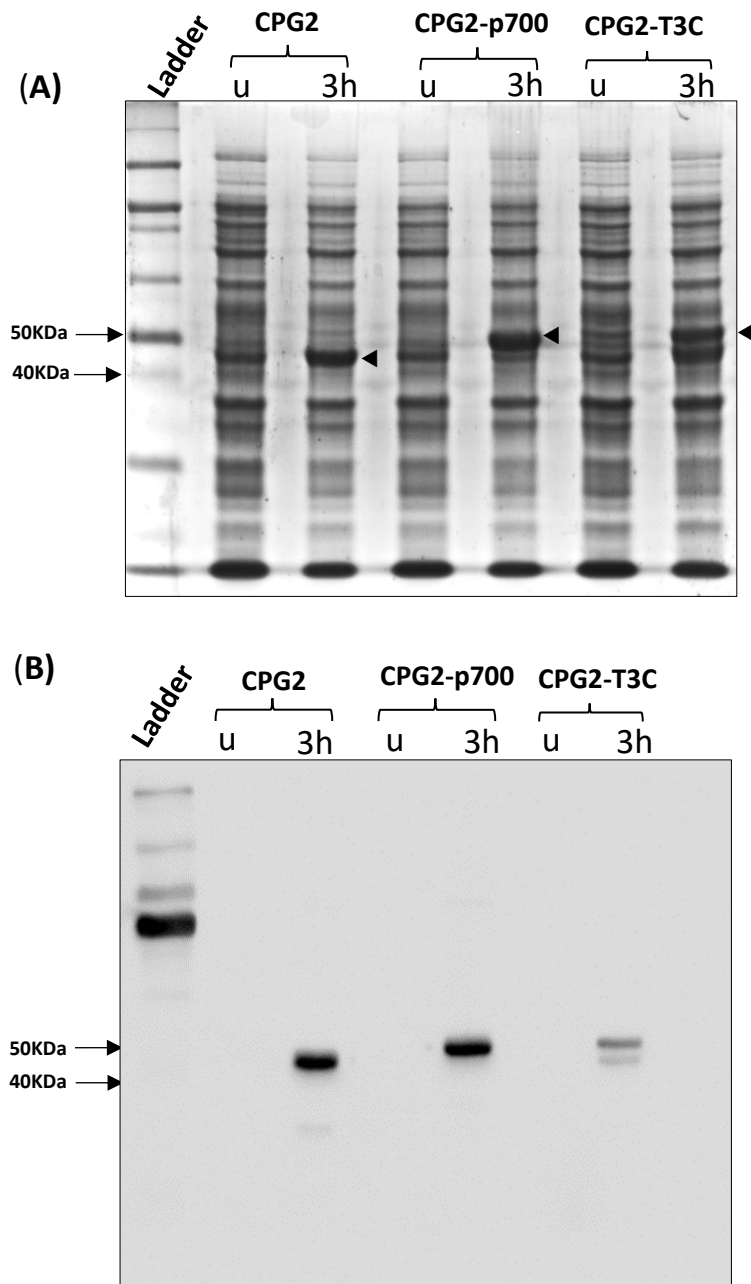


Figure 4.7 Large-scale expression of CPG2 recombinant proteins in BL21 *E. coli*

Panel A: Coomassie blue staining following SDS-PAGE of paired samples (whole cell lysate) taken pre- (u) and 3 hs post-IPTG induction (3h) of CPG2, CPG2-p700, and CPG2-T3C recombinant protein expression, respectively from left to right, compared with a ladder (extreme left). The arrow-heads highlight the protein bands of the expected sizes (43-47kDa).

Panel B: Western blotting analysis using anti-histidine antibody on identical samples corresponding to the top panel, compared with a protein ladder (extreme left). Histidine-tagged recombinant proteins of the expected sizes (43-47kDa) were detected in post-induction samples, but not in corresponding pre-induction samples.

4.3.5. Inclusion body preparation for CPG2

The solubility testing had confirmed that the recombinant proteins localised almost exclusively to the inclusion bodies of the bacteria which would necessitate extraction of the proteins with a denaturing agent that would permit refolding of functional proteins. Urea is commonly used for this purpose and, in the protocol for CPG2 expression described by Goda *et al.* (2009), the pellets were initially washed in three changes of 2M urea before complete dissolution in 6M urea, and so this procedure was replicated here. However, in our case, considerable amounts of relatively pure recombinant proteins were found in the 2M urea washes, as shown in Figure 4.8. While most of the protein was still found in the remaining pellets, it was thought that the protein found in the washes may not be fully denatured and would probably be sufficient to carry out initial functional screening assays, while the protein in the remaining pellets would require much more aggressive denaturation, and subsequent renaturation, that may result in loss of function. Again, the CPG2-T3C protein showed signs of degradation and so this protein was not used in subsequent assays.

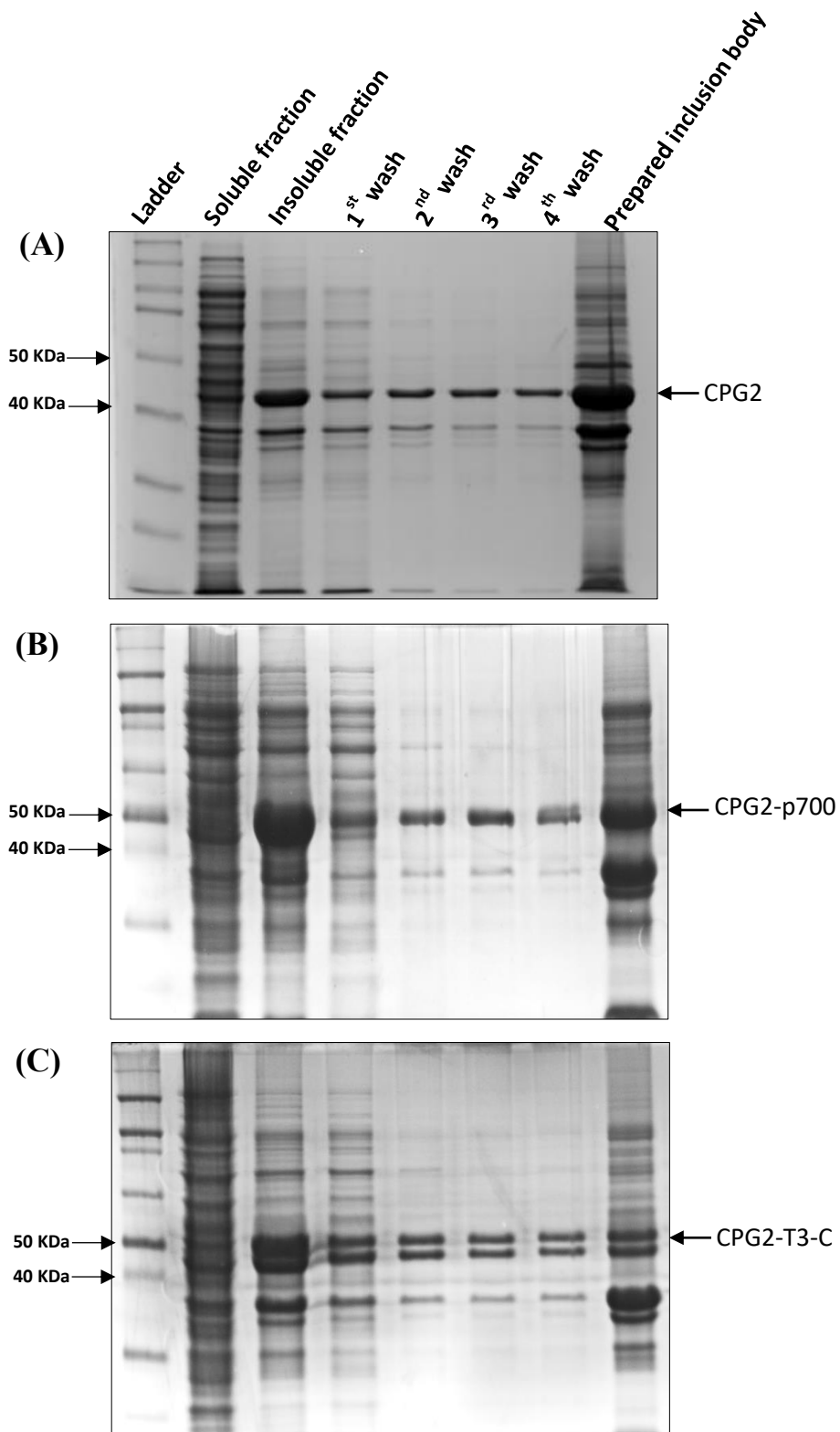


Figure 4.8 CPG2 proteins present in different fractions of BL21 *E. coli* cell lysate

Lanes (left to right) represent Coomassie Blue staining following SDS-PAGE of standard protein ladder; soluble fraction; insoluble fraction; four sequential urea washes; and remaining inclusion body, respectively of IPTG-induced BL21 *E. coli* cells expressing (A) CPG2, (B) CPG2-p700 and (C) CPG2-T3C recombinant proteins.

4.3.6. Purified CPG2 recombinants proteins:

As alluded to above, instead of extracting the CPG2 recombinant proteins from the pellets remaining after the urea washes, the recombinant proteins were purified from the four pooled 2M urea washes using Ni-NTA affinity chromatography (section 4.2.10). The result of the purification step is shown in Figure 4.9. and we were able to acquire sufficient purified protein (1 mg/ml) for subsequent functional assays.

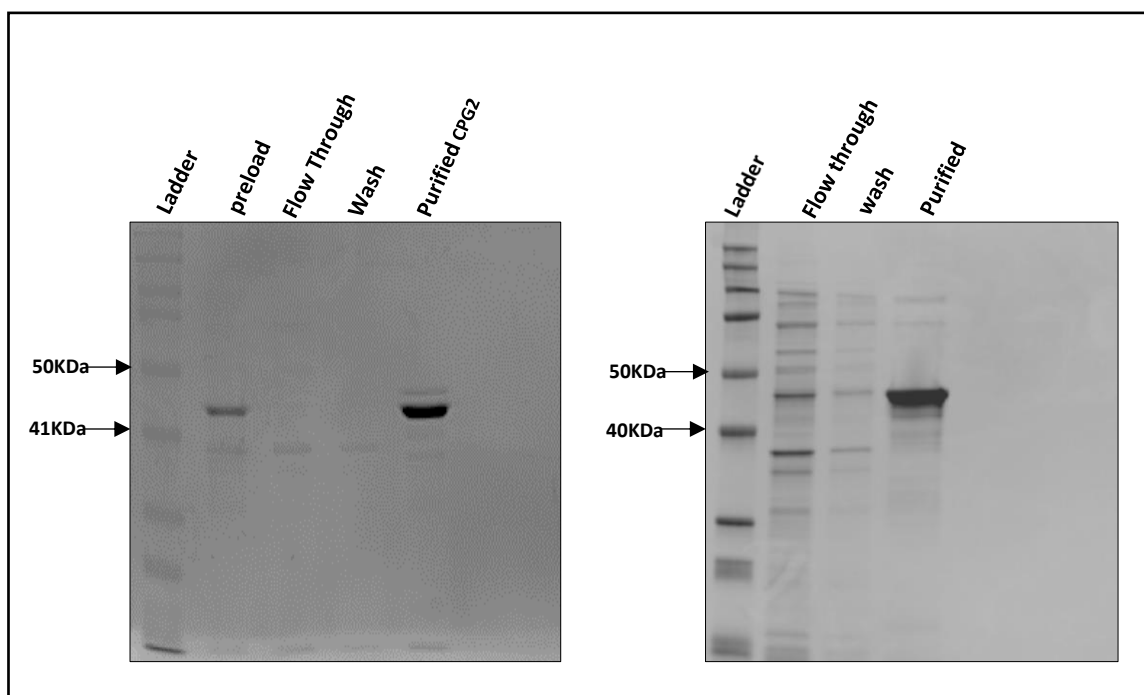


Figure 4.9 Purification of recombinant CPG2 proteins on nickel-chelate resin from urea washes derived from the insoluble fraction of BL21 *E. coli* cell lysates

Pooled washes (1 to 4) from the insoluble fraction of lysates derived the IPTG-induced BL21 *E. coli* cells expressing His-tagged recombinant CPG2 (left panel) and CPG2-p700 (right panel) were purified using a Ni²⁺ chelate column. Lanes (left to right) represent Coomassie Blue staining following SDS-PAGE of standard protein ladder; initial flow-through; wash; and eluent (purified recombinant protein).

4.3.7. Assessment of the enzymatic activity of the purified recombinant CPG2 proteins

The catalytic activity of the purified proteins was assessed using a methotrexate (MTX) cleavage assay. As CPG2 is a zinc-dependent enzyme the assay was carried out in the presence or absence of zinc, and in the presence of zinc and EDTA (a zinc chelator) in order to confirm that any cleavage seen was most likely due to CPG2 and not any other potentially contaminating protein. MTX was used as it is readily cleaved by CPG2 resulting in a reduction in its absorbance at a wavelength of 320nm which can be observed spectrophotometrically. Figure 4.10 shows that both CPG2 and CPG2-p700 were able to metabolise MTX in the presence of zinc, but not in its absence nor in the presence of zinc and EDTA. The rate of breakdown was almost identical between CPG2 and CPG2-p700 indicating that the purified enzyme is both functionally active and that the p700 sequence does not interfere with this activity.

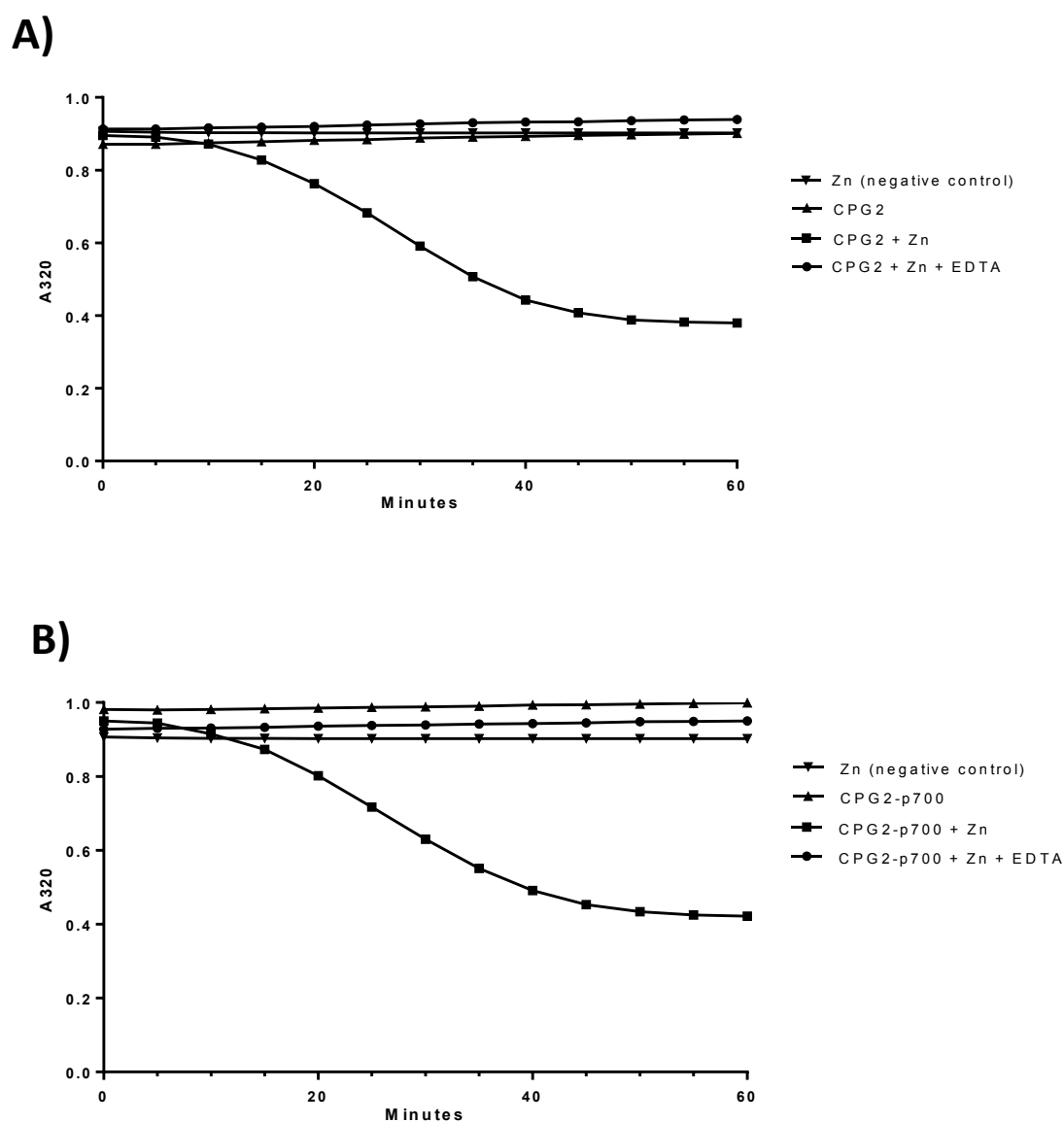


Figure 4.10 Confirmation of the zinc-dependent enzymatic activity of purified recombinant CPG2 proteins.

Recombinant proteins were incubated with methotrexate at 37°C for 0-60 min. The absorbance of each reaction at 320nm was plotted against time. A similar reduction in absorbance (representing catalysis of MTX) was seen for both CPG2 (A) or CPG2-p700 (B) in the presence of ZnSO₄ but not in its absence nor when the zinc chelating agent, EDTA, was added.

4.3.8. Determination of the ability of CPG2-p700 recombinant protein to bind to VEGFR2 by bio-layer interferometry.

The aim of this chapter was to use the p700 peptide to target CPG2 to cancer cells overexpressing growth factor receptors, such as VEGFR2. However, it is possible that coupling of the peptide to CPG2 inhibits this binding activity.

Bio-layer interferometry enables kinetic analysis to be carried out on very small sample volumes. As a recombinant VEGFR2-immunoglobulin Fc fusion protein was commercially available, enabling ready binding of VEGFR2 to the protein A sensor chips of the BLItz machine in the correct orientation, this receptor was used to test the ability CPG2-p700 to bind to VEGFR2, relative to CPG2 alone. Analysis of the association and dissociation data at a range of CPG2 concentrations indicated that p700 increased the affinity of CPG2 for VEGFR2 about 100-fold, with a calculated dissociation constant (K_d) of 130nM compared 15μM for CPG2 alone. A representative experiment, at a single protein concentration, is shown in Figure 4.11. This confirmed that p700 facilitates high affinity binding of CPG2 to VEGFR2.

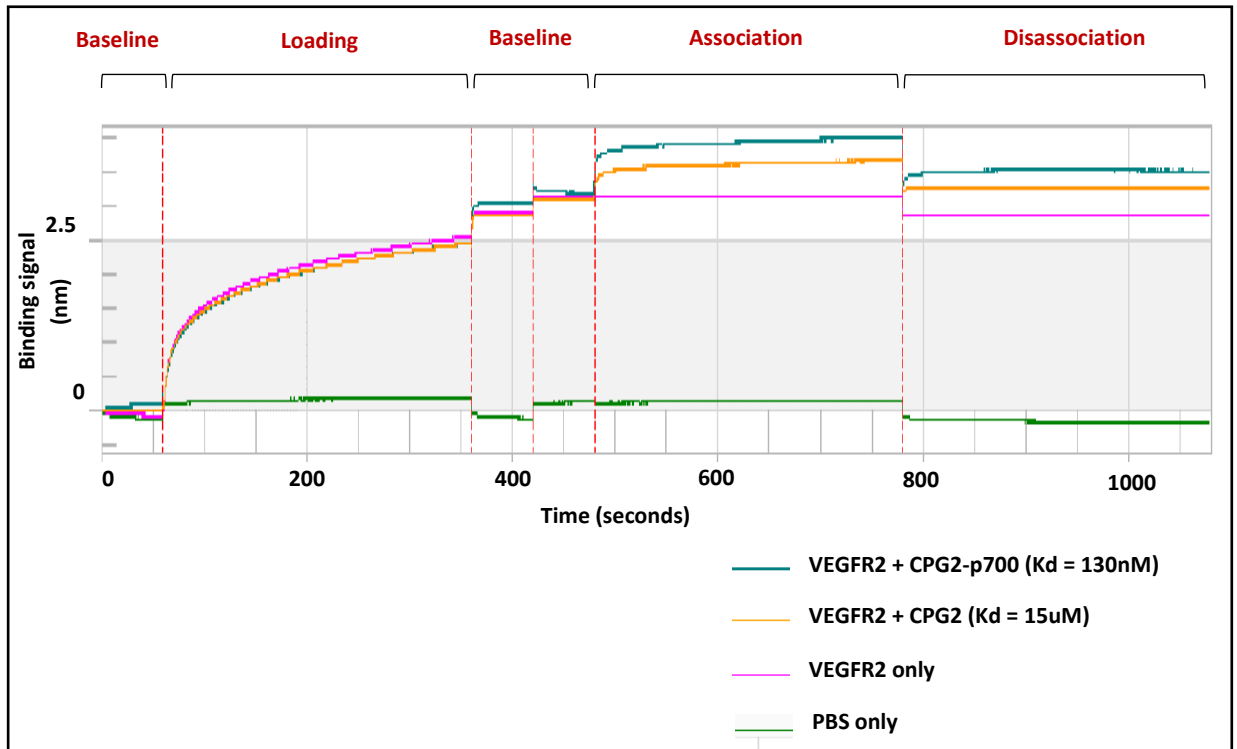


Figure 3.11 A representative bio-layer interferometry experiment comparing the interaction between recombinant CPG2 or CPG2-p700 and VEGFR2

The binding signal is the wavelength shift detected by the BLItz machine and corresponds to the change in thickness of the bilayer as a result of the interaction between the recombinant proteins (CPG2 or CPG2-p700) and a VEGFR2-coated biosensor and is plotted against the duration of the interactions. Four runs are shown with PBS only loaded (green line); VEGFR2 only loaded (purple line) and VEGFR2 loaded followed by CPG2 (yellow line) or CPG2-p700 (green line). The first loading curve is the binding of VEGFR2-Fc to the protein A coated sensor. The sensor is then washed by dipping into PBS (baseline) before dipping into the CPG2 protein solutions (association). The sensor is then transferred to PBS and dissociation measured. Binding affinity (dissociation constant, K_d) was calculated using the BLItz software based on five repeats using increasing concentrations (300nM to 10mM) of recombinant proteins. CPG2-p700 showed a 100-fold increase in binding affinity compared with CPG2.

4.3.9. Cytotoxicity assays to determine the ability of recombinant CPG2 proteins to activate the ZD2676P prodrug:

The effectiveness of both CPG2 and CPG2-p700 to convert the nitrogen mustard prodrug, ZD2676P, into a cytotoxic drug, and so kill 4T1 mouse breast tumour cells, was evaluated using an MTS cytotoxicity assay (section 2.1.13). Using a range of concentrations of the prodrug, based on a previous study (Blakey *et al.*, 1996), it was found that there was no significant difference in cell death between cells treated with ZD2676P alone or those treated with ZD2676P and CPG2 enzyme. However, at the highest dose of ZD2676P (14 μ M), there was a significant increase in cell death with cells treated with CPG2-p700, relative to both prodrug alone and prodrug with unlabelled CPG2 (Figure 4.12).

- ▲ CPG2 incubated cells treated with ZD2676P
- CPG2-p700 incubated cells treated with ZD2676P
- Cells treated with ZD2676P alone

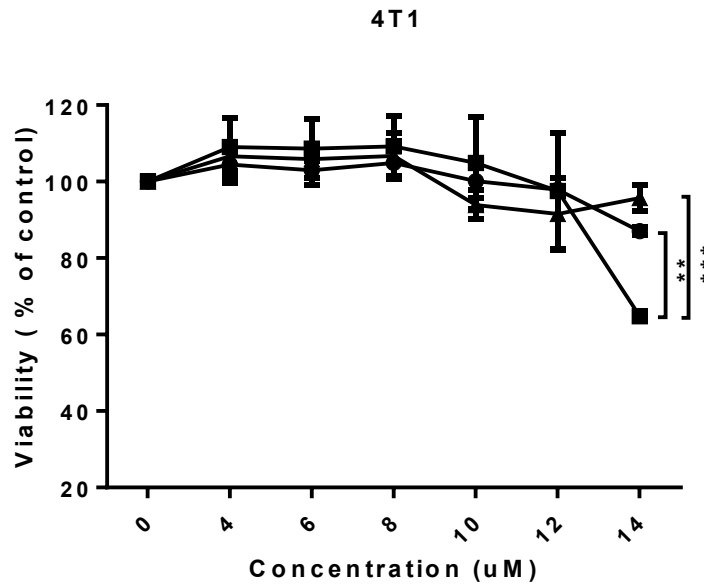


Figure 4.12 The effect of increasing concentrations of prodrug ZD2676P on the viability of the mouse breast cancer cell line 4T1 in the presence or absence of CPG2 or CPG2-p700. Experiments were performed in triplicate and data is presented as mean \pm SEM of three independent repeats. (**= $p < 0.01$, ***= $p < 0.001$) indicates significance, two-way ANOVA, multiple comparison test).

4.4. Discussion

Antibody-directed prodrug therapy (ADEPT) offered the promise of specific activation of cancer pro-drugs only at tumour sites. However, for reasons outlined earlier (section 4.1), this approach has not yet resulted in commercially viable drugs, and in fact CPG2 is the only enzyme to have been tested in clinical trials, which were not altogether successful (Sharma and Bagshawe, 2017).

We reasoned that the use of p700 to target enzymes to tumour sites, rather than antibodies, could overcome some of these issues, potentially reducing immunogenicity, decreasing clearance times and decreasing potential drug resistance due to the ability of p700 to target multiple receptors (Chen *et al.*, 2014). Nevertheless, whether p700 would retain its ability to bind receptors once covalently coupled to an enzyme could only be determined empirically.

In this chapter, we coupled p700 to the N-terminus of CPG2 via a [Gly₄Ser]₄ linker and showed that it could be purified from the insoluble fraction of bacteria in a form that retained both the catalytic activity of the CPG2 enzyme, as determined by methotrexate cleavage, and also the ability of p700 to bind to VEGFR2 with a high affinity, as determined by BLI. Additionally, p700 enabled association of CPG2 to the surface of 4T1 tumour cells, increasing cytotoxicity in the presence of the ZD2676P prodrug.

Interestingly, coupling the T3C peptide to CPG2 in the same way appeared to trigger degradation of the complex and so was not pursued further. The reason for this is uncertain but clearly lies in the difference between the two TIMP3 peptide sequences as the fusion proteins were otherwise identical in sequence.

The fact that the fusion proteins were largely confined to the insoluble fraction was not altogether surprising, considering the high level of expression seen, as this is often the

case when the overexpressed protein is more than 2% of the cellular protein (Singh *et al.*, 2015). This often leads to the formation of protein aggregates and subsequently denatured proteins. To obtain bioactive protein from inclusion bodies normally requires solubilisation in high concentrations (6-8M) of denaturing chaotropic agents, such as urea or guanidinium, followed by careful refolding by controlled dilution/dialysis to remove the chaotrope. However, in this case functional protein was extracted from the inclusion bodies with 2M urea. While much of the protein remained in the insoluble fraction, sufficient protein was extracted to enable subsequent purification and preliminary functional analysis.

Although budget constraints only enabled us to test binding of the CPG2-p700 complex to VEGFR2, and not the other closely related target receptors of p700, it would seem likely that this wider receptor binding profile is indeed retained, not only because these other receptors share a very similar ligand binding site in their D2/D3 immunoglobulin-like domains, but also due to the fact that p700 appeared to effectively associate CPG2 to the surface of 4T1 cells which do not express VEGFR2, the expression of which is largely limited to endothelial cells (Tseng *et al.*, 2010).

Although the improved ability CPG2-p700 to activate the pro-drug in the cytotoxicity assay, relative to CPG2 alone, was only seen at the highest dose of pro-drug, these concentrations were based on those from a previous study using a human colorectal cancer cell line and had not been optimised for 4T1 cells. A greater difference between the uncoupled- and p700-coupled CPG2 may have been seen if a higher dose range had been assessed. 4T1 cells were chosen here as our laboratory had previously shown p700 to be effective at inhibiting the growth of 4T1 tumours in a breast cancer model (Chen *et al.*, 2014) and so we intended using these cells in future *in vivo* studies. Indeed, another

advantage of p700 is that the peptide sequence is totally conserved between humans and mice and so it is unlikely to be immunogenic in either species.

While p700 is much less likely to elicit an immune response than a non-humanised monoclonal antibody, it is unlikely to reduce the potential immunogenicity of CPG2 itself. Nevertheless, our understanding of immunogenic epitopes is constantly improving and it is possible to predictively “deimmunise” proteins, as has been shown for certain β -lactamases that have applications in ADEPT (Osipovitch *et al.*, 2012), so it is likely that immunogenicity of the enzyme may become less of an issue in the future.

4.5. Conclusion

The data presented here verify the feasibility of using p700 as an alternative to monoclonal antibodies in directing CPG2 to tumour cells. As outlined above, p700 has many potential advantages over monoclonal antibodies. Moreover, we have shown that the CPG2-p700 fusion protein can be produced as a single functional protein in a bacterial expression system, greatly decreasing the potential production costs of such a molecule over ADEPT, where enzyme and antibody must be produced separately and chemically cross-linked, and where any antibody found to be effective in animal studies would need to be humanised prior to trials in humans.

Clearly the next step in validating the CPG2-p700 fusion protein would be to undertake an *in vivo* study to confirm efficacy in an animal model of cancer.

CHAPTER 5

**Assessment of the efficacy of Doxil-p700 in an *in vivo*
model of breast cancer**

5.1 Introduction

While *in vitro* experiments using cell lines are useful for the initial screening of any potential drug, they give little indication as to how that drug may act in a complex organism. This is particularly true of cancer drugs where tumour growth is not only dependent on how the drug affects the tumour cells themselves, but also how the drug acts in the complex tumour microenvironment in which multiple cell types exist, including those of the immune system. Additionally, many off-target effects, such as palmar-plantar erythrodysesthesia (PPE) are virtually impossible to predict *in vitro* (Gordon *et al.*, 1995, Charrois and Allen, 2003).

For these reasons, testing in animal models is an essential step in the development of any drug. Cost, ease of handling and the wealth of biochemical and genetic data available, make mouse models the most commonly used for initial drug screening. For cancer these models can be either syngeneic, i.e. the tumour is derived from the same organism, or xenografts, in which human tumours are grown in an immunocompromised mouse. Additionally, tumours can be implanted in a convenient location, e.g. sub-cutaneously in the flank, or orthotopically i.e. in the normal tumour site.

All of these models have their advantages and disadvantages. Xenografts are essential when the drug in question is specific to human cells but are also useful in examining the effect on the many well-established human tumour cell lines or on primary human tumour tissue. The main disadvantages of xenograft models are that they do not reflect a normal tumour microenvironment, and the human cells may not interact with host cells and molecules due to biochemical differences. Equally important, xenograft models lack a normal immune system. For these reasons, the engrafted solid human tumours are usually confined within sites of the graft and do not represent the metastatic capabilities of clinical tumours which account for most cancer related deaths (Guan, 2015).

The 4T1 mouse breast cancer cell line is widely used in cancer research and was derived from a BALB/c mouse mammary tumour that grew spontaneously (Tao *et al.*, 2008). The metastatic properties of the 4T1 cell line in syngeneic cancer models have been well studied and documented in the literature (Tao *et al.*, 2008, Heppner *et al.*, 2000). The cell line is highly aggressive *in vivo*, rapidly metastasising to the lungs, liver, brain, and bone, causing a lethal disease even after removal of the primary tumour, and bears a close semblance to metastatic human breast cancer (Fantozzi and Christofori, 2006) (Moase *et al.*, 2001).

The highly aggressive nature of the 4T1 model means it is a very robust model and therefore useful for testing cancer therapies. Our lab has previously reported that p700 alone was able to inhibit the growth of 4T1 tumours implanted subcutaneously (Chen *et al.*, 2014), although it did not prevent tumour metastasis, possibly due to an inability to actually kill the tumour cells.

For these reasons this cell line was chosen to test the efficacy of Doxil-p700 *in vivo*. In this case, however, the cells would be implanted orthotopically, providing a more realistic model of the disease.

5.1.1 Aim of this chapter

The aim of this study was to compare Doxil-p700 with the established drug, Doxil, to determine if there was any observable increase in efficacy and/or decrease in side effects as a result of p700 coupling. A preliminary study was carried out to determine the effects of using two different doses for each drug in the hope that this might give some indication as to the potential of p700 targeting of Doxil. The experiment was greatly facilitated by the publication of a detailed study of the effects of different dosing regimens for Doxil in orthotopically implanted 4T1 cells in BALB/c mice (Charrois and Allen, 2003). In that study a dosing regimen of 9mg/kg Doxil, administered twice with a one-week interval

between doses, was found to very significantly delay tumour growth with minimal side-effects. For this reason, we chose to compare doses of 5mg/kg or 10mg/kg, administering the two doses with a seven-day interval between doses. The health of the animals and growth of the tumour was monitored and then the animals were sacrificed and tissues taken for further analysis as described below.

5.2 Transplant of cancer cells into BALB/c mice

Six to seven week old female BALB/c mice were weighed and then anaesthetised in an induction box with 100% w/w inhalation vapour isoflurane (Zoetis) and 5% O₂ before being placed on a metal stage connected to 2.5% O₂. The abdominal area where the mammary fat pad is located was then shaved and wiped with antimicrobial skin cleaner. The skin was then raised with forceps and a small incision made to allow the orthotopic injection into the mammary fat pad of 5×10^5 4T1 cells (suspended in a 20 μ L mixture of PBS and growth factor-reduced-Matrigel in a 1:1 ratio) – see Figure 5.1. The incision was then closed with clips and the mice transferred to the incubator for 5 minutes to recover. The clips were removed after 72 hours and daily monitoring of the mammary fat pad tumour size was performed by measuring the diameter in two planes with callipers, and estimating tumour volume in mm³ using the formula: $\text{volume} = (a^2 \times b)/2$, where a is the smaller and b is the larger diameter in mm of the two dimensions. The mice were also weighed daily.

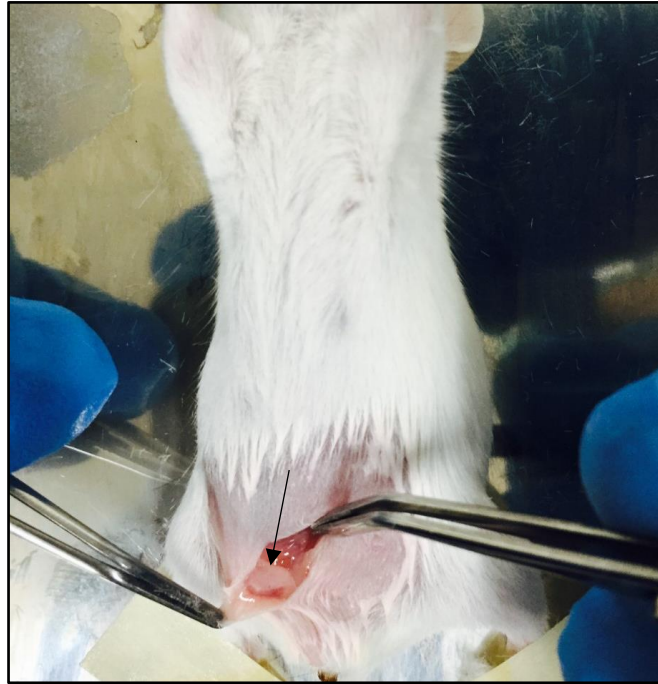


Figure 5.1 Abdominal cavity of BALB/c mice showing location of mammary fat pad (white) and 4T1 cell injection site (indicated by black arrow).

5.2.1 Treatment

Mice were divided into five treatment groups, each consisting of 8 mice. Once the tumour size reached 150-200 mm³, the mice were treated with drug or vehicle by injections into the tail vein under local anaesthesia with EMLA™ Cream (Astra Zeneca) as outlined in Table 5.1. Treatment with the same agent at the same dose was repeated after 7 days.

Table 5.1 Treatment group and dosage of Doxil or Doxil-p700 per body weight of mice

| Group | Number of Mice | Treatment |
|----------------|----------------|--------------------|
| Group 1 | 8 | Doxil-p700 5mg/kg |
| Group 2 | 8 | Doxil-p700 10mg/kg |
| Group 3 | 8 | Doxil-FITC 5mg/kg |
| Group 4 | 8 | Doxil-FITC 10mg/kg |
| Group 5 | 8 | PBS (vehicle) |

Daily monitoring of the mouse weight and tumour size continued after treatment and any physical changes or side-effects recorded. Exactly 7 days after the second treatment, the mice were culled by cervical dislocation and then dissected to remove the tumour and lungs. The tumour was divided into two and one half was placed into a plastic cassette containing Bright-Cryo-M-BED-Embedding compound to preserve the architecture of the tumour and stored at -80°C until further analysis. The other half of the tumour, the liver and the lungs were stored in 4% paraformaldehyde (PFA) at room temperature followed by wax embedding.

5.2.2 Fixed Tissue Preparation

Tissue fixed in 4% PFA were dissected and placed into cassettes (Simport-M490-2). They were then processed on an automated tissue processor (Leica- TP2010) according to the manufacturer's instructions. Briefly, water was gradually removed from the samples and replaced with paraffin wax by immersion in graded alcohol solutions then wax. The samples were immersed for 2 hours (with agitation) each in a sequence of pots containing 70% alcohol (3 times), 95% alcohol (2 times), 100% alcohol (2 times), xylene (2 times), then molten wax (2 times). A vacuum was applied in the last molten wax pot to pull the wax through the samples after which the samples were embedded in the wax using metal moulds. Sections (5 µm thickness) were then cut for haematoxylin and eosin staining (Section 5.2.3) using a Leica RM2245 microtome.

5.2.3 Haematoxylin and eosin staining

H&E staining was used to evaluate necrosis and identify lung metastases. Briefly, sections were de-waxed by immersing for 5 minutes each in two pots of xylene. They were then gradually rehydrated by sequential 3-minute washes in 100% ethanol (2 times), 95% ethanol, 90% alcohol, 70% alcohol and then rinsed in tap water for 1 minute.

This was then followed by staining with Gill's Haematoxylin for approximately 2 minutes or longer, checking for adequate nuclear staining under a "wet use" microscope (Olympus). The slides were then washed under tap water until it ran clear, followed by washes in 70% and then 90% alcohol for 3 minutes each.

They were then stained with 1% eosin (diluted in 95% alcohol) for 30 seconds to 1 minute, followed by three washes in 100% alcohol for 3 minutes each. Another two five-minute washes in xylene were then performed before cover slips were mounted with DPX mountant and the slides allowed to dry at room temperature.

5.2.4 Immunohistochemistry staining for caspase-3

Sections were first de-waxed by immersing in two pots of xylene for 10 and 5 minutes, respectively. They were then gradually rehydrated by sequential 3-minute washes in 100% ethanol (2 times) and then 95% ethanol.

Endogenous tissue peroxidase was then blocked by placing the slides in a 1:9 mixture of hydrogen peroxide and methanol, respectively for 30 minutes on a shaker. The slides were then washed quickly for 2 minutes in running tap water.

Antigen retrieval was carried out by placing the slides in a chamber rack filled with target retrieval solution (DAKO) diluted 1 in 10 with distilled H₂O. The rack was then placed in a pressure cooker (2100 Retriever) containing 750ml of distilled water, switched on and incubated for 2 hours. The slides were then rinsed in 0.1 % PBST (5ml of Tween 20 added to 5 litres PBS) a few times followed by two 3-minute washes in fresh 0.1% PBST with gentle shaking. After removing excess liquid by tapping the edge of the slide on tissue paper, the sections on the slides were encircled using an Immedge Hydrophobic barrier pen (Vector- Cat H400). The sections were then immediately covered with 0.1% PBST to prevent drying. Blocking solution of 10% goat serum and 1% bovine serum albumin (BSA diluted in PBST) was then applied to the tissue sections and incubated for one hour at room temperature.

Primary rabbit anti-caspase-3 (Cell Signalling - 9661) antibody was prepared by diluting at 1:600 in 1% BSA in PBST. Blocking solution was then removed by tipping off the slides and each dilution of primary antibody added to three slides each in addition to a negative control slide to which 1% BSA in PBST was added. The slides were then incubated overnight at 4°C.

The slides were then quickly rinsed twice in PBST followed by two 5-minute washes in PBST, ensuring that the negative control slides were done separately (in fresh PBST) to prevent inadvertent transfer of primary antibody.

Secondary antibody was prepared by diluting 10µl goat anti-rabbit antibody in 2ml of 2% goat serum (diluted in PBS). The secondary antibody solution was then added to all the sections and incubated for 30 min at room temperature. During this incubation, ABC reagent (Vector Laboratories) was prepared according to the manufacturer's instructions and left to stand for at least for 30 min before use.

The slides were then rinsed in PBST a few times followed again by two 5-minute washes in PBST with gentle shaking. ABC reagent was applied and incubated for 30 minutes at room temperature. The slides were then rinsed a few times in PBST and washed twice in PBST for 5 minutes each wash with gentle shaking. DAB solution was freshly prepared, according to manufacturer's instructions and added onto the tissue sections at room temperature for approximately 3 minutes, monitoring for the development of brown colouration under a wet slide microscope. DAB is a chromogenic substrate for peroxidase and turns into a brown insoluble product that is detected microscopically. At this point the slides were washed in water to stop the reaction.

The slides were then washed with running tap water for around 5 minutes before being stained with Gill's Haematoxylin for 30 seconds. This was followed by washing in running tap water for around 3 minutes until the water ran clear.

The sections were then dehydrated by sequential 3-minute washes in 70% ethanol, 90% ethanol, then 100% ethanol (2 times) before being transferred to mounting xylene for 5 minutes. Without allowing the sections to dry, the slides were then mounted with coverslips using DPX and incubated at room temperature until set.

5.2.5 Immunofluorescence staining for CD31

Immunofluorescence was performed on 10 µm frozen sections of mouse tumour that were cut using a cryotome (Microm Cryostar HM560) and placed on clean glass slides (Thermo Fisher, Superfrost Plus Cat No. J1800AMNZ). The sections were stored at -80°C prior to staining.

Once ready for staining, the frozen sections were allowed defrost at room temperature, but not air dry. The tissue was then fixed by flooding the slide with 100% ice-cold acetone and incubating for 10 minutes with frequently application of additional acetone to prevent drying. The acetone was then removed and the slide allowed to air dry. The tissue section was encircled with a hydrophobic barrier pen and PBST (0.05% Tween-20) was added to the section with a pipette and left on for 10 minutes to allow rehydration.

During the rehydration, fresh blocking solution of 10% goat serum and Fc receptor blocking reagent, diluted in PBST was prepared. The blocking solution was then applied to the rehydrated tissue sections and incubated for 1 hour at room temperature.

The blocking solution was then removed and the endothelial cell marker, Alexa 488-labelled anti-mouse CD31 antibody (BioLegend) was diluted 1 in 100 in PBST and applied to the sections. This was followed by incubation for 1 hour in the dark at room temperature. DAPI staining solution was then prepared by diluting stock DAPI solution in PBST at a ratio of 1:100. The primary antibody was removed and the DAPI applied to sections for 1 minute.

Stained slides were subsequently placed on a slide rack and washed by immersing in a large excess volume of PBST placed on a rotating platform for 15 minutes. Excess PBST was then removed from the slide, a single drop of ProLong™ Gold antifade reagent (Life Technologies™) applied to the section and mounted with a coverslip. The slide was then left overnight at room temperature to allow the antifade reagent to set.

5.2.6 Analysis for stained tumour or lung sections:

After slides were stained, they were imaged by confocal microscopy (NIKON A1) and five random images per tumour section taken and analyzed by Image J software in order to work out the percentage of positively stained areas. All other stained tumour or lung sections were imaged at x200 magnification using an automated NanoZoomer-XR C1200 digital slide scanner (Hamamatsu) before analysing the images with ImageScope (Leica) software. The software creates a composite image of the entire stained section and images can be produced at different magnifications ranging from x10 up to x200.

For analysis of tumour necrosis, apoptosis and lung metastasis, images of whole tumour or lung sections were taken at x100 and five random images were also photographed at the same magnification. The images obtained were saved as TIFF image format and the proportion of positive staining, as a percentage, was evaluated for each image. The imaging software enables the user to select colours that corresponds to positive stain and then automatically estimate the percentage of the image area that is made up of this positive stain.

5.3 Results

5.3.1 Health assessment of mice

The appearance and weight of the mice were monitored daily for fourteen days after the initial treatment. Observation of >20% weight loss or other symptoms such as limping were considered significant and indicated that the animal should be culled immediately to minimise suffering. As shown in Figure 5.2, there was a steady increase in the mean body weight for all treatment groups following the first dose, indicating no adverse effect of treatment on the health status of the mice. However, mice treated with 10 mg/kg of Doxil and Doxil-p700 exhibited a slight drop in body weight at Day 7 (post second dose), relative to the other groups, maintaining the body weight at between 19 and 20 g until the 14th day. However, these apparent differences were not statistically significant and treatment was generally well tolerated with no other physical signs of ill health detected.

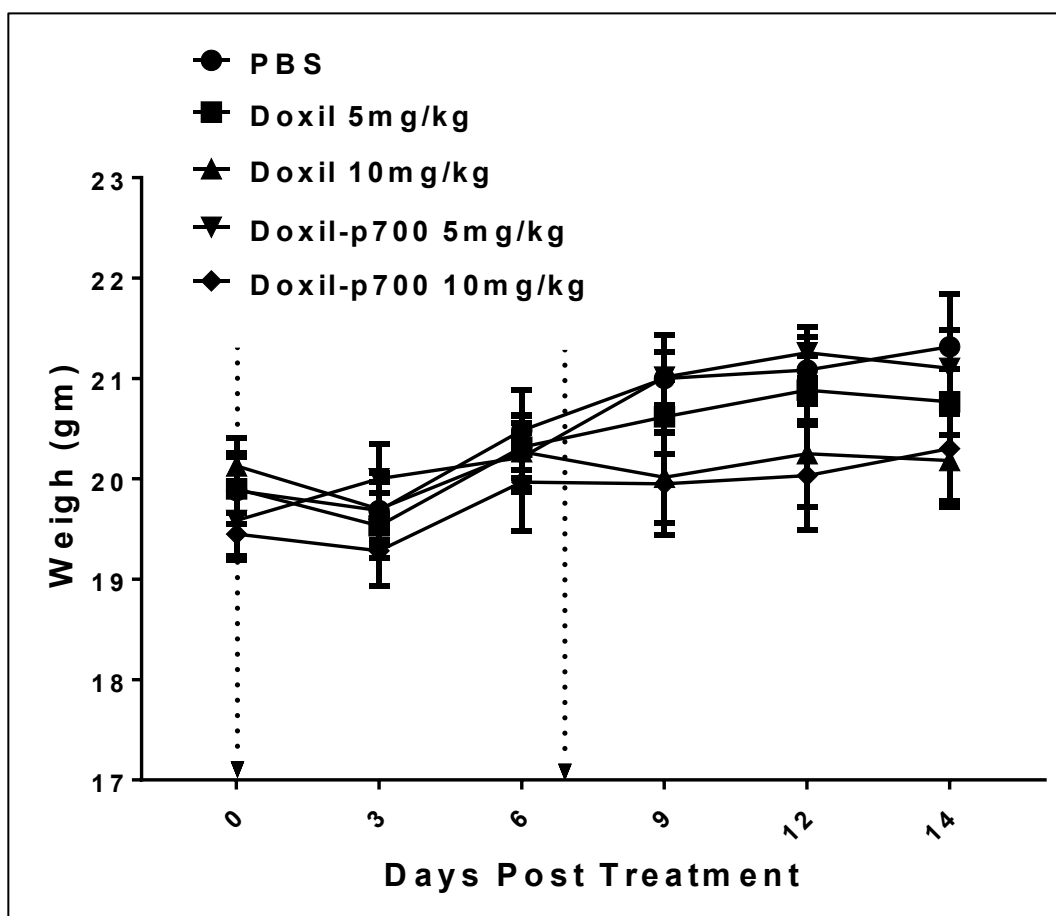


Figure 5.2 Doxil and Doxil-p700 do not significantly affect the weight of tumour bearing mice

Body weight of mice was measured daily for 14 days after first treatment as shown in the figure. Data is represented as mean \pm SEM of measurements in all mice in each treatment group (n = 8). Dotted arrows represent time-points (Day 0 and Day 7) at which treatment was given.

5.3.2 Effect of Doxil and Doxil-p700 treatment on tumour growth

As shown in Figure 5.3 (A), 5 mg/kg of both Doxil and Doxil-p700, and (B) 10 mg/kg Doxil and Doxil-p700 all induced a highly significant reduction in tumour size ($p < 0.0001$), with approximately 2-fold reduction in tumour volume for both dose levels when compared with the PBS-treated control group. However, there was no significant difference in efficacy between Doxil and Doxil-p700 nor between the two different doses of the drugs in tumour growth.

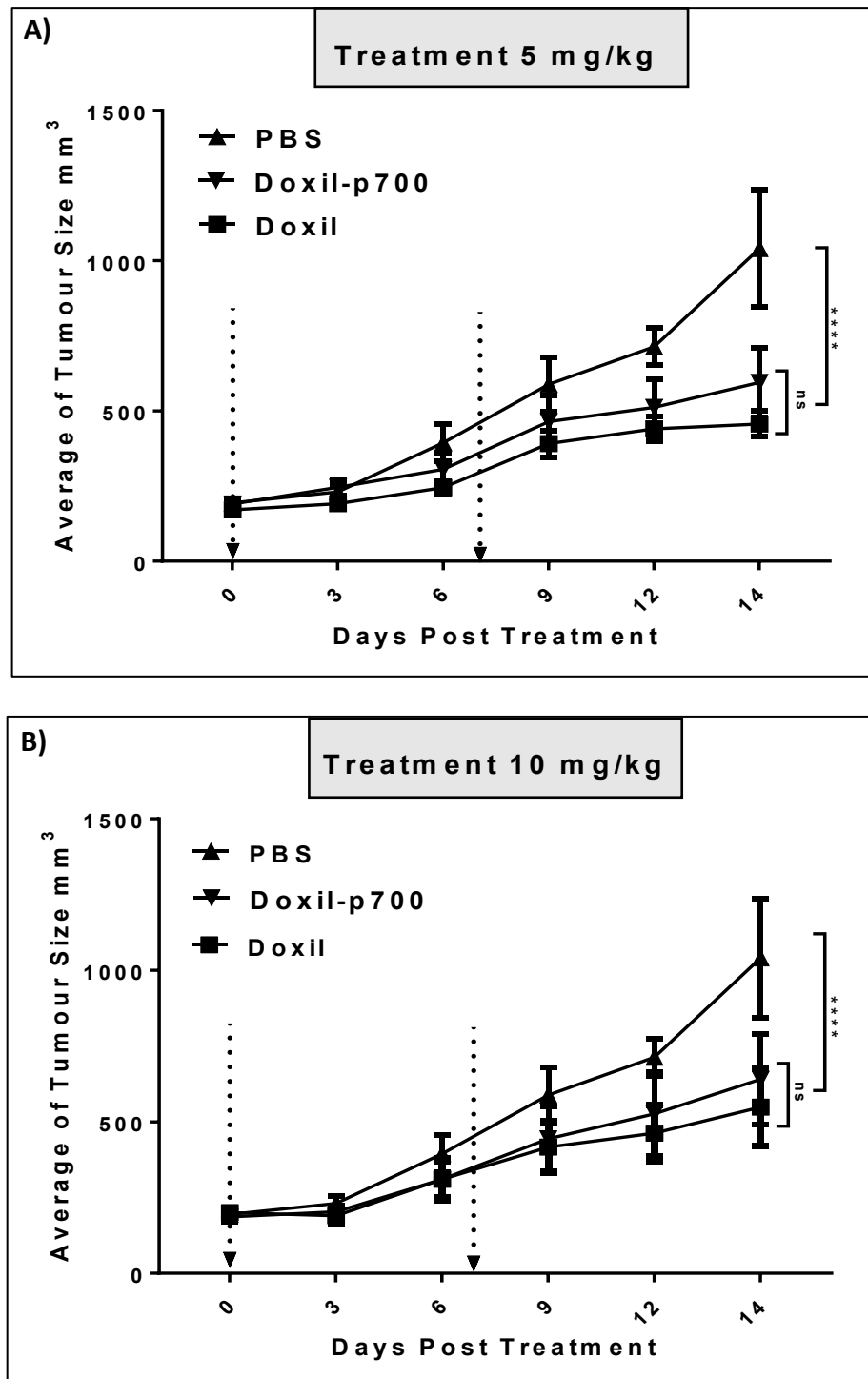


Figure 5.3 Doxil and Doxil-p700 significantly reduce tumour growth of orthotopically implanted 4T1 mammary tumours

Mice were first treated intravenously with Doxil or Doxil-p700 according to above dosage and the size of tumour measured by Vernier callipers both laterally and longitudinally for 14 days after treatment. Data is represented as mean \pm SEM of measurements in all mice in each treatment group (n = 8). (**** $p < 0.0001$. Two-way ANOVA, multiple comparison test). Dotted arrows represent time-points (Day 0 and Day 7) at which treatment was given.

5.3.3 Induction of necrosis by Doxil and Doxil-p700

Post-mortem analysis was performed on sections of tumour tissue removed from mice at the end of the experiment. Haematoxylin and eosin stained tissue sections were examined visually and scored using Image scope software. Necrotic cells are indicated by black arrows in Figure 5.4A. The necrotic cells are characterised by rounded morphology and they are detached from the tissue containing non-necrotic cells that are stained in blue. The percentage of necrotic cells determined by the area covered by necrotic cells as measured by Image Scope were similar amongst all the treatment groups including the control PBS-treated group (Figure 5.4B). This suggests, death by necrosis in these tumour tissues is independent of the treatment administered to the mice.

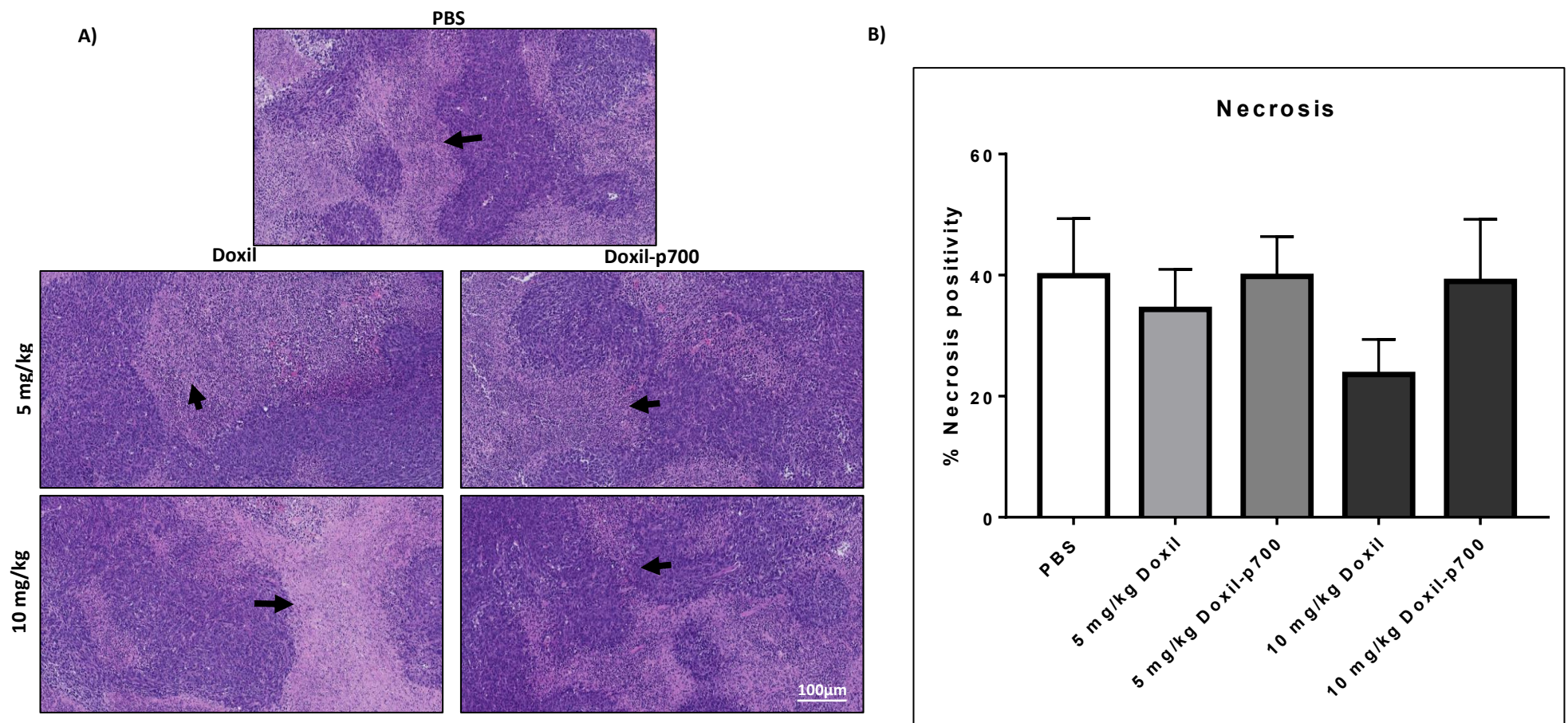


Figure 5.4 Identification and scoring of necrotic areas post-treatment with Doxil and Doxil-p700

A) Cross section of H&E stained mouse tumour tissue with the necrotic areas staining light blue and non-necrotic cells staining dark blue. B) Scoring of necrotic areas by Image Scope software at x10 magnification. Data represent mean area ± SEM. No significant difference ($p < 0.05$) was seen among the treatment groups using one-way ANOVA - multiple comparison test.

5.3.4 Caspase activation by Doxil and Doxil-p700

One of the mechanisms utilised by doxorubicin in inducing cancer cell death is through induction of caspase 3 mediated apoptosis (Yang *et al.*, 2006). We evaluated caspase 3 activation in the mouse tumour tissue section by measuring levels of caspase 3 cleavage using monoclonal anti-caspase 3 antibody. Using Image Scope software, images of the tumour tissue sections were scanned and the positive areas for caspase activation were estimated by Image J software. When compared with the control PBS-treated group, both 5 mg/kg and 10 mg/kg of Doxil and Doxil-p700 induced significant caspase 3 activation ($p < 0.01$ and $p < 0.0001$ respectively) that was also Doxil dose-dependent as shown in Figure 5.5. Conversely, there was no significant difference in the level of caspase 3 activation between Doxil and Doxil-p700 at 5 mg/kg and 10 mg/kg dosage. The negative control, without primary antibody showed no staining, confirming specificity of the antibody.

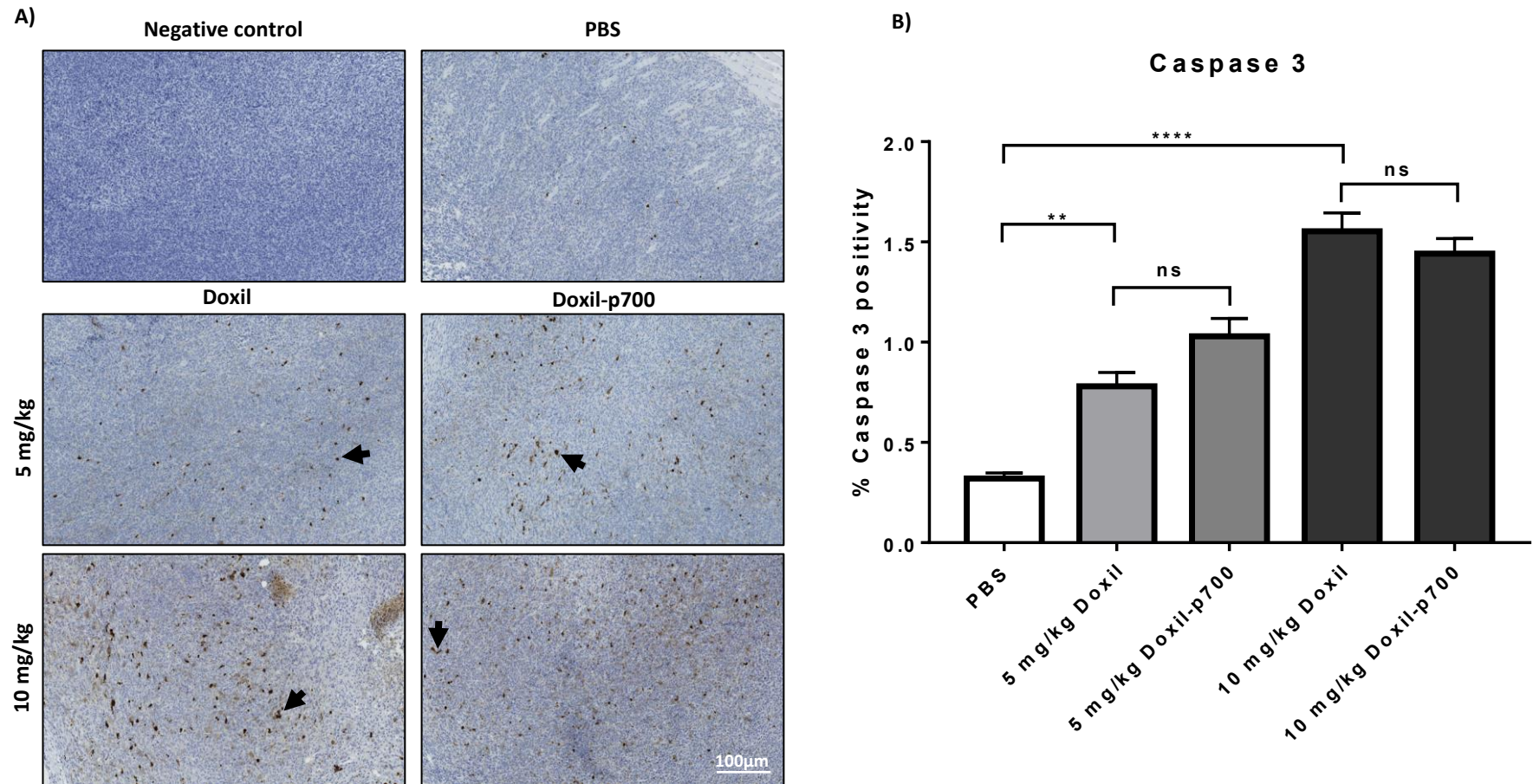


Figure 5.5 Caspase 3 activation after Doxil and Doxil-p700 treatment

A) Representative images of tumour tissue sections with anti-cleaved caspase-3 antibody at 1:600 dilution in 1% BSA in PBST. Brown DAB stained spots indicate cleaved caspase 3. B) Statistical analysis showed no significant difference between Doxil and Doxil-p700 treatment groups. Five randomly selected images were analysed for each treated tumour section. Data represented as mean \pm SEM. Significant differences ($p \leq 0.05$) among treatment groups were compared using ordinary one-way ANOVA - multiple comparison test [*ns* ($p > 0.05$); ** ($p < 0.01$); **** ($p < 0.0001$)]

5.3.5 Effect of Doxil and Doxil-p700 treatment on tumour vascularisation

Vascularisation is essential for tumour growth and metastasis and p700 should target tumour vasculature due to the upregulation of VEGF receptors on these cells. For this reason, vascularisation of the tumour tissues was evaluated by CD31 staining using monoclonal anti-CD31 antibody conjugated to Alexa 488 on frozen tissue sections from the mouse tumours. CD31, also known as platelet endothelial cell adhesion molecule-1 (PECAM-1) is highly expressed at endothelial cell junctions and is used as a marker for these cells, although it is also expressed by platelets and other blood cells, however these can generally be distinguished morphologically. Staining was evaluated visually and by image analysis using Image J software as described in section 5.2.6 above. While all treatment groups appeared to show some reduction in vascularisation relative to the PBS control, this was not statistically significant (Figure 5.6

A)

Isotype

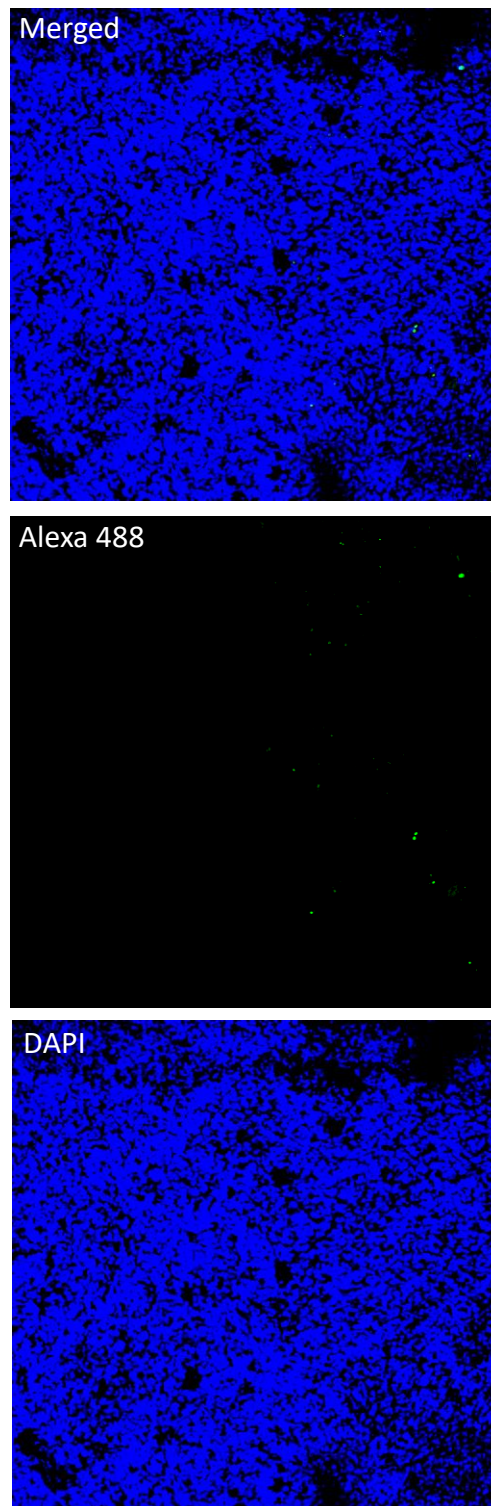


Figure 5.6A Effect of Doxil and Doxil-p700 on CD31 expression as a measure of vascularisation

Vascularisation on frozen tumour sections was determined by measuring CD31 staining using Alexa 488 conjugated anti-CD31 antibody (green). Panel A shows isotype controls with absent green CD31 staining. Blue indicates DAPI stained nuclei. Five randomly selected images were analysed for each treated tumour section.

B)

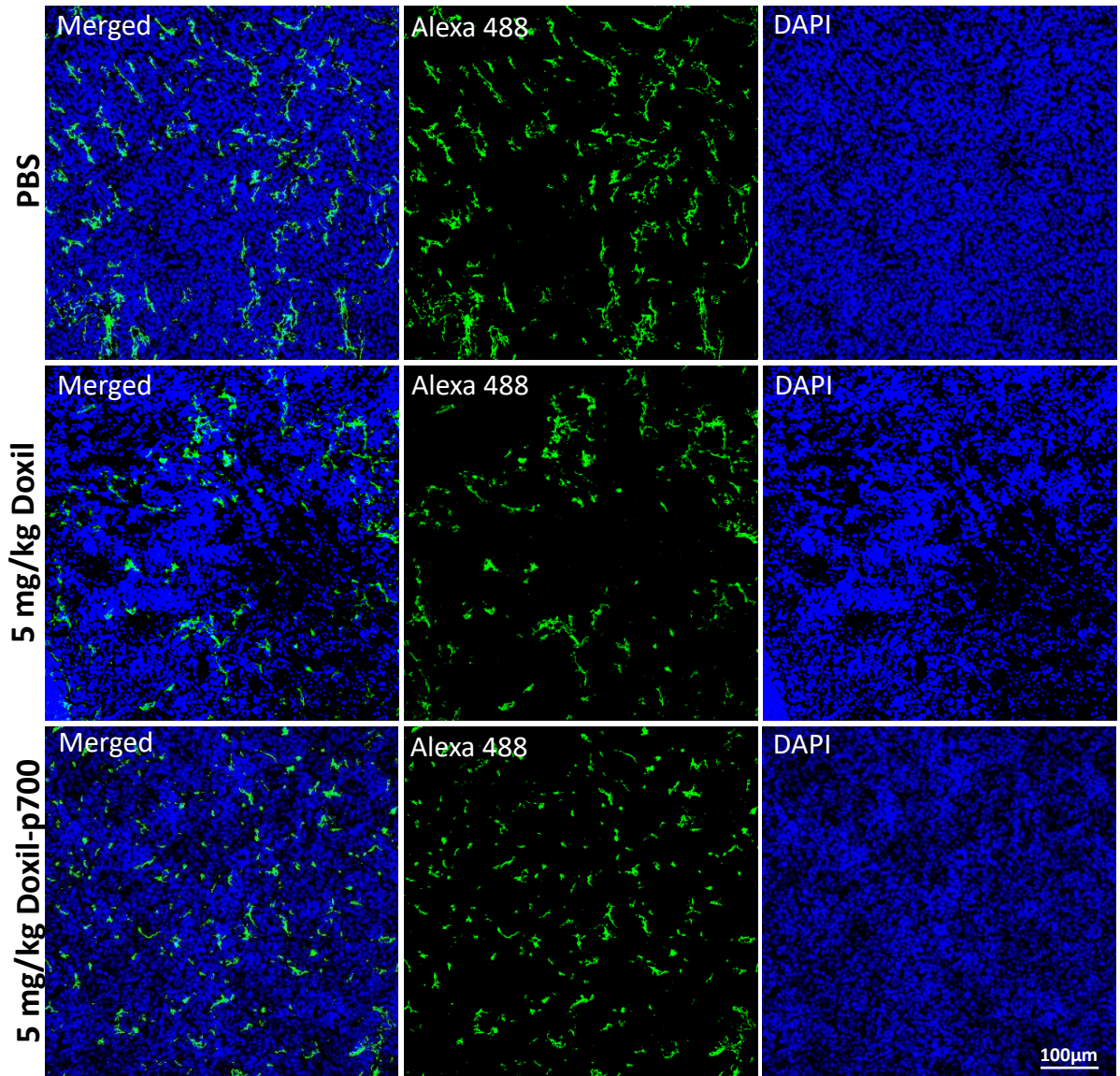


Figure 5.6B Effect of Doxil and Doxil-p700 on CD31 expression as a measure of vascularisation

Vascularisation on frozen tumour sections was determined by measuring CD31 staining using Alexa 488 conjugated anti-CD31 antibody (green). Panel B shows Doxil-p700- treated cells showing positive green CD31 stain. Blue indicates DAPI stained nuclei. Five randomly selected images were analysed for each treated tumour section.

C)

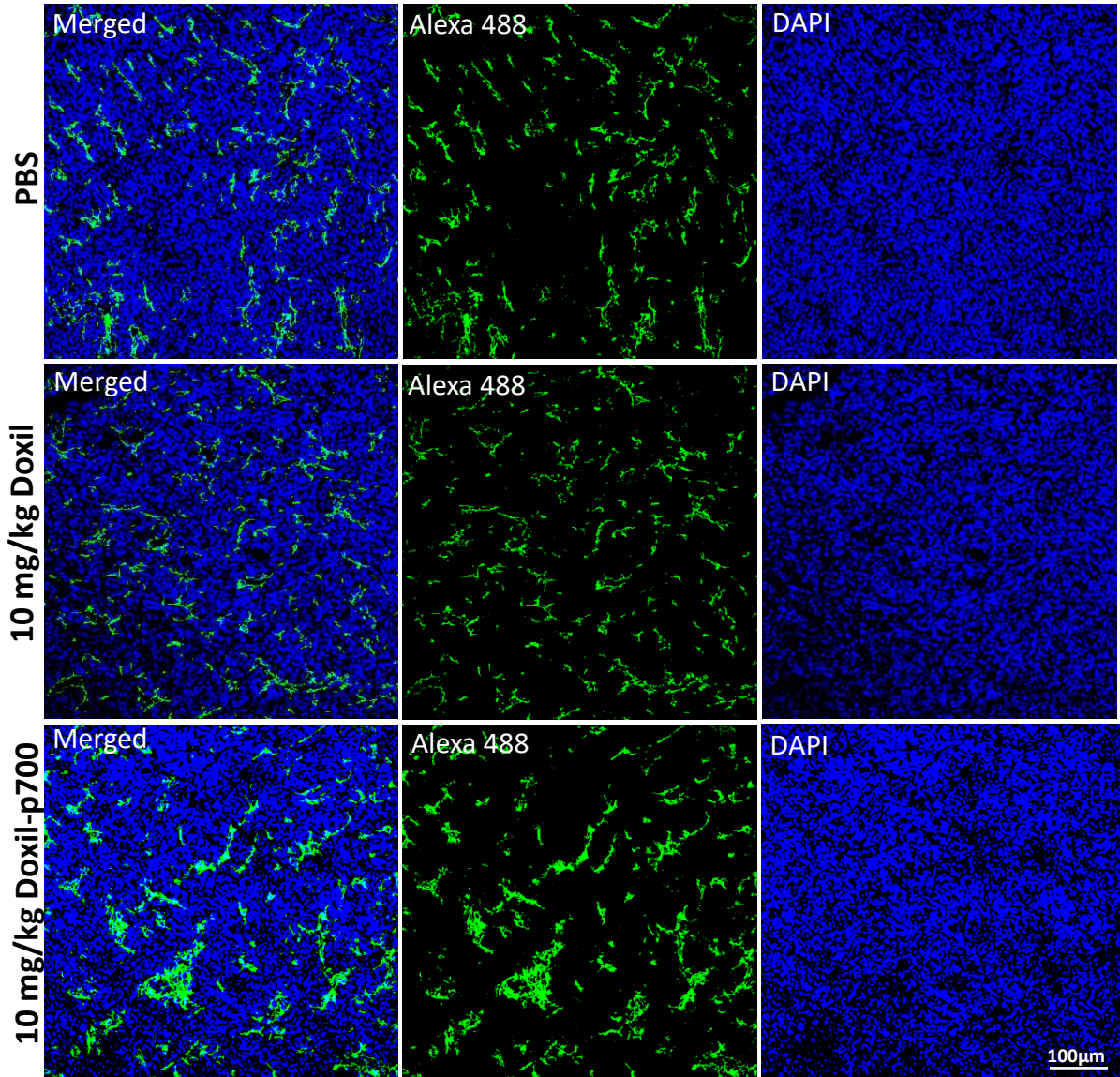


Figure 5.6C Effect of Doxil and Doxil-p700 on CD31 expression as a measure of vascularisation

Vascularisation on frozen tumour sections was determined by measuring CD31 staining using Alexa 488 conjugated anti-CD31 antibody (green). Panel C shows Doxil-treated cells showing positive green CD31 stain. Blue indicates DAPI stained nuclei.

D)

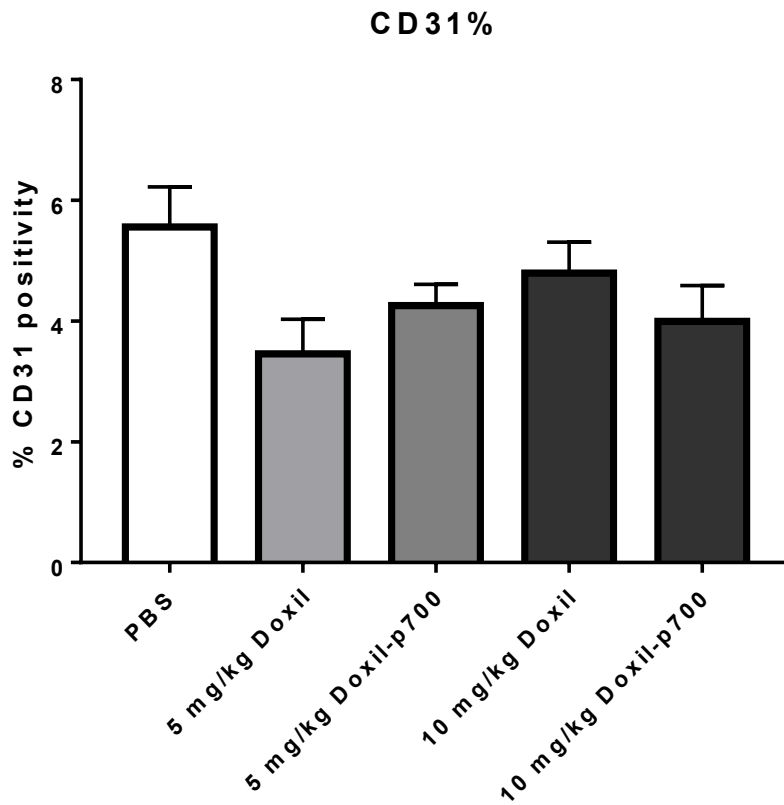


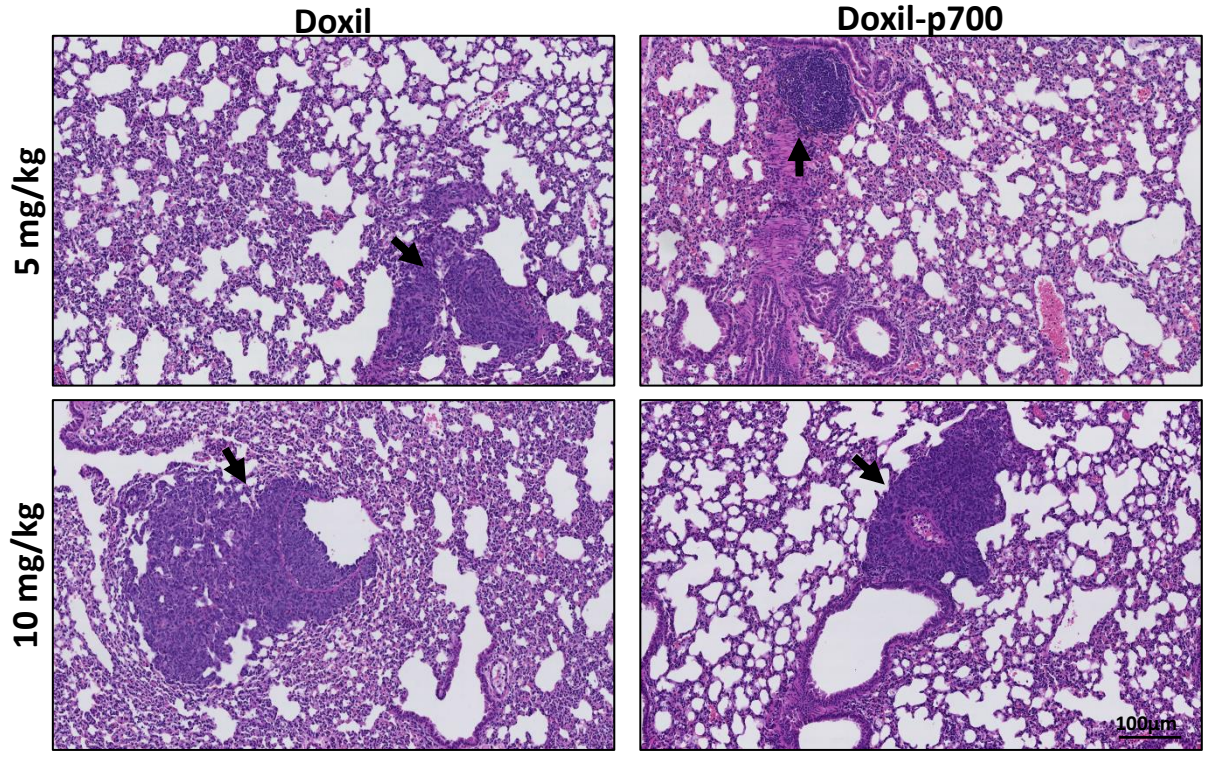
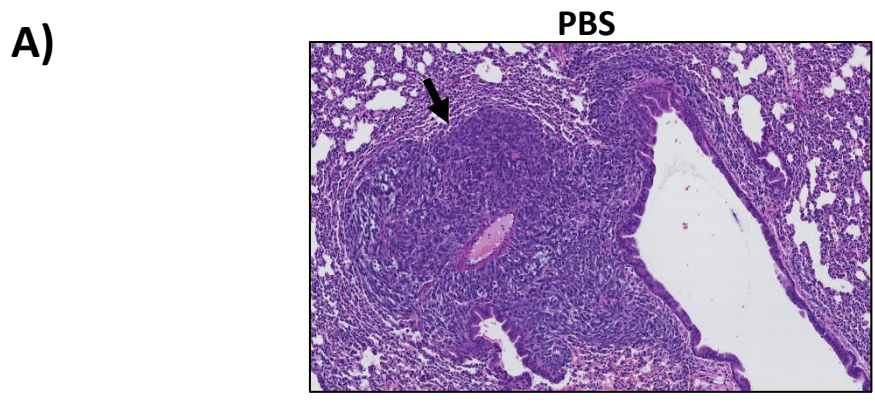
Figure 5.6D Effect of Doxil and Doxil-p700 on CD31 expression as a measure of vascularisation

Vascularisation on frozen tumour sections was determined by measuring CD31 staining using Alexa 488 conjugated anti-CD31 antibody and Image J software was used to score percentage of CD31 positive cells at x 10 magnification. For each tissue section, five randomly selected images were analysed. Data from five sections per mouse in each treatment group (n = 8) is presented as mean ± SEM. No significant difference ($p < 0.05$) was seen among the treatment groups using one-way ANOVA - multiple comparison test.

5.3.6 Effect of Doxil and Doxil-p700 treatment on lung metastasis of 4T1 cells

The effect of Doxil and Doxil-p700 treatment on the metastatic potential of 4T1 cancer cells was assessed in the lungs as this is one of the major metastatic sites for breast cancer and 4T1 cells, in particular, are known to spread to this location (Olkhanud *et al.*, 2009). Mice were treated as previously described and the lungs were collected from sacrificed mice seven days after the final dose. Tumour metastasis was determined by haematoxylin and eosin staining of lung sections and both numbers of metastasise (determined by counting random fields) and total area of metastatic sites (determined using Image Scope software) were measured (Figure 5.7A). There was a reduction in the number of lung metastatic foci seen in all four treatment groups compared to PBS control, but this was not significant, except for the 5mg/kg Doxil-p700 group ($p = 0.0069$). There was also no significant difference observed when the Doxil and Doxil-p700 groups at each dose level were compared with each other (Figure 5.7B).

As shown in Figure 5.7C, treatment with both Doxil and Doxil-p700 resulted in a highly significant reduction in the area of metastatic tissue in the lungs, relative to the vehicle control. While this area did appear to be slightly less with Doxil-p700 than Doxil at both doses, the difference was not significant.



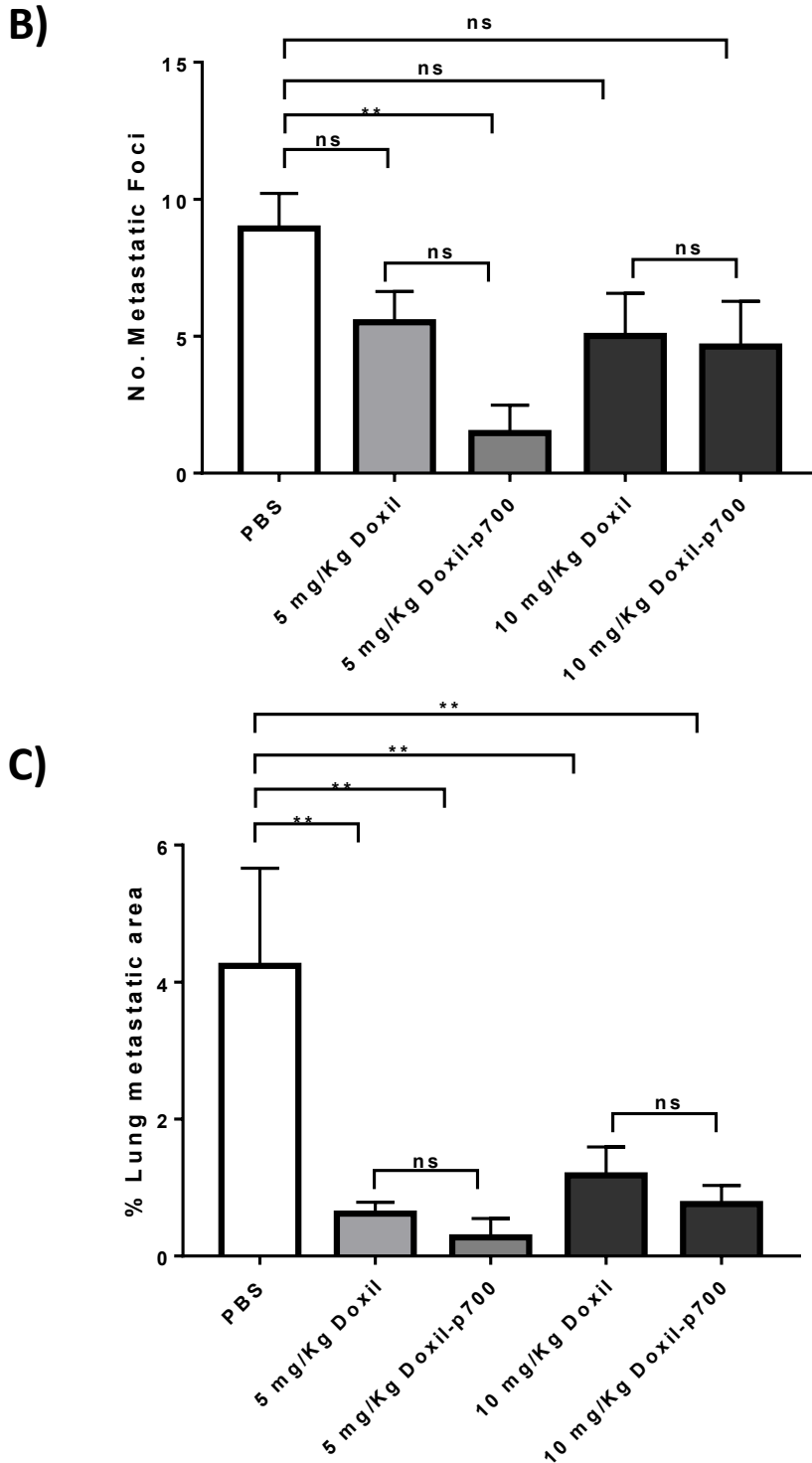


Figure 5.7 Effect of Doxil and Doxil-p700 on lung metastasis of 4T1 cancer cells

A) Representative images of lung tissue sections with haematoxylin and eosin showing pulmonary metastasis (dark blue), indicated by black arrows. B) Number of positive metastatic foci and C) area covered by metastatic cells were scored by Image Scope software as percentage of total area at x 10 magnification. For each lung section five randomly selected images were analysed. Data from five sections per mouse in each treatment group (n = 8) is presented as mean ± SEM. Significant differences ($p \leq 0.05$) among treatment groups were compared using ordinary one-way ANOVA - multiple comparison test [*ns* ($p > 0.05$); ** ($p < 0.01$)].

5.4 Discussion

The previous chapter clearly demonstrated that addition of p700 to the surface of liposomal doxorubicin greatly enhanced uptake and killing of tumour cells. The aim of this chapter, therefore, was to appraise the therapeutic potential of Doxil-p700, relative to Doxil alone, in an *in vivo* syngeneic mouse mammary cancer model where the effects of the tumour microenvironment and immune system may play a significant role in drug efficacy and where tumour metastasis and potential off-target effects could be examined. Here we used the 4T1 model because of its highly metastatic potential and previous studies have shown a response to doxorubicin (Bao *et al.*, 2011, McRae Page *et al.*, 2014). Nevertheless, although financial and time constraints meant that this was inevitably a very limited study, it was somewhat disappointing that the p700-conjugated Doxil failed to show any significant improvement in therapeutic effect, relative to the unmodified drug, in any of the criteria assessed with the one exception of a potential reduction in the number of lung metastasis at the lower dose of the drug. Although there is no clear-cut evidence on whether Doxil inhibits lung metastasis in patient with breast cancer, studies that investigated Doxil in metastatic breast cancer indicated it possess less cardiotoxicity and increases progression free interval by as much as 12 months compared with conventional doxorubicin (Ansari *et al.*, 2017, Rosati *et al.*, 2011, Rochlitz *et al.*, 2010).

It is possible that p700 may have been completely or partially removed by systemic proteases in our mouse model leading to a sub-therapeutic dose at the tumour tissue level. This could be confirmed by pharmacokinetic studies that involve measuring the levels of p700-conjugated Doxil in the tumour tissue and a full dose escalation study may have revealed a greater difference between the two drugs. The potential increased specificity of Doxil-p700 may enable a higher dose of the drug to be tolerated and therefore result in increased long-term efficacy. In these experiments, we did not detect any palmar planter

erythrodysesthesia nor any very significant weight loss with either drug, relative to the control, and so it would not be possible to assess this without using higher doses or a longer dosing regimen. On the other hand, it is also possible that Doxil-p700 may retain efficacy at lower doses, relative to Doxil alone. Again, this could only be ascertained using a much more thorough dosing regimen.

While there have been a number of studies reporting specific targeting of liposomal drugs to tumours (reviewed in (Khan *et al.*, 2015, Charrois and Allen, 2003)), some have only been carried out *in vitro* and the vast majority have used xenograft models, which are much less aggressive and, arguably, less realistic than the orthotopic 4T1 model used here. The other reason for choosing the 4T1 model was that we had previously shown successful tumour suppression in this model using p700 peptide alone (Chen *et al.*, 2014). However, 4T1 cells have been shown to readily develop resistance to doxorubicin by inducing expression of the MDR-1/P glycoprotein resulting its retention of the drug in the cytoplasm (Bao *et al.*, 2011) and so the 4T1 model may not have been the best choice when assessing the efficacy of Doxil. Another model that could be explored is the E0771.LMB mouse model of metastatic breast cancer to the lungs. This model exemplifies the metastasis of cancer cells from the mammary tumour to the lungs in the C57BL/6 mouse and it has been classified as a model that can be used to study aggressive form of metastatic breast cancer with poor prognosis (Johnstone *et al.*, 2015). Interestingly, the E0771 cell type has been shown in a previous study to be sensitive to doxorubicin in combination with interleukin-2 (IL-2) or sphingosine 1 phosphate, making it a plausible model to test the efficacy of Doxil (Ewens *et al.*, 2006, Katsuta *et al.*, 2017). Another model that can be explored is the MMTV-PyMT mouse model which expresses the polyoma middle T antigen (PyMT), which mimics growth factors under the control of the MMTV promoter for development of multifocal lesions and tumours in different

tissues including the lungs (Zhou *et al.*, 2011). Tumour formation in this mouse model is in stages that are characteristic of metastatic breast cancer and it is a model that has been shown to be responsive to doxorubicin treatment (Nakasone *et al.*, 2012). This makes it a perfect model to study the stage of breast cancer metastasis which Doxil actively targets. It is of course possible that, while p700 appears to greatly enhance localisation of Doxil to tumour cells *in vitro*, this may not necessarily be the case in a complex organism where the drug may be taken up by the mononuclear phagocyte system, differentially metabolised or simply not provide any enhancement in localisation above that due to the enhanced permeability and retention (EPR) effect (Maeda, 2012). Had time and budget permitted, it would have been informative to examine drug uptake in different tissues in the mice, which can be done by measuring doxorubicin fluorescence from different tissue slices (Song *et al.*, 2015).

5.5 Conclusion

In this preliminary study, Doxil-p700 at doses of 5mg/kg and 10mg/kg did not show significant effects on tumour growth, necrosis, apoptosis, vascularisation or metastasis compared to Doxil alone at equivalent doses in orthotopically implanted 4T1 cells in BALB/c mice. While it is possible that the choice of disease model may have decreased the likelihood that this *in vivo* study would be able to demonstrate a clear advantage in using p700 to target Doxil, there were some positive notes. Doxil-p700 did not show any loss of efficacy or increased toxicity, relative to Doxil only, and there was some indication that there was a decrease in the number of lung metastases at the lower dose. This, together with an observable if not statistically significant decrease in metastatic area in both Doxil-p700 groups, relative to the Doxil only groups, leaves some hope that a more comprehensive *in vivo* study may yet demonstrate therapeutic potential in p700-mediated drug delivery.

CHAPTER 6

**Identifying TIMP3 residues responsible for inhibition
of VEGFR2 to facilitate rational drug design**

6.1 Introduction

While we have already shown the therapeutic potential of the p700 peptide, obtaining a more precise understanding of the sites of interaction between TIMP3 and VEGFR2 may prove valuable in the rational design of novel inhibitors of VEGFR2. The fact that p700 is also able to inhibit a broader family of proangiogenic growth factor receptors indicates that it might also be possible to rationally design drugs that selectively inhibit groups of these receptors.

While our laboratory has shown that the p700 peptide, which corresponds to loop five and part of loop four of the C-terminal domain of TIMP3, plays an important role in this interaction (Chen *et al* 2014), this is by no means the only VEGFR2 binding domain on TIMP3. Qi *et al.* (2013) screened various peptides corresponding to both the N- and C-domains of TIMP3 and found that the most potent of these at inhibiting the VEGFR2 interaction were a peptide corresponding to the carboxyl tail (sequence GYCSWYRGWAPPDKSIINATDP) and one corresponding to loop 6 (sequence KNECLWTDMLSNGYPGYQSKHYACIRQKG). Somewhat surprisingly they found little effect with a slightly shorter version of our p700 sequence (KIKSCYYLPCFVTS). As already discussed in section 1.9, a similar study in our laboratory, (Mujamammi, 2014) using a series of TIMP3/TIMP4 chimeras and synthetic peptides, had also implicated the carboxyl-tail sequence and loop 6 in addition to the p700 sequence. By combining this information with computer based modelling we had identified eleven potential VEGFR2-interacting residues on TIMP3, however only six of these differed from the equivalent residues found on TIMP4, which does not bind VEGFR2, these being F133, V134, S147, Q164, W175 and A176 (numbering for the secreted TIMP3 sequence).

6.1.1 Aim of this chapter

In order to test the hypothesis that the above named residues are critical for the specific interaction of TIMP3 with VEGFR2, we aimed replace the equivalent residues in the C-terminal domain of TIMP4 with these residues to see if this would impart an ability to inhibit VEGFR2 signalling. While both TIMP2 and TIMP4 show a similar degree of sequence identity to TIMP3 in the C-terminal domain (43% and 44% respectively), unlike TIMP4, TIMP2 also inhibits angiogenesis in an MMP-independent manner. In this case, TIMP2 binds $\alpha 3\beta 1$ integrin resulting in an elevated level of protein tyrosine phosphatase that dephosphorylates FGFR-1 and VEGFR2, thus modulating the activity of these receptors (Seo *et al.*, 2003). As a consequence, this would have a confounding effect on any results obtained from the creation of TIMP3-TIMP2 chimeras as regards VEGFR2 inhibition.

A TIMP3-TIMP4 chimera was previously created in our lab and shown not to inhibit VEGFR2. It was decided to introduce potential VEGFR2 binding residues into this chimera, rather than into TIMP4 itself for 2 main reasons. While the N-domain of TIMP3 alone does not inhibit VEGFR2, *in silico* modelling indicated that some residues in the N-domain may also play a role in receptor binding (Chen *et al.*, 2014). Additionally, TIMP4 is a completely soluble molecule that would not localise to the ECM, potentially reducing the concentration at the cell surface. This would particularly be an issue when carrying out the VEGFR2 phosphorylation assay as it is necessary to replace medium that would contain the recombinant protein with starvation medium prior to the assay resulting in almost complete loss of TIMP4 in the medium.

The initial experiments aimed to compare inhibition VEGFR2 phosphorylation by three molecules: wild-type TIMP3, an unmodified TIMP3-TIMP4 chimera (T3T4) and a TIMP3-TIMP4 chimera in which the 6 amino acid residues identified above replaced the

equivalent residues in TIMP4 (T3T4V). Vectors containing TIMP3 and the T3T4 chimera had previously been prepared in our laboratory (Mujamammi 2014). The T3T4V construct was gene synthesised. This enabled codon optimisation for mammalian cell expression and the silent introduction of additional restriction sites that would enable different regions of the TIMP4 C-domain to be replaced back to the wild-type sequence in order to further localise individual residues, should swapping all six residues result in an VEGFR2-inhibitory molecule (see Appendix A2). In order to facilitate detection of these molecules, and enable distinction from any endogenous TIMP proteins, the sequences were tagged with the V5-[His]₆ sequence on the C-terminus. V5 is a 14-amino acid sequence derived from simian virus 5 to which highly specific antibodies have been raised. The [His]₆ tag also enables binding to metal chelate columns which could be used to purify the recombinant proteins if desired.

The H5V mouse endothelial cell line was chosen to express the TIMP construct because, as has already been discussed, this cell line expresses readily detectable levels of VEGFR2 which show robust autophosphorylation in response to VEGF (Kanthou *et al* 2014).

6.2 Methods

6.2.1 Polymerase chain reaction (PCR) for adding the V5-[His]₆ tag to TIMP chimeras

PCR was used to add a V5-[His]-6 tag to the existing TIMP3/TIMP4 chimeras by inclusion of the sequence in the reverse primer; 5'T3-HindIII (5'-GCCGGATCCAAGCTTGCCACCATGACCCCTTGGCTCGG-3'); 3'V5His-T4 (5'-CCAGCGCTCGAGCTAGTGGTGGTGGTGGTGGTGACCGGTACGGGT). For the PCR reaction, a PCR master mix was prepared for 8 reactions as in Table 6.1 PCR mastermix preparation enabling a series of annealing temperatures to be tested simultaneously. The gradient PCR machine was set up for 30 cycles, with a melting temperature of 98°C for 10 seconds, an

annealing temperature ranging from 50-70°C for the first cycle and 60-70°C for subsequent cycles, and an extension temperature of 72°C for 30 seconds.

The lower temperature of the first cycle was due to the fact that much of the reverse primer (the V5-His sequence) would not anneal to the template in the first cycle but would fully anneal to the full-length products. After the cycles had completed, the PCR products of the correct size were gel purified.

Table 6.1 PCR mastermix preparation used to add the V5-[His]₆ tag

| Component | Volume per 25µl Reaction | Final Concentration |
|--------------------------------------|---------------------------------|----------------------------|
| Nuclease free water | Up to 25µl | |
| 10µM Forward Primer | 1.25µl | 0.5µM |
| 10µM Reverse Primer | 1.25µl | 0.5µM |
| Template DNA | 1µl | 100ng/µl |
| Phusion Hot Start Flex 2X master mix | 12.5µl | 1X |

6.2.2 Digestion and ligation of PCR products and pcDNA6 vector

T3T4V-V5-His was digested with HindIII HF and XhoI restriction enzymes and T3T4-V5-His was digested with XhoI and BamHI before being ligated into similarly cut pcDNA6 vector, as described in sections 2.1.4 and 2.1.6 pcDNA6 contains the blasticidin resistant gene for selection of stable transfectants in mammalian cells.

6.2.3 Transformation of T3T4 constructs into competent E-coli

All constructs were transformed into α -Select Chemically-competent *E. coli* (section 2.1.1). Miniprep and maxiprep plasmid purification were then performed (section 2.1.3).

6.2.4 Diagnostic restriction digest

The same enzymes used in the ligation were used to carry out a diagnostic digest of the minipreps in order to confirm the presence of the insert followed by DNA sequencing to confirm cloned plasmid sequences (section 2.1.7).

6.2.5 Transfection of cell lines

Transfection of the H5V cells that were between 70-90% confluent was initially optimised by transfection in six-well plates with a plasmid containing the green fluorescent protein (GFP) under the CMV promoter (pmaxGFPTM) using both Lipofectamine 2000 and TransIT-LT1 reagents at various ratios.

TransIT-LT1 reagent was equilibrated to room temperature for 5 min and vortexed prior to use. 250µl of Opti-MEM I reduced-serum medium was placed in a sterilised tube and

2.5 µg (2.5 µl of a 1 µg/µl stock) plasmid DNA was added to the medium. The mixture was gently pipetted to mix completely. Afterwards, 15 µl or 7.5 µl Trans IT-LTI reagent (for 1:6 or 1:3 DNA:TransIT transfection ratios, respectively) was added to the diluted DNA mixture and the mixture pipetted gently. The mixture was incubated at RT for 25 min. The Trans IT-LTI reagent and DNA complexes were added to the cells drop wise and the plates gently rocked to allow even mixing.

For cell transfection using Lipofectamine 2000 reagent, a DNA:lipofectamine ratio of 1:4 (3 µl of DNA at 1µg/µl with 12 µl Lipofectamine) or 1:5 (3 µl of DNA with 15 µl Lipofectamine) were compared to determine the optimal ratio. The mixture was gently vortexed and incubated at RT for 5 mins and then added to 300 µl of serum free media and allowed to stand for 30 mins at RT. The reagent was then added to the wells in drop wise fashion and the plate rocked gently for even distribution. The cells were incubated at 37°C for 48 hrs and then examined under an inverted fluorescent microscope.

Following optimisation, H5V cells were transfected, as determined, and grown for 48 hours, followed by transfer into T75 flasks in preparation for selection in media containing 10 µg/ml of Blasticidin. After about 15-20 days, once the selection was complete, the antibiotic concentration in the medium was halved.

6.2.6 Phosphorylation assay

Untransfected H5V cells or those stably transfected with the TIMP3, T3T4 or T3T4V plasmids were maintained in complete medium until $\geq 90\%$ confluent and then harvested by trypsinisation. The cells were seeded into 100 mm dishes at a density of 1×10^5 cells/dish. At 90% confluence, the cells were washed twice in 1X DPBS followed by serum-starving (medium containing 0.5% serum) overnight for at least 17 hours followed by treatment with 0, 5, 10, 15 or 20 ng/ml of VEGF for 5 mins at room temperature. After treatment the cells were solubilised by scraping into 1x SDS-PAGE sample buffer and

centrifuging at 400,000g, in an ultracentrifuge at 20°C for 15 min to remove genomic DNA and the supernatant transferred into Eppendorf tubes for protein assay followed by western blotting (sections 2.1.10 - 2.1.12). Blots were initially probed with anti-phospho-VEGF Receptor 2 (Tyr1175 – clone (19A10) rabbit monoclonal antibody - Cell Signaling) before stripping and reprobing with anti VEGFR2 (clone 55B11) rabbit monoclonal antibody (Cell Signaling).

6.3 Results

6.3.1 Creation of V5-His-tagged chimeras

Following optimisation of the PCR reaction, V5-His tagged chimeras were produced and digested with the appropriate enzymes and the products separated on agarose gels, alongside similarly digested pcDNA6 vector (Figure 6.1). The bands corresponding to the chimeras and cut pcDNA6 vector gel were then purified and ligated. Minipreps of the ligated products were performed and these were digested with the same restriction enzymes and separated on an agarose gel to ensure the presence of the inserts (Figure 6.2). Following maxiprep purification of the ligated constructs, automated DNA sequencing confirmed the correct sequence and orientation of the chimeric products in the vector.

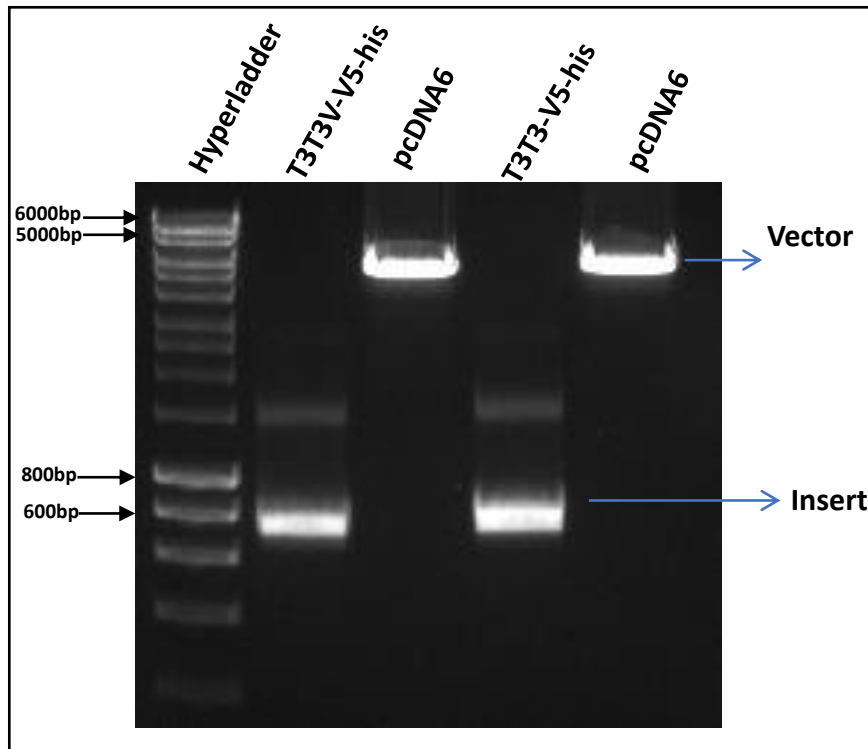


Figure 6.1 Preparation of T3T4 chimeras for insertion into the pcDNA6 vector

T3T4V-V5-His (lane1) and pcDNA6 (lane2) were digested with HindIII HF and XhoI. T3T4-V5-His (lane3) and pcDNA6 (lane4) were digested with XhoI and BamHI. They were all run on a 1% agarose gel and the arrows denote the bands that were gel purified and then ligated.

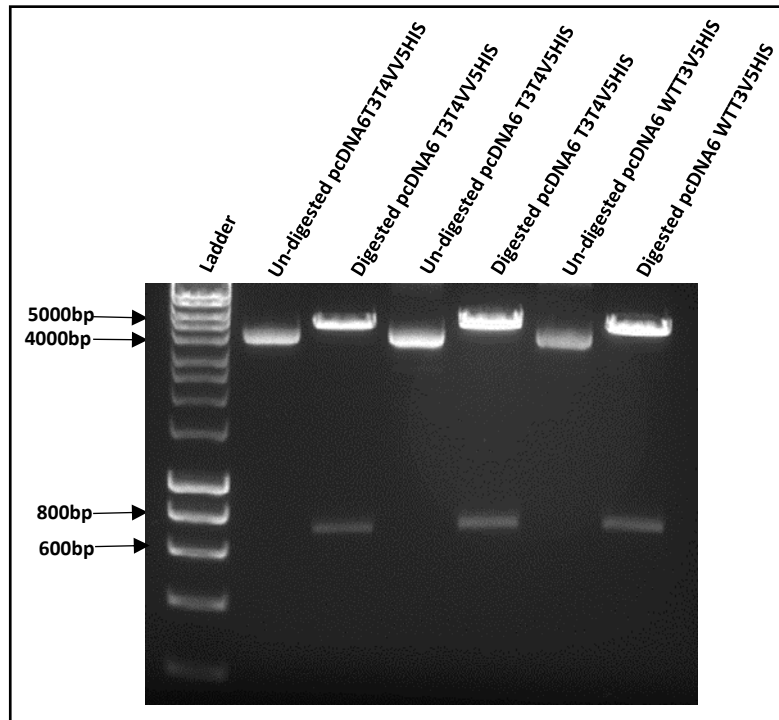


Figure 6.2 Diagnostic restriction digest of final TIMP constructs

100 ng of undigested pcDNA6T3T4VV5HIS (lane 1), digested pcDNA6 T3T4VV5HIS (lane 2), Un-digested pcDNA6 T3T4V5HIS (lane 3), Digested pcDNA6 T3T4V5HIS (lane 4), Un-digested pcDNA6 WTT3V5HIS (lane 5) and Digested pcDNA6 WTT3V5HIS (lane 6) were run on 1 % agarose gel after treatment with a cocktail of different restriction enzymes. The arrows denote the bands that were gel purified after digestion to confirm accuracy of restriction enzymes.

6.3.2 Optimisation of H5V cell transfection

Optimisation of transfection using Lipofectamine 2000 (Figure 6.3), or TransIT-LT1 (Figure 6.4), revealed Lipofectamine to be the more efficient reagent for transfecting H5V cells, with approximately 55% of cells being visibly fluorescence at a DNA:Lipofectamine ratio of 1:5. In contrast the maximum transfection for TransIT, at a DNA:TransIT ratio of 1:3, was only about 10%.

6.3.3 Stable transfection of H5V cells with the TIMP constructs

Following Blasticidin selection, western blotting using anti-V5 monoclonal antibody was used to confirm stable expression of all three TIMP constructs (Figure 6.5A). The level of expression of all three proteins was similar, as was confirmed with the anti-Histone antibody loading control (Figure 6.5B). TIMP3, unlike TIMP4, is N-glycosylated in the C-terminal domain, explaining the observation that only this protein gave rise to two distinct bands, corresponding to glycosylated and non-glycosylated protein.

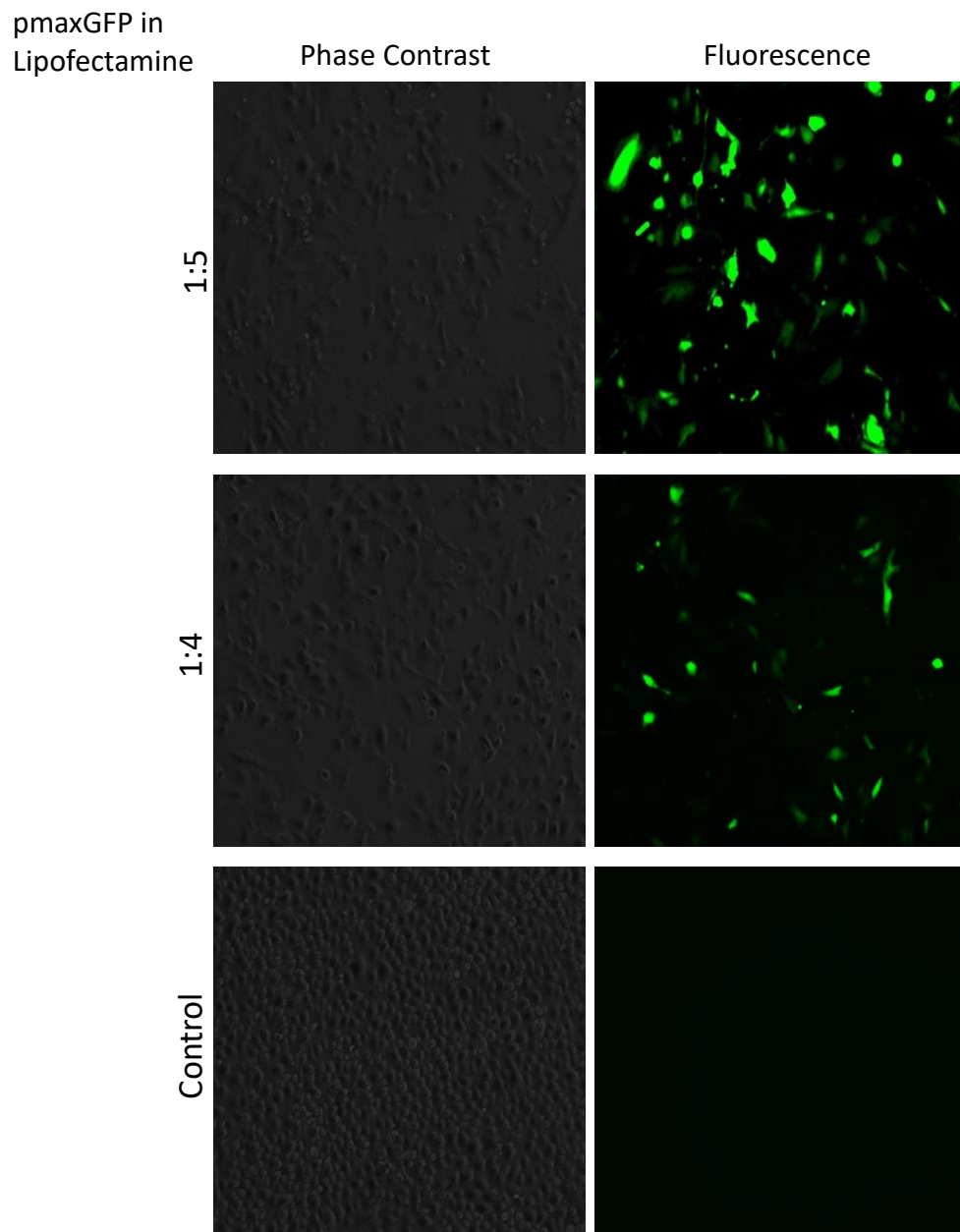


Figure 6.3 Transfection of H5V cells with pmaxGFP using Lipofectamine 2000

Cells were transfected with 3 μg of GFP plasmid and incubated for 48 hrs after which the cells were viewed under an inverted fluorescent microscope to observe the expression of the GFP protein. The control cells were mock transfected with Lipofectamine 2000 only.

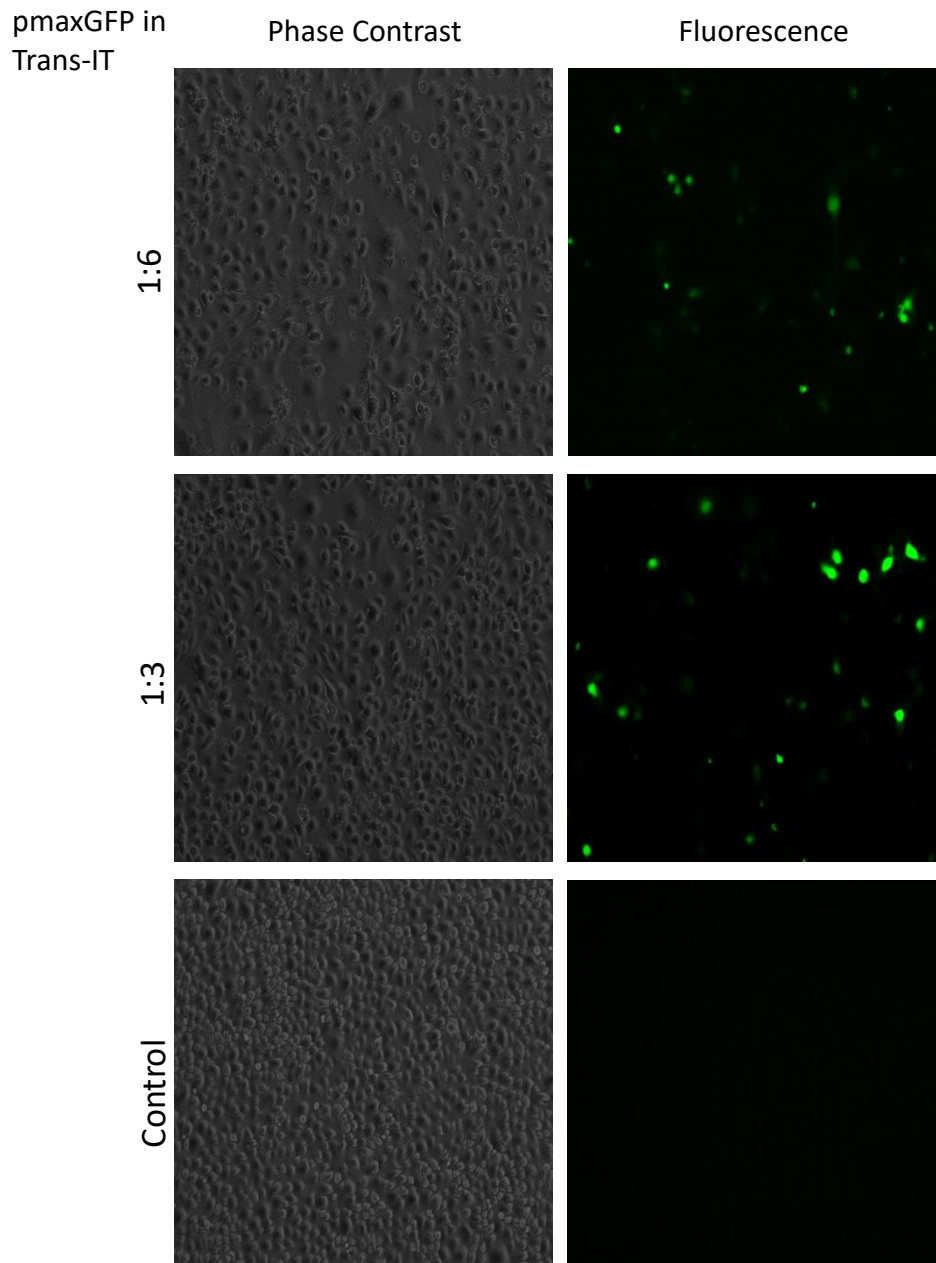


Figure 6.4 Transfection of H5V cells with pmaxGFP plasmid using TransIT-LT1

Cells were transfected with 3 μg of GFP plasmid in Trans IT reagent and incubated for 48 hrs after which the cells were viewed under an inverted fluorescent microscope to observe the expression of the GFP protein. The control cells were mock transfected with Trans IT reagent only.

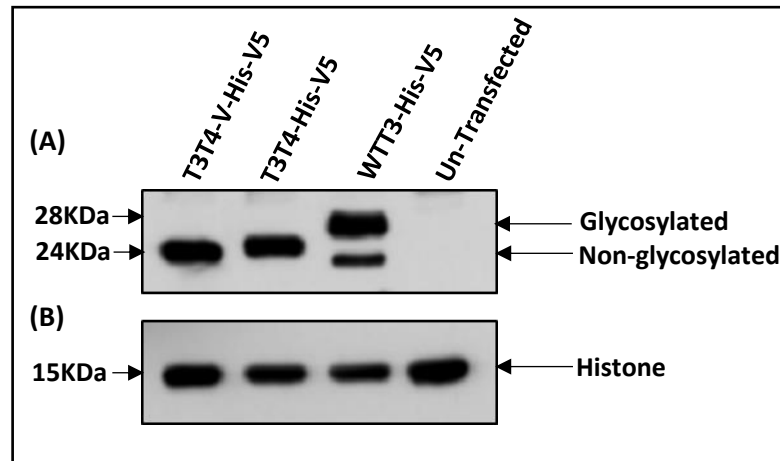


Figure 6.5 Expression of TIMP proteins by stably transfected H5V cells

H5V cells were stably transfected using Lipofectamine 2000 with the stated constructs and the solubilised protein extract from the cells subject to western blotting and probing with anti-V5 antibody (A) and then stripping and re-probing with anti-histone antibody as loading control (B).

6.3.4 Confirmation of VEGFR2 autophosphorylation in untransfected H5V cells

VEGF-induced phosphorylation of VEGFR2 in the H5V cell line was evaluated to ensure that phosphorylation could be easily detected in the cells using available antibodies and determine the sensitivity of the response to varying concentrations of VEGF. As can be seen in Figure 6.6, there was an apparent dose-dependent increase in the autophosphorylation of VEGFR2 in response to VEGF. To confirm that the increase was not due to variable sample loading, the blot was stripped and re-probed with an antibody against total VEGFR2 which confirmed equal sample loading and VEGFR2 protein expression.

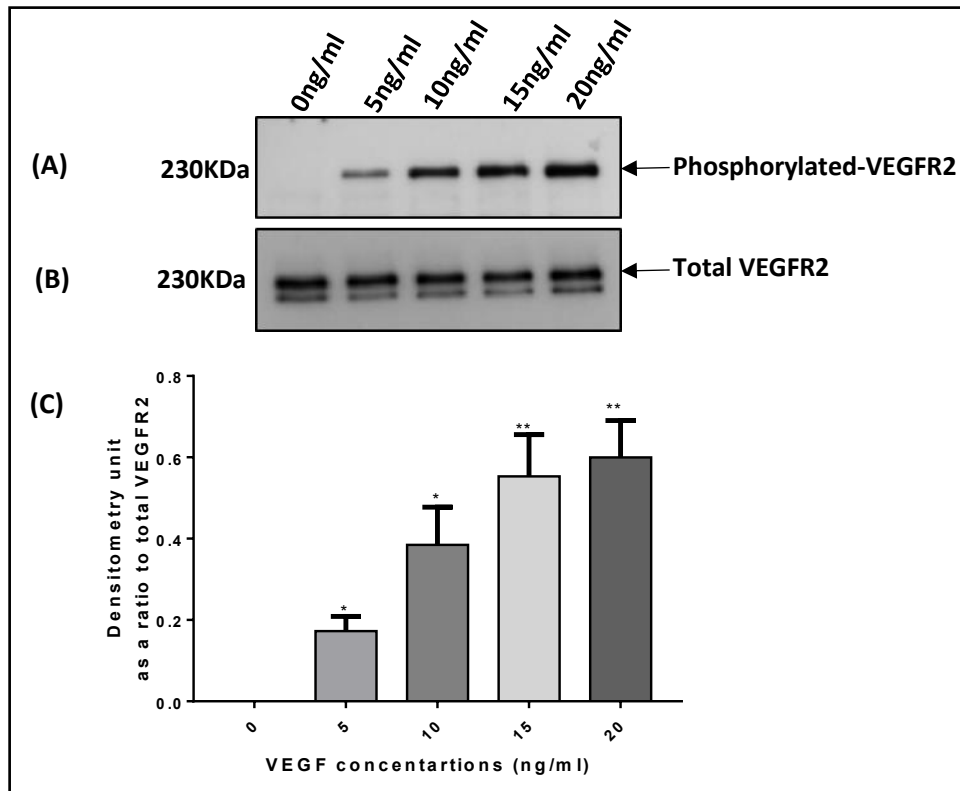


Figure 6.6 VEGFR2 phosphorylation in the H5V cell line

Untransfected H5V cells were lysed after stimulation with the indicated concentration of VEGF and whole cell lysate was electrophoretically transferred and immunoblotted with 1:2000 rabbit monoclonal anti-Phospho VEGFR2 antibody (A) or 1:3000 rabbit monoclonal anti-total VEGFR2 (B). Densitometry (graph C) shows VEGFR2 phosphorylation and total VEGFR2 expression as estimated from blots using image J software. Data is presented as mean \pm SEM from three independent repeats.

6.3.5 VEGFR2 autophosphorylation assay in H5V cells transfected with the TIMP chimeras

Stably transfected H5V cells were treated with varying concentrations of VEGF and western blotting performed, as described above, to determine whether the recombinant proteins affected the sensitivity of the response. As can be seen in Figure 6.7, all transfected cell lines seemed to exhibit some decrease in sensitivity to VEGF, relative to the untransfected controls; however the inhibition seen with the T3T4V chimera does appear to be appreciably higher than that seen with unmodified T3T4 and is very similar to that seen with the normal TIMP3 protein.

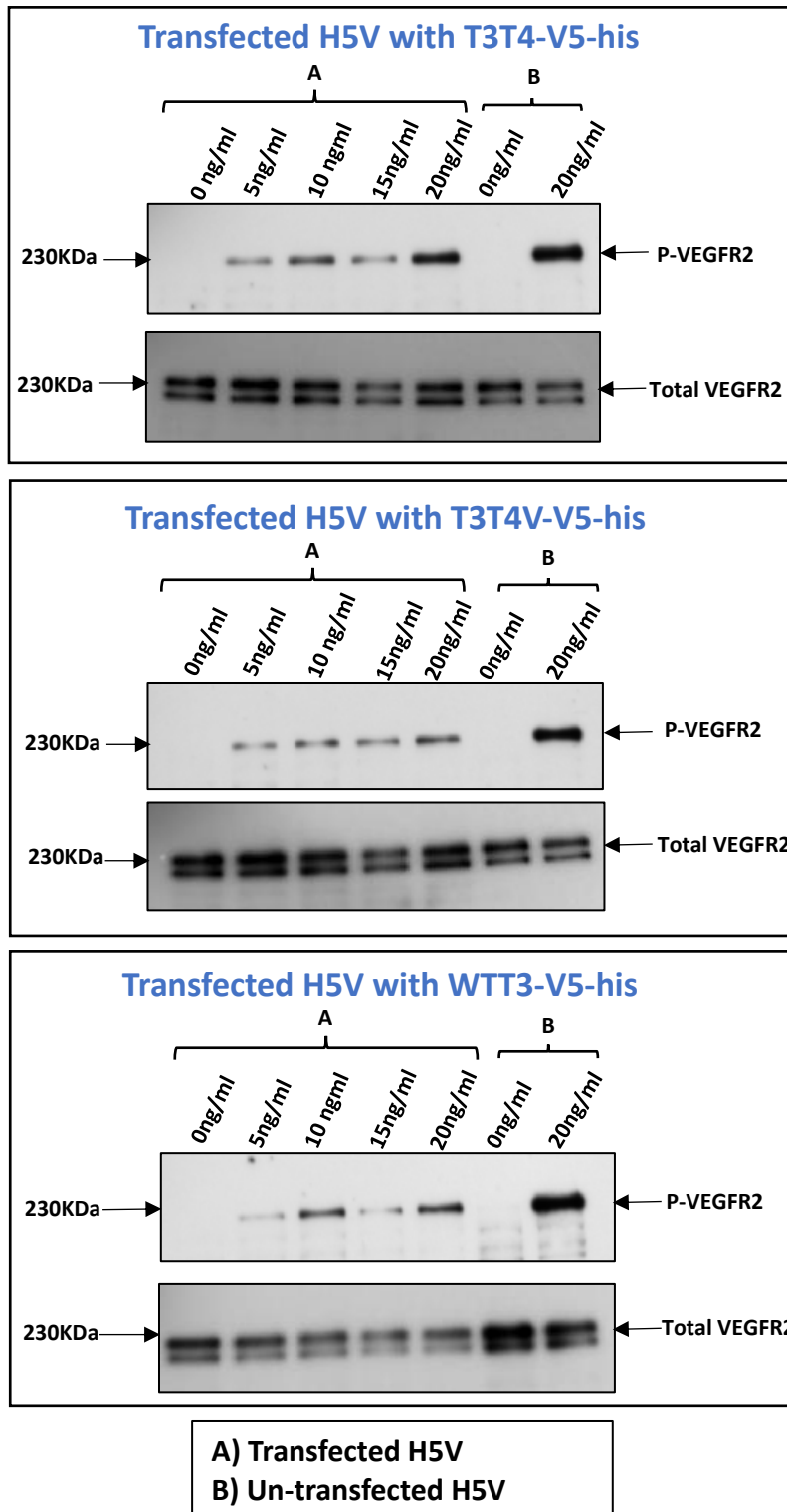


Figure 6.7 VEGFR2 phosphorylation in transfected H5V cell lines

Western blot showing the effect of the different TIMP constructs (A) on the stated concentrations of VEGF-induced phosphorylation of VEGFR2. P-VEGFR2 is phosphorylated VEGFR2 and VEGFR2 total receptor following stripping and re-probing. (B) are untransfected H5V cells treated at the highest dose of VEGF for comparison.

6.4 Discussion

Unfortunately, lack of time and finance prevented multiple repetition of this experiment that would be essential to make definitive conclusions as to the significance of the inhibition seen with the T3T4V construct. Nevertheless, it does seem to indicate that the TIMP3 amino acid residues introduced into the TIMP4 C-terminal domain of the T3T4 chimera increase the inhibitory activity of this molecule to a level indistinguishable from TIMP3 itself. If this indeed proves to be the case, it would provide compelling evidence that these six amino acid residues do indeed play a major part in the interaction of TIMP3 with VEGFR2. This could be further explored by methodically swapping back each amino acid to those seen in TIMP4 to see if some residues are particularly critical.

The six identified amino acids are found in loop 4, loop 6 and the carboxyl-tail sequence of TIMP3 in agreement with the peptide inhibitory data reported by Qi *et al* (2013) and data from our laboratory (Mujamammi 2014). As was mentioned in the introduction to this chapter, the one apparent contradiction here is that Qi *et al* (2013) found little inhibition with their loop4/5 peptide sequence, KIKSCYYLPCFVTS, which is only two amino acids shorter than p700 (KIKSCYYLPCFVTSKN) which clearly does inhibit the receptor and is the basis of this thesis. Moreover, the two amino acids identified in loop 4 as potentially directly interacting with VEGFR2, F133 and V134, are found in both peptides. There are several possible explanations for this. The most obvious is that that last two residues are also critical to the interaction or contribute to folding the peptide into the correct three-dimensional structure for binding. The correct folding of the peptide may also be determined by the disulfide bridge formed between the two cysteine residues, which is found in the full-length TIMP3 protein. All our p700 peptides have been oxidised after synthesis and the presence of the disulfide bond confirmed by mass spectrometry, this may not be the case for the peptide used by Qi *et al*. Less likely, but possible, is the

fact that Qi *et al* describe their peptide as being ten amino acids long, when in fact the quoted sequence is fourteen amino acids long. If the length is correct and the sequence in fact terminates at C132, this would conveniently omit the F133 and V134 residues!

6.5 Conclusion

While definitive conclusions regarding identification of VEGFR2-binding amino acid residues on TIMP3 are not possible from the limited data presented here, this is a promising approach for exploring the TIMP3/VEGFR2 interaction further. It may be possible to synthesise shorter peptide sequences that retain a high inhibitory potency or rationally design novel small molecule inhibitors based on the information gleaned. Moreover, the fact that p700 has a much wider receptor inhibitory profile than the full length TIMP3, indicates that it might be possible to design synthetic inhibitors that competitively inhibit several receptor families that are implicated in tumour growth and metastasis.

CHAPTER 7

General Discussion

7.1. Novelty of the p700 peptide

p700 is an exceptional peptide, being able to specifically bind to several different tyrosine kinase receptors gives it the potential to target a wide range of tumours with high avidity due to multivalent binding. Targeting multiple receptors also greatly decreases the likelihood of tumour cells developing resistance due to downregulation or mutation of any one receptor type. In addition to binding multiple targets, p700 also has several other advantages over monoclonal antibodies in that its small size will increase tissue penetration and the fact that it is derived from a highly conserved secreted human protein, means that immunogenicity is much less likely to be an issue.

While there are several small molecule drugs that also target a wider family of tyrosine kinase receptors, such as sorafenib and sunitinib, these all target the intracellular kinase domain and can also target other intracellular kinases with the potential for off-target effects. Extracellular, competitive inhibitors of these receptors may decrease the likelihood of side-effects and also offer the potential to act as ligands for targeted drug delivery.

Previous data from our laboratory had shown that p700 could potently inhibit tumour growth in a syngeneic breast tumour model (Chen *et al.*, 2014). However, on its own the molecule is not cytotoxic and tumours were found to regrow following treatment cessation or prolonged treatment (unpublished observation). This fuelled the idea that, in addition to inhibiting target receptors, p700 might be used as a delivery vehicle to target cytotoxic drugs to tumour sites, potentially enhancing the therapeutic potential of p700, while decreasing the off-target effects of chemotherapy.

At the outset to this thesis, we had no data to indicate whether the unique ability of p700 to target multiple receptors, unlike the parent TIMP3 which is VEGFR2 specific, would

be compromised by coupling to a larger entity. In fact this seemed a distinct possibility, as it is very likely that the ability of p700 to bind to several closely related target receptors is due to not being sterically constrained by the parent TIMP3 protein. Additionally, while we had shown p700 inhibits phosphorylation of its target receptors, we did not know if the peptide receptor complex would be internalised into the cell.

These potential issues guided the design of the experiments described in this thesis. Two different cytotoxic payloads were assessed. The first, CPG2, acts by converting an inactive prodrug into a cytotoxic one. This approach is largely dependent on CPG2 remaining outside the cell, as once internalised it would be degraded and inactivated. In contrast, the second approach of coupling to liposomal doxorubicin, is not dependent on the complex remaining outside the cell, indeed internalisation of its payload, doxorubicin, is essential for activity and so anything that enhances this uptake would be expected to be advantageous. However, both payloads are large molecules with potential to not only decrease the wider inhibitory profile of p700, but also abrogate it altogether. For this reason, in both cases, molecular spacers were employed to distance the peptide from the payload; for CPG2 this was in the form of a [Gly₄Ser]₄ linker, whereas for Doxil it was in the form of a twelve carbon PEG spacer, further extending the PEG moiety bearing the DBCO group already present on the surface of the liposome. Linking to the DBCO group of the modified Doxil via an azido group on the N-terminus of the peptide was the easiest option, synthetically. However, as we did not know if modifying either end of the peptide would be detrimental, we then chose to couple p700 via its C-terminus to CPG2.

7.2. Coupling of CPG2 to p700

Drug toxicity is a major challenge for anticancer chemotherapeutics and is the reason for the wealth of studies investigating delivery strategies that might suppress the toxic side effects of conventional drugs. CPG2 is sometimes used in the clinic to reduce excess concentration of methotrexate in cancer patients by converting it into 4-deoxy-4-amino-N 10-methylpteroic acid (DAMPA) and glutamate which are both non-toxic and metabolised by the liver (Green, 2012). CPG2 is also the only enzyme that has been tested in the clinic in ADEPT (Sharma and Bagshawe, 2017) and so, for these reasons, was chosen to test the feasibility of using p700 in what could be described as peptide-dependent pro-drug therapy.

The experiments described in Chapter 3 confirmed a number of issues. Most importantly that coupling of the peptide did not impair its ability to bind to VEGFR2, nor impair the activity of the CPG2 enzyme. It was perhaps fortuitous that the p700-CPG2 complex appeared stable whereas the C-terminal TIMP3 sequence (T3C) linked to CPG2, appeared to get degraded. T3C was intended as a positive control as it has been shown to be a potent inhibitor of VEGFR2 (Qi *et al.*, 2013) and, unlike p700, does not contain any disulfide bonds which are unlikely to form in the bacterial cytoplasm. While we could not readily determine whether the disulfide bond found in p700 was present in the fusion protein, it is possible that this might have played a role in protecting the N-terminus from degradation during purification. While, for cost reasons, the BLI kinetic analysis was limited to confirming the interaction of p700-CPG2 with VEGFR2, the fact that p700-CPG2 appeared to enhance the efficacy of CPG2 in the cytotoxicity assay on 4T1 cells which lack this receptor but express FGF receptors, seemed to confirm that the wider inhibitory profile of p700 was also retained when coupled to the enzyme. This, then, gave some confidence that the second strategy of coupling to Doxil may also be effective.

7.3 Coupling of p700 to liposomal doxorubicin (Doxil®)

Encapsulation of anticancer drugs in liposomes is a novel way of reducing toxicity and takes advantage of the enhanced permeability and retention effect of tumour vasculature in localising the drug to cancer tissue. However, such encapsulation can also inhibit release of the drug into the tumour. Targeted liposomal delivery aims to enhance localisation and internalisation and therefore increase drug uptake by cancer cells.

The many advantageous properties of p700, outlined in section 7.1, also made p700 a very promising candidate for targeting liposome-encapsulated cytotoxic drugs in what was the second drug-delivery approach of this thesis. Doxil was chosen here as it is a clinically proven drug and also commercially available with modified PEG groups that enable direct coupling of appropriately modified peptides and proteins.

Coupling of p700 to Doxil via DBCO-mediated click chemistry proved highly efficient. Moreover cell binding and uptake data not only confirmed that that p700 retained its receptor binding profile when coupled to Doxil via its N-terminus, but also that the complex was rapidly internalised by H5V mouse endothelial and MCF7 human and 4T1 mouse breast cancer cells lines relative to Doxil alone. In contrast little uptake was seen with primary human microvascular endothelial cells. The enhanced uptake of p700-Doxil over Doxil alone was also reflected in the cytotoxicity data on the cell lines. Interestingly, both Doxil and Doxil-p700 showed a similar cytotoxic effect on primary HuDMEC, indicating uptake of doxorubicin by these cells is not enhanced by p700, probably reflecting lower expression of the target growth factor receptors on primary cells.

7.4 Assessment of p700-Doxil® *in vivo*

In vivo assessment of any new drug requires very careful and thorough experimental design which would normally include a dose escalation study to determine the maximum tolerable dose. The time and cost of such a study was beyond the reach of this project. Nevertheless, the publication of a detailed study of the effects of different dosing regimens for Doxil in orthotopically implanted 4T1 cells in BALB/c mice (Charrois and Allen, 2003), gave hope that a small-scale study with a dosing regimen based on that publication might be informative as an initial appraisal of the therapeutic potential of p700-Doxil in cancer treatment. Unfortunately, however, this study failed to show any conclusive benefit of p700-Doxil over Doxil alone. As has already been discussed, there are a number of reasons why the limitations of the experimental design mean this cannot be taken as a definitive result and a different dosing regimen, different model or different encapsulated drug may yet show a demonstrable benefit of p700-mediated targeting.

Both payload systems tested in this thesis clearly demonstrate that the p700 peptide can be used as a vehicle for delivering different types of drug to diseased tissues, it remains to be seen how this may best be exploited therapeutically.

7.5 Identification of VEGFR2 binding residues on TIMP3

The final section of this thesis focussed on attempting to identify critical residues on TIMP3 essential for its interaction with VEGFR2. While p700 binds to and inhibits VEGFR2, we had not attempted to further localise which specific residues on the peptide are critical for this interaction, nor whether the disulfide bond that forms between the two cysteine residues contributes to the conformation and is necessary for binding. Moreover, several other regions of the TIMP3 C-terminal domain have also been shown to bind to VEGFR2 (Qi *et al.*, 2013, Mujamammi, 2014). By combining this information with computerised molecular modelling, our group had previously identified six key residues

that may be critical in this interaction (Chen *et al.*, 2014). The work described in Chapter 6 indicates that these residues alone may be sufficient to impart VEGFR2 inhibition to the C-terminal domain of TIMP4, which normally lacks this attribute, although this clearly needs to be confirmed by replication. If this does prove to be the case, it may be possible to rationally design small molecule inhibitors of this interaction. As p700 indicates, some of these molecules may effectively inhibit closely related families of growth factor receptors and could be further engineered for precise targeting of certain receptor families. Current drugs that inhibit multiple members of this receptor family target the tyrosine kinase domain, necessitating the ability to enter the cell where they may also inhibit other signalling molecules. In contrast, drugs that target the extracellular domain of these receptor are usually antibodies or ligand mimetics and are monospecific and generally very expensive to produce. The possibility of producing broader range, synthetic, extracellular inhibitors of this family of receptors may open up new therapeutic opportunities in cancer and other diseases.

7.6 Conclusion

The discovery of the p700 peptide was quite serendipitous as it was originally synthesised as a potential ECM binding site on TIMP3 and only after TIMP3 was identified as a VEGFR2 inhibitor was it tested in that context. Moreover, an almost identical peptide described by Qi *et al* (2013), but two amino acids shorter, showed little inhibitory activity and, unlike p700, all the peptides described by those authors are reported to be specific for VEGFR2 with no inhibition of VEGFR1. We are not aware of any other peptide with a similar broad, yet specific, inhibitory profile and this makes it a potentially valuable tool in targeting this particular family of receptors whose over-expression is associated with cancer tissue.

Nevertheless, at the outset of this thesis, the prospect of using p700 as a means of delivering or targeting cytotoxic drugs had seemed quite a remote possibility as there were many potential obstacles to success. Coupling of the peptide to any additional molecule may have instantly abrogated its unique inhibitory profile by steric inhibition. Also, while p700 was shown to inhibit several tyrosine kinase family receptors, we did not know if binding resulted in internalisation.

In this thesis we have shown that, with a suitable spacer sequence, p700 retains its ability to bind to this family of receptors, whether coupled via the N- or C-terminus. Moreover, when conjugated to Doxil, the whole complex is rapidly internalised. While we did not have any simple way to determine if this was also the case for the p700-CPG2 conjugate, this would seem likely and may explain the limited enhancement in efficacy over the unconjugated enzyme.

While the p700-Doxil complex proved to have limited additional efficacy over Doxil alone in our particular *in vivo* model, that study was extremely limited due to budget and time constraints and was only intended as a proof of principle of the drug delivery concept. The great advantage of coupling to liposomes is that they can be used to deliver any drug or combination of drugs that can be encapsulated in that way and this is not limited to water soluble drugs in the liposomal centre but could also apply to lipophilic drugs in the liposome itself.

7.7 Future work

Time and budget constraints meant that p700-mediated targeting was only tested on breast cancer cells and any future study would undoubtedly involve a more thorough screening against a panel of human tumour cells/cell lines that would undoubtedly include renal, lung and neuroendocrine cancers where VEGF/PDGFR targeting has been shown to be of clinical benefit. This might in turn dictate testing in different *in vivo* models.

In any case, a much more thorough *in vivo* study in the 4T1 mouse mammary cancer model is essential to determine what, if any, drug/drug regimen/tumour type could benefit from p700-targeted delivery. These studies would investigate the bio-distribution of the conjugate drug while concurrent dose escalation would demonstrate the possibility for greater tolerability with attendant potential for increased efficacy at higher doses of the drug conjugate compared with the cytotoxic component, Doxil. Not only could this provide an explanation for the lack of relative efficacy observed at the dose levels used in this study (section 5.4), the safety and efficacy data generated would inform the design of subsequent studies that would expand the application of the drug conjugate to xenograft models of human breast cancer as well as other cancers. Efficacy comparisons could also be made with receptor tyrosine kinase inhibitors that have a similar targeting profile to p700 such as nintedanib that has been shown to have clinical benefit when combined with cytotoxic agents in advanced lung cancer (Awasthi and Schwarz, 2015).

This thesis focussed exclusively on cancer, however p700 also showed some efficacy in inflammatory arthritis (Chen *et al.*, 2014) where it inhibits synovial cell invasion and inflammation, presumably due to its ability to inhibit FGF and/or PDGF receptors which are highly expressed by these cells. Combining p700 with either an anti-inflammatory payload or cytotoxic drug to destroy the invading pannus may significantly increase efficacy in this disease.

As p700 is derived from an extracellular human protein and would be used to target existing drugs, together with the evidence from this study indicating no additional toxic effects following p700 conjugation, any positive benefits found in an animal model could quite quickly be translated into an early stage exploratory clinical study in a small cohort of patients.

If repetition of the VEGFR2 phosphorylation experiment confirms inhibition with the T3T4V chimera, then additional mutants, in which individual or pairs of residues were mutated back to the TIMP4 equivalent, would be constructed to further narrow down key binding residues. As the p700 peptide is promiscuous with respect to receptor specificity, relative to other TIMP3 peptides tested, then particular focus might be applied to the VEGFR2 site that interacts with residues on this peptide sequence. Testing synthetic small molecules that could target this site may lead to the development of broader spectrum extracellular inhibitors of this family of growth factor receptors.

8 Bibliography

- AABERG-JESSEN, C., CHRISTENSEN, K., OFFENBERG, H., BARTELS, A., DREEHSEN, T., HANSEN, S., SCHRODER, H. D., BRUNNER, N. & KRISTENSEN, B. W. 2009. Low expression of tissue inhibitor of metalloproteinases-1 (TIMP-1) in glioblastoma predicts longer patient survival. *J Neurooncol*, 95, 117-28.
- ABECASIS, G. R., YASHAR, B. M., ZHAO, Y., GHIASVAND, N. M., ZAREPARSI, S., BRANHAM, K. E., REDDICK, A. C., TRAGER, E. H., YOSHIDA, S., BAHLING, J., FILIPPOVA, E., ELNER, S., JOHNSON, M. W., VINE, A. K., SIEVING, P. A., JACOBSON, S. G., RICHARDS, J. E. & SWAROOP, A. 2004. Age-related macular degeneration: a high-resolution genome scan for susceptibility loci in a population enriched for late-stage disease. *Am J Hum Genet*, 74, 482-94.
- ACUFF, H. B., SINNAMON, M., FINGLETON, B., BOONE, B., LEVY, S. E., CHEN, X., POZZI, A., CARBONE, D. P., SCHWARTZ, D. R., MOIN, K., SLOANE, B. F. & MATRISIAN, L. M. 2006. Analysis of host- and tumor-derived proteinases using a custom dual species microarray reveals a protective role for stromal matrix metalloproteinase-12 in non-small cell lung cancer. *Cancer Res*, 66, 7968-75.
- AFSHAR, S., ASAI, T. & MORRISON, S. L. 2009. Humanized ADEPT comprised of an engineered human purine nucleoside phosphorylase and a tumor targeting peptide for treatment of cancer. *Mol Cancer Ther*, 8, 185-93.
- AHONEN, M., BAKER, A. H. & KAHARI, V. M. 1998. Adenovirus-mediated gene delivery of tissue inhibitor of metalloproteinases-3 inhibits invasion and induces apoptosis in melanoma cells. *Cancer Res*, 58, 2310-5.
- AHONEN, M., POUKKULA, M., BAKER, A. H., KASHIWAGI, M., NAGASE, H., ERIKSSON, J. E. & KAHARI, V. M. 2003. Tissue inhibitor of metalloproteinases-3 induces apoptosis in melanoma cells by stabilization of death receptors. *Oncogene*, 22, 2121-34.
- AKOOL EL, S., DOLLER, A., MULLER, R., GUTWEIN, P., XIN, C., HUWILER, A., PFEILSCHIFTER, J. & EBERHARDT, W. 2005. Nitric oxide induces TIMP-1 expression by activating the transforming growth factor beta-Smad signaling pathway. *J Biol Chem*, 280, 39403-16.
- ALSAFFAR, F. A. 2017. The Molecular Characterisation of TIMP3 Mutations Responsible for Sorsby's Fundus Dystrophy: is there a link to Age-related Macular Degeneration. . *PhD Thesis, University of Sheffield, UK*.
- ANDRADY, C., SHARMA, S. K. & CHESTER, K. A. 2011. Antibody-enzyme fusion proteins for cancer therapy. *Immunotherapy*, 3, 193-211.
- ANDRAE, J., GALLINI, R. & BETSHOLTZ, C. 2008. Role of platelet-derived growth factors in physiology and medicine. *Genes Dev*, 22, 1276-312.
- ANSARI, L., SHIEHZADEH, F., TAHERZADEH, Z., NIKOOFAL-SAHLABADI, S., MOMTAZI-BOROJENI, A., SAHEBKAR, A. & ESLAMI, S. 2017. The most prevalent side effects of pegylated liposomal doxorubicin monotherapy in women with metastatic breast cancer: a systematic review of clinical trials. *Cancer gene therapy*.
- ANTONIOU, A. C., SPURDLE, A. B., SINILNIKOVA, O. M., HEALEY, S., POOLEY, K. A., SCHMUTZLER, R. K., VERSMOLD, B., ENGEL, C., MEINDL, A., ARNOLD, N., HOFMANN, W., SUTTER, C., NIEDERACHER, D., DESSLER, H., CALDES, T., KAMPJARVI, K., NEVANLINNA, H., SIMARD, J., BEESLEY, J., CHEN, X., KATHLEEN CUNINGHAM CONSORTIUM FOR RESEARCH INTO FAMILIAL BREAST, C., NEUHAUSEN, S. L., REBBECK, T. R., WAGNER, T., LYNCH, H. T., ISAACS, C., WEITZEL, J., GANZ, P. A., DALY, M. B., TOMLINSON, G., OLOPADE, O. I., BLUM, J. L., COUCH, F. J., PETERLONGO, P., MANOUKIAN, S., BARILE, M., RADICE, P., SZABO, C. I., PEREIRA, L. H., GREENE, M. H., RENNERT, G., LEJBKOWICZ, F., BARNETT-GRINESS, O., ANDRULIS, I. L., OZCELIK, H., OCGN, GERDES, A. M., CALIGO, M. A., LAITMAN, Y., KAUFMAN, B., MILGROM, R., FRIEDMAN, E., SWEDISH, B., COLLABORATORS, B. S.,

- DOMCHEK, S. M., NATHANSON, K. L., OSORIO, A., LLORT, G., MILNE, R. L., BENITEZ, J., HAMANN, U., HOGERVORST, F. B., MANDERS, P., LIGTENBERG, M. J., VAN DEN OUWELAND, A. M., COLLABORATORS, D.-H., PEOCK, S., COOK, M., PLATTE, R., EVANS, D. G., EELES, R., PICHERT, G., CHU, C., ECCLES, D., DAVIDSON, R., DOUGLAS, F., EMBRACE, GODWIN, A. K., BARJHOUX, L., MAZOYER, S., SOBOL, H., BOURDON, V., EISINGER, F., CHOMPRET, A., CAPOULADE, C., BRESSAC-DE PAILLERETS, B., LENOIR, G. M., GAUTHIER-VILLARS, M., HOUDAYER, C., STOPPA-LYONNET, D., GEMO, CHENEVIX-TRENCH, G., EASTON, D. F. & CIMBA 2008. Common breast cancer-predisposition alleles are associated with breast cancer risk in BRCA1 and BRCA2 mutation carriers. *Am J Hum Genet*, 82, 937-48.
- AWASTHI, N. & SCHWARZ, R. E. 2015. Profile of nintedanib in the treatment of solid tumors: the evidence to date. *Onco Targets Ther*, 8, 3691-701.
- BABA, Y., YASUDA, O., TAKEMURA, Y., ISHIKAWA, Y., OHISHI, M., IWANAMI, J., MOGI, M., DOE, N., HORIUCHI, M., MAEDA, N., FUKUO, K. & RAKUGI, H. 2009. Timp-3 deficiency impairs cognitive function in mice. *Lab Invest*, 89, 1340-7.
- BABINA, I. S. & TURNER, N. C. 2017. Advances and challenges in targeting FGFR signalling in cancer. *Nat Rev Cancer*, 17, 318-332.
- BACHMAN, K. E., HERMAN, J. G., CORN, P. G., MERLO, A., COSTELLO, J. F., CAVENEE, W. K., BAYLIN, S. B. & GRAFF, J. R. 1999. Methylation-associated silencing of the tissue inhibitor of metalloproteinase-3 gene suggests a suppressor role in kidney, brain, and other human cancers. *Cancer research*, 59, 798-802.
- BAHUDHANAPATI, H., BHATTACHARYA, S. & WEI, S. 2015. Evolution of Vertebrate Adam Genes; Duplication of Testicular Adams from Ancient Adam9/9-like Loci. *PLoS One*, 10, e0136281.
- BAKER, A. H., EDWARDS, D. R. & MURPHY, G. 2002. Metalloproteinase inhibitors: biological actions and therapeutic opportunities. *J Cell Sci*, 115, 3719-27.
- BAKER, A. H., GEORGE, S. J., ZALTSMAN, A. B., MURPHY, G. & NEWBY, A. C. 1999. Inhibition of invasion and induction of apoptotic cell death of cancer cell lines by overexpression of TIMP-3. *Br J Cancer*, 79, 1347-55.
- BALBIN, M., FUEYO, A., TESTER, A. M., PENDAS, A. M., PITIOT, A. S., ASTUDILLO, A., OVERALL, C. M., SHAPIRO, S. D. & LOPEZ-OTIN, C. 2003. Loss of collagenase-2 confers increased skin tumor susceptibility to male mice. *Nat Genet*, 35, 252-7.
- BAO, L., HAQUE, A., JACKSON, K., HAZARI, S., MOROZ, K., JETLY, R. & DASH, S. 2011. Increased Expression of P-Glycoprotein Is Associated with Doxorubicin Chemoresistance in the Metastatic 4T1 Breast Cancer Model. *The American Journal of Pathology*, 178, 838-852.
- BARBIERI, F., BAJETTO, A., PATTAROZZI, A., GATTI, M., WURTH, R., THELLUNG, S., CORSARO, A., VILLA, V., NIZZARI, M. & FLORIO, T. 2013. Peptide receptor targeting in cancer: the somatostatin paradigm. *Int J Pept*, 2013, 926295.
- BARLEON, B., SOZZANI, S., ZHOU, D., WEICH, H. A., MANTOVANI, A. & MARME, D. 1996. Migration of human monocytes in response to vascular endothelial growth factor (VEGF) is mediated via the VEGF receptor flt-1. *Blood*, 87, 3336-3343.
- BARSKI, D., WOLTER, M., REIFENBERGER, G. & RIEMENSCHNEIDER, M. J. 2010. Hypermethylation and transcriptional downregulation of the TIMP3 gene is associated with allelic loss on 22q12.3 and malignancy in meningiomas. *Brain Pathol*, 20, 623-31.
- BASU, R., FAN, D., KANDALAM, V., LEE, J., DAS, S. K., WANG, X., BALDWIN, T. A., OUDIT, G. Y. & KASSIRI, Z. 2012. Loss of Timp3 gene leads to abdominal aortic aneurysm formation in response to angiotensin II. *J Biol Chem*, 287, 44083-96.
- BASU, R., LEE, J., MORTON, J. S., TAKAWALE, A., FAN, D., KANDALAM, V., WANG, X., DAVIDGE, S. T. & KASSIRI, Z. 2013. TIMP3 is the primary TIMP to regulate agonist-induced vascular remodelling and hypertension. *Cardiovasc Res*, 98, 360-71.

- BATES, R. C., GOLDSMITH, J. D., BACHELDER, R. E., BROWN, C., SHIBUYA, M., OETTGEN, P. & MERCURIO, A. M. 2003. Flt-1-dependent survival characterizes the epithelial-mesenchymal transition of colonic organoids. *Current Biology*, 13, 1721-1727.
- BELOTTI, D., PAGANONI, P., MANENTI, L., GAROFALO, A., MARCHINI, S., TARABOLETTI, G. & GIAVAZZI, R. 2003. Matrix metalloproteinases (MMP9 and MMP2) induce the release of vascular endothelial growth factor (VEGF) by ovarian carcinoma cells: implications for ascites formation. *Cancer Res*, 63, 5224-9.
- BERNADOTTE, A., MIKHELSON, V. M. & SPIVAK, I. M. 2016. Markers of cellular senescence. Telomere shortening as a marker of cellular senescence. *Aging (Albany NY)*, 8, 3.
- BERNKOP-SCHNURCH, A. & DUNNHAUPT, S. 2012. Chitosan-based drug delivery systems. *Eur J Pharm Biopharm*, 81, 463-9.
- BIRRER, M. J., JOHNSON, M. E., HAO, K., WONG, K. K., PARK, D. C., BELL, A., WELCH, W. R., BERKOWITZ, R. S. & MOK, S. C. 2007. Whole genome oligonucleotide-based array comparative genomic hybridization analysis identified fibroblast growth factor 1 as a prognostic marker for advanced-stage serous ovarian adenocarcinomas. *J Clin Oncol*, 25, 2281-7.
- BLAKEY, D. C., BURKE, P. J., DAVIES, D. H., DOWELL, R. I., EAST, S. J., ECKERSLEY, K. P., FITTON, J. E., MCDAID, J., MELTON, R. G. & NICULESCU-DUVAZ, I. A. 1996. ZD2767, an improved system for antibody-directed enzyme prodrug therapy that results in tumor regressions in colorectal tumor xenografts. *Cancer research*, 56, 3287-3292.
- BLOBEL, C. P., WOLFSBERG, T. G., TURCK, C. W., MYLES, D. G., PRIMAKOFF, P. & WHITE, J. M. 1992. A potential fusion peptide and an integrin ligand domain in a protein active in sperm-egg fusion. *Nature*, 356, 248-52.
- BOLKESTEIN, M., DE BLOIS, E., KOELEWIJN, S. J., EGGERMONT, A. M., GROSVELD, F., DE JONG, M. & KONING, G. A. 2016. Investigation of Factors Determining the Enhanced Permeability and Retention Effect in Subcutaneous Xenografts. *J Nucl Med*, 57, 601-7.
- BOMMARITO, A., RICHIUSA, P., CARISSIMI, E., PIZZOLANTI, G., RODOLICO, V., ZITO, G., CRISCIMANNA, A., DI BLASI, F., PITRONE, M., ZERILLI, M., AMATO, M. C., SPINELLI, G., CARINA, V., MODICA, G., LATTERI, M. A., GALLUZZO, A. & GIORDANO, C. 2011. BRAFV600E mutation, TIMP-1 upregulation, and NF-kappaB activation: closing the loop on the papillary thyroid cancer trilogy. *Endocr Relat Cancer*, 18, 669-85.
- BOONJARASPINYO, S., BOONMARS, T., WU, Z., LOILOME, W., SITHITHAWORN, P., NAGANO, I., PINLAOR, S., YONGVANIT, P., NIELSEN, P. S., PAIROJKUL, C. & KHUNTIKEO, N. 2012. Platelet-derived growth factor may be a potential diagnostic and prognostic marker for cholangiocarcinoma. *Tumour Biol*, 33, 1785-802.
- BOURBOULIA, D., JENSEN-TAUBMAN, S., RITTLER, M. R., HAN, H. Y., CHATTERJEE, T., WEI, B. & STETLER-STEVENSON, W. G. 2011. Endogenous angiogenesis inhibitor blocks tumor growth via direct and indirect effects on tumor microenvironment. *Am J Pathol*, 179, 2589-600.
- BOURLEV, V., VOLKOV, N., PAVLOVITCH, S., LETS, N., LARSSON, A. & OLOVSSON, M. 2006. The relationship between microvessel density, proliferative activity and expression of vascular endothelial growth factor-A and its receptors in eutopic endometrium and endometriotic lesions. *Reproduction*, 132, 501-9.
- BRIDGES, L. C. & BOWDITCH, R. D. 2005. ADAM-Integrin Interactions: potential integrin regulated ectodomain shedding activity. *Curr Pharm Des*, 11, 837-47.
- BROWN, S. & KHAN, D. R. 2012. The treatment of breast cancer using liposome technology. *Journal of drug delivery*, 2012.
- BRYANT, D. M., WYLIE, F. G. & STOW, J. L. 2005. Regulation of endocytosis, nuclear translocation, and signaling of fibroblast growth factor receptor 1 by E-cadherin. *Mol Biol Cell*, 16, 14-23.

- BURKS, S. R., LEGENZOV, E. A., MARTIN, E. W., LI, C., LU, W. & KAO, J. P. 2015. Co-encapsulating the fusogenic peptide INF7 and molecular imaging probes in liposomes increases intracellular signal and probe retention. *PLoS One*, 10, e0120982.
- CAIRNEY, C. J. & KEITH, W. N. 2008. Telomerase redefined: integrated regulation of hTR and hTERT for telomere maintenance and telomerase activity. *Biochimie*, 90, 13-23.
- CAL, S. & LOPEZ-OTIN, C. 2015. ADAMTS proteases and cancer. *Matrix Biol*, 44-46, 77-85.
- CARMELIET, P. 2003. Angiogenesis in health and disease. *Nature medicine*, 9, 653-660.
- CARMELIET, P. & JAIN, R. K. 2000. Angiogenesis in cancer and other diseases. *Nature*, 407, 249-57.
- CARMELIET, P. & JAIN, R. K. 2011. Molecular mechanisms and clinical applications of angiogenesis. *Nature*, 473, 298-307.
- CASTAGNA, A., CESARI, E., GAROFALO, R., GIGANTE, A., CONTI, M., MARKOPOULOS, N. & MAFFULLI, N. 2013. Matrix metalloproteases and their inhibitors are altered in torn rotator cuff tendons, but also in the macroscopically and histologically intact portion of those tendons. *Muscles Ligaments Tendons J*, 3, 132-8.
- CATUSUS, L., PONS, C., MUNOZ, J., ESPINOSA, I. & PRAT, J. 2013. Promoter hypermethylation contributes to TIMP3 down-regulation in high stage endometrioid endometrial carcinomas. *Histopathology*, 62, 632-41.
- CATHCART, J., PULKOSKI-GROSS, A. & CAO, J. 2015. Targeting Matrix Metalloproteinases in Cancer: Bringing New Life to Old Ideas. *Genes Dis*, 2, 26-34.
- CAVALLARO, U. & CRISTOFORI, G. 2004. Multitasking in tumor progression: signaling functions of cell adhesion molecules. *Ann N Y Acad Sci*, 1014, 58-66.
- CHARROIS, G. J. & ALLEN, T. M. 2003. Multiple injections of pegylated liposomal Doxorubicin: pharmacokinetics and therapeutic activity. *J Pharmacol Exp Ther*, 306, 1058-67.
- CHEN, T. T., LUQUE, A., LEE, S., ANDERSON, S. M., SEGURA, T. & IRUELA-ARISPE, M. L. 2010. Anchorage of VEGF to the extracellular matrix conveys differential signaling responses to endothelial cells. *J Cell Biol*, 188, 595-609.
- CHEN, X., DING, G., GAO, Q., SUN, J., ZHANG, Q., DU, L., QIU, Z., WANG, C., ZHENG, F. & SUN, B. 2013a. A human anti-c-Met Fab fragment conjugated with doxorubicin as targeted chemotherapy for hepatocellular carcinoma. *PloS one*, 8, e63093.
- CHEN, X., ZARO, J. L. & SHEN, W. C. 2013b. Fusion protein linkers: property, design and functionality. *Adv Drug Deliv Rev*, 65, 1357-69.
- CHEN, Y. Y., BROWN, N. J., JONES, R., LEWIS, C. E., MUJAMAMMI, A. H., MUTHANA, M., SEED, M. P. & BARKER, M. D. 2014. A peptide derived from TIMP-3 inhibits multiple angiogenic growth factor receptors and tumour growth and inflammatory arthritis in mice. *Angiogenesis*, 17, 207-19.
- CLARK, I. M., SWINGLER, T. E., SAMPIERI, C. L. & EDWARDS, D. R. 2008. The regulation of matrix metalloproteinases and their inhibitors. *The international journal of biochemistry & cell biology*, 40, 1362-1378.
- COLEY, H. M. 2008. Mechanisms and strategies to overcome chemotherapy resistance in metastatic breast cancer. *Cancer Treat Rev*, 34, 378-90.
- DAS, A., FANSLAW, W., CERRETTI, D., WARREN, E., TALARICO, N. & MCGUIRE, P. 2003. Angiopoietin/Tek interactions regulate mmp-9 expression and retinal neovascularization. *Lab Invest*, 83, 1637-45.
- DAS, A. M., SEYNHAEVE, A. L., RENS, J. A., VERMEULEN, C. E., KONING, G. A., EGGERMONT, A. M. & TEN HAGEN, T. L. 2013. Differential TIMP3 expression affects tumor progression and angiogenesis in melanomas through regulation of directionally persistent endothelial cell migration. *Angiogenesis*, 25, 25.
- DAVIES, H., HUNTER, C., SMITH, R., STEPHENS, P., GREENMAN, C., BIGNELL, G., TEAGUE, J., BUTLER, A., EDKINS, S., STEVENS, C., PARKER, A., O'MEARA, S., AVIS, T., BARTHORPE, S., BRACKENBURY, L., BUCK, G., CLEMENTS, J., COLE, J., DICKS, E., EDWARDS, K., FORBES,

- S., GORTON, M., GRAY, K., HALLIDAY, K., HARRISON, R., HILLS, K., HINTON, J., JONES, D., KOSMIDOU, V., LAMAN, R., LUGG, R., MENZIES, A., PERRY, J., PETTY, R., RAINE, K., SHEPHERD, R., SMALL, A., SOLOMON, H., STEPHENS, Y., TOFTS, C., VARIAN, J., WEBB, A., WEST, S., WIDAA, S., YATES, A., BRASSEUR, F., COOPER, C. S., FLANAGAN, A. M., GREEN, A., KNOWLES, M., LEUNG, S. Y., LOOIJENGA, L. H., MALKOWICZ, B., PIEROTTI, M. A., TEH, B. T., YUEN, S. T., LAKHANI, S. R., EASTON, D. F., WEBER, B. L., GOLDSTRAW, P., NICHOLSON, A. G., WOOSTER, R., STRATTON, M. R. & FUTREAL, P. A. 2005. Somatic mutations of the protein kinase gene family in human lung cancer. *Cancer Res*, 65, 7591-5.
- DE FRANCESCO, E. M., LAPPANO, R., SANTOLLA, M. F., MARSICO, S., CARUSO, A. & MAGGIOLINI, M. 2013. HIF-1alpha/GPER signaling mediates the expression of VEGF induced by hypoxia in breast cancer associated fibroblasts (CAFs). *Breast Cancer Res*, 15, R64.
- DE MOERLOOZE, L., SPENCER-DENE, B., REVEST, J. M., HAJIHOSEINI, M., ROSEWELL, I. & DICKSON, C. 2000. An important role for the IIIb isoform of fibroblast growth factor receptor 2 (FGFR2) in mesenchymal-epithelial signalling during mouse organogenesis. *Development*, 127, 483-92.
- DE VISSER, K. E., EICHTEN, A. & COUSSENS, L. M. 2006. Paradoxical roles of the immune system during cancer development. *Nat Rev Cancer*, 6, 24-37.
- DEAN, G., YOUNG, D. A., EDWARDS, D. R. & CLARK, I. M. 2000. The human tissue inhibitor of metalloproteinases (TIMP)-1 gene contains repressive elements within the promoter and intron 1. *Journal of Biological Chemistry*, 275, 32664-32671.
- DECHAPHUNKUL, A., PHUKAOLOUN, M., KANJANAPRADIT, K., GRAHAM, K., GHOSH, S., SANTOS, C. & MACKEY, J. R. 2012. Prognostic significance of tissue inhibitor of metalloproteinase-1 in breast cancer. *Int J Breast Cancer*, 2012, 290854.
- DEFAMIE, V., SANCHEZ, O., MURTHY, A. & KHOKHA, R. 2015. TIMP3 controls cell fate to confer hepatocellular carcinoma resistance. *Oncogene*, 34, 4098.
- DOWELL, R. I., SPRINGER, C. J., DAVIES, D. H., HADLEY, E. M., BURKE, P. J., BOYLE, F. T., MELTON, R. G., CONNORS, T. A., BLAKEY, D. C. & MAUGER, A. B. 1996. New mustard prodrugs for antibody-directed enzyme prodrug therapy: alternatives to the amide link. *J Med Chem*, 39, 1100-5.
- DUDLEY, A. C. 2012. Tumor endothelial cells. *Cold Spring Harbor perspectives in medicine*, 2, a006536.
- EBRAHEM, Q., QI, J. H., SUGIMOTO, M., ALI, M., SEARS, J. E., CUTLER, A., KHOKHA, R., VASANJI, A. & ANAND-APTE, B. 2011. Increased neovascularization in mice lacking tissue inhibitor of metalloproteinases-3. *Invest Ophthalmol Vis Sci*, 52, 6117-23.
- ELLERBROEK, S. M., WU, Y. I., OVERALL, C. M. & STACK, M. S. 2001. Functional interplay between type I collagen and cell surface matrix metalloproteinase activity. *J Biol Chem*, 276, 24833-42.
- EWENS, A., LUO, L., BERLETH, E., ALDERFER, J., WOLLMAN, R., HAFEEZ, B. B., KANTER, P., MIHICH, E. & EHRKE, M. J. 2006. Doxorubicin plus interleukin-2 chemoimmunotherapy against breast cancer in mice. *Cancer Res*, 66, 5419-26.
- FANTOZZI, A. & CHRISTOFORI, G. 2006. Mouse models of breast cancer metastasis. *Breast Cancer Res*, 8, 212.
- FARISS, R. N., APTE, S. S., LUTHER, P. J., BIRD, A. C. & MILAM, A. H. 1998. Accumulation of tissue inhibitor of metalloproteinases-3 in human eyes with Sorsby's fundus dystrophy or retinitis pigmentosa. *Br J Ophthalmol*, 82, 1329-34.
- FERNALD, K. & KUROKAWA, M. 2013. Evading apoptosis in cancer. *Trends Cell Biol*, 23, 620-33.
- FERRARA, N. 2010. Binding to the extracellular matrix and proteolytic processing: two key mechanisms regulating vascular endothelial growth factor action. *Mol Biol Cell*, 21, 687-90.

- FRANTZ, C., STEWART, K. M. & WEAVER, V. M. 2010. The extracellular matrix at a glance. *J Cell Sci*, 123, 4195-4200.
- FUTAKI, S., SUZUKI, T., OHASHI, W., YAGAMI, T., TANAKA, S., UEDA, K. & SUGIURA, Y. 2001. Arginine-rich peptides. An abundant source of membrane-permeable peptides having potential as carriers for intracellular protein delivery. *J Biol Chem*, 276, 5836-40.
- GAO, G., WESTLING, J., THOMPSON, V. P., HOWELL, T. D., GOTTSCHALL, P. E. & SANDY, J. D. 2002. Activation of the proteolytic activity of ADAMTS4 (aggrecanase-1) by C-terminal truncation. *J Biol Chem*, 277, 11034-41.
- GARCIA-IRIGOYEN, O., CAROTTI, S., LATASA, M. U., URIARTE, I., FERNANDEZ-BARRENA, M. G., ELIZALDE, M., URTASUN, R., VESPASIANI-GENTILUCCI, U., MORINI, S., BANALES, J. M., PARKS, W. C., RODRIGUEZ, J. A., ORBE, J., PRIETO, J., PARAMO, J. A., BERASAIN, C. & AVILA, M. A. 2013. Matrix metalloproteinase-10 expression is induced during hepatic injury and plays a fundamental role in liver tissue repair. *Liver Int*, 4, 12337.
- GARLANDA, C., PARRAVICINI, C., SIRONI, M., DE ROSSI, M., WAINSTOK DE CALMANOVICI, R., CAROZZI, F., BUSSOLINO, F., COLOTTA, F., MANTOVANI, A. & VECCHI, A. 1994. Progressive growth in immunodeficient mice and host cell recruitment by mouse endothelial cells transformed by polyoma middle-sized T antigen: implications for the pathogenesis of opportunistic vascular tumors. *Proc Natl Acad Sci U S A*, 91, 7291-5.
- GIALELLI, C., THEOCHARIS, A. D. & KARAMANOS, N. K. 2011. Roles of matrix metalloproteinases in cancer progression and their pharmacological targeting. *FEBS J*, 278, 16-27.
- GILL, J. H., LOADMAN, P. M., SHNYDER, S. D., COOPER, P., ATKINSON, J. M., RIBEIRO MORAIS, G., PATTERSON, L. H. & FALCONER, R. A. 2014. Tumor-targeted prodrug ICT2588 demonstrates therapeutic activity against solid tumors and reduced potential for cardiovascular toxicity. *Mol Pharm*, 11, 1294-300.
- GIRI, D., ROPIQUET, F. & ITTMANN, M. 1999. Alterations in expression of basic fibroblast growth factor (FGF) 2 and its receptor FGFR-1 in human prostate cancer. *Clin Cancer Res*, 5, 1063-71.
- GODA, S. K., RASHIDI, F. A., FAKHARO, A. A. & AL-OBAIDLI, A. 2009. Functional overexpression and purification of a codon optimized synthetic glucarpidase (carboxypeptidase G2) in Escherichia coli. *Protein J*, 28, 435-42.
- GORDON, K. B., TAJUDDIN, A., GUITART, J., KUZEL, T. M., ERAMO, L. R. & VONROENN, J. 1995. Hand-foot syndrome associated with liposome-encapsulated doxorubicin therapy. *Cancer*, 75, 2169-73.
- GOUGH, P. J., GARTON, K. J., WILLE, P. T., RYCHLEWSKI, M., DEMPSEY, P. J. & RAINES, E. W. 2004. A disintegrin and metalloproteinase 10-mediated cleavage and shedding regulates the cell surface expression of CXC chemokine ligand 16. *The Journal of Immunology*, 172, 3678-3685.
- GREEN, A. E. & ROSE, P. G. 2006. Pegylated liposomal doxorubicin in ovarian cancer. *Int J Nanomedicine*, 1, 229-39.
- GREEN, J. M. 2012. Glucarpidase to combat toxic levels of methotrexate in patients. *Ther Clin Risk Manag*, 8, 403-13.
- GRIGNON, D. J., SAKR, W., TOTH, M., RAVERY, V., ANGULO, J., SHAMSA, F., PONTES, J. E., CRISSMAN, J. C. & FRIDMAN, R. 1996. High levels of tissue inhibitor of metalloproteinase-2 (TIMP-2) expression are associated with poor outcome in invasive bladder cancer. *Cancer Res*, 56, 1654-9.
- GRUNEWALD, F. S., PROTA, A. E., GIESE, A. & BALLMER-HOFER, K. 2010. Structure-function analysis of VEGF receptor activation and the role of coreceptors in angiogenic signaling. *Biochim Biophys Acta*, 1804, 567-80.
- GRÜNWARD, B., HARANT, V., SCHATEN, S., FRÜHSCHÜTZ, M., SPALLEK, R., HÖCHST, B., STUTZER, K., BERCHTOLD, S., ERKAN, M. & PROKOPCHUK, O. 2016. Pancreatic premalignant lesions secrete tissue inhibitor of metalloproteinases-1, which activates hepatic stellate

- cells via CD63 Signaling to create a premetastatic niche in the liver. *Gastroenterology*, 151, 1011-1024. e7.
- GU, P., XING, X., TANZER, M., ROCKEN, C., WEICHERT, W., IVANAUSKAS, A., PROSS, M., PEITZ, U., MALFERTHEINER, P., SCHMID, R. M. & EBERT, M. P. 2008. Frequent loss of TIMP-3 expression in progression of esophageal and gastric adenocarcinomas. *Neoplasia*, 10, 563-72.
- GUAN, F., WANG, X. & HE, F. 2015. Promotion of Cell Migration by Neural Cell Adhesion Molecule (NCAM) Is Enhanced by PSA in a Polysialyltransferase-Specific Manner. *PLoS ONE*, 10, e0124237.
- GUAN, X. 2015. Cancer metastases: challenges and opportunities. *Acta Pharm Sin B*, 5, 402-18.
- GUPTA, S., LI, H. & SAMPSON, N. S. 2000. Characterization of fertilin beta-disintegrin binding specificity in sperm-egg adhesion. *Bioorg Med Chem*, 8, 723-9.
- GUTSCHNER, T. & DIEDERICHS, S. 2012. The hallmarks of cancer: a long non-coding RNA point of view. *RNA Biol*, 9, 703-19.
- HAGEMANN, T., GUNAWAN, B., SCHULZ, M., FÜZESI, L. & BINDER, C. 2001. mRNA expression of matrix metalloproteases and their inhibitors differs in subtypes of renal cell carcinomas. *European Journal of Cancer*, 37, 1839-1846.
- HAN, Y. P., NIEN, Y. D. & GARNER, W. L. 2002. Tumor necrosis factor-alpha-induced proteolytic activation of pro-matrix metalloproteinase-9 by human skin is controlled by down-regulating tissue inhibitor of metalloproteinase-1 and mediated by tissue-associated chymotrypsin-like proteinase. *J Biol Chem*, 277, 27319-27.
- HANAHAH, D. & WEINBERG, R. A. 2000. The hallmarks of cancer. *cell*, 100, 57-70.
- HANAHAH, D. & WEINBERG, R. A. 2011. Hallmarks of cancer: the next generation. *Cell*, 144, 646-74.
- HEINRICH, M. C., CORLESS, C. L., DUENSING, A., MCGREEVEY, L., CHEN, C. J., JOSEPH, N., SINGER, S., GRIFFITH, D. J., HALEY, A., TOWN, A., DEMETRI, G. D., FLETCHER, C. D. & FLETCHER, J. A. 2003. PDGFRA activating mutations in gastrointestinal stromal tumors. *Science*, 299, 708-10.
- HELDIN, C. H. 2013. Targeting the PDGF signaling pathway in tumor treatment. *Cell Commun Signal*, 11, 97.
- HELLEMAN, J., JANSEN, M. P., RUIGROK-RITSTIER, K., VAN STAVEREN, I. L., LOOK, M. P., MEIJER-VAN GELDER, M. E., SIEUWERTS, A. M., KLIJN, J. G., SLEIJFER, S., FOEKENS, J. A. & BERNS, E. M. 2008. Association of an extracellular matrix gene cluster with breast cancer prognosis and endocrine therapy response. *Clin Cancer Res*, 14, 5555-64.
- HEPPNER, G. H., MILLER, F. R. & SHEKHAR, P. M. 2000. Nontransgenic models of breast cancer. *Breast Cancer Res*, 2, 331-4.
- HERZOG, B., PELLET-MANY, C., BRITTON, G., HARTZOULAKIS, B. & ZACHARY, I. C. 2011. VEGF binding to NRP1 is essential for VEGF stimulation of endothelial cell migration, complex formation between NRP1 and VEGFR2, and signaling via FAK Tyr407 phosphorylation. *Molecular biology of the cell*, 22, 2766-2776.
- HIRAOKA, Y., YOSHIDA, K., OHNO, M., MATSUOKA, T., KITA, T. & NISHI, E. 2008. Ectodomain shedding of TNF-alpha is enhanced by nardilysin via activation of ADAM proteases. *Biochem Biophys Res Commun*, 370, 154-8.
- HIRATSUKA, S., NAKAMURA, K., IWAI, S., MURAKAMI, M., ITOH, T., KIJIMA, H., SHIPLEY, J. M., SENIOR, R. M. & SHIBUYA, M. 2002. MMP9 induction by vascular endothelial growth factor receptor-1 is involved in lung-specific metastasis. *Cancer Cell*, 2, 289-300.
- HONKAVUORI, M., TALVENSAARI-MATTILA, A., PUISTOLA, U., TURPEENNIEMI-HUJANEN, T. & SANTALA, M. 2008. High serum TIMP-1 is associated with adverse prognosis in endometrial carcinoma. *Anticancer research*, 28, 2715-2719.

- HOUGHTON, A. M., GRISOLANO, J. L., BAUMANN, M. L., KOBAYASHI, D. K., HAUTAMAKI, R. D., NEHRING, L. C., CORNELIUS, L. A. & SHAPIRO, S. D. 2006. Macrophage elastase (matrix metalloproteinase-12) suppresses growth of lung metastases. *Cancer Res*, 66, 6149-55.
- HU, L. 2004. Prodrugs: effective solutions for solubility, permeability and targeting challenges. *IDrugs*, 7, 736-42.
- HUANG, K., ANDERSSON, C., ROOMANS, G. M., ITO, N. & CLAESSEON-WELSH, L. 2001. Signaling properties of VEGF receptor-1 and -2 homo- and heterodimers. *Int J Biochem Cell Biol*, 33, 315-24.
- HUANG, L., DAI, T., LIN, X., ZHAO, X., CHEN, X., WANG, C., LI, X., SHEN, H. & WANG, X. 2012. MicroRNA-224 targets RKIP to control cell invasion and expression of metastasis genes in human breast cancer cells. *Biochem Biophys Res Commun*, 425, 127-33.
- HURSKAINEN, T. L., HIROHATA, S., SELDIN, M. F. & APTE, S. S. 1999. ADAM-TS5, ADAM-TS6, and ADAM-TS7, novel members of a new family of zinc metalloproteases. General features and genomic distribution of the ADAM-TS family. *J Biol Chem*, 274, 25555-63.
- IACOVELLI, R., STERNBERG, C. N., PORTA, C., VERZONI, E., DE BRAUD, F., ESCUDIER, B. & PROCOPIO, G. 2015. Inhibition of the VEGF/VEGFR pathway improves survival in advanced kidney cancer: a systematic review and meta-analysis. *Curr Drug Targets*, 16, 164-70.
- ICHIM, G. & TAIT, S. W. 2016. A fate worse than death: apoptosis as an oncogenic process. *Nature Reviews Cancer*, 16, 539-548.
- ILLMAN, S. A., LEHTI, K., KESKI-OJA, J. & LOHI, J. 2006. Epilysin (MMP-28) induces TGF-beta mediated epithelial to mesenchymal transition in lung carcinoma cells. *J Cell Sci*, 119, 3856-65.
- JACKSON, H. W., DEFAMIE, V., WATERHOUSE, P. & KHOKHA, R. 2017. TIMPs: versatile extracellular regulators in cancer. *Nat Rev Cancer*, 17, 38-53.
- JACKSON, H. W., HOJILLA, C. V., WEISS, A., SANCHEZ, O. H., WOOD, G. A. & KHOKHA, R. 2015. Timp3 Deficient Mice Show Resistance to Developing Breast Cancer. *PLoS ONE*, 10, e0120107.
- JECHLINGER, M., SOMMER, A., MORIGGL, R., SEITHER, P., KRAUT, N., CAPODIECCI, P., DONOVAN, M., CORDON-CARDO, C., BEUG, H. & GRUNERT, S. 2006. Autocrine PDGFR signaling promotes mammary cancer metastasis. *J Clin Invest*, 116, 1561-70.
- JENKINSON, C., ELLIOTT, V., MENON, U., APOSTOLIDOU, S., FOURKALA, O., GENTRY-MAHARAJ, A., PEREIRA, S., JACOBS, I., COX, T. & GREENHALF, W. 2015. Evaluation in pre-diagnosis samples discounts ICAM-1 and TIMP-1 as biomarkers for earlier diagnosis of pancreatic cancer. *Journal of proteomics*, 113, 400-402.
- JOHNSTONE, C. N., SMITH, Y. E., CAO, Y., BURROWS, A. D., CROSS, R. S., LING, X., REDVERS, R. P., DOHERTY, J. P., ECKHARDT, B. L., NATOLI, A. L., RESTALL, C. M., LUCAS, E., PEARSON, H. B., DEB, S., BRITT, K. L., RIZZITELLI, A., LI, J., HARMEY, J. H., POULIOT, N. & ANDERSON, R. L. 2015. Functional and molecular characterisation of EO771.LMB tumours, a new C57BL/6-mouse-derived model of spontaneously metastatic mammary cancer. *Dis Model Mech*, 8, 237-51.
- JONES, G. C. & RILEY, G. P. 2005. ADAMTS proteinases: a multi-domain, multi-functional family with roles in extracellular matrix turnover and arthritis. *Arthritis Res Ther*, 7, 160-169.
- JUBB, A. M., STRICKLAND, L. A., LIU, S. D., MAK, J., SCHMIDT, M. & KOEPPEN, H. 2012. Neuropilin-1 expression in cancer and development. *J Pathol*, 226, 50-60.
- JUDSON, I., RADFORD, J. A., HARRIS, M., BLAY, J. Y., VAN HOESEL, Q., LE CESNE, A., VAN OOSTEROM, A. T., CLEMONS, M. J., KAMBY, C., HERMANS, C., WHITTAKER, J., DONATO DI PAOLA, E., VERWEIJ, J. & NIELSEN, S. 2001. Randomised phase II trial of pegylated liposomal doxorubicin (DOXIL/CAELYX) versus doxorubicin in the treatment of advanced or metastatic soft tissue sarcoma: a study by the EORTC Soft Tissue and Bone Sarcoma Group. *Eur J Cancer*, 37, 870-7.

- KAMEI, M. & HOLLYFIELD, J. G. 1999. TIMP-3 in Bruch's membrane: changes during aging and in age-related macular degeneration. *Invest Ophthalmol Vis Sci*, 40, 2367-75.
- KANTHOU, C., DACHS, G. U., LEFLEY, D. V., STEELE, A. J., CORALLI-FOXON, C., HARRIS, S., GRECO, O., DOS SANTOS, S. A., REYES-ALDASORO, C. C., ENGLISH, W. R. & TOZER, G. M. 2014. Tumour cells expressing single VEGF isoforms display distinct growth, survival and migration characteristics. *PLoS One*, 9, e104015.
- KASHIWAGI, M., TORTORELLA, M., NAGASE, H. & BREW, K. 2001. TIMP-3 is a potent inhibitor of aggrecanase 1 (ADAM-TS4) and aggrecanase 2 (ADAM-TS5). *J Biol Chem*, 276, 12501-4.
- KASSIRI, Z., OUDIT, G. Y., KANDALAM, V., AWAD, A., WANG, X., ZIOU, X., MAEDA, N., HERZENBERG, A. M. & SCHOLEY, J. W. 2009. Loss of TIMP3 enhances interstitial nephritis and fibrosis. *J Am Soc Nephrol*, 20, 1223-35.
- KATOH, M. & NAKAGAMA, H. 2014. FGF receptors: cancer biology and therapeutics. *Medicinal research reviews*, 34, 280-300.
- KATSUTA, E., YAN, L., NAGAHASHI, M., RAZA, A., STURGILL, J. L., LYON, D. E., RASHID, O. M., HAIT, N. C. & TAKABE, K. 2017. Doxorubicin effect is enhanced by sphingosine-1-phosphate signaling antagonist in breast cancer. *journal of surgical research*, 219, 202-213.
- KAUR, I., RATHI, S. & CHAKRABARTI, S. 2010. Variations in TIMP3 are associated with age-related macular degeneration. *Proc Natl Acad Sci U S A*, 107, E112-3.
- KAYGUSUZ, I., ESER, A., INEGOL GUMUS, I., KOSUS, A., YENIDUNYA, S., NAMUSLU, M. & KAFALI, H. 2014. Effect of Anti-Vascular Endothelial Growth Factor Antibody During Early Fetal Development in Rats. *J Matern Fetal Neonatal Med*.
- KAZEROUNIAN, S., YEE, K. O. & LAWLER, J. 2008. Thrombospondins in cancer. *Cell Mol Life Sci*, 65, 700-12.
- KESSENBROCK, K., PLAKS, V. & WERB, Z. 2010. Matrix metalloproteinases: regulators of the tumor microenvironment. *Cell*, 141, 52-67.
- KHADKA, P., RO, J., KIM, H., KIM, I., KIM, J. T., KIM, H., CHO, J. M., YUN, G. & LEE, J. 2014. Pharmaceutical particle technologies: an approach to improve drug solubility, dissolution and bioavailability. *asian journal of pharmaceutical sciences*, 9, 304-316.
- KHAN, D. R., WEBB, M. N., CADOTTE, T. H. & GAVETTE, M. N. 2015. Use of Targeted Liposome-based Chemotherapeutics to Treat Breast Cancer. *Breast Cancer (Auckl)*, 9, 1-5.
- KITSUKAWA, T., SHIMIZU, M., SANBO, M., HIRATA, T., TANIGUCHI, M., BEKKU, Y., YAGI, T. & FUJISAWA, H. 1997. Neuropilin-semaphorin III/D-mediated chemorepulsive signals play a crucial role in peripheral nerve projection in mice. *Neuron*, 19, 995-1005.
- KLENOTIC, P. A., MUNIER, F. L., MARMORSTEIN, L. Y. & ANAND-APTE, B. 2004. Tissue inhibitor of metalloproteinases-3 (TIMP-3) is a binding partner of epithelial growth factor-containing fibulin-like extracellular matrix protein 1 (EFEMP1). Implications for macular degenerations. *J Biol Chem*, 279, 30469-73.
- KOBAYASHI, N., KOSTKA, G., GARBE, J. H., KEENE, D. R., BACHINGER, H. P., HANISCH, F. G., MARKOVA, D., TSUDA, T., TIMPL, R., CHU, M. L. & SASAKI, T. 2007. A comparative analysis of the fibulin protein family. Biochemical characterization, binding interactions, and tissue localization. *J Biol Chem*, 282, 11805-16.
- KOO, B. H., KIM, Y. H., HAN, J. H. & KIM, D. S. 2012. Dimerization of matrix metalloproteinase-2 (MMP-2): functional implication in MMP-2 activation. *J Biol Chem*, 287, 22643-53.
- KUVAJA, P., TALVENSAARI-MATTILA, A., PÄÄKKÖ, P. & TURPEENIEMI-HUJANEN, T. 2005. The absence of immunoreactivity for tissue inhibitor of metalloproteinase-1 (TIMP-1), but not for TIMP-2, protein is associated with a favorable prognosis in aggressive breast carcinoma. *Oncology*, 68, 196-203.
- LAMALICE, L., HOULE, F., JOURDAN, G. & HUOT, J. 2004. Phosphorylation of tyrosine 1214 on VEGFR2 is required for VEGF-induced activation of Cdc42 upstream of SAPK2/p38. *Oncogene*, 23, 434-45.

- LAMBERT, E., DASSÉ, E., HAYE, B. & PETITFRÈRE, E. 2004. TIMPs as multifacial proteins. *Critical reviews in oncology/hematology*, 49, 187-198.
- LAMOREAUX, W. J., FITZGERALD, M. E., REINER, A., HASTY, K. A. & CHARLES, S. T. 1998. Vascular endothelial growth factor increases release of gelatinase A and decreases release of tissue inhibitor of metalloproteinases by microvascular endothelial cells in vitro. *Microvasc Res*, 55, 29-42.
- LANGTON, K. P., BARKER, M. D. & MCKIE, N. 1998. Localization of the functional domains of human tissue inhibitor of metalloproteinases-3 and the effects of a Sorsby's fundus dystrophy mutation. *J Biol Chem*, 273, 16778-81.
- LANGTON, K. P., MCKIE, N., CURTIS, A., GOODSHIP, J. A., BOND, P. M., BARKER, M. D. & CLARKE, M. 2000. A novel tissue inhibitor of metalloproteinases-3 mutation reveals a common molecular phenotype in Sorsby's fundus dystrophy. *J Biol Chem*, 275, 27027-31.
- LANGTON, K. P., MCKIE, N., SMITH, B. M., BROWN, N. J. & BARKER, M. D. 2005. Sorsby's fundus dystrophy mutations impair turnover of TIMP-3 by retinal pigment epithelial cells. *Hum Mol Genet*, 14, 3579-86.
- LEE, J.-Y., PARK, S.-W., CHANG, H. K., KIM, H. Y., RHIM, T., LEE, J.-H., JANG, A.-S., KOH, E.-S. & PARK, C.-S. 2006a. A disintegrin and metalloproteinase 33 protein in patients with asthma: relevance to airflow limitation. *American journal of respiratory and critical care medicine*, 173, 729-735.
- LEE, M. H., ATKINSON, S. & MURPHY, G. 2007. Identification of the extracellular matrix (ECM) binding motifs of tissue inhibitor of metalloproteinases (TIMP)-3 and effective transfer to TIMP-1. *J Biol Chem*, 282, 6887-98.
- LEE, M. H., KNAUPER, V., BECHERER, J. D. & MURPHY, G. 2001. Full-length and N-TIMP-3 display equal inhibitory activities toward TNF-alpha convertase. *Biochem Biophys Res Commun*, 280, 945-50.
- LEE, M. H., RAPTI, M. & MURPHY, G. 2005a. Total conversion of tissue inhibitor of metalloproteinase (TIMP) for specific metalloproteinase targeting: fine-tuning TIMP-4 for optimal inhibition of tumor necrosis factor- α -converting enzyme. *J Biol Chem*, 280, 15967-75.
- LEE, S., DESAI, K. K., ICZKOWSKI, K. A., NEWCOMER, R. G., WU, K. J., ZHAO, Y. G., TAN, W. W., ROYCIK, M. D. & SANG, Q. X. 2006b. Coordinated peak expression of MMP-26 and TIMP-4 in preinvasive human prostate tumor. *Cell Res*, 16, 750-8.
- LEE, S., JILANI, S. M., NIKOLOVA, G. V., CARPIZO, D. & IRUELA-ARISPE, M. L. 2005b. Processing of VEGF-A by matrix metalloproteinases regulates bioavailability and vascular patterning in tumors. *J Cell Biol*, 169, 681-91.
- LEE, Y.-J., KOCH, M., KARL, D., TORRES-COLLADO, A. X., FERNANDO, N. T., ROTHROCK, C., KURUPPU, D., RYEOM, S., IRUELA-ARISPE, M. L. & YOON, S. S. 2010. Variable inhibition of thrombospondin 1 against liver and lung metastases through differential activation of metalloproteinase ADAMTS1. *Cancer research*, 70, 948-956.
- LEMMON, M. A. & SCHLESSINGER, J. 2010. Cell signaling by receptor tyrosine kinases. *Cell*, 141, 1117-34.
- LERICHE, G., CIFELLI, J. L., SIBUCAO, K. C., PATTERSON, J. P., KOYANAGI, T., GIANNESCHI, N. C. & YANG, J. 2017. Characterization of drug encapsulation and retention in archaea-inspired tetraether liposomes. *Org Biomol Chem*, 15, 2157-2162.
- LI, C. F., HE, H. L., WANG, J. Y., HUANG, H. Y., WU, T. F., HSING, C. H., LEE, S. W., LEE, H. H., FANG, J. L., HUANG, W. T. & CHEN, S. H. 2014. Fibroblast growth factor receptor 2 overexpression is predictive of poor prognosis in rectal cancer patients receiving neoadjuvant chemoradiotherapy. *J Clin Pathol*, 67, 1056-61.
- LI, L. & LI, H. 2013. Role of microRNA-mediated MMP regulation in the treatment and diagnosis of malignant tumors. *Cancer Biol Ther*, 14, 796-805.

- LI, Q., GAO, X. R., CUI, H. P., LANG, L. L., XIE, X. W. & CHEN, Q. 2016. Time-dependent matrix metalloproteinases and tissue inhibitor of metalloproteinases expression change in fusarium solani keratitis. *Int J Ophthalmol*, 9, 512-8.
- LIAO, D. & JOHNSON, R. S. 2007. Hypoxia: a key regulator of angiogenesis in cancer. *Cancer Metastasis Rev*, 26, 281-90.
- LIN, R. J., BLUMENKRANZ, M. S., BINKLEY, J., WU, K. & VOLLRATH, D. 2006. A novel His158Arg mutation in TIMP3 causes a late-onset form of Sorsby fundus dystrophy. *Am J Ophthalmol*, 142, 839-48.
- LISS, M., SREEDHAR, N., KESHGEGIAN, A., SAUTER, G., CHERNICK, M. R., PRENDERGAST, G. C. & WALLON, U. M. 2009. Tissue inhibitor of metalloproteinase-4 is elevated in early-stage breast cancers with accelerated progression and poor clinical course. *The American journal of pathology*, 175, 940-946.
- LIU, H., ZHANG, T., LI, X., HUANG, J., WU, B., HUANG, X., ZHOU, Y., ZHU, J. & HOU, J. 2008. Predictive value of MMP-7 expression for response to chemotherapy and survival in patients with non-small cell lung cancer. *Cancer Sci*, 99, 2185-92.
- LOFFEK, S., SCHILLING, O. & FRANZKE, C. W. 2011. Series "matrix metalloproteinases in lung health and disease": Biological role of matrix metalloproteinases: a critical balance. *Eur Respir J*, 38, 191-208.
- LOPEZ, P. F., SIPPY, B. D., LAMBERT, H. M., THACH, A. B. & HINTON, D. R. 1996. Transdifferentiated retinal pigment epithelial cells are immunoreactive for vascular endothelial growth factor in surgically excised age-related macular degeneration-related choroidal neovascular membranes. *Invest Ophthalmol Vis Sci*, 37, 855-68.
- LU, P., WEAVER, V. M. & WERB, Z. 2012. The extracellular matrix: a dynamic niche in cancer progression. *J Cell Biol*, 196, 395-406.
- LUKASZEWICZ-ZAJAC, M., MROCZKO, B., GUZINSKA-USTYMOWICZ, K., PRYCYNICZ, A., GRYKO, M., KEMONA, A., KEDRA, B. & SZMITKOWSKI, M. 2013. Matrix metalloproteinase 2 (MMP-2) and their tissue inhibitor 2 (TIMP-2) in gastric cancer patients. *Adv Med Sci*, 13, 1-9.
- LUKYANOV, A. N., ELBAYOUMI, T. A., CHAKILAM, A. R. & TORCHILIN, V. P. 2004. Tumor-targeted liposomes: doxorubicin-loaded long-circulating liposomes modified with anti-cancer antibody. *J Control Release*, 100, 135-44.
- MAEDA, H. 2012. Vascular permeability in cancer and infection as related to macromolecular drug delivery, with emphasis on the EPR effect for tumor-selective drug targeting. *Proc Jpn Acad Ser B Phys Biol Sci*, 88, 53-71.
- MAEKAWA, S., IWASAKI, A., SHIRAKUSA, T., ENATSU, S., KAWAKAMI, T., KUROKI, M. & KUROKI, M. 2007. Correlation Between Lymph Node Metastasis and the Expression of VEGF-C, VEGF-D and VEGFR-3 in T1 Lung Adenocarcinoma. *Anticancer Research*, 27, 3735-3741.
- MAHMOODI, M., SAHEBJAM, S., SMOOKLER, D., KHOKHA, R. & MORT, J. S. 2005. Lack of tissue inhibitor of metalloproteinases-3 results in an enhanced inflammatory response in antigen-induced arthritis. *Am J Pathol*, 166, 1733-40.
- MAJOR JOURDEN, J. L. & COHEN, S. M. 2010. Hydrogen peroxide activated matrix metalloproteinase inhibitors: a prodrug approach. *Angew Chem Int Ed Engl*, 49, 6795-7.
- MAJUMDAR, S. & SIAHAAN, T. J. 2012. Peptide-mediated targeted drug delivery. *Med Res Rev*, 32, 637-58.
- MARETZKY, T., REISS, K., LUDWIG, A., BUCHHOLZ, J., SCHOLZ, F., PROKSCH, E., DE STROOPER, B., HARTMANN, D. & SAFTIG, P. 2005. ADAM10 mediates E-cadherin shedding and regulates epithelial cell-cell adhesion, migration, and beta-catenin translocation. *Proc Natl Acad Sci U S A*, 102, 9182-7.
- MARMORSTEIN, L. Y., MUNIER, F. L., ARSENIJEVIC, Y., SCHORDERET, D. F., MCLAUGHLIN, P. J., CHUNG, D., TRABOULSI, E. & MARMORSTEIN, A. D. 2002. Aberrant accumulation of

- EFEMP1 underlies drusen formation in Malattia Leventinese and age-related macular degeneration. *Proc Natl Acad Sci U S A*, 99, 13067-72.
- MASTROBATTISTA, E., KONING, G. A. & STORM, G. 1999. Immunoliposomes for the targeted delivery of antitumor drugs. *Adv Drug Deliv Rev*, 40, 103-127.
- MASUI, T., HOSOTANI, R., TSUJI, S., MIYAMOTO, Y., YASUDA, S., IDA, J., NAKAJIMA, S., KAWAGUCHI, M., KOBAYASHI, H., KOIZUMI, M., TOYODA, E., TULACHAN, S., ARII, S., DOI, R. & IMAMURA, M. 2001. Expression of METH-1 and METH-2 in pancreatic cancer. *Clin Cancer Res*, 7, 3437-43.
- MATES, J. M. & SANCHEZ-JIMENEZ, F. M. 2000. Role of reactive oxygen species in apoptosis: implications for cancer therapy. *Int J Biochem Cell Biol*, 32, 157-70.
- MATSUDA, Y., ISHIWATA, T., YAMAHATSU, K., KAWAHARA, K., HAGIO, M., PENG, W. X., YAMAMOTO, T., NAKAZAWA, N., SEYA, T., OHAKI, Y. & NAITO, Z. 2011. Overexpressed fibroblast growth factor receptor 2 in the invasive front of colorectal cancer: a potential therapeutic target in colorectal cancer. *Cancer Lett*, 309, 209-19.
- MATTHEWS, R. T., GARY, S. C., ZERILLO, C., PRATTA, M., SOLOMON, K., ARNER, E. C. & HOCKFIELD, S. 2000. Brain-enriched hyaluronan binding (BEHAB)/brevican cleavage in a glioma cell line is mediated by a disintegrin and metalloproteinase with thrombospondin motifs (ADAMTS) family member. *Journal of Biological Chemistry*, 275, 22695-22703.
- MCCAWLEY, L. J., CRAWFORD, H. C., KING, L. E., JR., MUDGETT, J. & MATRISIAN, L. M. 2004. A protective role for matrix metalloproteinase-3 in squamous cell carcinoma. *Cancer Res*, 64, 6965-72.
- MCGOWAN, E. M., ALLING, N., JACKSON, E. A., YAGOUB, D., HAASS, N. K., ALLEN, J. D. & MARTINELLO-WILKS, R. 2011. Evaluation of cell cycle arrest in estrogen responsive MCF-7 breast cancer cells: pitfalls of the MTS assay. *PLoS one*, 6, e20623.
- MCRAE PAGE, S., HENCHEY, E., CHEN, X., SCHNEIDER, S. & EMRICK, T. 2014. Efficacy of polyMPC-DOX prodrugs in 4T1 tumor-bearing mice. *Mol Pharm*, 11, 1715-20.
- MELENDEZ-ZAJGLA, J., DEL POZO, L., CEBALLOS, G. & MALDONADO, V. 2008. Tissue inhibitor of metalloproteinases-4. The road less traveled. *Mol Cancer*, 7, 85.
- MENG, J., GUO, F., XU, H., LIANG, W., WANG, C. & YANG, X.-D. 2016. Combination therapy using co-encapsulated resveratrol and paclitaxel in liposomes for drug resistance reversal in breast cancer cells in vivo. *Scientific reports*, 6.
- MIGUEL, R. F., POLLAK, A. & LUBEC, G. 2005. Metalloproteinase ADAMTS-1 but not ADAMTS-5 is manifold overexpressed in neurodegenerative disorders as Down syndrome, Alzheimer's and Pick's disease. *Molecular brain research*, 133, 1-5.
- MINN, A. J., KANG, Y., SERGANOVA, I., GUPTA, G. P., GIRI, D. D., DOUBROVIN, M., PONOMAREV, V., GERALD, W. L., BLASBERG, R. & MASSAGUÉ, J. 2005. Distinct organ-specific metastatic potential of individual breast cancer cells and primary tumors. *Journal of Clinical Investigation*, 115, 44.
- MIX, K. S., ATTUR, M. G., AL-MUSSAWIR, H., ABRAMSON, S. B., BRINCKERHOFF, C. E. & MURPHY, E. P. 2007. Transcriptional repression of matrix metalloproteinase gene expression by the orphan nuclear receptor NURR1 in cartilage. *J Biol Chem*, 282, 9492-504.
- MOASE, E. H., QI, W., ISHIDA, T., GABOS, Z., LONGENECKER, B. M., ZIMMERMANN, G. L., DING, L., KRANTZ, M. & ALLEN, T. M. 2001. Anti-MUC-1 immunoliposomal doxorubicin in the treatment of murine models of metastatic breast cancer. *Biochim Biophys Acta*, 1510, 43-55.
- MUJAMAMMI, A. H. 2014. *Characterisation and Therapeutic Targeting of TIMP3 in Sorsby's Fundus Dystrophy*. PhD, University of Sheffield.
- MULLER, P. A. & VOUSDEN, K. H. 2013. p53 mutations in cancer. *Nat Cell Biol*, 15, 2-8.
- NAGASE, H. & MURPHY, G. 2008. Tailoring TIMPs for Selective Metalloproteinase Inhibition. In: EDWARDS, D., HØYER-HANSEN, G., BLASI, F. & SLOANE, B. (eds.) *The Cancer Degradome*. Springer New York.

- NAGASE, H., VISSÉ, R. & MURPHY, G. 2006. Structure and function of matrix metalloproteinases and TIMPs. *Cardiovasc Res*, 69, 562-73.
- NAKAMURA, M., ISHIDA, E., SHIMADA, K., KISHI, M., NAKASE, H., SAKAKI, T. & KONISHI, N. 2005. Frequent LOH on 22q12.3 and TIMP-3 inactivation occur in the progression to secondary glioblastomas. *Lab Invest*, 85, 165-75.
- NAKASONE, E. S., ASKAUTRUD, H. A., KEES, T., PARK, J. H., PLAKS, V., EWALD, A. J., FEIN, M., RASCH, M. G., TAN, Y. X., QIU, J., PARK, J., SINHA, P., BISSELL, M. J., FRENGEN, E., WERB, Z. & EGEHLAD, M. 2012. Imaging tumor-stroma interactions during chemotherapy reveals contributions of the microenvironment to resistance. *Cancer Cell*, 21, 488-503.
- NALLURI, S., GHOSHAL-GUPTA, S., KUTIYANAWALLA, A., GAYATRI, S., LEE, B. R., JIWANI, S., ROJIANI, A. M. & ROJIANI, M. V. 2015. TIMP-1 Inhibits Apoptosis in Lung Adenocarcinoma Cells via Interaction with Bcl-2. *PLoS One*, 10, e0137673.
- NAYAK, S., GOEL, M. M., MAKKER, A., BHATIA, V., CHANDRA, S., KUMAR, S. & AGARWAL, S. 2015. Fibroblast Growth Factor (FGF-2) and Its Receptors FGFR-2 and FGFR-3 May Be Putative Biomarkers of Malignant Transformation of Potentially Malignant Oral Lesions into Oral Squamous Cell Carcinoma. *PloS one*, 10, e0138801.
- NEVE, A., CANTATORE, F. P., MARUOTTI, N., CORRADO, A. & RIBATTI, D. 2014. Extracellular matrix modulates angiogenesis in physiological and pathological conditions. *Biomed Res Int*, 2014, 756078.
- NILSSON, I., BAHRAM, F., LI, X., GUALANDI, L., KOCH, S., JARVIUS, M., SODERBERG, O., ANISIMOV, A., KHOLOVA, I., PYTOWSKI, B., BALDWIN, M., YLA-HERTTUALA, S., ALITALO, K., KREUGER, J. & CLAESSEON-WELSH, L. 2010. VEGF receptor 2/-3 heterodimers detected in situ by proximity ligation on angiogenic sprouts. *EMBO J*, 29, 1377-88.
- NOE, V., FINGLETON, B., JACOBS, K., CRAWFORD, H. C., VERMEULEN, S., STEELANT, W., BRUYNEEL, E., MATRISIAN, L. M. & MAREEL, M. 2001. Release of an invasion promoter E-cadherin fragment by matrilysin and stromelysin-1. *J Cell Sci*, 114, 111-118.
- NUTTALL, R. K., SAMPIERI, C. L., PENNINGTON, C. J., GILL, S. E., SCHULTZ, G. A. & EDWARDS, D. R. 2004. Expression analysis of the entire MMP and TIMP gene families during mouse tissue development. *FEBS Lett*, 563, 129-34.
- OLFERT, I. M. 2016. Physiological Capillary Regression is not Dependent on Reducing VEGF Expression. *Microcirculation*, 23, 146-56.
- OLKHANUD, P. B., BAATAR, D., BODOGAI, M., HAKIM, F., GRESS, R., ANDERSON, R. L., DENG, J., XU, M., BRIEST, S. & BIRAGYN, A. 2009. Breast cancer lung metastasis requires expression of chemokine receptor CCR4 and regulatory T cells. *Cancer Res*, 69, 5996-6004.
- ONDER, T. T., GUPTA, P. B., MANI, S. A., YANG, J., LANDER, E. S. & WEINBERG, R. A. 2008. Loss of E-cadherin promotes metastasis via multiple downstream transcriptional pathways. *Cancer Res*, 68, 3645-54.
- OSIPOVITCH, D. C., PARKER, A. S., MAKOKHA, C. D., DESROSIERS, J., KETT, W. C., MOISE, L., BAILEY-KELLOGG, C. & GRISWOLD, K. E. 2012. Design and analysis of immune-evading enzymes for ADEPT therapy. *Protein Eng Des Sel*, 25, 613-23.
- OTROCK, Z. K., MAKAREM, J. A. & SHAMSEDDINE, A. I. 2007. Vascular endothelial growth factor family of ligands and receptors: review. *Blood Cells Mol Dis*, 38, 258-68.
- OVERALL, C. M. & KLEIFELD, O. 2006. Validating matrix metalloproteinases as drug targets and anti-targets for cancer therapy. *Nature Reviews Cancer*, 6, 227.
- PAN, X., WU, G., YANG, W., BARTH, R. F., TJARKS, W. & LEE, R. J. 2007. Synthesis of cetuximab-immunoliposomes via a cholesterol-based membrane anchor for targeting of EGFR. *Bioconjug Chem*, 18, 101-8.
- PARK, Y. H., SEO, S. Y., HA, M., KU, J. H., KIM, H. H. & KWAK, C. 2011. Inhibition of prostate cancer using RNA interference-directed knockdown of platelet-derived growth factor receptor. *Urology*, 77, 1509.e9-15.

- PATIL, R. R., GUHAGARKAR, S. A. & DEVARAJAN, P. V. 2008. Engineered nanocarriers of doxorubicin: a current update. *Crit Rev Ther Drug Carrier Syst*, 25, 1-61.
- PATTABIRAMAN, D. R. & WEINBERG, R. A. 2014. Tackling the cancer stem cells—what challenges do they pose? *Nature reviews Drug discovery*, 13, 497-512.
- PENN, J. S., MADAN, A., CALDWELL, R. B., BARTOLI, M., CALDWELL, R. W. & HARTNETT, M. E. 2008. Vascular endothelial growth factor in eye disease. *Prog Retin Eye Res*, 27, 331-71.
- POLLARD, J. W. 2004. Tumour-educated macrophages promote tumour progression and metastasis. *Nat Rev Cancer*, 4, 71-8.
- PORTER, S., CLARK, I. M., KEVORKIAN, L. & EDWARDS, D. R. 2005. The ADAMTS metalloproteinases. *Biochem J*, 386, 15-27.
- POSTINA, R., SCHROEDER, A., DEWACHTER, I., BOHL, J., SCHMITT, U., KOJRO, E., PRINZEN, C., ENDRES, K., HIEMKE, C. & BLESSING, M. 2004. A disintegrin-metalloproteinase prevents amyloid plaque formation and hippocampal defects in an Alzheimer disease mouse model. *The Journal of clinical investigation*, 113, 1456-1464.
- POULSEN, H. S., URUP, T., MICHAELSEN, S. R., STABERG, M., VILLINGSHOJ, M. & LASSEN, U. 2014. The impact of bevacizumab treatment on survival and quality of life in newly diagnosed glioblastoma patients. *Cancer Manag Res*, 6, 373-87.
- PRADOS, J., MELGUIZO, C., RAMA, A. R., ORTIZ, R., SEGURA, A., BOULAIZ, H., VELEZ, C., CABA, O., RAMOS, J. L. & ARANEGA, A. 2010. Gef gene therapy enhances the therapeutic efficacy of doxorubicin to combat growth of MCF-7 breast cancer cells. *Cancer Chemother Pharmacol*, 66, 69-78.
- PULUKURI, S. M., PATIBANDLA, S., PATEL, J., ESTES, N. & RAO, J. S. 2007. Epigenetic inactivation of the tissue inhibitor of metalloproteinase-2 (TIMP-2) gene in human prostate tumors. *Oncogene*, 26, 5229-37.
- PUPUTTI, M., TYNNINEN, O., SIHTO, H., BLOM, T., MAENPAA, H., ISOLA, J., PAETAU, A., JOENSUU, H. & NUPPONEN, N. N. 2006. Amplification of KIT, PDGFRA, VEGFR2, and EGFR in gliomas. *Mol Cancer Res*, 4, 927-34.
- QI, J. H., EBRAHEM, Q., ALI, M., CUTLER, A., BELL, B., PRAYSON, N., SEARS, J., KNAUPER, V., MURPHY, G. & ANAND-APTE, B. 2013. Tissue inhibitor of metalloproteinases-3 peptides inhibit angiogenesis and choroidal neovascularization in mice. *PLoS One*, 8, e55667.
- QI, J. H., EBRAHEM, Q., MOORE, N., MURPHY, G., CLAESSEON-WELSH, L., BOND, M., BAKER, A. & ANAND-APTE, B. 2003. A novel function for tissue inhibitor of metalloproteinases-3 (TIMP3): inhibition of angiogenesis by blockage of VEGF binding to VEGF receptor-2. *Nat Med*, 9, 407-15.
- QUANTE, M., TU, S. P., TOMITA, H., GONDA, T., WANG, S. S., TAKASHI, S., BAIK, G. H., SHIBATA, W., DIPRETE, B., BETZ, K. S., FRIEDMAN, R., VARRO, A., TYCKO, B. & WANG, T. C. 2011. Bone marrow-derived myofibroblasts contribute to the mesenchymal stem cell niche and promote tumor growth. *Cancer Cell*, 19, 257-72.
- RADISKY, E. S. & RADISKY, D. C. 2010. Matrix metalloproteinase-induced epithelial-mesenchymal transition in breast cancer. *J Mammary Gland Biol Neoplasia*, 15, 201-12.
- RAUTIO, J., KUMPULAINEN, H., HEIMBACH, T., OLIYAI, R., OH, D., JARVINEN, T. & SAVOLAINEN, J. 2008. Prodrugs: design and clinical applications. *Nat Rev Drug Discov*, 7, 255-70.
- REID, M. J., CROSS, A. K., HADDOCK, G., ALLAN, S. M., STOCK, C. J., WOODROOFE, M. N., BUTTLE, D. J. & BUNNING, R. A. 2009. ADAMTS-9 expression is up-regulated following transient middle cerebral artery occlusion (tMCAo) in the rat. *Neuroscience letters*, 452, 252-257.
- RESTIFO, N. P., DUDLEY, M. E. & ROSENBERG, S. A. 2012. Adoptive immunotherapy for cancer: harnessing the T cell response. *Nat Rev Immunol*, 12, 269-81.
- RISTIC, D., VUKOSAVLJEVIC, M., DRAGANIC, B., CEROVIC, V., PETROVIC, N. & JANICIJEVIC-PETROVIC, M. 2013. The effect of intravitreal administration of bevacizumab on macular edema and visual acuity in age-related macular degeneration with subfoveal choroidal neovascularisation. *Vojnosanit Pregl*, 70, 660-3.

- RIVERA, S., KHRESTCHATISKY, M., KACZMAREK, L., ROSENBERG, G. A. & JAWORSKI, D. M. 2010a. Metzincin proteases and their inhibitors: foes or friends in nervous system physiology? *The Journal of Neuroscience*, 30, 15337-15357.
- RIVERA, S., KHRESTCHATISKY, M., KACZMAREK, L., ROSENBERG, G. A. & JAWORSKI, D. M. 2010b. Metzincin proteases and their inhibitors: foes or friends in nervous system physiology? *Journal of Neuroscience*, 30, 15337-15357.
- ROCHLITZ, C., RUHSTALLER, T., LERCH, S., SPIRIG, C., HUOBER, J., SUTER, T., BÜHLMANN, M., FEHR, M., SCHÖNENBERGER, A. & VON MOOS, R. 2010. Combination of bevacizumab and 2-weekly pegylated liposomal doxorubicin as first-line therapy for locally recurrent or metastatic breast cancer. A multicenter, single-arm phase II trial (SAKK 24/06). *Annals of oncology*, 22, 80-85.
- ROSATI, M. S., RAIMONDI, C., BACIARELLO, G., GRASSI, P., GIOVANNONI, S., PETRELLI, E., BASILE, M. L., GIROLAMI, M., DI SERI, M. & FRATI, L. 2011. Weekly combination of non-pegylated liposomal doxorubicin and taxane in first-line breast cancer: wALT trial (phase I-II). *Ann Oncol*, 22, 315-20.
- RUHRBERG, C., GERHARDT, H., GOLDING, M., WATSON, R., IOANNIDOU, S., FUJISAWA, H., BETSHOLTZ, C. & SHIMA, D. T. 2002. Spatially restricted patterning cues provided by heparin-binding VEGF-A control blood vessel branching morphogenesis. *Genes Dev*, 16, 2684-98.
- RUSSELL, M. R., JAMIESON, W. L., DOLLOFF, N. G. & FATATIS, A. 2009. The alpha-receptor for platelet-derived growth factor as a target for antibody-mediated inhibition of skeletal metastases from prostate cancer cells. *Oncogene*, 28, 412-21.
- SAHIN, U., WESKAMP, G., KELLY, K., ZHOU, H. M., HIGASHIYAMA, S., PESCHON, J., HARTMANN, D., SAFTIG, P. & BLOBEL, C. P. 2004. Distinct roles for ADAM10 and ADAM17 in ectodomain shedding of six EGFR ligands. *J Cell Biol*, 164, 769-79.
- SAMPIERI, C. L., NUTTALL, R. K., YOUNG, D. A., GOLDSPINK, D., CLARK, I. M. & EDWARDS, D. R. 2008. Activation of p38 and JNK MAPK pathways abrogates requirement for new protein synthesis for phorbol ester mediated induction of select MMP and TIMP genes. *Matrix Biol*, 27, 128-38.
- SANDY, J. D., WESTLING, J., KENAGY, R. D., IRUELA-ARISPE, M. L., VERSCHAREN, C., RODRIGUEZ-MAZANEQUE, J. C., ZIMMERMANN, D. R., LEMIRE, J. M., FISCHER, J. W. & WIGHT, T. N. 2001. Versican V1 proteolysis in human aorta in vivo occurs at the Glu441-Ala442 bond, a site that is cleaved by recombinant ADAMTS-1 and ADAMTS-4. *Journal of Biological Chemistry*, 276, 13372-13378.
- SANTOS, S. C. R., MIGUEL, C., DOMINGUES, I., CALADO, A., ZHU, Z., WU, Y. & DIAS, S. 2007. VEGF and VEGFR-2 (KDR) internalization is required for endothelial recovery during wound healing. *Experimental cell research*, 313, 1561-1574.
- SAWADA, K., MITRA, A. K., RADJABI, A. R., BHASKAR, V., KISTNER, E. O., TRETIAKOVA, M., JAGADEESWARAN, S., MONTAG, A., BECKER, A., KENNY, H. A., PETER, M. E., RAMAKRISHNAN, V., YAMADA, S. D. & LENGYEL, E. 2008. Loss of E-cadherin promotes ovarian cancer metastasis via alpha 5-integrin, which is a therapeutic target. *Cancer Res*, 68, 2329-39.
- SEO, D. W., LI, H., GUEDEZ, L., WINGFIELD, P. T., DIAZ, T., SALLOUM, R., WEI, B. Y. & STETLER-STEVENSON, W. G. 2003. TIMP-2 mediated inhibition of angiogenesis: an MMP-independent mechanism. *Cell*, 114, 171-80.
- SHARMA, S. K. & BAGSHAW, K. D. 2017. Translating antibody directed enzyme prodrug therapy (ADEPT) and prospects for combination. *Expert Opin Biol Ther*, 17, 1-13.
- SHARMA, S. K., BAGSHAW, K. D., MELTON, R. G. & SHERWOOD, R. F. 1992. Human immune response to monoclonal antibody-enzyme conjugates in ADEPT pilot clinical trial. *Cell Biophys*, 21, 109-20.

- SHINOJIMA, T., YU, Q., HUANG, S. K., LI, M., MIZUNO, R., LIU, E. T., HOON, D. S. & LESSARD, L. 2012. Heterogeneous epigenetic regulation of TIMP3 in prostate cancer. *Epigenetics*, 7, 1279-89.
- SHOJI, T., TAKATORI, E., KAIDO, Y., OMI, H., YOKOYAMA, Y., MIZUNUMA, H., KAIHO, M., OTSUKI, T., TAKANO, T., YAEGASHI, N., NISHIYAMA, H., FUJIMORI, K. & SUGIYAMA, T. 2014. A phase I study of irinotecan and pegylated liposomal doxorubicin in recurrent ovarian cancer (Tohoku Gynecologic Cancer Unit 104 study). *Cancer Chemother Pharmacol*, 73, 895-901.
- SILLETI, S., KESSLER, T., GOLDBERG, J., BOGER, D. L. & CHERESH, D. A. 2001. Disruption of matrix metalloproteinase 2 binding to integrin alpha vbeta 3 by an organic molecule inhibits angiogenesis and tumor growth in vivo. *Proc Natl Acad Sci U S A*, 98, 119-24.
- SIMONS, M., GORDON, E. & CLAESSION-WELSH, L. 2016. Mechanisms and regulation of endothelial VEGF receptor signalling. *Nat Rev Mol Cell Biol*, 17, 611-25.
- SINGH, A., UPADHYAY, V., UPADHYAY, A. K., SINGH, S. M. & PANDA, A. K. 2015. Protein recovery from inclusion bodies of Escherichia coli using mild solubilization process. *Microbial cell factories*, 14, 41.
- SMITH, N. R., BAKER, D., JAMES, N. H., RATCLIFFE, K., JENKINS, M., ASHTON, S. E., SPROAT, G., SWANN, R., GRAY, N., RYAN, A., JURGENSMEIER, J. M. & WOMACK, C. 2010. Vascular endothelial growth factor receptors VEGFR-2 and VEGFR-3 are localized primarily to the vasculature in human primary solid cancers. *Clin Cancer Res*, 16, 3548-61.
- SOGAWA, K., KONDO, K., FUJINO, H., TAKAHASHI, Y., MIYOSHI, T., SAKIYAMA, S., MUKAI, K. & MONDEN, Y. 2003. Increased expression of matrix metalloproteinase-2 and tissue inhibitor of metalloproteinase-2 is correlated with poor prognostic variables in patients with thymic epithelial tumors. *Cancer*, 98, 1822-9.
- SONG, X., REN, Y., ZHANG, J., WANG, G., HAN, X., ZHENG, W. & ZHEN, L. 2015. Targeted delivery of doxorubicin to breast cancer cells by aptamer functionalized DOTAP/DOPE liposomes. *Oncol Rep*, 34, 1953-60.
- SOUDY, R., CHEN, C. & KAUR, K. 2013. Novel peptide-doxorubicin conjugates for targeting breast cancer cells including the multidrug resistant cells. *J Med Chem*, 56, 7564-73.
- SPAN, P. N., LINDBERG, R. L., MANDERS, P., TJAN-HEIJNEN, V. C., HEUVEL, J. J., BEEH, L. V. & SWEEP, C. 2004. Tissue inhibitors of metalloproteinase expression in human breast cancer: TIMP-3 is associated with adjuvant endocrine therapy success. *The Journal of pathology*, 202, 395-402.
- STEWART, J. A., CHAIKEN, M. F., WANG, F. & PRICE, C. M. 2012. Maintaining the end: roles of telomere proteins in end-protection, telomere replication and length regulation. *Mutat Res*, 730, 12-9.
- TACAR, O., SRIAMORNSAK, P. & DASS, C. R. 2013. Doxorubicin: an update on anticancer molecular action, toxicity and novel drug delivery systems. *J Pharm Pharmacol*, 65, 157-70.
- TAKAGI, S., SIMIZU, S. & OSADA, H. 2009. RECK negatively regulates matrix metalloproteinase-9 transcription. *Cancer Res*, 69, 1502-8.
- TAMMELA, T., ZARKADA, G., WALLGARD, E., MURTOMAKI, A., SUCHTING, S., WIRZENIUS, M., WALTARI, M., HELLSTROM, M., SCHOMBER, T., PELTONEN, R., FREITAS, C., DUARTE, A., ISONIEMI, H., LAAKKONEN, P., CHRISTOFORI, G., YLA-HERTTUALA, S., SHIBUYA, M., PYTOWSKI, B., EICHMANN, A., BETSHOLTZ, C. & ALITALO, K. 2008. Blocking VEGFR-3 suppresses angiogenic sprouting and vascular network formation. *Nature*, 454, 656-60.
- TANAKA, Y., MIYAMOTO, S., SUZUKI, S. O., OKI, E., YAGI, H., SONODA, K., YAMAZAKI, A., MIZUSHIMA, H., MAEHARA, Y. & MEKADA, E. 2005. Clinical significance of heparin-binding epidermal growth factor-like growth factor and a disintegrin and metalloprotease 17 expression in human ovarian cancer. *Clinical Cancer Research*, 11, 4783-4792.

- TAO, K., FANG, M., ALROY, J. & SAHAGIAN, G. G. 2008. Imagable 4T1 model for the study of late stage breast cancer. *BMC Cancer*, 8, 228.
- TCHAIKOVSKI, V., FELLBRICH, G. & WALTENBERGER, J. 2008. The molecular basis of VEGFR-1 signal transduction pathways in primary human monocytes. *Arterioscler Thromb Vasc Biol*, 28, 322-8.
- TEWARI, K. S., SILL, M. W., LONG, H. J., 3RD, PENSON, R. T., HUANG, H., RAMONDETTA, L. M., LANDRUM, L. M., OAKNIN, A., REID, T. J., LEITAO, M. M., MICHAEL, H. E. & MONK, B. J. 2014. Improved survival with bevacizumab in advanced cervical cancer. *N Engl J Med*, 370, 734-43.
- THIELE, W. & SLEEMAN, J. P. 2006. Tumor-induced lymphangiogenesis: a target for cancer therapy? *J Biotechnol*, 124, 224-41.
- TIAN, Y., ZHANG, P., XIAO, X., ZHANG, J., ZHAO, J., KANG, Q., CHEN, X., QIU, F. & LIU, Y. 2007. The quantification of ADAMTS expression in an animal model of cerebral ischemia using real-time PCR. *Acta anaesthesiologica scandinavica*, 51, 158-164.
- TROEBERG, L., LAZENBATT, C., ANOWER-E-KHUDA, MD F., FREEMAN, C., FEDEROV, O., HABUCHI, H., HABUCHI, O., KIMATA, K. & NAGASE, H. 2014. Sulfated Glycosaminoglycans Control the Extracellular Trafficking and the Activity of the Metalloprotease Inhibitor TIMP-3. *Chemistry & Biology*, 21, 1300-1309.
- TSENG, W. W., WINER, D., KENKEL, J. A., CHOI, O., SHAIN, A. H., POLLACK, J. R., FRENCH, R., LOWY, A. M. & ENGLEMAN, E. G. 2010. Development of an orthotopic model of invasive pancreatic cancer in an immunocompetent murine host. *Clin Cancer Res*, 16, 3684-95.
- TSENG, Y. L., LIU, J. J. & HONG, R. L. 2002. Translocation of liposomes into cancer cells by cell-penetrating peptides penetratin and tat: a kinetic and efficacy study. *Mol Pharmacol*, 62, 864-72.
- TURKINGTON, R. C., LONGLEY, D. B., ALLEN, W. L., STEVENSON, L., MCLAUGHLIN, K., DUNNE, P. D., BLAYNEY, J. K., SALTO-TELLEZ, M., VAN SCHAEYBROECK, S. & JOHNSTON, P. G. 2014. Fibroblast growth factor receptor 4 (FGFR4): a targetable regulator of drug resistance in colorectal cancer. *Cell Death Dis*, 5, e1046.
- TURNER, N. & GROSE, R. 2010. Fibroblast growth factor signalling: from development to cancer. *Nat Rev Cancer*, 10, 116-29.
- UNEMORI, E. N., FERRARA, N., BAUER, E. A. & AMENTO, E. P. 1992. Vascular endothelial growth factor induces interstitial collagenase expression in human endothelial cells. *J Cell Physiol*, 153, 557-62.
- VALTOLA, R., SALVEN, P., HEIKKILA, P., TAIPALE, J., JOENSUU, H., REHN, M., PIHLAJANIEMI, T., WEICH, H., DEWAAL, R. & ALITALO, K. 1999. VEGFR-3 and its ligand VEGF-C are associated with angiogenesis in breast cancer. *Am J Pathol*, 154, 1381-90.
- VANDENBROUCKE, R. E. & LIBERT, C. 2014. Is there new hope for therapeutic matrix metalloproteinase inhibition? *Nature reviews. Drug discovery*, 13, 904.
- WAGSTAFF, L., KELWICK, R., DECOCK, J. & EDWARDS, D. R. 2011. The roles of ADAMTS metalloproteinases in tumorigenesis and metastasis. *Front Biosci (Landmark Ed)*, 16, 1861-72.
- WANG, J., HUANG, Y., ZHANG, J., WEI, Y., MAHOUD, S., BAKHEET, A. M., WANG, L., ZHOU, S. & TANG, J. 2016. Pathway-related molecules of VEGFC/D-VEGFR3/NRP2 axis in tumor lymphangiogenesis and lymphatic metastasis. *Clin Chim Acta*, 461, 165-71.
- WANG, M., LIU, Y. E., GREENE, J., SHENG, S., FUCHS, A., ROSEN, E. M. & SHI, Y. E. 1997. Inhibition of tumor growth and metastasis of human breast cancer cells transfected with tissue inhibitor of metalloproteinase 4. *Oncogene*, 14, 2767-74.
- WANG, W., JONES, C., CIACCI-ZANELLA, J., HOLT, T., GILCHRIST, D. G. & DICKMAN, M. B. 1996. Fumonisin and Alternaria alternata lycopersici toxins: sphinganine analog mycotoxins induce apoptosis in monkey kidney cells. *Proceedings of the National Academy of Sciences*, 93, 3461-3465.

- WESTMAN, E. L., CANOVA, M. J., RADHI, I. J., KOTEVA, K., KIREEVA, I., WAGLECHNER, N. & WRIGHT, G. D. 2012. Bacterial inactivation of the anticancer drug doxorubicin. *Chem Biol*, 19, 1255-64.
- WHITAKER, G. B., LIMBERG, B. J. & ROSENBAUM, J. S. 2001. Vascular endothelial growth factor receptor-2 and neuropilin-1 form a receptor complex that is responsible for the differential signaling potency of VEGF165 and VEGF121. *Journal of Biological Chemistry*, 276, 25520-25531.
- WILCZYNSKA, K. M., GOPALAN, S. M., BUGNO, M., KASZA, A., KONIK, B. S., BRYAN, L., WRIGHT, S., GRISWOLD-PRENNER, I. & KORDULA, T. 2006. A novel mechanism of tissue inhibitor of metalloproteinases-1 activation by interleukin-1 in primary human astrocytes. *J Biol Chem*, 281, 34955-64.
- WISNIEWSKA, M., GOETTIG, P., MASKOS, K., BELOUSKI, E., WINTERS, D., HECHT, R., BLACK, R. & BODE, W. 2008. Structural determinants of the ADAM inhibition by TIMP-3: crystal structure of the TACE-N-TIMP-3 complex. *J Mol Biol*, 381, 1307-19.
- WITSCH, E., SELA, M. & YARDEN, Y. 2010. Roles for growth factors in cancer progression. *Physiology (Bethesda)*, 25, 85-101.
- WONG, R. S. 2011. Apoptosis in cancer: from pathogenesis to treatment. *J Exp Clin Cancer Res*, 30, 87.
- WU, J., LIU, Q. & LEE, R. J. 2006. A folate receptor-targeted liposomal formulation for paclitaxel. *Int J Pharm*, 316, 148-53.
- WU, Y., WEI, S., VAN DOREN, S. R. & BREW, K. 2011. Entropy increases from different sources support the high-affinity binding of the N-terminal inhibitory domains of tissue inhibitors of metalloproteinases to the catalytic domains of matrix metalloproteinases-1 and -3. *J Biol Chem*, 286, 16891-9.
- WYATT, M. K., TSAI, J. Y., MISHRA, S., CAMPOS, M., JAWORSKI, C., FARISS, R. N., BERNSTEIN, S. L. & WISTOW, G. 2013. Interaction of complement factor h and fibulin3 in age-related macular degeneration. *PLoS One*, 8, e68088.
- XU, P., LIU, J., SAKAKI-YUMOTO, M. & DERYNCK, R. 2012. TACE activation by MAPK-mediated regulation of cell surface dimerization and TIMP3 association. *Sci Signal*, 5, ra34.
- YABLUCHANSKIY, A., MA, Y., IYER, R. P., HALL, M. E. & LINDSEY, M. L. 2013. Matrix metalloproteinase-9: Many shades of function in cardiovascular disease. *Physiology (Bethesda)*, 28, 391-403.
- YANG, H. W., CHUNG, M., KUDO, T. & MEYER, T. 2017. Competing memories of mitogen and p53 signalling control cell-cycle entry. *Nature*, 549, 404-408.
- YANG, S., THOR, A. D., EDGERTON, S. & YANG, X. 2006. Caspase-3 mediated feedback activation of apical caspases in doxorubicin and TNF-alpha induced apoptosis. *Apoptosis*, 11, 1987-97.
- YONG, V. W. 2005. Metalloproteinases: mediators of pathology and regeneration in the CNS. *Nat Rev Neurosci*, 6, 931-44.
- YU, W. H., YU, S., MENG, Q., BREW, K. & WOESSNER, J. F., JR. 2000. TIMP-3 binds to sulfated glycosaminoglycans of the extracellular matrix. *J Biol Chem*, 275, 31226-32.
- YUAN, W., MATTHEWS, R., SANDY, J. & GOTTSCHALL, P. 2002. Association between protease-specific proteolytic cleavage of brevican and synaptic loss in the dentate gyrus of kainate-treated rats. *Neuroscience*, 114, 1091-1101.
- ZHOU, A. Y., ICHASO, N., ADAMAREK, A., ZILA, V., FORSTOVA, J., DIBB, N. J. & DILWORTH, S. M. 2011. Polyomavirus middle T-antigen is a transmembrane protein that binds signaling proteins in discrete subcellular membrane sites. *Journal of virology*, 85, 3046-3054.
- ZHOU, B., REN, J., DING, C., WU, Y., HU, D., GU, G. & LI, J. 2013. Rapidly in situ forming platelet-rich plasma gel enhances angiogenic responses and augments early wound healing after open abdomen. *Gastroenterol Res Pract*, 2013, 926764.

- ZHOU, L., DU, L., CHEN, X., LI, X., LI, Z., WEN, Y., LI, Z., HE, X., WEI, Y., ZHAO, X. & QIAN, Z. 2010a. The antitumor and antimetastatic effects of N-trimethyl chitosan-encapsulated camptothecin on ovarian cancer with minimal side effects. *Oncol Rep*, 24, 941-8.
- ZHOU, Z., NGUYEN, T. C., GUCHHAIT, P. & DONG, J. F. 2010b. Von Willebrand factor, ADAMTS-13, and thrombotic thrombocytopenic purpura. *Semin Thromb Hemost*, 36, 71-81.
- ZHU, L., KATE, P. & TORCHILIN, V. P. 2012. Matrix metalloprotease 2-responsive multifunctional liposomal nanocarrier for enhanced tumor targeting. *ACS Nano*, 6, 3491-8.
- ZSCHIESCHE, W., SCHONBORN, I., BEHRENS, J., HERRENKNECHT, K., HARTVEIT, F., LILLEN, P. & BIRCHMEIER, W. 1997. Expression of E-cadherin and catenins in invasive mammary carcinomas. *Anticancer Res*, 17, 561-7.

9 Appendix

Reagents and other materials

| Reagents for cell culture | Supplier |
|--|---|
| Cells | |
| ARPE19 cells | American Type Culture Collection (ATCC) |
| HuDMEC | PromoCell |
| H5V mouse cardiac endothelial cell | Provided by Dr Chryso Kanthou, Tumour Microcirculation Group, University of Sheffield, with kind permission from Dr Annunciata Vecchi, Direzione Scientifica Istituto Clinico Humanitas, Rozzano, Italy |
| α -Select chemically competent <i>E. coli</i> | Bioline |
| 4T1 mouse breast cancer cell | Provided by Dr Russell Hughes, Tumour Targeting Group, University of Sheffield |
| MCF-7 Human breast cancer cell | ATCC® HTB-133™ |
| <i>E. coli</i> BL21 (DE3) cells | Bioline |
| Antibodies | |
| Anti P-VEGF Receptor 2 (cat 19A10) | Cell Signalling |
| Anti VEGF Receptor 2 (cat 55B11) | |
| Anti-Histone H3 (cat 4499P) | Cell Signalling |
| Alexa Fluor® 488 anti-mouse CD31 (cat 102513) | BioLegend® |
| Alexa Fluor® 488 Rat IgG2a, κ Isotype Ctrl (cat 400525) | BioLegend® |
| Anti-Caspase 3 (Rabbit)-Ab9661 | Cell Signalling |
| Mouse anti-Histidine (cat 37-2900) | Invitrogen |
| Anti-V5 Mouse Antibody (cat R960-25) | Invitrogen |
| Commercial DNA and Protein kits | |
| GenElute™ Gel Extraction Kit | Sigma-Aldrich |
| GenElute™ PCR Clean-up Kit | Sigma-Aldrich |
| GenElute™ HP Plasmid Miniprep Kit | Sigma-Aldrich |
| GenElute™ HP Plasmid Maxiprep Kit | Sigma-Aldrich |
| LumiGLO Reverse Chemiluminescent Substrate | KPL |
| BCA Protein Assay Kit | Pierce |
| Other Chemical, substances and reagents | |
| Resolving Gel Buffer | Bio-Rad |
| Stacking Gel Buffer | Bio-Rad |
| Acrylamide 40% | Bio-Rad |
| Ammonium Persulphate | GE Healthcare Sciences |

| | |
|---|----------------------|
| 10% SDS | Bio-Rad |
| TEMED | Amersham Biosciences |
| LB Broth Granulated | Melford |
| LB Agar High Salt Granulated | Melford |
| Tween 20 | Fisher Scientific |
| Dulbecco's Phosphate Buffered Saline | BioWhittaker |
| Caps | Fisher Scientific |
| Bicinchoninic | Sigma Aldrich |
| Copper II Sulphate | Sigma Aldrich |
| Isopropanol | Fisher Scientific |
| Ethanol 96% vol | VWR |
| Methanol | VWR |
| Bromophenol Blue | BDH |
| Triton X-100 | Fisher Scientific |
| Glycerol | Fisher Scientific |
| DAB | Vector Laboratories |
| Avidin–biotinylated enzyme complex (ABC) | Vector Laboratories |
| CellTiter 96® AQueous One Solution Cell Proliferation Assay (MTS) | Promega |
| Enzymes for digestion and ligation | |
| NotI-HF | New England Biolabs |
| HindIII | New England Biolabs |
| NdeI | New England Biolabs |
| NotI | New England Biolabs |
| AgeI | New England Biolabs |
| XhoI | New England Biolabs |
| BamHI | New England Biolabs |
| HindIII HF | New England Biolabs |
| T4 DNA ligase | Promega |
| 10X Ligase Buffer | Promega |
| Vectors | |
| pcDNA6B plasmid | Invitrogen |
| Pet28a | Monogenic |

Preparation of solutions and buffers

Tris acetate EDTA buffer (TAE) preparation:

TAE was prepared by adding up 242 g of Tris-base, 57.1 ml of 100% acetate (100% acetic acid), 100 ml 0.5M sodium EDTA and volume made up to 1 L with H₂O to make 50X TAE. 10 ml of 50X TAE was then added to 490 ml dH₂O to make 1X.

Agarose gel for DNA strand separation:

1% agarose mini gels were prepared by dissolving 0.6 g of agarose in 60 ml of 1X TAE buffer. The solution was heated in a microwave for about 3 mins and allowed to cool to 80°C at room temperature (RT). Afterwards, 3 µl of 10 mg/ml of ethidium bromide (EtBr) was then added to the solution and mixed carefully before pouring into a gel tray and allowing to set. To prepare larger gels of different gel concentration, the agarose and TAE volume were adjusted as required.

Antibiotics:

For selection of transformed bacteria, carbenicillin was prepared by dissolving carbenicillin powder in 70% ethanol to make a 100 mg/ml stock solution. Kanamycin stock solution was also prepared by dissolving 1 g kanamycin powder in 10 ml deionised water (dH₂O) to make 100 mg/ml stock and filter sterilised. The antibiotic stock solutions prepared were then stored at -20°C. For the selection of transfected mammalian cells, 50 mg of Blasticidin was dissolved in 10 ml of deionised water (dH₂O) to make 5 mg/ml stock, then it was sterile filtered and stored at -20°C.

Ammonium persulphate (APS):

10% solution of APS was freshly prepared by dissolving 100 mg of APS in 1 ml of dH₂O.

FACs buffer (0.1% BSA and 0.1% sodium azide):

FACS buffer was prepared by dissolving 0.1 g of sodium azide in 100 ml with of cold Dulbecco's phosphate buffer saline (DPBS). After which 285µl of BSA (35%) was added

DAPI (4',6-diamidino-2-phenylindole):

The nucleic acid stain DAPI was prepared by dissolving 10 mg powder in 2 ml of deionised water (dH₂O) to make 5 mg/ml stock. This was then stored, protected from light, at -20°C.

4% paraformaldehyde:

The 4% paraformaldehyde fixative was prepared by dissolving 1.2 g of paraformaldehyde in 30 ml of pre-warmed DPBS and allowed to dissolve on a magnetic stirrer for an hour. The pH was then adjusted to 7.3 before the solution was stored in -80°C.

Tris buffer saline solution (10x TBS):

TBS (10x) was prepared by dissolving 24.22 g Tris and 87.66 g NaCl in 800 mL of dH₂O. The pH was adjusted to 7.5 using 1 M HCl and then the volume made up to 1 L with dH₂O.

Tris buffer saline with tween 20 (1X TBST):

To prepare 1X TBST, 100 ml of 10X TBS was added to 900ml of dH₂O. 500µl of Tween 20 was then added to the solution (0.05%) and mixed thoroughly before storing at room temperature.

5% (w/v) milk blocking buffer:

Blocking buffer was prepared by dissolving 2.5 g of dried skimmed milk powder in 50 ml of 1X TBST.

3% (w/v) BSA blocking buffer:

BSA blocking buffer was prepared by dissolving 1.5 g of BSA in 50 ml of 1X TBST.

N-cyclohexyl-3-aminopropanesulfonic acid (CAPS) buffer:

2.2 g of CAPS powder was added to 800 ml of dH₂O after which the pH was adjusted to 11 using 1M sodium hydroxide (NaOH). Afterwards, 100 ml of methanol was added and the volume was made up to 1 L with dH₂O.

Preparation of stripping buffer:

The stripping buffer was prepared by mixing 6.28 mM Tris-HCl at pH 6.7, 2% SDS and 100mM 2-Mercaptoethanol.

LB Broth:

LB broth was prepared by adding 12.5 g of granulated LB broth in 500 ml of dH₂O. The solution was autoclaved at 121°C for 20 min.

LB agar:

37 g of LB agar granules were added to 1 L of dH₂O and autoclaved at 121°C. The autoclaved agar was allowed to cool to below 50°C and 100 µg/ml of carbenicillin was added. The agar was immediately poured into the agar plates at 20 ml/plate covering the base of the plate and then allowed to solidify at RT. The agar plates were stored at 4°C until needed. For kanamycin-containing agar plates, kanamycin was added to agar when cooling as before to make 30 µg/ml kanamycin final concentration in agar.

Recombinant Human TIMP3 preparation (rhTIMP3):

Ten microgram of rhTIMP3 was added to 2 ml sterile deionised water to give a concentration of 5 µg/ml which is then kept at -20°C as 25 µl aliquots.

Starving medium:

This was prepared by adding 0.5 % foetal bovine serum (FBS) to Dulbecco's modified eagle's medium (DMEM) serum free medium. The medium was used immediately or stored at 4°C until needed.

VEGF:

10 µg of VEGF was dissolved in 100 µl of 1X DPBS in a class II safety cabinet. Aliquots of 5 µl were prepared and stored at -20°C until needed.

Sequence: CPG2 codon optimised no periplasmic seq + His tag single AgeI Range: 1 to 1223

```
>NdeI
|
| 10    20    30    40    50    60    70    80    90
CATATGGCGCTGGCCAGAAAACGTGATAACGTGCTGTTTCAGGCGGCGACCGATGAACAGCCGGCGGTGATTAACCGTGGAAAACTG
GTATACCGCGACCGGGTCTTTGCACTATTGCACGACAAAGTCCGCCGCTGGCTACTTGTGCGCCGCACTAATTTTGCACCTTTTAC
M A L A Q K R D N V L F Q A A T D E Q P A V I K T L E K L >
CDS >

>AgeI
|
100    110    120    130    140    150    160    170    180
GTGAACATTGAAACCGGCACCGGTGATGCGGAAGGTATTGCGGCAGCGGGTAACTTCTGGAAGCGGAACGAAAAACCTGGGCTTACC
CACTTGTAACTTTGGCCGTGGCCACTACGCCCTCCATAACGCCGTGCGCCATTGAAAGACCTTCGCCCTGACTTTTGGACCGGAATGG
V N I E T G T G D A E G I A A A G N F L E A E L K N L G F T >
CDS >

190    200    210    220    230    240    250    260    270
GTGACCCGTAGCAAAGCGCGGTCTGGTGGTGGCGGATAACATTGTGGGCAAATTAAGGCCGTGGCGGTAACAACTGCTGCTGATG
CACTGGGCATCGTTTTCCGCCAGACACCGCGCTATTGTAACACCGGTTTAATTTCCGGCACCGCCATTTTGGACGACGACTAC
V T R S K S A G L V V G D N I V G K I K G R G G K N L L L M >
CDS >

280    290    300    310    320    330    340    350    360
AGCCACATGGATACCGTGTATCTGAAAGGCATTCTGGCCAAAGCGCGCTTTCGTGTGGAAGCGGATAAAGCGTATGGCCCGGGTATTGG
TCGGTGTACCTATGGCACATAGACTTTCCGTAAGACCGGTTTCGGCGCAAAGCACACCTTCCGCTATTTGCGCATACCGGGCCATAACGC
S H M D T V Y L K G I L A K A P F R V E G D K A Y G P G I A >
CDS >

370    380    390    400    410    420    430    440    450
GATGATAAAGGCGGCAACCGGTGATTCTGCATACCGTAAACTGCTGAAAGAATATGGCGTGCGTGATTATGGCACCATACCGTGCCTG
CTACTATTTCCGCCGTTGCGCCACTAAGCGTATGGGACTTTGACGACTTTCTTATACCGCACGCACTAATACCGTGGTAATGGCACGAC
D D K G G N A V I L H T L K L L K E Y G V R D Y G T I T V L >
CDS >

460    470    480    490    500    510    520    530    540
TTAACACCGATGAAGAAAAAGGCAGCTTTGGCAGCCGTGATCTGATTAGGAAGAAGCGAAACTGGCCGATTATGTTCTGAGCTTTGAA
AAATTTGGCTACTTCTTTTTCCGTCGAAACCGTCGGCACTAGACTAAGTCTTCTTCGCTTTGACCGGCTAATACAAGACTCGAAACTT
F N T D E E K G S F G S R D L I Q E E A K L A D Y V L S F E >
CDS >

550    560    570    580    590    600    610    620    630
CCGACCAAGCGGGTGTGAAAAACTGAGCCTGGGCAACAGCGGCATTGCGTATGTGCAAGTGAACATTACCGGCAAAGCGAGCCATCGG
GGCTGGTCGCGCCACTACTTTTTGACTCGGACCGGTGGTCCCGTAACGCATACACGTCCTACTTGAATGGCCGTTTCGCTCGGTACGC
P T S A G D E K L S L G T S G I A Y V Q V N I T G K A S H A >
CDS >

640    650    660    670    680    690    700    710    720
GGTCCGCGCACCGAACTGGGTGTGAACGCGCTGGTTGAAGCGAGCGATCTGGTGTGCTGCTACCATGAACATTGATGATAAAGCGAAAAAC
CCACGCCGTGGCCTTGACCCACACTTGGCGGACCAACTTCGCTCGTAGACCACGACGCATGGTACTTGTAACTACTATTTCCGCTTTTGG
G A A P E L G V N A L V E A S D L V L R T M N I D D K A K N >
CDS >

730    740    750    760    770    780    790    800    810
CTGCGTTTTAACTGGACCATGCGAAAGCGGGCAACGTGAGCAACATTATCCGGCGAGCGGACCCCTGAATGCGGATGTGCGTTATGGG
GACGCAAAATGACCTGGTAACGCTTTCCGCCGTTGCACCTGTTGTAATAAGCGCGCTCGCGCTGGGACTTACGCTACACGCAATACGC
L R F N W T I A K A G N V S N I I P A S A T L N A D V R Y A >
CDS >

820    830    840    850    860    870    880    890    900
CGTAACGAAGATTTTGTGCGGCCATGAAAACGCTGGAAGAAGCTGCGCAGCAGAAAAAACTGCCGGAAGCGGATGTGAAAGTGATTGTG
GCATTGCTTCTAAAACACCGCGTACTTTTGGACCTTCTTGCACGCGTCTTTTTTGGACGGCCTTCGCCCTACACTTTCACTAACAC
R N E D F D A A M K T L E E R A Q Q K K L P E A D V K V I V >
CDS >
```

910 920 930 940 950 960 970 980 990
 ACCCGTGGCCGTCCGGCGTTTAAACGCGGGCGAAGGCGGCAAAAACTGGTGGATAAAGCGGTGGCGTATTATAAAGAAGCAGGCGGGCACC
 TGGGCACCGGCAGGCCGAAATTGCGCCCGCTTCCGGCGTTTTTTGACCACCTATTTGCGCACCGCATAATATTTCTCGTCCGGCGTGG
 T R G R P A F N A G E G G K K L V D K A V A Y Y K E A G G T>
 CDS >

1000 1010 1020 1030 1040 1050 1060 1070 1080
 CTGGGTGTGGAAGAACGTACCGGCGGTGGCACCGATGCGGCGTATGCGGCCCTGAGCGGCAAGCCGGTGATTGAAAGCCTGGGCCTGCCG
 GACCCACACCTTCTTGCATGGCCGCCACCGTGGCTACGCCGCATACGCCGGGACTCGCCGTTCCGGCCACTAACTTTCCGGACCCGGACGGC
 L G V E E R T G G G T D A A Y A A L S G K P V I E S L G L P>
 CDS >

1090 1100 1110 1120 1130 1140 1150 1160 1170
 GGCTTTGGCTATCATAGCGATAAAGCGGAATATGTGGATATTAGCGCGATTCCGCGTGTCTGTATATGGCGCGTGTCTGATTATGGAT
 CCGAAACCGATAGTATCGCTATTTGCGCTTATACACCTATAATCGCGCTAAGGCGCAGCAGACATATACCGCGCAGCAGACTAATACCTA
 G F G Y H S D K A E Y V D I S A I P R R L Y M A R R L I M D>
 CDS >

>HindIII
 |
 1180 1190 1200 1210 | 1220
 CTGGGTGCGGGCAAACATCATCACCATCATCATTATAAAAAGCTTGGCGCCGC
 GACCCACGCCCGTTTGTAGTAGTGGTAGTAGTAATATTTTGAACGCCGGCG
 L G A G K H H H H H H *>
 CDS >

Sequence: p700 for CPG2 modified for synthesis Range: 1 to 222

```
>NdeI
|
| 10      20      30      40      50      60      70      80      90
CATATGAAATCAAATCCTGCTACTATCTGCCGTGTTTCGTAACCAGCAAGAATGGCGGTGGTGGCTCAGGTGGAGGCGGCAGTGGCGGC
GTATACTTTTAGTTTAGGACGATGATAGACGGCACAAAGCATTGGTCGTTCTTACCGCCACCACCGAGTCCACCTCCGCCGTACCCGCCG
  K I K S C Y Y L P C F V T S K N>
  _____
                    P700
                                     G G G G S G G G G S G G>
                                     _____
                                           [GLY4SER]4 LINKER

100      110      120      130      140      150      160      170      180
GGTGGTCTGGCGGAGGTGGGTGGCATTAGCGCAGAAACGGGATAACGTTCTGTTTCAGGCTGCGACTGACGAACAACCAGCCGTCATT
CCACCAAGACCGCTCCACCCAGCCGTAATCGCGTCTTTGCGCTATTGCAAGACAAAGTCCGACGCTGACTGCTTGTGGTCGGCAGTAA
  G G S G G G G S>
  _____
    [GLY4SER]4 LINKER
                                     A L A Q K R D N V L F Q A A T D E Q P A V I>
                                     _____
                                           CPG2

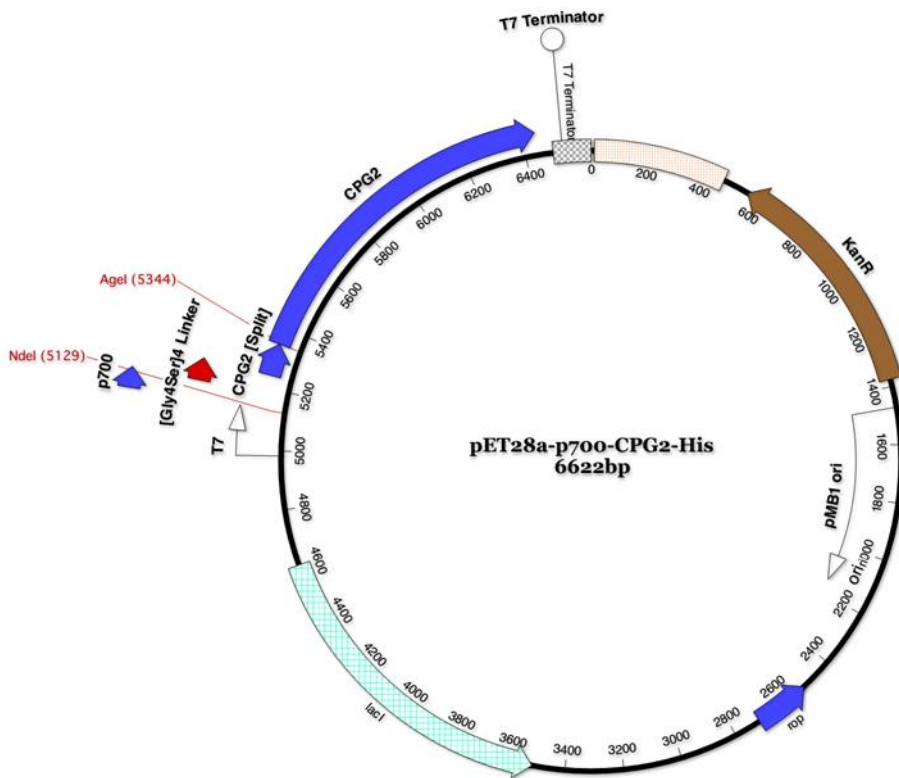
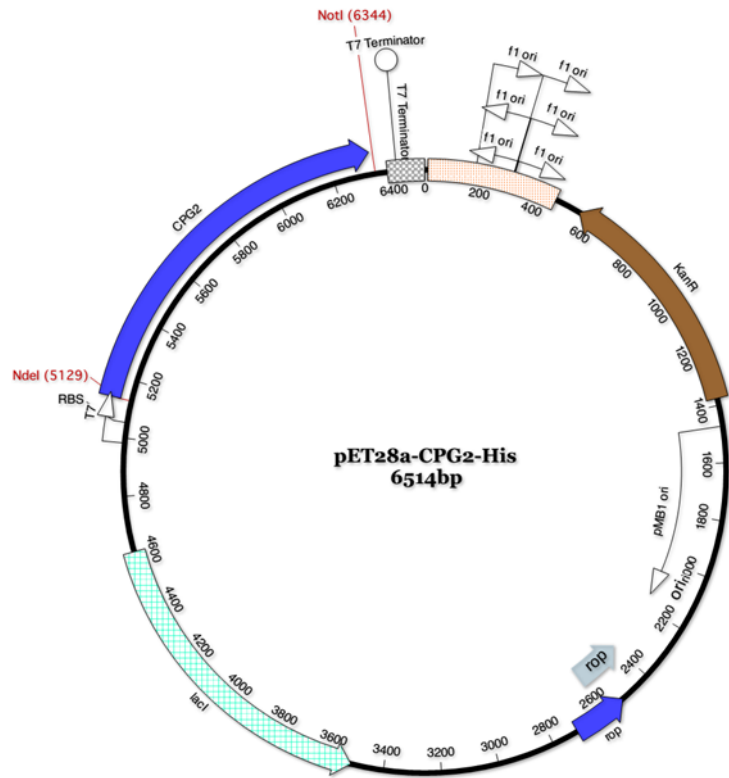
                                     >AgeI
                                     |
190      200      210      220 |
AAAACGTTGGAGAACTGGTGAACATTGAAACCGGGACCGGT
TTTTGCAACCTCTTTGACCACTTGAACCTTTGGCCCTGGCCA
  K T L E K L V N I E T G T G>
  _____
                    CPG2
```

Sequence: T3 C-term for CPG2 modified for synthesis Range: 1 to 231

```
>NdeI
|
| 10      20      30      40      50      60      70      80      90
CATATGCTCGGTATCGTGGTTGGGCTCCTCCGGATAAAAGCATCATTAAACCGGACTGATCCAGGCGGTGGAGGCGAGTGGCGGTGGTGGG
GTATACAGGACCATAGCACCAACCGAGGAGGCCTATTTTCGTAGTAATTGCGCTGACTAGGTCCGCCACCTCCGTACCCGCCACCACCC
  S W Y R G W A P P D K S I I N A T D P>
  _____
                    TIMP3 C-TERM
                                     G G G G S G G G G G>
                                     _____
                                           [GLY4SER]4 LINKER

100      110      120      130      140      150      160      170      180
TCTGGCGCGGTGGGTGAGGAGGCGGTGGCTCGGCTTAGCCAGAAACGGGACAATGTGCTGTTTCAGGCAGCGACCGATGAACAACCG
AGACCGCCGCCACCCAGTCTCCGCCACCGAGCCGAATCGGGTCTTTGCGCTGTTACACGACAAAGTCCGTCGCTGGCTACTTGTGGC
  S G G G G S G G G G S>
  _____
    [GLY4SER]4 LINKER
                                     A L A Q K R D N V L F Q A A T D E Q P>
                                     _____
                                           CPG2

                                     >AgeI
                                     |
190      200      210      220      230|
GCCGTTATCAAGACGTTGGAGAACTGGTCAACATTGAAACCGGGACCGGT
CGGCAATAGTTCTGCAACCTCTTTGACCACTTGAACCTTTGGCCCTGGCCA
  A V I K T L E K L V N I E T G T G>
  _____
                    CPG2
```



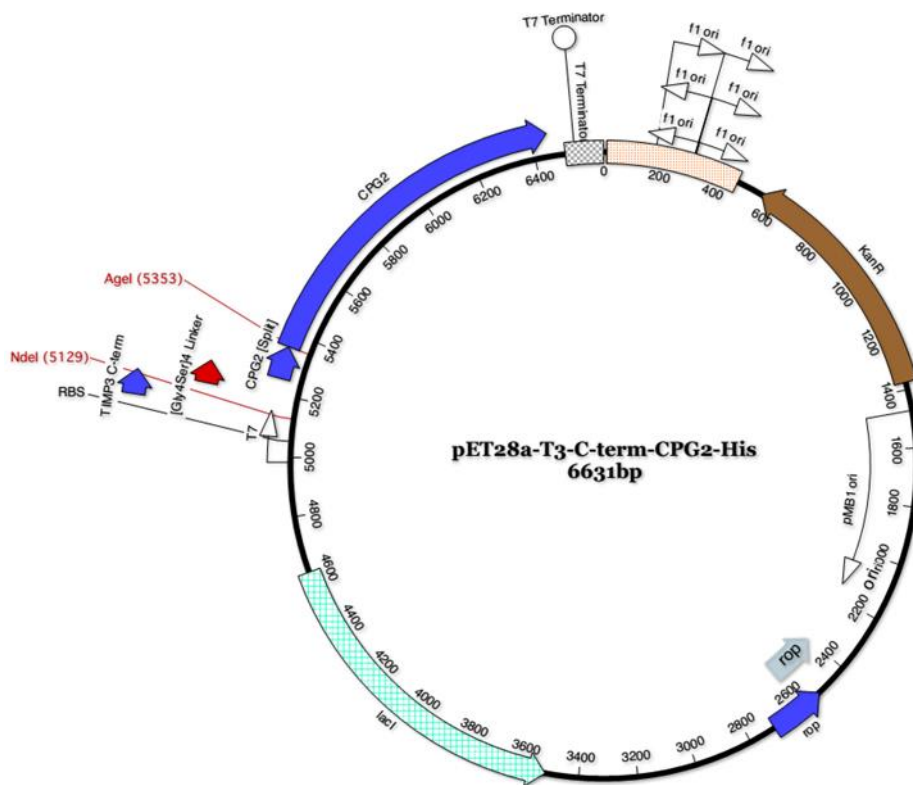


Figure A1: Insertion of codon optimised CPG2, CPG2-T3C and CPG2-p700 into pET28a plasmid vector

CPG2 (long blue) inserted between NdeI and NotI sites while T3C plus linker, and p700 plus linker (short blue and short red) are inserted at AgeI and NdeI sites to align the sequences in a correct open reading frame for a codon optimised vector.

Sequence: TIMP3-TIMP4 chimera + VEGFR2 + extra rest sites Range: 1 to 668

```
>NheI   >HindIII
|       |
|       | 10      20      30      40      50      60
GCTAGCAAGCTTGCCACCATGACCCCTTGGCTCGGGCTCATCGTGCTCCTGGGCAGCTGG
CGATCGTTCGAACGGTGGTACTGGGGAACCGAGCCCGAGTAGCACGAGGACCGTCGACC
      M T P W L G L I V L L G S W>

      70      80      90      100     110     120
AGCCTGGGGGACTGGGGCGCCGAGGC TGCACATGCTC CCCAGCCACCCCAGGACGCC
TCGGACCCCTGACCCCGCGGCTCCG ACGTGTACGAG GGGTCGGTGGGGTCTCGCGG
S L G D W G A E A C T C S P S H P Q D A>

      130     140     150     160     170     180
TTC T G C A A C T C C G A C A T C G T G A T C C G G G C C A A G G T G G T G G G G A A G A G C T G G T G A A G G A G
A A G A C G T T G A G G C T G T A G C A C T A G G C C C G G T T C C A C C A C C C C T T C T T C G A C C A C T T C C T C
F C N S D I V I R A K V V G K K L V K E>

      190     200     210     220     230     240
GGGCCCTTCGGCACCCTGGTCTACACCATCAAGCAGATGAAGATGTACCGAGGCTTCACC
CCCGGGAAGCCGTGCGACACAGATGTGGTAGTTTCGTCTACTTCTACATGGCTCCGAAGTGG
G P F G T L V Y T I K Q M K M Y R G F T>

                                          >AflIII
                                          |
      250     260     270     280     290     | 300
AAGATGCCCATGTGCAGTACATCCACACGGAAGCCTCCGAGAGTCTCTGTGGCCTTAAG
TTCTACGGGGTACACGTCATGTAGGTGTGCCTTCGGAGGCTCTCAGAGACACCGGAATTC
K M P H V Q Y I H T E A S E S L C G L K>

                                          >BsrGI
                                          |
      310     320     330     340     350     | 360
CTGGAGGTCAACAAGTACCAGTACCTGCTGACAGGTCCGGTCTATGATGGCAAGATGTAC
GACCTCCAGTTGTTTCATGGTTCATGGACGACTGTCCAGCGCAGATACTACCGTTCTACATG
L E V N K Y Q Y L L T G R V Y D G K M Y>

      370     380     390     400     410     420
ACGGGGCTGTGCAACTTCGTGGAGAGGTGGGACCAGCTCACCCCTCTCCAGCGCAAGGGG
TGCCCCGACACGTTGAAGCACCTCTCCACCCTGGTCGAGTGGGAGAGGGTCCGTTCCCC
T G L C N F V E R W D Q L T L S Q R K G>
```

TIMP3

TIMP4

```

                                >PmlI
                                |
          430      440      450      460      |      470      480
CTGAACATACGGTATCACCTGGGTTGTAACAGCCAAATCACCACGTGCTACACAGTCCC
GACTTGATAGCCATAGTGGACCCAACATTGACGGTTTAGTGGTGCACGATGTGTCAAGG
L N Y R Y H L G C N C Q I T T C Y T V P

          >AfeI
          |
          490      |      500      510      520      530      540
TGTTTTGTTAGCGCTCCTAACGAGTGCCTCTGGACAGACTGGCTGTCCGAACGAAAGCTC
ACAAACAATCGCGAGGATTGCTCAGGAGACCTGTCTGACCGACAGGCTTGCTTCGAG
C F V S A P N E C L W T D W L S E R K L

          >BlpI
          |
          550      |      560      570      580      590      600
TATGGTTACCAGGCTCAGCATTATGCTGTATGAAGCAGGTTGACGGCACCTGCTCCTGG
ATACCAATGGTCCGAGTCGTAATACAGACATACTTCGTCCAACCTGCCGTGGACGAGGACC
Y G Y Q A Q H Y V C M K Q V D G T C S W

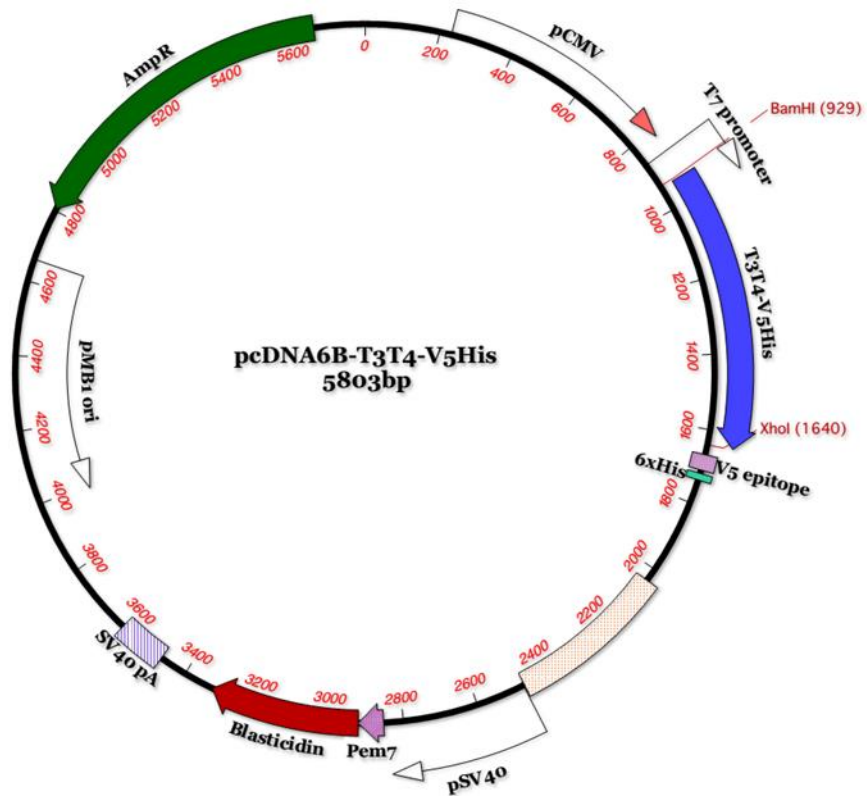
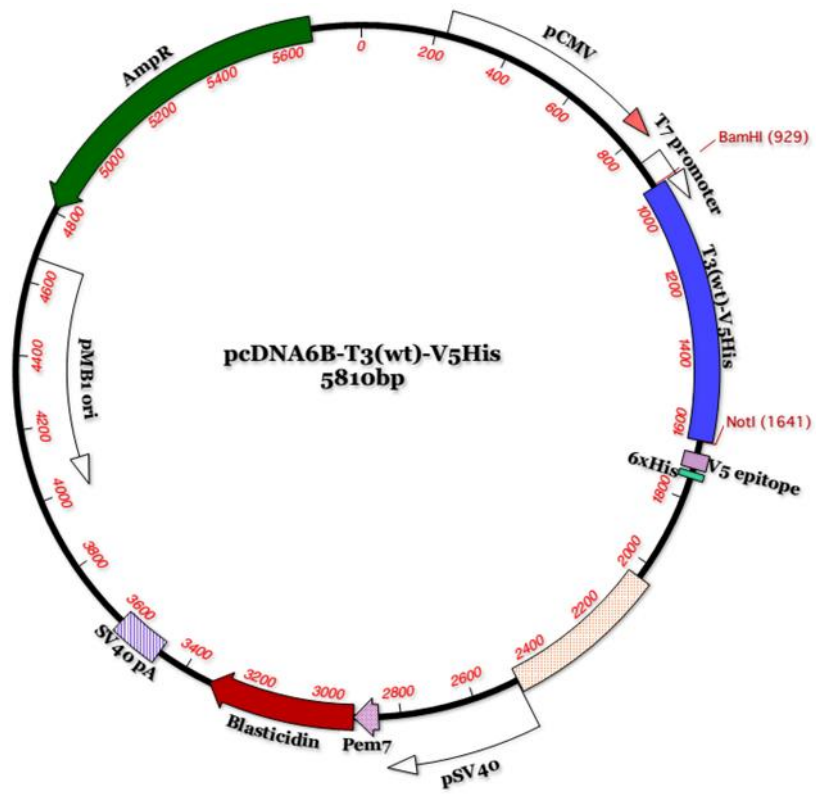
          >SacII
          |
          >KpnI |
          | | 610      620      630      640      650      | 660
TACCGCGGCTGGGCCCTCTCAGGAAGGAGTTTGTGACATCGTTCAGCCCTAGGCGGGC
ATGGCGCGGACCCGGGAGAGTCCTTCCTCAAACAACGTAGCAAGTCGGGATCCGCGGG
Y R G W A P L R K E F V D I V Q P *

          >EcoRI
          |
          GCGAATTC
          CGCTTAAG
  
```

Red residues are VEGFR2 binding residues from TIMP3

Blocked red bases are human optimised codons

NB DNA sequence silently modified to incorporate extra restriction sites. All those shown are absent from pcDNA3 except 5' and 3' ends for cloning into MCS.



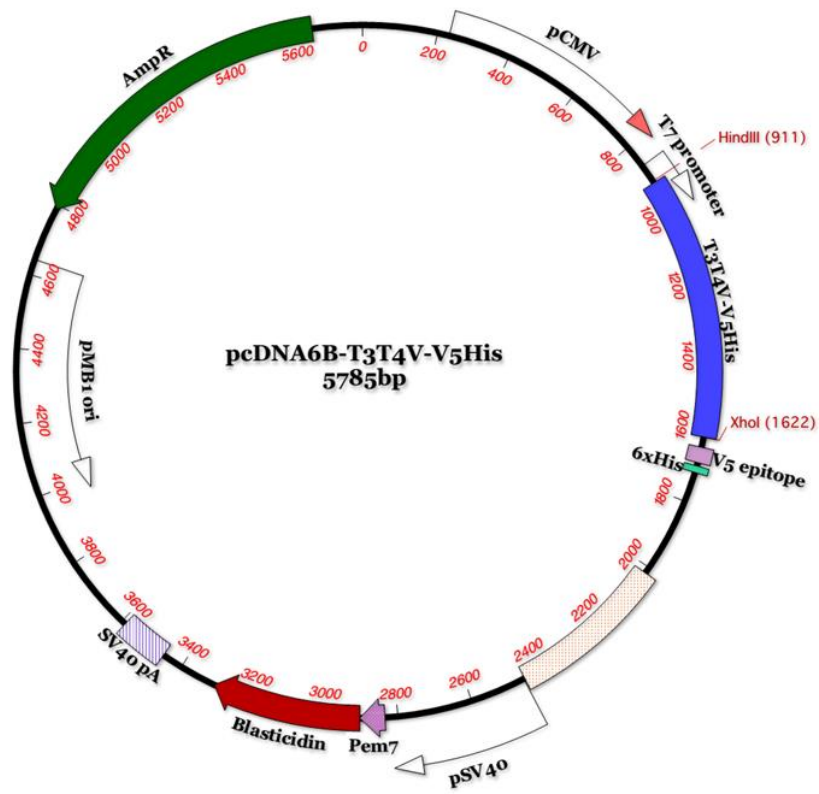


Figure A2: Map of the final pcDNA6-T3T4-V5-His constructs